DISSERTATION THESIS

Characterization of Glutamate Carboxypeptidase II,

its Close Homologs and their Interactions with Ligands

by

Jan Tykvart, MSc

Scientific Supervisor: Jan Konvalinka, PhD

Department of Biochemistry

Faculty of Science

Charles University

Institute of Organic Chemistry and Biochemistry

Gilead Sciences & IOCB Research Centre

Academy of Sciences of the Czech Republic

Prague 2015

Prohlašuji, že jsem tuto disertační práci vypracoval samostatně pod vedením školitele Doc. RNDr. Jana Konvalinky, CSc. a všechny použité prameny jsem řádně citoval.

V Praze dne 2.4.2015   ....

Acknowledgement

Abstract

Cancer, group of diseases characterized by an uncontrolled cell growth, represents one of the great challenges of modern clinical research. Currently, the standard treatment of the cancer disease relies mainly on the whole body exposition to various factors, which targets the dividing cells, combined with surgical resection of the tumor. Unfortunately, this treatment is sometimes accompanied by numerous severe side-effects (e.g., nausea, loss of hair, infertility etc.). Therefore, in the past 40 years enormous resources and effort have been invested into finding a way how to specifically target and destroy the cancerous cells. This goal has been primarily addressed by the search for molecules, mainly proteins, which are predominantly expressed in the cancerous tissues compared to the healthy cells.

Glutamate carboxypeptidase II (GCPII), also known as prostate specific membrane antigen (PSMA), represents such a target since it is highly expressed in a prostate carcinoma as well as in a solid tumor neovasculature. Additionally, GCPII is widely used as a model target molecule for proof-of-principle studies on targeted drug delivery. GCPII thorough biochemical characterization is essential for its appropriate use. Therefore, our laboratory has been investigating GCPII from various perspectives for more than 15 years.

The studies presented in this thesis aim to introduce new advanced methodologies for GCPII expression, purification and characterization. These methodologies should enable more simple and reliable study of GCPII and facilitate its application as a specific address for targeted drug delivery. In order to achieve this goal, we established a one-step reliable and versatile affinity purification protocol for GCPII. Subsequently, we performed a thorough comparative study characterizing majority of currently used monoclonal antibodies (mAbs) against GCPII in both quantitative and qualitative manner. Finally, we characterized one of the closest GCPII homolog, *N*-acetylated alpha-linked acidic dipeptidase-like (NAALADase L) protein in terms of its tertiary structure, expression profile, and enzymatic activity.

Abstrakt

Nádorová onemocnění, skupina nemocí vyznačující se nekontrolovaným buněčným růstem, představuje jednu z velkých výzev moderního klinického výzkumu. V současnosti se standardní postup léčby spoléhá převážně na systémovou terapii, která využívá různé látky účinkující proti dělícím se buňkám, v kombinaci s chirurgickým odstraněním nádoru. Tento přístup je bohužel někdy doprovázen řadou nežádoucích vedlejších účinků (jako jsou například nevolnost, ztráta vlasů, neplodnost apod.) a navíc může docházet k opakovanému návratu nemoci. Z těchto důvodu se v posledních 40 letech investovalo mnoho prostředků a úsilí do nalezení způsobu jak ničit nádorové buňky více specificky. Nejběžnějším způsobem získání specifity se stalo hledání molekul (primárně proteinů), které by se vyskytovaly převážně v rakovinné a ne ve zdravé tkáni.

Glutamátkarboxypeptidasa II (GCPII), známá též jako nádorový antigen specifický pro prostatu (PSMA), představuje jeden z takovýchto proteinů, jelikož je produkovaná ve velkém množství buňkami adenokarcinomu prostaty a navíc je přítomna v neovaskulaturách dalších pevných nádorů. GCPII se také často využívá jako modelová molekula při testování nových metod pro cílenou dopravu léčiv. Důkladná biochemická charakterizace GCPII je proto nezbytná pro její správné využití při výše zmíněných aplikacích. Již více než 15 let naše laboratoř studuje GCPII a snaží se tento protein co nejdůkladněji charakterizovat, aby umožnila jeho efektivní využití.

Primárním cílem publikací uvedených v této práci je prohloubení znalostí o GCPII a zavedení pokročilých metod umožňujících jednodušší práci s tímto proteinem. Je zde popsán vývoj efektivní a univerzální purifikační metody pro GCPII a detailní charakterizace monoklonálních protilátek proti GCPII. Tyto protilátky se využívají jak v běžné laboratorní praxi, tak při vývoji diagnostických a terapeutických léčiv, jejichž současná špatná charakterizace může vést k jejich nesprávnému použití. Na závěr je zde také prezentována charakterizace blízkého homologu GCPII, proteinu NAALADase L, kdy byla určena jeho prostorová struktura, enzymová aktivita a také distribuce v lidských tkáních.

Contents

Chapter 1: Introduction

1.1 History and nomenclature of GCPII

First reference of GCPII in scientific literature dates back to 1987 when it emerged simultaneously from two completely unrelated research areas. Robinson *et al.* presented a study identifying a protein, denominated *N*-acetylated alpha-linked acidic dipeptidase (NAALADase), responsible for hydrolysis of neurotransmitter *N*-acetyl-L-aspartyl-L-glutamate (NAAG) in rat brain [1]. In the meantime Horoszewicz *et al.* raised monoclonal antibody 7E11-C5.3 against a new marker of epithelial prostatic cancer cell line LNCaP (lymph node carcinoma of the prostate) which was entitled prostate specific membrane antigen (PSMA) [2]. To make things even more complicated, in 1991, Halsted *et al* identified a new enzyme, designated folate hydrolase (FOLH), in jejunal brush-border which hydrolyses and thus enable subsequent absorption of dietary folates [3].

Probably due to the very distant research fields, for the following five years neuroscientists studied NAALADase, urologists PSMA and dietologists FOLH without realizing that all these names refer to a single protein entity. In 1996, two publications emerged showing that the PSMA possesses folate hydrolase activity [4] and that it also embodies the characteristics of a neuropeptidase [5]. Shortly after, the laboratory of Joseph T. Coyle made an attempt to unify the nomenclature by performing a thorough analysis of NAALADase, PSMA and FOLH. They demonstrated the equal properties of these proteins and suggested the usage of the name "glutamate carboxypeptidase II" [6-9]. This designation was subsequently adopted by International Union of Biochemistry and Molecular Biology (IUBMB).

However, even after 15 years the original names for GCPII, mainly PSMA, are still frequently used. Unfortunately, this makes the orientation in the GCPII research field quite complicated. Throughout this thesis the name GCPII will be used preferentially.

1.2 GCPII on DNA level

Gene *FOLH1* coding for GCPII spans over 60 kbp region at chromosome 11 arm p11.2 and is formed by 19 exons and 18 introns [10]. A promoter for *FOLH1* gene lies upstream and contains several potential transcription factor binding sites. Interestingly, none of them is responsible for high GCPII expression in the prostate [10, 11]. This phenotype is probably caused by a 72 bp enhancer (PSME), localized in the third intron of

FOLH1, which activates GCPII expression in prostate cancer cell lines and is repressed by androgens [12, 13].

1.3 GCPII on RNA level

1.3.1 Alternative splicing

An mRNA coding for full-length GCPII protein (ENTREZ code NM_004476.1) undergoes various alternative splicing. Several different splice variants such as PSM', PSM-C, PSM-D, PSM-E and PSM-F have been identified [14-18]. Additionally, many other alternatively spliced transcripts of *FOLH1* gene can be found among the ESTs (expressed sequence tags) at the NCBI database UniGene (http://www.ncbi.nlm.nih.gov/unigene), which indicates that the list of described splice variants is probably not complete.

The PSM' was the first identified and the most studied GCPII splice variant. PSM' lacks the nucleotides 114-379 at the 3' end of the first exon compared to the "wild-type" mRNA. On a protein level this deletion would led to the loss of intracellular as well as transmembrane region of GCPII thus yielding a protein which would start with methionine at position 58 (compared to the "wild type" protein) [17]. Indeed, a protein, which cleaved NAAG and started with alanine at position 60, was identified in the LNCaP cells and in the prostate carcinoma. This protein was named PSM' since it was considered to be a translational product of PSM' mRNA [19, 20].

However, the true origin of PSM' protein is probably more complex. GCPII protein was shown to be N-glycosylated and this post-translational modification was proven to be essential for its enzymatic activity [21, 22]. On the other hand, PSM' protein originating from PSM' mRNA would not contain a signal sequence which would guide the protein into the ER and Golgi apparatus, where N-glycosylation occurs. Moreover, it was recently shown that identified PSM' protein is N-glycosylated and is also produced by full-length GCPII transfectants [23]. These data suggest that PSM' protein probably does not originate from PSM' mRNA but is rather a product of a post-translational processing of a full-length GCPII protein.

1.3.2 Expression of mRNA in human tissues

All studies determining the expression profile of mRNA coding for GCPII showed a significantly increased mRNA level in the prostate compared to other tissues [24-28].

Furthermore, Chang *et al.* suggested that GCPII mRNA expression is induced in malignant non-prostatic tissues such as the bladder, lung, or pancreas [25]. However, a subsequent study by Pangalos *et al.* detected mRNA expression in variety of human tissues including brain, colon, heart, kidneys, lungs, ovary, pancreas, spleen, small intestine and testis [27]. These data suggest that the GCPII mRNA expression is widespread in human but it may be further induced by the malignant processes within the cell.

1.4 GCPII on protein level

GCPII (E.C. 3.4.17.21) is a type II transmembrane di-zinc metallopeptidase which, based on the sequence homology with the aminopeptidases from *Streptomyces griseus* and *Vibrio proteolyticus*, belongs to the MEROPS clan MH; subfamily M28B [29, 30]. It consists of short intracellular N-terminal part (AAs 1-18), one transmembrane helix (AAs 19-43) and large extracellular C-terminal part (AAs 44-750) [31]. GCPII contains 10 N-glycosylation motifs (Asn-X-Ser/Thr) within its primary sequence and these post-translational modifications were shown to be necessary for GCPII enzymatic activity [21, 22]. Properly modified GCPII molecule embodies a molecular weight of approximately 100 kDa while the protein without posttranslational modifications has a molecular weight of 84 kDa [26].

Additionally, the short intracellular portion of GCPII contains an internalization motif (MXXXL) which is responsible for its internalization via clathrin-coated pits [32].

1.4.1 GCPII overall 3D structure

Structural information about GCPII has been primarily gained from the X-ray crystallography experiments. The first X-ray structure of GCPII refined at 3.5 Å was published in 2005. It revealed overall homodimer fold of this protein and also a coordination sphere for two zinc ions, which is conserved throughout the whole clan of MH peptidases [33]. However, the detailed description of GCPII active site and its mechanism of substrate recognition were not known until 2006 when a series of high-resolution structures (refined at up to 2.0 Å) was published; it is worth mentioning that this study also pointed out some major misinterpretations in the original structure [31].

A homodimeric structure of GCPII extracellular part is shown in Figure 1, p. 4. The GCPII monomer can be divided into three distinct domains: protease-like domain (AAs 59-116 and 352-590), apical domain (AAs 117-351) and C-terminal domain (AAs 591-750).

Additionally, four inorganic ions (two Zn^{2+}, one Cl^- and one Ca^{2+}) and seven N-glycosylation sites have been identified within the crystal structure model of GCPII.
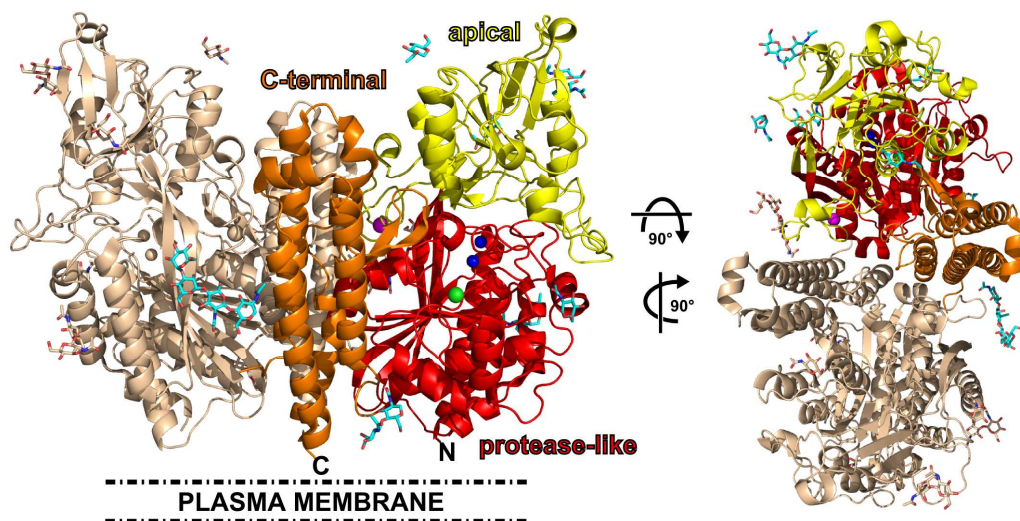
Figure 1: X-ray structure model of extracellular portion of GCPII.
One monomer is shown in wheat and the other is colored according to the domain organization; protease-like domain in red (AAs 57-116 and 352-590), apical domain in yellow (AAs 117-351) and C-terminal domain in orange (AAs 591-750). Carbon atoms of carbohydrate moieties of colored monomer are shown in cyan while in other monomer are shown in wheat. All carbohydrates are shown as stick and their oxygen atoms are shown in red and nitrogen atoms in blue. Protein backbone is shown in ribbon representation while zinc ions are depicted as blue, chloride ion as green and calcium ion as magenta spheres. N- and C-termini of the GCPII extracellular domain are labeled as **N** and **C**, respectively. The orientation of GCPII homodimer towards the cell is schematically depicted by the illustration of the plasma membrane.

A major breakthrough in the field came a year later, when a new crystallization conditions for GCPII, which led to the structures refined to as low as 1.65 Å, were identified [34]. Since then, the X-ray crystallography has become a method routinely applied for investigation of GCPII substrate specificity and enabled to perform several structure-activity relationship (SAR) studies which aimed to design potent and specific inhibitors of GCPII [35-43]. Currently, more than 40 different X-ray structures of GCPII have been deposited in RCSB Protein Data Bank.

1.4.2 Specific structural features of GCPII

The large series of X-ray structures led to the identification of many GCPII structural features. These features were shown to be responsible for a stabilization of the overall protein fold (e.g., the N-glycosylation at position Asn638 or the Ca^{2+} coordination sphere), for the substrate specificity (e.g., the arginine patch, the Cl^- coordination sphere, or the positioning of the entrance lid), and for the enzymatic activity (e.g., the Zn^{2+} coordination sphere together with catalytic acid/base Glu424). Majority of these structural features is illustrated and described in more detail in Figure 2, p. 5.
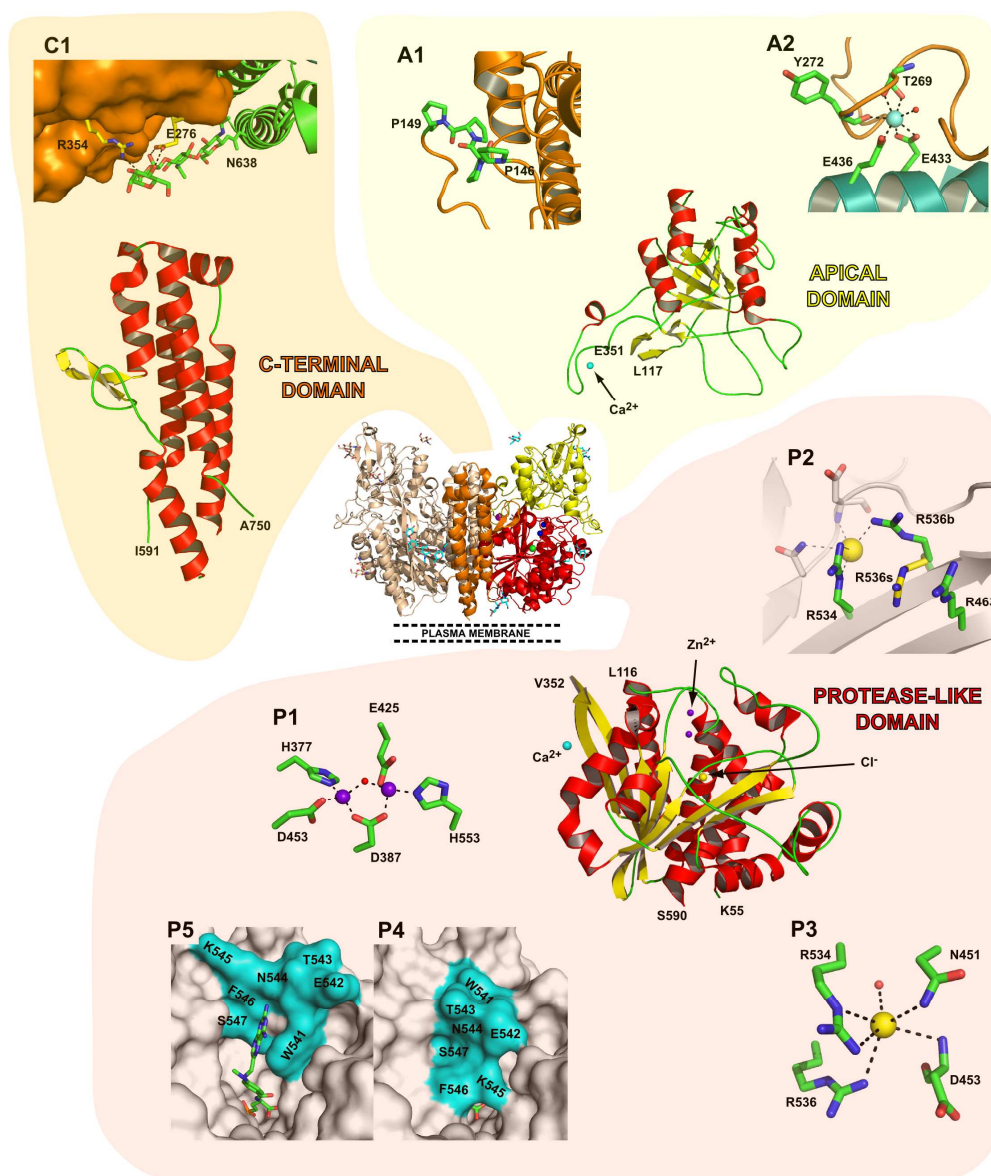
Figure 2: Selected structural features of human GCPII.

GCPII homodimer in the center of the figure is shown identically as in Figure 1. The ribbon representations of individual isolated domains are shown within shaded areas with α-helices, β-strands, and loops colored red, yellow, and green, respectively. **C1**, detailed view of protein-carbohydrate interactions in the GCPII structure. An oligosaccharide chain anchored at Asn638 side chain (green sticks) of the first monomer (green cartoon) interacts with the side chains of Glu276 and Arg354 (yellow sticks) of the second GCPII monomer (orange surface) and thus contributes to dimer formation. Hydrogen bonding interactions are shown as dashed lines. **A1**, solvent exposed type-II polyproline helix (Pro146–Pro149). **A2**, detailed architecture of the calcium-binding site. Residues from the apical (Tyr272 and Thr269) and the protease-like (Glu433 and Glu436) domains contribute to the Ca^{2+} (cyan sphere) coordination sphere. This motif is involved in GCPII dimerization by stabilizing the loop 272–279 at the dimerization interface. **P1**, coordination sphere of active site zinc ions (purple spheres). **P2**, flexibility of the arginine patch residues. Side chains of the arginine patch (Arg534, Arg536, and Arg463) are shown in stick representation, the chloride ion as a yellow sphere. While the side chain of Arg534 is virtually immobile, the Arg536 side chain can adopt two conformations depending on the occupancy of the S1 site – the binding conformation (R536b, green) and stacking conformation (R536s, yellow) with the S1 site empty or occupied, respectively. **P3**, coordination sphere of the chloride anion (yellow sphere). **P4, 5**, entrance lid (Trp541-Gly548) in the closed (**P4**) and open (**P5**) conformation. GCPII is shown in surface representation with the entrance lid colored cyan. Adopted from [44].

Additionally, a detailed reaction mechanism of NAAG hydrolysis by GCPII was described by the combination of computational and X-ray crystallography methods [43]. For more information, the reader is referred to a recently published review article which comprehensively summarizes and describes the current knowledge about GCPII structure and its reaction mechanism in more detail [44].

1.5 GCPII as an enzyme

1.5.1 GCPII substrates

As the name suggests, GCPII is a hydrolase which cleaves off C-terminal glutamate from its substrate. In a human body this enzymatic activity executes two different but important physiological functions. Firstly, GCPII is responsible for the cleavage of *N*-acetyl-L-aspartyl-L-glutamate (NAAG), the most abundant peptide neurotransmitter in human brain [45], yielding *N*-acetyl-L-aspartate and L-glutamate (see Figure 3) [1].

N-acetyl-L-aspartyl-L-glutamic acid   *N*-acetyl-L-aspartatic acid   L-glutamic acid
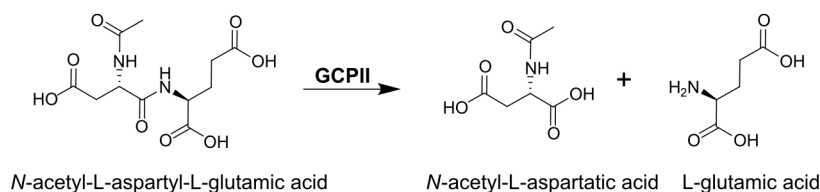
Figure 3: Cleavage of *N*-acetyl-L-aspartyl-L-glutamic acid (NAAG) by GCPII in the brain.

Secondly, GCPII enzymatic activity is crucial for the metabolism of dietary folates. People accept folate (known also as pteroyl-γ-L-glutamate or vitamin B9) in a polyglutamylated form. GCPII located in the brush border membrane of the small intestine is responsible for the consecutive cleavage of these glutamates (see Figure 4) and thus enables the absorption of the folates by epithelial cells [3, 4].

folylpoly$_{(n)}$-γ-L-glutamic acid   folylpoly$_{(n-1)}$-γ-L-glutamic acid   L-glutamic acid
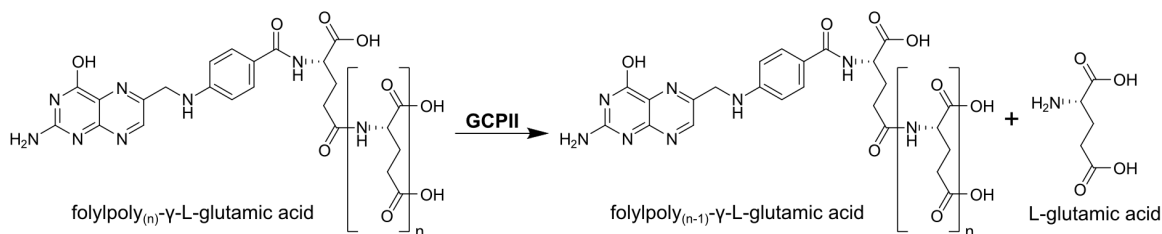
Figure 4: Cleavage of folylpoly-γ-L-glutamate by GCPII in the small intestine.
Generally, the polyglutamylated folates contain 5-7 glutamate residues (n=5-7).

Beside these two endogenous substrates, GCPII is able to process other peptidic substrates. Study by Barinka *et al.* showed that GCPII efficiently processes *N*-acetylated

dipeptides which contain acidic residues (Glu/Asp) in P1 position and either acidic residues (Glu/Asp) or methionine in P1' position (e.g., *N*-acetyl-L-glutamyl-L-glutamate or *N*-acetyl-L-aspartyl-L-methionine) [46].

1.5.2 GCPII inhibitors

As all other metallopeptidases, GCPII is inhibited by chelating agents (e.g., EDTA, EGTA), but these compounds are neither specific nor potent enough to enable their practical use. Additionally, the product analogues (e.g., quisqualic acid) and substrate analogues (e.g., β-NAAG) were shown to inhibit GCPII activity effectively [1, 47].

However, it took another 10 years until a first potent nanomolar inhibitor of GCPII 2-(phosphonomethyl)pentanedioic acid (2-PMPA) was prepared [48]. Generally, GCPII inhibitors often comprise a glutamate residue, which binds to a P1' site of GCPII, and a zinc binding group. Based on the different zinc binding groups, GCPII inhibitors can be divided into three different groups: (1) phosphonate-, phosphate-, and phosphoramidate-based inhibitors (e.g., 2-PMPA); (2) thiol-based inhibitors (e.g., 2-(3-mercapto-propyl)pentanedioic acid (2-MPPA) [49]); and (3) urea-based inhibitors (e.g., ZJ-43, DCIBzL, and ARM-P2 [39, 40, 50, 51]). The chemical formulae together with respective inhibition constants of each group representatives are shown in Figure 5, p. 8.

The inhibitor 2-PMPA was the first developed tight and specific GCPII inhibitor [48] and served as an inhibitor scaffold for many derivatives [52]. However, these inhibitors are highly polar and therefore not orally available which diminished their practical applicability. To reduce the polarity, the phosphonate group was replaced with thiol moiety which led to slightly decreased inhibitory potency, but made the whole molecule less polar and therefore orally available [49, 53]. Interestingly, even though 2-PMPA showed different inhibition potency of its two enantiomers, the corresponding thio analog 2-MPPA did not exhibit this phenomenon [54].

In the meantime, Kozikowski *et al.* developed quite simple and original approach which utilizes a urea group as a zinc binding group. They prepared series of highly potent, specific and also easily accessible compounds [55, 56]. Further optimization of the urea-based inhibitors led to the preparation of low-picomolar inhibitors DCIBzL and ARM-P2 [40, 51].
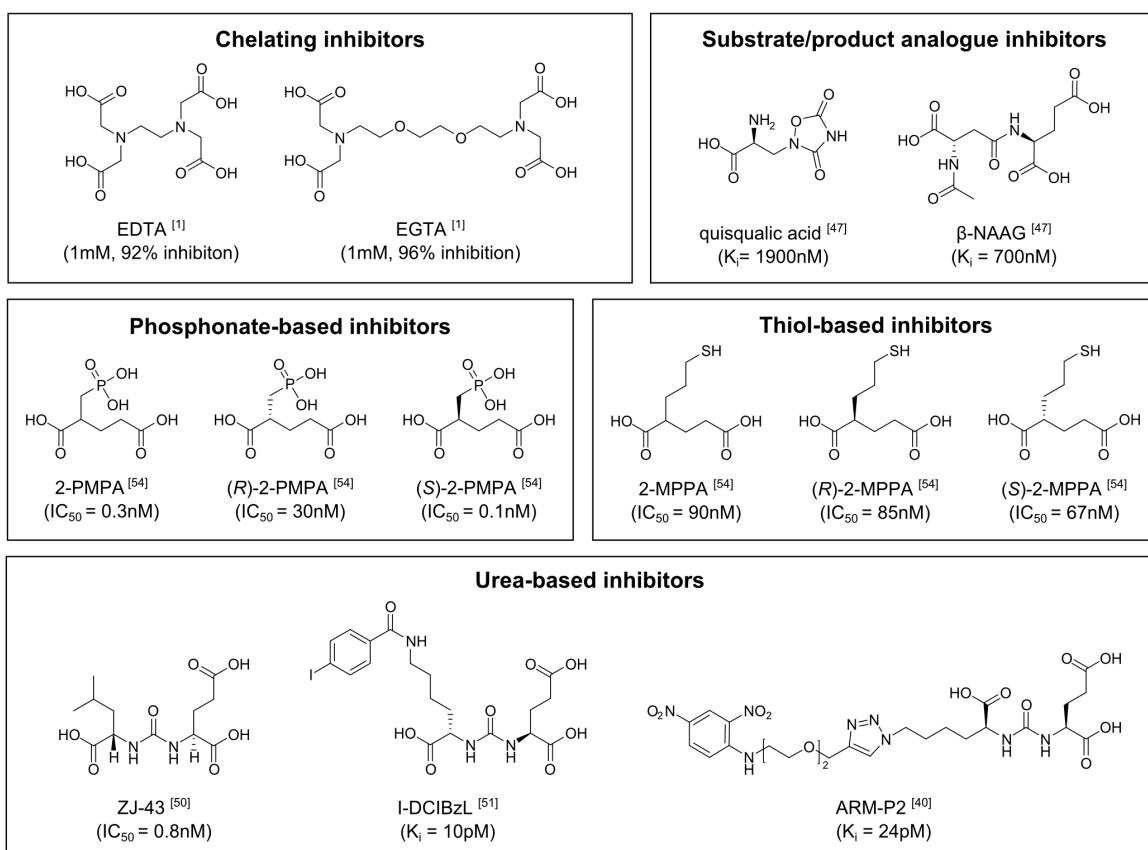
Figure 5: Chemical formulae and inhibition constants of selected GCPII inhibitors.
Inhibitors are divided based on their active moieties to 5 different groups. Inhibition constant of each inhibitor together with the citation source is stated bellow the name of inhibitor. EDTA - 2,2',2'',2'''-(ethane-1,2-diylbis(azanetriyl))tetraacetic acid; EGTA - 3,12-bis(carboxymethyl)-6,9-dioxa-3,12-diazatetra-decanedioic acid; 2-PMPA - 2-(phosphonomethyl)pentanedioic acid; 2-MPPA - 2-(3-mercapto-propyl)pentanedioic acid; β-NAAG - ((S)-3-acetamido-3-carboxy propanoyl) -L-glutamic acid; ZJ-43 - (((S)-1-carboxy-3-methylbutyl)carbamoyl)-L-glutamic acid; DCIBzL - (((S)-1-carboxy-5-(4-iodobenzamido)pentyl)carbamoyl)-L-glutamic acid; ARM-P2 - (((S)-1-carboxy-5-(4-((2-(2-((2,4-dinitrophenyl)amino)ethoxy)ethoxy)methyl)-1H-1,2,3-triazol-1-yl)pentyl)carbamoyl)-L-glutamic acid. Systematic names of the inhibitors were generated using ChemBioDraw Ultra software v13.0 (PerkinElmer).

As GCPII inhibitors find their application in many areas of clinical research, such as prostate cancer diagnostics and therapy or in the neuroprotective studies (see below), the urea-based scaffold is currently used preferentially for GCPII inhibitor design. A more complex and detailed description of the GCPII inhibitor field was recently reviewed by Ferraris *et al.* [57]. Additionally, a Braunschweig enzyme database (BRENDA) can also serve as a valuable source of data on GCPII enzymological profile [58].

1.6 GCPII expression in human body

GCPII protein expression in human healthy and malignant tissues has been intensively studied throughout the past two decades. Unfortunately, except for a high protein

expression in both benign and malignant prostate tissue, the data on GCPII expression in other human tissues are somewhat inconsistent (see Table 1, p. 10).

The explanation for such big discrepancy may lie in a variety of detection methods (western blotting (WB) [59], immunohistochemistry (IHC) [60-65], enzyme-linked immunosorbent assay (ELISA) [66]) and monoclonal antibodies (7E11-C5.3 [59, 61-66], J591 and J415 [63], PEQ226.5 [63, 66], PM2J004.5 [63], 24.4E6 [60], and YPSMA-1 [67]) used in these studies. Different methods have variable detection limits and their results also often rely on the experience of the researcher. Moreover, different mAbs recognize distinct epitopes (e.g., within intracellular or extracellular portion of GCPII) and may bind to its antigen in different forms (e.g., native or denatured form of GCPII). Unfortunately, these basic mAbs characteristics are often not even known or specified for majority of the commonly used mAbs and additionally many researchers do not provide sufficient information (e.g., concentration of used mAb) to enable reliable assessment and/or reproducibility of their experiments.

Nevertheless, the data from healthy tissue samples indicate that GCPII expression is not exclusive for the prostate, but can also be found in other tissues such as brain, small intestine, colon and kidney. In malignant tissues, the only clear consistency of the data relates to the strong GCPII expression in prostate carcinoma. On the other hand, considering histological localization, a majority of the studies demonstrated that GCPII is primarily expressed in tumor-associated neovasculature of various types of solid carcinomas [25, 63, 68-70].

1.7 GCPII role in human pathological conditions

1.7.1 GCPII role in neuropathies

GCPII role in neuropathological conditions is quite complex. Generally, GCPII inhibition leads to the increase of NAAG concentration in a neuronal synaptic cleft which has a neuroprotective effect in a model of glutamate-mediated excitotoxicity. The detailed description of this field is beyond the scope of this Introductory section. However, a whole issue of the Current Medicinal Chemistry (2012, vol.19, no.9) was recently published containing review articles exclusively related to this topic. In this chapter, only a basic description of the excitotoxicity mechanism and the role of NAAG in this process will be presented.

Table 1: Summary of reported GCPII expression in human healthy and malignant tissues.
" + " stands for detected protein expression. " - " stands for no expression detected. Empty spot indicates that the tissue was not analyzed in the study. [1]marks studies which used WB as a detection method. [2]marks studies which used IHC as a detection method. [3]marks studies which used ELISA as a detection method. mAbs used for individual studies were: J591 and J415 used in [63], PEQ226.5 used in [63, 66], 7E11-C5.3 (widely marked as 7E11) used in [59, 61-66], PM2J004.5 used in [63], 24.4E6 used in [60], and YPSMA-1 used in [67]. Adopted from [71].

Healthy tissue	Troyer et al. [59][1]	Kinoshita et al. [60][2]	Dumas et al. [61][2]	Gala et al. [62][2]	Chang et al. [63][2]	Lopes et al. [64][2]	Silver et al. [65][2]	Sokoloff et al. [66][3]	Mhawech-Fauceglia et al. [67][2]
adrenal glands		+			-	-	-		
bladder		+			-		-		+
brain	+	+			-	-	-		+
breast	-	+			+		-	+	-
colon	-	+			+	-	+		-
duodenum					+		+		
esophagus		+			-				-
heart									+
kidney - glomerulus					-	-	-		-
kidney - proximal tubule			+		+	+			
kidney - distal tubule					-	-			
liver	-	+			-	-	-		
lung	-	-			-	-			-
lymph node							-		-
ovary	-	+			-			+	-
pancreas					-		-		
peripheral ganglion							-		
prostate		+			+	+	+	+	+
salivary gland	+								-
skeletal muscle	-				+	+	-		
seminal fluid	+							+	
skin					-	-	-		-
small intestine	+	+				-		+	-
spleen						-			-
stomach		+			-	-	-		-
testis					-	-	-		+
thyroid gland					-	-	-		-
urine								+	
urothelium				+					+
Malignant tissue									
adrenal gland		+							-
bladder	-	+		+	-	-			+
breast	-	+			-	-		+	-
colon	-	+			-	-	-		+
connective tissue					-				
esophagus		+							+
gallbladder									+
kidney		+	+		-	-	-		+
liver	-								+
lung	-	+			-	-			
ovary		-							+
pancreas					-				
prostate	+	+			+	+	+		+
salivary gland									+
skin					-	-			+
small intestine		+							+
stomach		+							
testis		+			-				-
thyroid gland									+
urinary bladder									+

- 10 -

1.7.1.1 Model of glutamate-mediated excitotoxicity

L-glutamate is generally acknowledged as a main excitatory amino acid neurotransmitter in mammals with glutamate receptors expressed in majority of neurons and glial cells [72-74]. These glutamate receptors can be divided in two major classes: ionotropic glutamate receptors (iGluRs) and metabotropic glutamate receptors (mGluRs) [75, 76].

Based on the exogenous agents activating them, iGluRs are further subdivided to three groups: AMPA (α-amino-3-hydroxy-5-methyl-4-isoxasolepropionate), NMDA (*N*-methyl-D-aspartate), and kainate receptors (see Figure 6). Upon ligand binding, iGluRs become permeable for extracellular ions (mostly Na^+, but in case of NMDA also for Ca^{2+}) which causes membrane depolarization of a postsynaptic neuron [77].
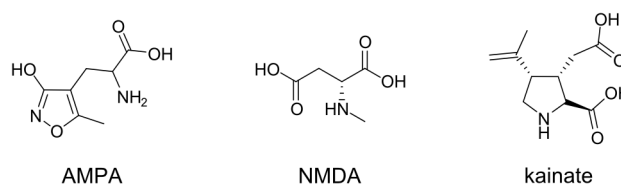
Figure 6: Structures of ionotropic glutamate receptor agonists.
AMPA - 2-amino-3-(3-hydroxy-5-methylisoxazol-4-yl)propanoic acid, NMDA - methyl-*D*-aspartic acid, kainate - (2*R*,3*S*,4*S*)-3-(carboxymethyl)-4-(prop-1-en-2-yl)pyrrolidine-2-carboxylic acid. Systematic names of the inhibitors were generated using ChemBioDraw Ultra software v13.0 (PerkinElmer).

Contrary to iGluRs, mGluRs do not facilitate straightforward influx of ions into the cell but are rather coupled with G-proteins and thus regulate the production of second messengers (e.g., cAMP). mGluRs are expressed in both presynaptic and postsynaptic neurons as well as in glial cells and can be divided into three subgroups I-III. Activation of mGluRs group I acts excitatory leading to the propagation of the neuronal signals, while activation of mGluRs group II and III leads to the attenuation of the signaling [78].

During signal transduction, the L-glutamate is released from presynaptic neuron, reaching as high as 1 mM concentration in a synaptic cleft for few milliseconds. Its rapid reuptake is secured by specific amino acid transporters in both neurons and astrocytes [79]. However, a prolonged exposition of the post-synaptic neurons to high L-glutamate concentration may lead to the overstimulation of the glutamate receptors. This causes a rapid influx of Ca^{2+} ion into the cells, mainly through the activation of NMDA receptors. Consequently, high Ca^{2+} concentration triggers processes leading to the death of the postsynaptic neuronal cell followed by additional release of glutamate which starts cascade effect of cell death. This phenomenon is called glutamate-mediated excitotoxicity [80-83].

Glutamate-mediated excitotoxicity has been shown to be involved in many neuropathological conditions such as amyotrophic lateral sclerosis (ALS), Alzheimer disease, diabetic neuropathy, inflammatory and neuropathic pain, ischemia, and traumatic brain injury [81, 84, 85].

1.7.1.2 Neuroprotective mechanism of GCPII inhibition

NAAG, the most abundant peptide neurotransmitter in mammals [45] and substrate of GCPII [1], plays pivotal role in an attenuation of a postsynaptic neuron excitation and thus acts as a protective agent against the excitotoxicity.

There are two distinct mechanisms of action of NAAG which both participate in a protection of postsynaptic neurons. Firstly, NAAG was shown to specifically activate group II of metabotropic glutamate receptors, mainly $mGluR_3$ [86, 87]. The $mGluR_3$ are expressed in astrocytes, where their activation leads to the secretion of TGF-β (tumor growth factor β) which has a neuroprotective effect on the neurons [88-90]. Additionally, the $mGluR_3$ are expressed in presynaptic neurons where they inhibit additional secretion of glutamate [91, 92].

Second mechanism of action lies in the ability of NAAG to bind specifically to NMDA receptors, but not to AMPA and kainate receptors [93]. Even though this mechanism may seem counter-intuitive, NAAG demonstrated much less activation potency than glutamate upon binding to NMDA receptor [94, 95]. Therefore, NAAG acts as a partial antagonist of NMDA receptors competing with excitatory neurotransmitter glutamate. However, the ability of NAAG to bind NMDA receptors is not ubiquitous and probably depends on the composition of the NMDA receptor subunits since there are studies reporting this binding [94-98] and also studies which do not observe NAAG binding to NMDA receptor [99, 100]. Therefore, this type of neuroprotective role of NAAG may probably be restricted to defined regions in the nervous system. Nevertheless, neuroprotective role of the NAAG in nervous system is undeniable.

GCPII is responsible for NAAG inactivation in a synaptic cleft by its cleavage to *N*-acetyl-L-aspartate and L-glutamate. The inhibition of GCPII activity, leading to subsequent increase of NAAG concentration in synaptic cleft, was shown to be neuroprotective in several models of neurodegenerative conditions. Therefore, GCPII is being considered and evaluated as a potential therapeutic target against various neuropathies [89, 90, 101-108]. Zhong *et al.* recently summarized a current state of the art in this field [85].

A simplified model of the proposed NAAG and GCPII role in glutamatergic synapse is illustrated in Figure 7.
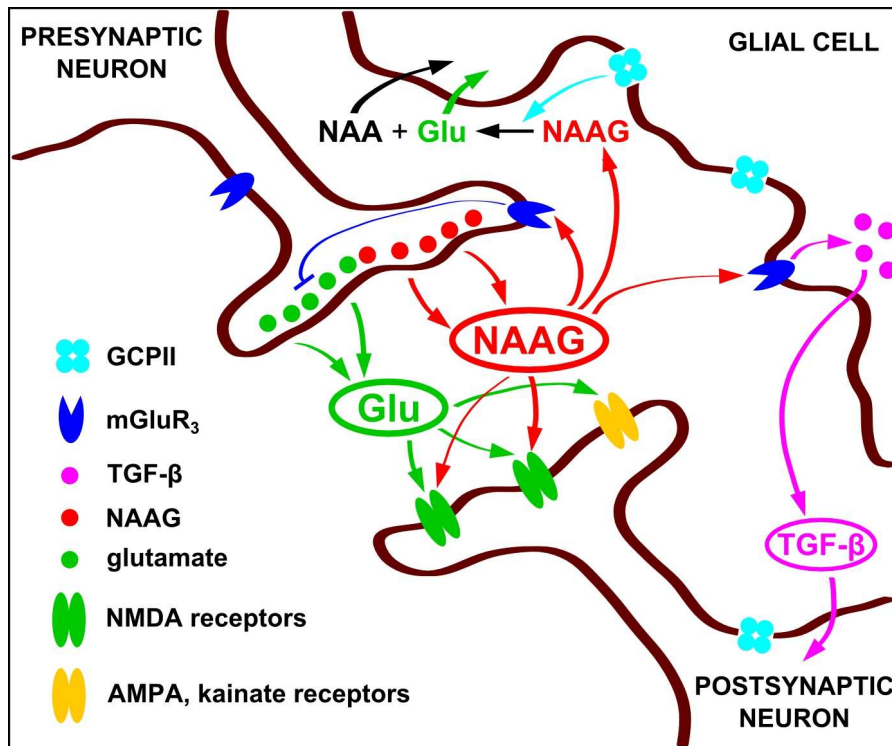
Figure 7: A model of the proposed NAAG role in a glutamatergic synapse.
When released from the presynaptic neuron, NAAG can activate $mGluR_3$ on both the presynaptic neuron and the glial cells. The activation of presynaptic $mGluR_3$ decreases the release of the primary neurotransmitter glutamate, while the activation of glial $mGluR_3$ leads to the secretion of neuroprotective TGF-β, which is absorbed by postsynaptic neuron and acts there as a neuroprotective agent. Simultaneously, NAAG is also competing with glutamate for the binding to NMDA receptors in some types of neuronal synapses. The action of NAAG is terminated by GCPII which hydrolyses NAAG to *N*-acetyl-aspartate (NAA) and glutamate (Glu) which are then absorbed by glial cells.

1.7.2 GCPII role in prostate cancer and angiogenesis

High level of GCPII expression in prostate carcinoma (PCa) indicates its potentially important role in the development of this pathological condition. However, unlike its role in neuropathies, the GCPII mechanism of action in the PCa is not known.

One hypothesis suggested that GCPII may serve as a folate transporter [109, 110]. Other, based on the close sequence and structural homology with transferrin receptor [31, 111, 112] and an ability of GCPII to internalize upon ligand binding [32, 69], hypothesized that GCPII may serve as a receptor for yet unknown ligand. However, since nearly 100 % of prostate cancer metastases express GCPII, it seems likely that the protein contributes to a successful transport and colonization of the cells at distant body sites [113, 114].

Unfortunately, not enough evidence has been gathered yet for any theory to be widely accepted by the scientific community.

Additionally, GCPII was also detected in endothelial cells of newly formed blood vessels associated with most of the solid tumors as well as with normal proliferative tissues such as endometrium and wounds [63, 68, 115-117]. In analogy to the role in prostate, GCPII function in the process of angiogenesis (i.e., formation of new blood vessels) still remains to be elucidated. One hypothesis speculated that GCPII increases the invasiveness of the endothelial cells by feedback loop activation of p21-associated kinase (PAK) [118], while the other suggested that GCPII mechanism of action resides in the absorption of extracellular folate into the cell. Folate is subsequently converted to 5-methyl-tetrahydrofolate (THF) that reduces and recycles tetrahydrobiopterin (BH4). Then BH4, as a cofactor of endothelial isoform of nitric oxide synthase (eNOS), sustains the production of nitric oxide, a potent stimulator of angiogenesis [119-121]. Unfortunately, none of these hypotheses have been reliably proven yet.

1.8 GCPII as a diagnostic and therapeutic target of prostate carcinoma

Cancerous diseases are a major public health problem. Statistics for the USA show that more than 1 600 000 new cases and over 580 000 deaths are projected to occur in the USA in 2014. Among males, the prostate carcinoma (PCa) is the most commonly diagnosed type of cancer and the leading cause of death with the expected number of diagnoses and deaths exceeding 233 000 and 30 000, respectively [122]. As the numbers suggest, the need for effective diagnosis and treatment of PCa is immense.

1.8.1 GCPII in prostate cancer imaging

Imaging can be defined as a set of techniques, such as positron emission tomography (PET), single-photon emission computed tomography (SPECT), nuclear magnetic resonance (NMR), or computed tomography (CT), which enable non-invasive detection and measurement of cellular processes in living beings. Imaging has become routinely used in cancer research, clinical trials as well as medical practice. In a cancer management, the molecular imaging enables detection of tumor metastatic malignancies, determination of tumor stage, and also therapeutic monitoring, which is particularly important early after the start of the therapy [123].

In case of the PCa, the primary goal of imaging techniques is detection of potential metastases and also early identification of possible recurrence after initial primary therapy

(most often prostatectomy). GCPII, in this field almost exclusively known as PSMA, represents a promising molecular target for the PCa imaging. The agents targeting GCPII can be divided into two distinct groups: (1) monoclonal antibodies and (2) low-molecular-weight molecules [121, 124, 125].

1.8.1.1 Monoclonal antibodies as imaging agents

Monoclonal antibodies (mAbs) are widely used in basic research, but they can be also utilized in a diagnosis and therapy of PCa. Many different mAbs against GCPII have been prepared since its identification as a prostate cancer marker.

The first mAbs against GCPII, 7E11-C5.3, was prepared in 1987 [1]. Its radio-conjugate with ^{111}In, sold under the commercial name ProstaScint™, currently represents the only imaging agent which was approved by U.S. Food and Drug Administration (FDA) for human imaging [126]. The ProstaScint™ is reported to stage primary PCa with 68 % accuracy, 62 % sensitivity and 72 % specificity [127], which shows that the agents is useful but not optimal. The sub-optimal function of ProstaScint™ may be caused by the fact that it recognizes intracellular portion of GCPII [128] and thus is probably able to visualize only necrotic cells of PCa which have disrupted cell membrane. This drawback led to the development of second-generation mAbs which target extracellular portion of GCPII [129].

The mAb J591, developed in the laboratory of Dr. N. Bander at the Comell University, is by far the most intensively studied second-generation mAb [63]. To facilitate its use in clinical practice, the humanized form of J591 was prepared in 2003 [130]. Subsequently, several radio-conjugates of J591 with ^{64}Cu, ^{111}In, ^{177}Lu, [89]Zr and ^{99m}Tc were prepared and tested [131-135]. In majority of the studies the J591 radio-conjugates showed specific targeting of GCPII positive cells. Therefore, intensive research involving ^{99m}Tc-J591 [136], [89]Zr-J591 [137], and ^{177}Lu-J591 [138, 139], which can serve conveniently as both imaging and therapeutic agent, is currently undergoing to enable application of these imaging agents in clinical practice [137]. Additionally, ^{111}In-J591 has already entered phase I of the clinical trials (in combination with ^{90}Y-J591 which served as therapeutic agent) [140].

The mAb 3/A12 represents one of the several mAbs against GCPII developed in the laboratory of Dr. U. Elsässer-Beile [141]. The ^{64}Cu radio-conjugate of 3/A12 showed highly specific uptake to GCPII-positive tumors in animal models suggesting its potential to become useful diagnostic agent [142, 143].

1.8.1.2 Low-molecular-weight molecules as imaging agents

One of the drawbacks of the mAb-based imaging agents is their delayed clearance from the non-targeted tissues resulting in a span of several days between agent injection and imaging [121]. This issue may be overcome by the usage of small molecules [144]. Since GCPII is an enzyme, its specific and potent inhibitors (see section 1.5.2), can be used as the scaffolds for the design of specific low-molecular-weight imaging agents. Chemical formulae of further discussed imaging agents are depicted in Figure 8.

As suggested earlier, the urea-based inhibitors have been preferentially utilized as a scaffold for GCPII specific low-molecular-weight imaging agents. The first imaging agents were derived from tyrosine-glutamate urea (conjugated with ^{125}I; compound **1**) [145] and cystein-glutamate urea (conjugated with ^{18}F; compound **2**) [146]. Both these compounds showed high affinity towards GCPII, selective binding to GCPII-positive cells and specific uptake in GCPII-positive xenografts. Afterwards, a lysine-glutamate urea scaffold was utilized to prepare ^{123}I radio-conjugate (compound **3**). In clinical SPECT imaging study, this compound was able to detect metastatic prostate cancer lesions in soft tissues [147].

To enable the use of heavy metal radionuclides such as ^{99m}Tc, bulky radiometal chelate group was attached to the lysine-glutamate urea scaffold (compound **4**) yielding imaging agent that demonstrated specific uptake in GCPII-positive xenografts [148]. Last but not least, a ^{99m}Tc-labeled agent was prepared from glutamine-glutamate urea scaffold (compound **5**) which also showed specific accumulation in GCPII-positive xenograft models [149].
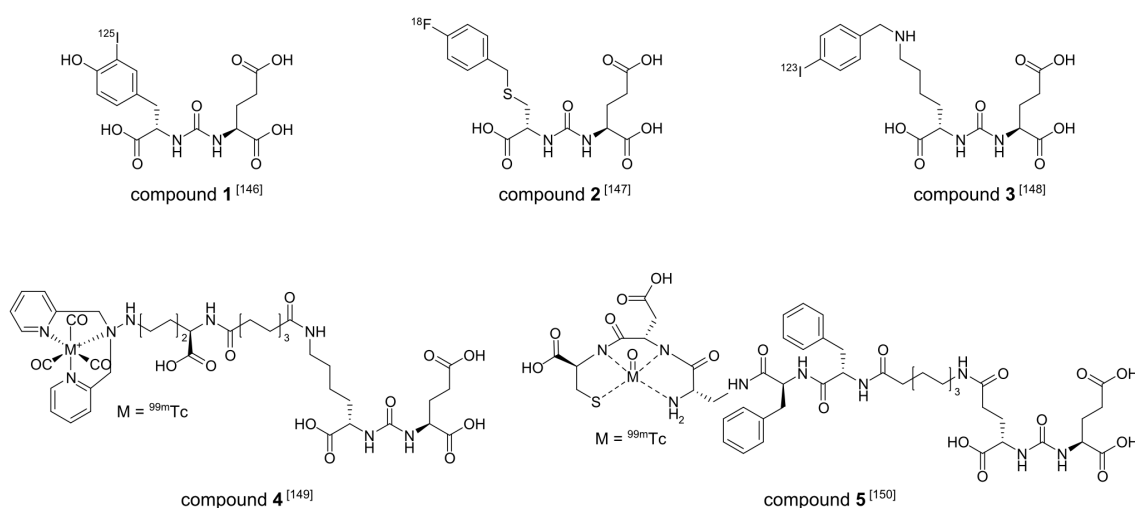

Figure 8: Examples of structures of imaging agents based on the specific GCPII inhibitors.
The citation of the corresponding literature source is stated for each compound.

The abovementioned GCPII imaging agents do not represent all prepared compound so far. For additional information, the reader is referred to a recently published review which summarizes the field more thoroughly [121].

1.8.2 GCPII in the targeted therapy of prostate cancer

Majority of carcinomas are still treated by the whole body exposition to various cytotoxic agents which might bring serious side-effects such as nausea, hair and weight loss, compromised immunity and infertility to the patients. Specific targeted delivery of the therapeutic agents represents an attractive approach to diminish these side-effects. Unfortunately, even though the idea of targeted therapy has been actively investigated by scientific community for several decades, it has started to be used in clinical practice just recently [150, 151]. Similarly to PCa diagnostics, GCPII is also intensively studied as a target for PCa targeted therapy. Both mAbs and specific small molecule conjugates with cytotoxic agents or radionuclides have been prepared and their therapeutic application tested in the past decades [152, 153].

1.8.2.1 Monoclonal antibodies as therapeutic agents

Second-generation mAb conjugates are mostly investigated as potential therapeutic agents. Understandably, mAbs used in diagnostic (see section 1.8.1.1) are also heavily utilized in therapy together with one additional mAb called PSMA-ADC (ADC stands for antibody-drug conjugate) [154]. PSMA-ADC is fully humanized mAb conjugated with monomethylauristatin E, a potent inhibitor of tubulin dimerization. This conjugate showed potent *in vivo* activity against GCPII-positive xenografts [155] and is now tested in phase I clinical trials [156].

Antibody J591 has been widely investigated mainly for its potential use in radioimmunotherapy. It was conjugated with α-emitting radioisotope ^{215}Bi [157-160] and with β-emitters ^{131}I, ^{90}Y and ^{177}Lu [133, 134, 161-163]. All these conjugates specifically target GCPII-positive cells *in vitro*, PCa *in vivo* [157, 159, 162] and show no side-effects [158]. A ^{177}Lu-J591 conjugate is currently in the final stage of phase II clinical trials and registration for phase III trial is planned [139]. J591 conjugation with immunotoxins is not so profoundly studied even though the conjugate with maytansine derivative DM1, a microtubule depolymerizing compound, was shown to specifically target GCPII-positive xenografts and inhibit its growth [164].

Unlike J591, mAbs from Dr. U. Elsässer-Beile laboratory have been predominantly conjugated with immunotoxins. Single-chain variable fragment (scFv) antibody A5 was conjugated with truncated form of *Pseudomonas* exotoxin (PE40) yielding A5-PE40. This construct demonstrated specific binding and cytotoxic effect against GCPII-positive tissue culture and mouse xenografts [165, 166]. A comparable potency was also achieved by using construct which consisted of different scFv (D7) and the same exotoxin (PE40) [167]. Both these constructs are now aiming to the clinical trials.

A different approach of therapy, utilizing human own immune system, was also investigated by preparation of diabody combining scFv A5 and scFv against CD3, a protein expressed in T-cells. Testing on the cell cultures showed ability of this conjugate to activate immune response of the T-cells [168, 169].

1.8.2.2 Low-molecular-weight molecules as imaging agents

Direct radio-labeling of small molecules is not frequently used in GCPII targeted therapy. One representative may be the inhibitor [^{131}I]-MIP-1375 (^{131}I analogue of compound **3**, Figure 8, p. 16) which was able to inhibit the growth of GCPII-positive cell cultures and xenografts [170].

Besides the specific GCPII inhibitors, the aptamers, a 8-15 kDa oligonucleotide or protein molecules which are selected for specific binding to targeted molecule through affinity maturation [171], are also investigated for their potential usage in targeted therapy [172]. Short hairpin RNA (shRNA) aptamer A10 specific against GCPII was developed [173] and its conjugate with small interfering RNA (siRNA) demonstrated GCPII-positive tumor regression in mouse xenografts [174, 175]. Additionally, A10 aptamer was also used for preparation of aptamer-nanoparticle conjugate which was loaded with various cytotoxic compounds. Such nanoparticles then demonstrated growth inhibition of GCPII-positive cells *in vitro* and *in vivo* [176-180]. Even though the preliminary results of aptamer conjugates are encouraging, additional research needs to be done before its potential application in the clinical practice will be feasible.

1.9 GCPII homologs

1.9.1 GCPII orthologs

GCPII orthologs (i.e., proteins derived from the common ancestral gene and separated by a speciation event) can be found throughout the whole eukaryotic domain [111]. For

successful development of diagnostic and therapeutic agents targeting GCPII, an animal model testing is an essential methodology. Therefore, reliable data on GCPII activity, inhibition profile and tissue expression in these animal models are crucial for their efficient utilization.

Given the frequently used animal models in drug-development testing, mouse, rat, pig and canine GCPII are the most extensively investigated GCPII orthologs. Since all those orthologs share more than 90 % sequence similarity to human GCPII, it is not surprising that all were found to be good models of human GCPII in enzymological studies [1, 7, 14, 181-183]. On the other hand, the GCPII expression profiles of these orthologs differ considerably in prostate and small intestine compared to human. Most importantly, no expression of GCPII was detected in mouse, rat and pig prostate [70, 181, 184]. Interestingly, GCPII expression in canine prostate was firstly not detected [184], but subsequent studies showed GCPII expression on both mRNA and protein level [185, 186] leaving this issue controversial. In small intestine, GCPII expression was detected in pig, but not in mouse and rats [70, 181]. In other tissues, the mouse, rat and pig orthologs showed similar tissue distribution as human GCPII being expressed primarily in brain, kidney and testes [70, 181].

To sum up, the data suggest that common animal models can be used for GCPII-based diagnostic and therapeutic testing, but there are some caveats, mainly considering GCPII protein tissue distribution, which needs to be taken into account. Due to similar enzymatic activity of these orthologs, the agents based on the GCPII-specific inhibitors can be used in the animal models without restriction, while in the case of the agents based on GCPII-specific mAbs, differences in primary and tertiary structures among the orthologs need to be accounted for. Unfortunately, the proper characterization of these mAbs binding specificity and their potential cross-reactivity towards GCPII orthologs has not been carried out yet.

1.9.2 Paralogs of human GCPII

Human GCPII has several very close paralogs (i.e., proteins derived from a gene which was created by a duplication event of an ancestral gene within the genome). Unfortunately, these proteins, due to the sometimes very similar enzymatic properties, have been designated based on the one of the several GCPII historic names, which makes the orientation in the literature highly complicated. The various names used for GCPII and its closest paralogs prostate specific membrane antigen-like (PSMAL), glutamate

carboxypeptidase III (GCPIII), and *N*-acetylated α-linked acidic dipeptidase-like (NAALADase L) proteins are summarized in Table 2. For clarity, the table also contains references to their mRNA and protein sequences and basic protein characteristics.

Table 2: List of human GCPII paralogs and their basic nomenclature.
The most commonly used names for GCPII and its closest human paralogs are highlighted while the other names found in literature are listed bellow. Corresponding mRNA and protein sequences can be accessed via ENTREZ code at http://www.ncbi.nlm.nih.gov/gene or http://www.ncbi.nlm.nih.gov/protein, respectively. Additionally, the number of amino acids of each protein and protein identities towards human GCPII are also listed. Adopted from [187].

Protein name (abbreviation)	Gene name / localization	ENTREZ code for mRNA	ENTREZ code for protein	identity	AAs
Glutamate **C**arboxy**p**eptidase II (GCPII or GCP2) **P**rostate **S**pecific **M**embrane **A**ntigen (PSMA or PSM) *N*-acetylated α-linked **A**cidic **D**ipeptidase (NAALADase) **Fo**lylpoly-γ-glutamate **C**arboxy**p**eptidase (FGCP) **Fol**ate **H**ydrolase (FOLH)	*FOLH1* 11p11.2	NM_004476.1	NP_004467.1	100 %	750
Prostate **S**pecific **M**embrane **A**ntigen-**l**ike (PSMAL)	*FOLH1B* 11q14.3	NM_153696.2	NP_710163.1	98 %*	442
Glutamate **C**arboxy**p**eptidase III (GCPIII or GCP3) β-**C**itrylglutamate **H**ydrolase (BCG hydrolase) *N*-acetylated α-linked **A**cidic **D**ipeptidase II (NAALADase II)	*NAALAD2* 11q14.3-q21	NM_005467.3	NP_005458.1	68 %	740
N-a**c**etylated α-linked **A**cidic **D**ipeptidase-**l**ike (NAALADase L) **100**kDa **I**leal Brush Border Membrane Protein (I100)	*NAALADL1* 11q12	NM_005468.2	NP_005459.2	37 %	740

* Percentage of protein identity is calculated regarding to the whole sequence of PSMAL and corresponding part of GCPII.

1.9.2.1 Prostate-specific membrane antigen-like (PSMAL)

Gene *FOLH1B*, which is localized at the chromosome 11 arm q11.4 and codes for PSMAL, was initially thought of as a *FOLH1* pseudogene [10]. However, the subsequent investigation indicated that the identified DNA region is actually the evolutionary closest GCPII paralog found only in primates [111].

The genomic identity of *FOLH1B* and *FOLH1* is 98 %, but *FOLH1B* lacks more than 1 kb region which corresponds to the end of a promoter, first exon and part of the first intron of *FOLH1* gene [188]. Therefore, putative protein construct from this gene, PSMAL, would be substantially shortened (442 AAs) compared to GCPII (750 AAs). Even though PSMAL shares more than 98 % sequence identity with GCPII, due to its N-terminal truncation and architecture of GCPII active site, where all three protein domains contribute to the proper folding of the active site, the PSMAL protein is likely to be inactive [189]. mRNA coding for PSMAL was detected in liver and kidney [188], but no data are available on the PSMAL protein expression.

1.9.2.2 Glutamate carboxypeptidase III (GCPIII)

With 68 % primary sequence identity, GCPIII represents the closest enzymatically active homolog of GCPII coded by *NAALAD2* gene localized at chromosome 11 arm q14.3-q21. mRNA coding for GCPIII was found well-spread in human tissues such as brain, colon, heart, ovary, spleen, prostate and testis, but generally showed lower expression level compared to GCPII [27].

No data on GCPIII protein expression are available. The likely reason for that is the fact that a specific mAb, which would recognize GCPIII but not GCPII, has not been prepared yet. Interestingly, this issue has not been taken into account in almost any studies mapping GCPII protein expression profile. With regard to very high primary sequence identity of GCPII and GCPIII, the chance of cross-reactivity of some mAbs recognizing mainly denatured GCPII is substantial. Unfortunately, currently used mAbs against GCPII are not characterized enough with respect to their potential cross-reactivity with GCPIII.

Bzdega *et al.* demonstrated that mouse GCPIII cleaves NAAG with similar efficiency as mouse GCPII [190]. Subsequent comparative analysis of human GCPII and GCPIII revealed different pH and salt dependency on the enzymatic activity for these enzymes, which makes their direct comparison quite difficult [191].

Interestingly, GCPIII was recently shown to process β-citryl-L-glutamate (BCG), a compound structurally similar to NAAG (see Figure 9) [192]. BCG is a pseudopeptide found in rat testis and prenatal as well as perinatal CNS [193-195]. Its role in these tissues is still unknown. Interestingly, GCPIII cleavage specificity was shown to be metal dependent. In the presence of Zn^{2+}, GCPIII cleaved preferentially NAAG, whereas in the presence of Ca^{2+}, GCPIII cleaved preferentially BCG. In the presence of Mn^{2+}, GCPIII processed both substrates with a similar efficiency. Surprisingly, GCPII did not process BCG at all [192].
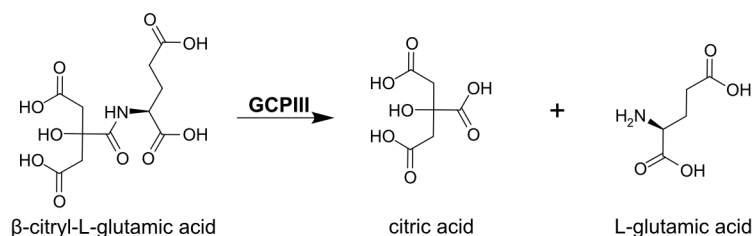

Figure 9: Hydrolysis of β-citryl-L-glutamic acid (BCG) by GCPIII.

X-ray structure of GCPIII was recently solved [196]. The overall GCPIII structure is highly similar to that of GCPII, but some interesting differences have been identified. The

most important one involved the coordination of zinc ions in the GCPIII active site. Compared to GCPII, zinc ions in GCPIII displays much lower occupancies (0.80-0.95 for catalytic Zn1 and 0.45-0.80 for co-catalytic Zn2) [196]. This observation suggests that GCPIII is able to create heterometallic clusters, replacing zinc ion with different metal ion, which supports the enzymological data determined for BCG and NAAG hydrolysis.

To date, no selective inhibitor of GCPII/GCPIII has been identified. However, knowledge of 3D structure and identification of GCPIII specific substrate may hopefully facilitate the development of such inhibitor, which would be essential for a proper dissection of GCPII and GCPIII physiological roles.

1.9.2.3 *N*-acetylated α-linked acidic dipeptidase-like (NAALADase L)

NAALADase L represents a more distant paralog of GCPII with just 37 % protein identity. It is coded by *NAALADL1* gene which is located at chromosome 11 arm q12 [27].

NAALADase L, approximately 100 kDa large protein, was identified in 1997 by its isolation from rat ileum and based on its molecular weight named I100 [197]. Subsequently, a large comparative study by Pangalos *et al.* revealed its close homology to GCPII and GCPIII and the protein was re-named to NAALADase L, because at that time the researchers worked with "NAALADase" instead of "GCPII" [27]. Since this was actually the last publication investigating NAALADase L, the name still prevailed.

mRNA coding for NAALADase L was shown to be expressed in several human tissues such as heart, colon, ovary, blood, prostate, small intestine, spleen and testis and additionally was shown to undergo heavy alternative splicing [27]. To date, no data on NAALADase L protein expression in human tissues have been published.

Both abovementioned studies detected DPP-IV activity of NAALADase L, but none of these studies used purified recombinant protein [27, 197]. This may be quite crucial since DPP-IV activity is highly promiscuous [198] and therefore false positive results may be easily obtained; as was probably the case for GCPII and GCPIII, which were both shown to possess DPP-IV activity by Pangalos *et al.* and subsequently disproved by the experiments with pure recombinant protein [27, 46, 191]. Finally, unlike GCPII and GCPIII, NAALADase L was shown to be unable to cleave NAAG [27].

Undoubtedly, additional studies characterizing NAALADase L will be necessary for the determination of its physiological role which is currently unknown.

Chapter 2: Results

2.1 Research aims

The research aims of this thesis are as follows:

- To develop and establish the affinity-tag based purification protocol for extracellular portion of recombinant human GCPII (rhGCPII) heterologously expressed in *Drosophila* S2 Schneider cells which would be also applicable for topologically identical proteins.

- To perform thorough comparative analysis of all available mAbs recognizing human GCPII. To quantitatively characterize their binding, to investigate their potential cross-reactivity with close GCPII homologs, and to compare their efficacies on the standard antibody-based molecular biology methods.

- To characterize human NAALADase L protein in terms of its 3D structure, its enzymatic activity, and its expression on mRNA and protein levels in order to elucidate its physiological function.

2.2 Publications

Publications included in the dissertation thesis

I. Tykvart, J., Sacha, P., Barinka, C., Knedlik, T., Starkova, J., Lubkowski, J., and Konvalinka, J. (2012) **Efficient and versatile one-step affinity purification of in vivo biotinylated proteins: expression, characterization and structure analysis of recombinant human glutamate carboxypeptidase II**, *Protein Expr Purif 82*, 106-115.

II. Tykvart, J., Navratil, V., Sedlak, F., Corey, E., Colombatti, M., Fracasso, G., Koukolik, F., Barinka, C., Sacha, P., and Konvalinka, J. (2014) **Comparative analysis of monoclonal antibodies against prostate-specific membrane antigen (PSMA)**, *Prostate 74(16)*, 1674-1690.

III. Tykvart, J., Barinka, C., Svoboda, M., Navratil, V., Soucek R., Hubalek M., Hradilek, M., Sacha, P., Lubkowski, J., and Konvalinka, J. (2015) **Structural and biochemical characterization of a novel aminopeptidase from human intestine**, *J Biol Chem,* Epub 2015/03/11, doi: 10.1074/jbc.M114.628149.

Publications not included in the dissertation thesis

Tykvart, J., Schimer, J., Barinkova, J., Pachl, P., Postova-Slavetinska, L., Majer, P., Konvalinka, J., and Sacha, P. (2014) **Rational design of urea-based glutamate carboxypeptidase II (GCPII) inhibitors as versatile tools for specific drug targeting and delivery,** *Bioorgan Med Chem 22*, 4099-4108.

Mlcochova, P., Barinka, C., Tykvart, J., Sacha, P., and Konvalinka, J. (2009) **Prostate-specific membrane antigen and its truncated form PSM'**, *Prostate 69*, 471-479.

Hlouchova, K., Navratil, V., Tykvart, J., Sacha, P., and Konvalinka, J. (2012) **GCPII variants, paralogs and orthologs,** *Curr Med Chem 19*, 1316-1322.

2.2.1 Paper I: Efficient and versatile one-step affinity purification of GCPII

Motivation of the study

Since GCPII requires N-glycosylation for its proper enzymatic activity [21, 22], the eukaryotic systems have to be used for its preparation. One option is to purify GCPII from its natural sources (e.g., brain tissue or LNCaP cells [19, 199, 200]). Unfortunately, even though this approach yields full-length GCPII with endogenous post-translational modifications, it provides low yields and is rather expensive.

The other possibility is to use a eukaryotic heterologous expression system, such as insect cells, designed for a large-scale protein expression. A baculoviral expression system combined with affinity chromatography can be used to express and purify recombinant GCPII with N-terminal His-tag [33, 201]. However, utilization of His-tag for GCPII, which is a metallopeptidase, is not optimal and may influence the protein enzymatic activity.

A "tag-free" stable cell line expression system using *Drosophila melanogaster* Schneider S2 cells was established by Barinka *et al.* in our laboratory in 2002 [46]. This system is rather cost-effective providing GCPII in high yields; tens of milligrams per liter of culture media. Even though this set-up produces just extracellular portion of GCPII (rhGCPII) the subsequent analysis showed that protein is properly folded and enzymatically active. Furthermore, the omission of transmembrane domain enabled much easier work with the protein. The down-sides of this purification set-up were its complexity, four purification steps, and its non-versatility towards other enzymes highly homologous to GCPII, such as GCPIII or NAALADase L.

Therefore, we set out to establish new expression system for GCPII which would be less laborious, more versatile and additionally enables specific modification of a purified protein.

Summary

In this study, we present a new large-scale expression system for extracellular portion of GCPII utilizing Avi-tag as an affinity anchor and *Drosophila melanogaster* Schneider S2 cells as host cells. The prepared protein construct as well as purification analysis by SDS-PAGE are show in Figure 10, p.26.

The protein construct (Avi-GCPII) comprises the Avi-tag sequence [202], TEV cleavage site and extracellular portion of human GCPII (rhGCPII). The Avi-GCPII is endogenously biotinylated by *E. coli* biotin ligase (*BirA*) on the lysine residue of the Avi-

tag during its expression; S2 cells were stably transfected with *BirA* prior Avi-GCPII production. We prepared three different S2 stable cell lines with *BirA* localized in the cytoplasm, in the endoplasmic reticulum (ER) or secreted outside the cell. We investigated these stable transfectants and found out that *BirA* localization within ER leads to the highest biotinylation efficacy of Avi-GCPII and used these cells for large-scale expression.

Subsequently, we used the site-specific biotinylation of Avi-GCPII for one-step affinity purification via commercially available Streptavidin Mutein Matrix (Roche) yielding highly homogenous protein in good yields, 6 mg per liter of culture media.
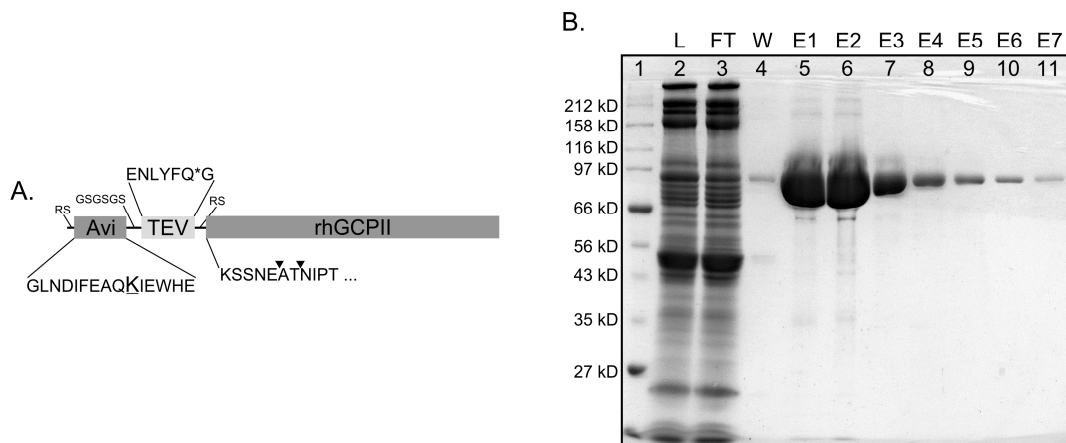
Figure 10: Schematic representation of Avi-GCPII and analysis of its purification.
Panel A: Schematic representation of Avi-GCPII with detailed primary sequence; Avi −15 AAs sequence known as AviTag with underlined Lys residue which undergoes biotinylation; TEV – TEV protease cleavage site marked with *; rhGCPII – extracellular portion of GCPII (AAs 44–750).
Panel B: Analysis of Avi-GCPII purification by SDS–PAGE. (1) Molecular weight marker; (2) Load; (3) Flow-through; (4) Wash; (5–11) Elutions 1–7. 4 µl of the sample was loaded to each lane.

Additionally, we demonstrated that this purification set-up provides protein which readily crystallizes yielding diffraction quality crystals. We solved the 3D X-ray structure of Avi-GCPII and confirmed that our protein construct embodies the same overall structure and enzymatic activity as its tag-free counterpart (rhGCPII). Finally, we confirmed the versatility of our expression system by preparation and purification of close GCPII homolog, NAALADase L, with similar yields and purity.

My contribution:

I prepared expression plasmid for Avi-tagged proteins, established and optimized the purification protocol, purify Avi-GCPII and refined its X-ray structure. I also conducted all experiment involving AviTEV cleavage, by TEV protease or unknown host protease, and Avi-GCPII enzymatic activity analysis and wrote the draft of the manuscript.

Efficient and versatile one-step affinity purification of *in vivo* biotinylated proteins: Expression, characterization and structure analysis of recombinant human glutamate carboxypeptidase II

J. Tykvart [a,b], P. Šácha [a,b], C. Bařinka [c], T. Knedlík [a,b], J. Starková [a], J. Lubkowski [d], J. Konvalinka [a,b,*]

[a] Gilead Sciences and IOCB Research Centre, Institute of Organic Chemistry and Biochemistry, Academy of Sciences of the Czech Republic, Flemingovo n. 2, Prague 6, Czech Republic
[b] Department of Biochemistry, Faculty of Natural Science, Charles University, Albertov 6, Prague 2, Czech Republic
[c] Institute of Biotechnology, Academy of Sciences of the Czech Republic, Videnska 1083, Prague 4, Czech Republic
[d] Center for Cancer Research, National Cancer Institute at Frederick, Frederick, MD, USA

ABSTRACT

Affinity purification is a useful approach for purification of recombinant proteins. Eukaryotic expression systems have become more frequently used at the expense of prokaryotic systems since they afford recombinant eukaryotic proteins with post-translational modifications similar or identical to the native ones.

Here, we present a one-step affinity purification set-up suitable for the purification of secreted proteins. The set-up is based on the interaction between biotin and mutated streptavidin. *Drosophila* Schneider 2 cells are chosen as the expression host, and a biotin acceptor peptide is used as an affinity tag. This tag is biotinylated by *Escherichia coli* biotin-protein ligase *in vivo*. We determined that localization of the ligase within the ER led to the most effective *in vivo* biotinylation of the secreted proteins. We optimized a protocol for large-scale expression and purification of AviTEV-tagged recombinant human glutamate carboxypeptidase II (Avi-GCPII) with milligram yields per liter of culture. We also determined the 3D structure of Avi-GCPII by X-ray crystallography and compared the enzymatic characteristics of the protein to those of its non-tagged variant. These experiments confirmed that AviTEV tag does not affect the biophysical properties of its fused partner.

Purification approach, developed here, provides not only a sufficient amount of highly homogenous protein but also specifically and effectively biotinylates a target protein and thus enables its subsequent visualization or immobilization.

© 2011 Elsevier Inc. All rights reserved.

Introduction

Purification of recombinant proteins via diverse affinity tags has recently largely replaced approaches utilizing the biophysical features of the proteins. Affinity tags based on the well-characterized biotin–avidin interaction (or its analogs) were among the first candidates for this application since this interaction is the strongest ($K_D \sim 10^{-15}$ M) non-covalent bond known in biology [1].

Ironically, the strength of the binding is a major drawback for its use as a purification technique, since the elution conditions would have to be so harsh that they would lead to destruction of the purified protein. One possible way to overcome this problem is to use site-directed mutagenesis to modify the streptavidin

molecule to have a K_D for biotin in the micromolar range, which is more suitable for purification purposes [2,3].

Enzymatic biotinylation of target proteins by biotin-protein ligase from *Escherichia coli* (*BirA*; EC 6.3.4.15) is often used instead of the less specific *in vitro* chemical biotinylation of free amino groups. In *E. coli*, this ligase recognizes and biotinylates the ε-amino group of a specific lysine residue within the biotin carboxyl carrier protein subunit of acetyl-CoA carboxylase [4,5]. Using combinatorial peptide libraries, a 15 amino acid peptide with one lysine residue specifically biotinylated by *BirA* was identified. The sequence was referred to as biotin acceptor peptide (BAP) or, more frequently, AviTag and it bears little similarity to the natural *BirA* substrate [6,7].

The biotinylation via *BirA* can proceed either *in vitro* or *in vivo*. The *in vivo* biotinylation, being a part of intracellular, post-translational modification of target proteins represents an elegant, high-yield approach [8–10]. AviTag is specifically recognized only by the *BirA*, therefore if other expression systems than *E. coli* are used for production of biotinylated proteins, the expressing cells

have to be co-transfected with plasmids coding for both targeted protein and *BirA*. Proteins biotinylated *in vivo* were successfully expressed in both mammalian [8,10–13] and insect [9,14,15] expression systems. In some of these studies, different cellular localizations of *BirA* (in cytoplasm, within the ER, or in the secretory pathway) were investigated showing a strong dependency of *BirA* localization on its biotinylation efficiency. In all these experiments, the biotinylated proteins were expressed as secreted proteins [10,11,15].

Besides the AviTag/*BirA*/mutated streptavidin system, there are other affinity purification approaches utilizing avidin or its analogs. Above all, the Strep-tag II/Strep-Tactin system is commonly used [16,17]. This system does not require additional transfection with *BirA* since the Strep-tag II binds directly to the Strep-Tactin molecule. On the other hand, the Strep-tag II affinity to Strep-Tactin is in the micromolar range, which is suitable for purification but might represent a drawback during visualization, immobilization, or specific uptake of a target protein. Generally, purification approaches based on the avidin–biotin interaction are very specific, ensuring a high homogeneity of the purified proteins. Achieving such a homogeneity may be an occasional problem with the use of other affinity tags, e.g. His-tag [18].

In this paper, we present an optimized one-step protocol for affinity purification of recombinant proteins expressed via the secretory pathway in insect cells with *BirA* localized within the ER. The purified protein, the extracellular portion of glutamate carboxypeptidase II (rhGCPII, amino acids 44–750)[1], is a 90 kD N-glycosylated metalloprotease [19,20]. GCPII (EC 3.4.17.21) belongs to the family of type II transmembrane proteins and is an interesting pharmaceutical target for prostate cancer imaging and treatment [21–23]. It is also implicated in neuropathological disorders [24] and has an unknown function in angiogenesis [25,26].

Materials and methods

Preparation of expression plasmid for N-terminally AviTEV-tagged proteins

DNA encoding the AviTEV tag was prepared *de novo* from six individual oligonucleotides with complementary overlaps. Short 5′ overhangs were filled in with Phusion polymerase (Finnzymes). The following primers were used: Avi0-F (5′-aaaaa*tgatc*aggcctgaac gacatc-3′), Avi1-R (5′-atcttctgggcctcgaagatgtcgttcaggcc-3′), Avi2-F (5′-ttcgaggcccagaagatcgagtggcacg-3′), Avi3-R (5′-**ggttctc**gctgccgctg ccgctgcc*ctcgtgccactcg*-3′), Uni3-F (5′-gcagcggcagc**gagaacctgtact tccagggc***agatct*gaattcaaaaa-3′), and Uni4-R (5′-tttttgaattc*agatct***g c**-3′). Sequences encoding AviTag™ (Avidity) are underlined, and sequences encoding the TEV cleavage site are in bold. Two restriction sites introduced into the DNA are shown in italics, *BclI* at the 5′ end and *BglII* at the 3′ end of the sequence.

A standard PCR reaction was performed with a mixture of all primers. The resulting DNA construct was cleaved by *BclI* and *BglII* and inserted into the pMNAEXST, pre-cleaved with *BglII*, to create a plasmid for expression of N-terminally AviTEV-tagged rhGCPII. Both correct orientation and sequence of the prepared plasmid

were verified by sequencing. The resulting plasmid was denoted pMT/BiP/AviTEV/rhGCPII and contained AviTEV tag immediately downstream of the BiP peptide signal sequence for secretion. Additionally, the DNA encoding rhGCPII can be easily excised with *BglII* and *XhoI/XbaI* restriction enzymes, and DNA encoding a different secreted protein can be substituted.

Preparation of plasmids encoding differently localized BirA

The commercially available plasmid pBirAcm (Avidity) was used as a template for PCR reactions. To obtain a plasmid encoding cytoplasmic *BirA*, primers BirAKpnI-F (5′-atc*ggggtacc*atgaaggataaa caccgtgcc-3′) and BirAnoKDELXhoI-R (5′-tctaga*ctcgag*ttattctgcac tacgcaggg-3′) were used (restriction sites are italicized). The DNA amplicon was cleaved with *KpnI* and *XhoI* and ligated into the vector pMT/V5-HisA (Invitrogen). The resulting plasmid was denoted pMT/BirA. To obtain DNA encoding *BirA* retained within the endoplasmic reticulum (ER), primers BirABglII-F (5′-ctcggg*agatc* t*atgaaggataacaccgtgcc-3′) and BirAXhoI-R (5′-tctaga*ctcgag*ttaca gctcatcttttctgcactacgcaggg-3′) were used to amplify DNA from pBirAcm. The DNA was cleaved with *BglII* and *XhoI* and ligated into the vector pMT/BiP/V5-HisA (Invitrogen). The resulting plasmid was named pMT/BiP/BirA/KDEL. A plasmid encoding secreted *BirA* was obtained similarly, but primer BirAXhoI-R was substituted with BirAnoKDELXhoI-R. The resulting plasmid encoding secreted *BirA* was denoted pMT/BiP/BirA.

The correct sequences of all three plasmids were subsequently verified by sequencing.

Preparation of stable Drosophila S2 cell lines expressing Avi-GCPII and BirA

Drosophila S2 cells were transfected consecutively, first with 9 μg of pMT/BiP/AviTEV/rhGCPII together with 0.5 μg of pCoBlast (Invitrogen) and selected with the appropriate antibiotic. Afterwards, they were transfected with 9 μg of one of the three different plasmids encoding differently localized *BirA* together with 0.5 μg of pCoHygro (Invitrogen), as previously published [27]. The transfected cells were selected by cultivation with both Blasticidin (5 μg/ mL, Invitrogen) and Hygromycin B (300 μg/mL, Invitrogen) until they regained growth. Two transfections were performed in case of *BirA* localized within ER to prepared two individual polyclonal stable cell lines of S2 cells.

The 2.10^6 cells of each stable transfectant were transferred to 35 mm Petri dish supplemented with 2 mL SF900II medium (Invitrogen). The protein expression was induced next day by 1 mM CuSO$_4$ (Sigma). Three days post-induction, the cells were harvested by centrifugation, and the medium was analyzed by Western blot.

Large-scale expression of Avi-GCPII and rhGCPII in Drosophila S2 cells

The protocol for large-scale expression of Avi-GCPII was almost identical to that previously described [19]. The only modification was the final volume of the cell suspension, which changed from 0.5 to 1 L. Different volumes of cell culture supplements were used accordingly. The protocol for large-scale expression and purification of rhGCPII was identical to that described previously [19].

Purification of Avi-GCPII on Streptavidin Mutein Matrix

The commercial protocol for Streptavidin Mutein Matrix™ (Roche) was used as a starting point for optimization of the purification protocol. Phosphate buffer was replaced with Tris–HCl buffer, since phosphate acts as a weak inhibitor of GCPII [28]. Additional optimization experiments were performed on a small-scale with 9 mL of conditioned medium and 200 μL of mutein resin

---

[1] *Abbreviations used:* GCPII, glutamate carboxypeptidase II; rhGCPII, extracellular portion of GCPII consisting of amino acids 44–750; Avi-GCPII, molecule of rhGCPII fused at its N-terminus with AviTEV tag; TEV protease, tobacco etch virus protease; Ac-Asp-Glu, *N*-acetyl-ʟ-aspartyl-ʟ-glutamate; Ac-Asp-Met, *N*-acetyl-ʟ-aspartyl-ʟ-methionine; 2-PMPA, 2-(phosphonomethyl)-pentanedioic acid; BAP, biotin acceptor peptide; BirA, biotin-protein ligase from *Escherichia coli*; ER, endoplasmic reticulum; SDS–PAGE, sodium dodecyl sulfate–polyacrylamide gel electrophoresis; FBS, fetal bovine serum; PBS, phosphate buffered saline; TBS, tris buffered saline; Tris, tris(hydroxymethyl)aminomethane; HPLC, high-performance liquid chromatography; HRP, horseradish peroxidase; Neu, NeutrAvidin; S2 cells, Schneider 2 cells; r.m.s.d, root mean square deviation.

(i.e. 400 μL of resin mixture with 20% ethanol). Following optimization, large-scale purification of Avi-GCPII was performed.

Conditioned medium from S2 cells (0.8 L) was centrifuged at 3400g for 30 min and then concentrated to 70 mL at 4 °C using a LabScale™ TFF system (Millipore) with a Pellicon XL Biomax50 cassette (Millipore). All subsequent purification steps were performed at 4 °C. The concentrated medium was mixed with equilibration buffer (450 mM NaCl, 300 mM Tris–HCl, pH 7.2) in a 2:1 ratio (fraction L). Equilibrated medium was mixed with 1.6 mL of mutein resin, which had been washed several times with washing buffer (150 mM NaCl, 100 mM Tris–HCl, pH 7.2), and incubated overnight on a rocker. The next day, a disposable gravity column (Thermo Scientific) was used to separate the resin from the equilibrated medium (fraction FT). The mutein resin was washed with 30 mL of washing buffer and then 1.6 mL of elution buffer (150 mM NaCl, 2 mM D-biotin, 100 mM Tris–HCl, pH 7.2) was applied to the column to replace the remaining wash buffer (fraction W). The column was sealed and the resin was incubated with elution buffer for 1 h. Then, the bound Avi-GCPII protein was eluted with 7 mL of elution buffer to obtain seven 1 mL elution fractions (fractions E1–7). Following the purification procedure, the Streptavidin Mutein Matrix™ was regenerated and stored according to the manufacturer's protocol.

After the first purification and regeneration, the flow-through fraction and regenerated resin were mixed again and the whole purification procedure was repeated. All fractions were analyzed by reducing SDS–PAGE. The E1 and E2 fractions were dialyzed against appropriate buffer overnight, aliquoted and stored at −80 °C until further use.

SDS–PAGE and Western blotting

Protein samples were resolved by reducing, 0.1% sodium dodecyl sulfate (SDS), polyacrylamide gel electrophoresis (PAGE). Following SDS–PAGE, gels were either stained using Coomassie Brilliant Blue R-250 (Thermo Scientific), silver-stained, or electroblotted. For N-terminal sequencing, the proteins were transferred onto a polyvinylidene difluoride (PVDF) membrane, which was stained with Coomassie Brilliant Blue G-250 (Thermo Scientific).

Proteins were transferred onto a nitrocellulose membrane for detection by a specific antibody against rhGCPII (GCP-04) or Neu-HRP (Thermo Scientific). The membrane was blocked with Blocker™ Casein in TBS (Thermo Scientific) for 1 h. For detection of rhGCPII, GCP-04 (1 mg/mL) was diluted 1:5000 in casein blocker, incubated overnight, washed several times with 0.05% Tween 20 in PBS, and incubated for 1 h with HRP-conjugated goat anti-mouse antibody (1 mg/mL; Thermo Scientific) diluted in casein blocker in a 1:25000 ratio. For detection of biotinylated proteins, Neu-HRP (1 mg/mL) was diluted 1:2500 in casein blocker and incubated with the membrane for 1 h.

Afterwards, the membranes were washed with 0.05% Tween 20 in PBS several times to remove either Neu-HRP or HRP-conjugated goat anti-mouse antibody. The blots were developed using SuperSignal West Dura Chemiluminiscence Substrate (Thermo Scientific) according to the manufacturer's protocol. Reactive bands were visualized on a LAS-3000 CCD camera (FujiFilm). If necessary, densitometry analysis was performed using ImageJ software v1.43 [29].

Cleavage of AviTEV tag from Avi-GCPII by TEV protease

Purified Avi-GCPII was diluted to a final concentration of 1 μg/mL and mixed with His-TEV(S219 V)-Arg protease in an equimolar ratio or with a 100-fold molar excess of TEV protease. Equivalent reference mixture, without TEV protease, was also prepared. Five microliters of concentrated TBS buffer (1.5 M NaCl, 0.5 M Tris–HCl, pH 7.6) was added to each reaction, and the final volume

was adjusted to 50 μL with distilled water. Mixtures were incubated overnight at 4 °C and analyzed on Western blots. Similar experiments were performed under identical conditions substituting concentrated TBS buffer with concentrated TEV buffer (10 mM β-mercaptoethanol, 5 mM EDTA, 0.5 M Tris–HCl, pH 8.0) or concentrated MOPS buffer (0.2 M NaCl, 0.2 M MOPS, pH 7.4).

Inhibition of Avi-GCPII degradation

Twenty microliters of purified Avi-GCPII (40 μg/mL) was mixed with 5 μL of inhibitor or water (negative control) to achieve a final concentration of 200 μM for EDTA (Sigma–Aldrich), 2-PMPA, Pefabloc SC (Roche) and E-64 (Sigma–Aldrich) or 2 μM for Pepstatin A (Sigma–Aldrich). Reactions were incubated at room temperature and 6 μL samples were taken sequentially every other day and analyzed by SDS–PAGE.

Crystallization and data collection

The Avi-GCPII stock solution (10 mg/mL) was mixed with 1/10 volume of 1 mM 2-PMPA inhibitor, and the crystallization droplets were prepared by combining 2 μL of the complex solution with 2 μL of the reservoir solution containing 33% pentaerythritol propoxylate (Hampton Research), 1% polyethylene glycol 3350 (Fluka), and 100 mM Tris–HCl, pH 8.0. Crystals were grown by the hanging drop vapor diffusion method at 293 K.

Crystals were flash-frozen in liquid nitrogen directly from the reservoir solution, and the diffraction data were collected at 100 K using synchrotron radiation at the Southeast Regional Collaborative Access Team sector 22 beamlines BM of the Advanced Photon Source (Argonne, IL, USA) at an X-ray wavelength of 1.0 Å. The complete dataset was collected from a single crystal using the MarMosaic 225 mm CCD detector. Data processing was performed with the HKL2000 software package [30].

Structure determination and refinement

Since the crystal of the Avi-GCPII/2-PMPA complex was isomorphous with the crystals of rhGCPII containing the same inhibitor (PDB entry 2PVW) [31], the latter (without the inhibitor and water molecules) was used as the starting model for the structural refinement based on the X-ray data collected from a crystals of the Avi-GCPII/2-PMPA complex. Calculations were performed with the program Refmac 5.1 [32], and the refinement protocol was interspersed with manual corrections to the model using Coot [33]. The stereochemical quality of the final model was evaluated using MolProbity [34] and the final model, together with experimental amplitudes, deposited in the RCSB Protein Data Bank (entry code 3RBU). During the refinement process, 1363 of the randomly selected reflections were kept aside for cross-validation (Rfree).

Radioenzymatic assay of carboxypeptidase activity

To determine the kinetic constants of Ac-Asp-Glu cleavage, radioenzymatic assays using [3H]-Ac-Asp-Glu (radiolabelled on the terminal glutamate; 50 Ci/mmol in Tris buffer, Perkin–Elmer) were performed as previously described [27,28] with several modifications.

Briefly, appropriate amount of enzyme solution in reaction buffer (20 mM NaCl, 20 mM MOPS, pH 7.4) was pre-incubated for 10 min at 37 °C in a final volume of 90 μL. The reaction was started by addition of a 10 μL mixture of unlabeled and radioactive Ac-Asp-Glu with different overall concentration ranging from 200 nM to 50 μM (containing 50 nM 3H-Ac-Asp-Glu together with corresponding amount of unlabeled Ac-Asp-Glu) and 100 μM

to 400 μM (containing 100 nM ^{3}H-Ac-Asp-Glu together with corresponding amount of unlabeled Ac-Asp-Glu). Reactions were then incubated at 37 °C and after 20 min were stopped with 100 μL of ice-cold stopping solution (2 mM β-mercaptoethanol, 200 mM sodium phosphate, pH 7.4). Free glutamate was separated from the uncleaved substrate by ion exchange chromatography, and quantified by liquid scintillation using the Rotiszint ECO Plus scintillation cocktail (Roth) and Tri-Carb 2900TR liquid scintillation counter (Perkin–Elmer).

Reactions were performed in duplicate for each measurement, and substrate turnovers ranged between 14% and 20%. For Avi-GCPII, two separate measurements were performed. The K_m and k_{cat} values were determined from reaction rate versus substrate concentration plots using the GraFit program [35].

HPLC assay of carboxypeptidase activity

Kinetic constants of *N*-acetyl-ʟ-aspartyl-ʟ-methionine (Ac-Asp-Met) cleavage by Avi-GCPII and rhGCPII were determined using HPLC for quantification of the hydrolysis products. An appropriate amount of enzyme was added to reaction buffer (20 mM NaCl, 20 mM MOPS, pH 7.4) to final volume of 45 μL. The reaction mixtures were pre-incubated for 10 min at 37 °C. Then, 5 μL of substrate was added into each reaction (final concentration of substrate ranged from 2.8 μM to 360 μM). The reaction mixtures were incubated for 15 min at 37 °C and then stopped by adding 125 μL of ice-cold 0.2 M sodium borate, pH 10.0, and 4 μM ʟ-glutamate (internal standard). Subsequently, the amount of free ʟ-methionine was determined following a previously described method based on *o*-phthaldialdehyde (OPA) derivatization [36] and analyzed on an Agilent 1200 Series system using an AccQ-Tag Ultra column (2.1 × 100 mm; Waters).

Reactions were performed with substrate turnovers ranging from 10% to 15%. Methionine quantification was performed using a calibration curve constructed from known concentrations of methionine standard. The measurements were performed in duplicate for both proteins. The K_m and k_{cat} values were determined from reaction rate versus substrate concentration plots using the GraFit program [35].

Active site titration of Avi-GCPII and rhGCPII

Mixtures of an appropriate amount of enzyme (to achieve 10–15% substrate turnover for the non-inhibited reaction) and the tight-binding inhibitor 2-PMPA (final concentration ranging from 0 nM to 500 nM) in reaction buffer (20 mM NaCl, 20 mM MOPS, pH 7.4) were pre-incubated for 10 min at 37 °C. Reactions were started by addition of Ac-Asp-Met (final concentration 100 μM) and stopped after 15 min by addition of ice-cold 0.2 M sodium borate, pH 10.0, and 4 μM ʟ-glutamate (internal standard). Reaction volumes and determination of free ʟ-methionine were the same as for the carboxypeptidase activity assay.

The active site concentrations and K_i' values were determined from proportional velocity versus 2-PMPA concentration plots using the GraFit program [35].

Determination of the inhibition constant of 2-PMPA for Avi-GCPII and rhGCPII

The K_i for 2-PMPA was calculated from the K_i' value obtained during active site titration measurements following the formula: $K_i = K_i'/(1+[S]/K_m)$ where [S] stands for Ac-Asp-Met concentration and K_m for the Michaelis constant of the enzyme towards Ac-Asp-Met.

Amino acid analysis

The total protein concentration of Avi-GCPII and rhGCPII stock solution was determined by analysis performed on a Biochrom30 amino acid analyzer (Biochrom) following the manufacturer's protocol.

Results

Preparation of the stable insect cell line expressing biotinylated Avi-GCPII

The DNA encoding AviTEV tag was prepared from oligonucleotides by the gene fusion approach and inserted into the plasmid pMNAEXST, which enables inducible expression in *Drosophila* Schneider 2 (S2) cells [19]. Cells stably transfected with this plasmid expressed rhGCPII N-terminally fused with AviTEV tag (Avi-GCPII) into the medium (the composition of the tag is schematically shown in Fig. 1, panel A). The cells were subsequently transfected with a plasmid encoding *E. coli* biotin-protein ligase (*BirA*). In order to analyze the efficiency of Avi-GCPII *in vivo* biotinylation, three different plasmids were prepared encoding *BirA* localized in cytoplasm (pMT/BirA), within the ER (pMT/BiP/BirA/KDEL), and secreted into the media (pMT/BiP/BirA). Two peptide signal sequences for *BirA* targeting were used: the BiP sequence for the secretory pathway and the KDEL sequence for retaining *BirA* within the ER.

The expression of Avi-GCPII in the cell lines stably transfected with *BirA* and Avi-GCPII was monitored by the Western blot (see Fig. 2). To determine the biotinylation efficiency, two visualizing agents were used: the monoclonal antibody GCP-04, which specifically recognizes the extracellular portion of GCPII (rhGCPII) [37], and NeutrAvidin conjugated with horseradish peroxidase (Neu-HRP), which visualizes only the biotinylated fraction of Avi-GCPII (and potential other endogenously biotinylated proteins). The cytoplasmic localization of *BirA* led to a very low biotinylation yield. On the other hand, the localization of *BirA* either within the ER or the secretory pathway caused the effective biotinylation of Avi-GCPII. Densitometry analysis of the Western blot revealed that *BirA* localization within the ER resulted in a slightly higher biotinylation yield compared to *BirA* localized in the secretory pathway (the ratio of the signals of biotinylated and total Avi-GCPII for *BirA* localized within the ER was approximately 15% higher than for *BirA* localized in secretory pathway). Based on these results, the cell line containing *BirA* within the ER (stable cell line 1) was used for large-scale expression of Avi-GCPII.

Previous work suggested that the addition of exogenous ᴅ-biotin into the cell medium might influence the *BirA* biotinylation efficiency [15]. However, this approach did not lead to any significant improvement in biotinylation efficiency in our hands (data not shown).

Avi-GCPII is successfully purified on Streptavidin Mutein Matrix

The purification protocol given by the manufacturer of Streptavidin Mutein Matrix (Roche) was changed for the purpose of Avi-GCPII purification. The appropriate amount of resin, buffer composition and its ionic strength, and incubation times were all optimized to provide the highest possible yield while sustaining high homogeneity of the purified protein.

After optimization of the purification protocol, large-scale purification of concentrated conditioned media was performed (see "Materials and methods" section for details). Fractions collected during purification were analyzed and their purity assessed by reducing SDS–PAGE (see Fig. 1, panel B for analysis of fractions
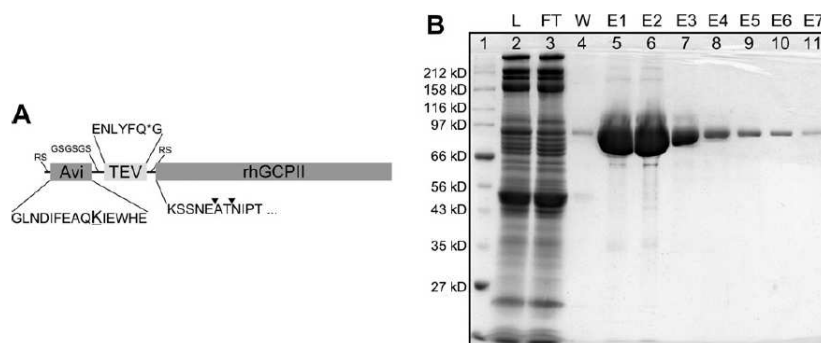
Fig. 1. Schematic representation of Avi-GCPII and analysis of its purification. *Panel A:* Schematic representation of Avi-GCPII with amino acid sequences detailed for all AviTEV tag parts; Avi – sequence of 15 amino acids known as AviTag, which is specifically recognized by biotin-protein ligase and biotinylated on the ε-amino group of the lysine residue (underlined); TEV – protein sequence specifically recognized by TEV protease (cleavage site is marked with *); rhGCPII – extracellular portion of GCPII consisting of amino acids 44–750.▼ - identified cleavage site within Avi-GCPII recognized by an unknown host protease which is co-purified with Avi-GCPII. Spacer sequence and amino acids introduced during molecular cloning are depicted in a smaller font size. *Panel B:* Analysis of Avi-GCPII purification on Streptavidin Mutein Matrix. Equilibrated concentrated conditioned medium from S2 cells was mixed with resin and incubated overnight at 4 °C. The resin was separated from the medium on a gravity-flow column, and purified protein was eluted with an excess of ᴅ-biotin. Individual fractions obtained during purification were subsequently analyzed by SDS–PAGE and stained by Coomassie blue. (1). Molecular weight marker; (2). Load; (3). Flow-through; (4). Wash; (5–11). Elutions 1–7. Four microliters of the sample was loaded to each lane. Detailed descriptions of individual fractions can be found in "Materials and methods" section.
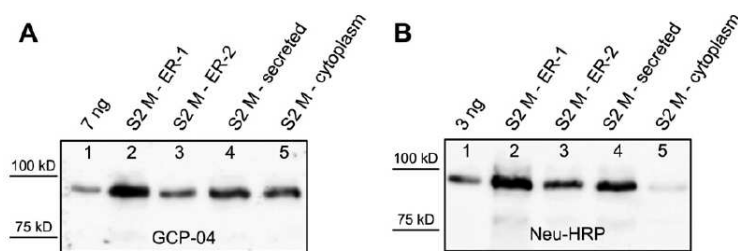

Fig. 2. Comparison of the biotinylation efficiency of *BirA* in different cellular compartments of S2 cells. Conditioned media from the cells, expressing Avi-GCPII and *BirA* (targeted to three different cellular compartments - cytoplasmic, secreted, or within the ER), were harvested 3 days post-induction and analyzed on Western blot. Western blots were visualized with the monoclonal antibody GCP-04, which recognizes total Avi-GCPII (panel A), and Neu-HRP, which recognizes only the biotinylated Avi-GCPII (panel B). (1) 7 ng (panel A) or 3 ng (panel B) of Avi-GCPII standard; (2) medium from cells with *BirA* localized within the ER (stable cell line 1); (3) medium from cells with *BirA* localized within the ER (stable cell line 2); (4) medium from cells with secreted *BirA*; (5) medium from cells with *BirA* localized in cytoplasm. Lanes 2–5 in both panels contained identical volumes of the analyzed samples.

from first purification). To increase the yield of purified Avi-GCPII, the affinity purification was performed in two rounds, with the flow-through from the first round used as an input for the second. The yields from the first and second round of purification were 4.3 mg and 0.7 mg of Avi-GCPII protein, respectively. The homogeneity of the purified protein was more than 95% and more than 90% of the protein was present in the first two elution fractions (E1, E2). The amount of Avi-GCPII in the cell conditioned medium before concentration and purification was estimated by densitometry analysis to be approximately 20 mg of overall and 12 mg of biotinylated Avi-GCPII in 0.8 L of the cell culture, suggesting that the purification yield was approximately 40%.

The purified Avi-GCPII was characterized and compared to its non-tagged version, the rhGCPII. We analyzed the influence of AviTEV tag on Avi-GCPII activity and crystallizability. We also investigated the possibility of removing the AviTEV tag with TEV protease.

The Avi-GCPII structure is not influenced by the attachment of the AviTEV tag

Purified Avi-GCPII was concentrated to 10 mg/mL and co-crystallized with a potent GCPII inhibitor, 2-(phosphonomethyl)-

pentanedioic acid (2-PMPA), using conditions identical to those used for rhGCPII crystallization [38]. The Avi-GCPII structure was obtained by the structural refinement of isomorphous structure of rhGCPII (PDB entry 2PVW) at 1.60 Å resolution, using the X-ray data collected for Avi-GCPII crystals. The new structure was deposited in the Protein Data Bank (PDB entry 3RBU). Detailed information about data collection and refinement statistics are summarized in Table 1.

The structure is virtually identical to that of rhGCPII (PDB entry 2PVW) with r.m.s.d. of 0.14 Å for 649 equivalent Cα atoms (see Fig. 3, panel A). In particular, residues participating in Zn^{2+} chelation and inhibitor binding retain their spatial arrangement (see Fig. 3, panels B and C). The AviTEV tag and the first 11 residues of rhGCPII are not visible in the electron density map, suggesting a high flexibility of the N-terminal part of the protein.

Avi-GCPII activity is not affected by the presence of the AviTEV tag

As a prerequisite for a careful quantitative comparison of Avi-GCPII and rhGCPII enzymatic activity, the total protein concentrations and the active site concentrations of both enzymes were determined by quantitative amino acid analysis and active site titration by a specific inhibitor. Relative portion of the

Table 1
Data collection and refinement statistics for the Avi-GCPII structure (3RBU).

Data collection statistics	
Wavelength (Å)	1.000
Temperature (K)	100
Space group	I222
Unit cell parameters a, b, c (Å)	101.3, 130.6, 158.9
Resolution limits (Å)	30.0–1.60 (1.66–1.60)[a]
Number of unique reflections	136,479 (12,595)
Redundancy	7.0 (4.4)
Completeness (%)	99.0 (91.9)
I/mean$I$	19.8 (2.4)
Rmerge	0.081 (0.517)
Refinement statistics	
Resolution limits (Å)	28.46–1.60 (1.64–1.60)
Total No. of reflections	134,416
No. of reflections in working	133,053 (8872)
No. of reflections in test set	1363 (68)
R	0.158 (0.251)
Rfree	0.182 (0.255)
Total No. of non-H atoms	6770
No. of protein atoms	6050
No. of inhibitor atoms	14
No. of ions	4
No. of water molecules	702
Average B-factor (Å^2)	30.31
Protein atoms	28.32
Waters	42.11
Inhibitor	28.00
RMS deviations	
Bond lengths (Å)	0.018
Bond angles (deg)	1.689
Ramachandran plot (%)	
Favoured region	97.8%
Allowed region	2.05%
Disallowed region	0.15% (Gly335)
Missing residues	T1–T32, 44–54, 541–544, 655

The amino acids which belong to the AviTEV tag are denoted as Txy.
[a] Values in parentheses correspond to the highest resolution shell.

enzymatically active molecules in the stock solution was assessed to be 102 ± 2% for Avi-GCPII and 72 ± 2% for the rhGCPII, respectively. The rhGCPII was purified according to the protocol established in our laboratory [19].

Kinetic constants characterizing cleavage of the prototypical GCPII substrate Ac-Asp-Glu [28], the less-efficient substrate Ac-Asp-Met [19], and the potent inhibitor 2-PMPA [39] were determined in order to characterize the effect of AviTEV tag on Avi-GCPII enzymatic activity. As shown in Table 2, all kinetic constants are comparable for both Avi-GCPII and rhGCPII, indicating that AviTEV tag does not affect the enzymatic characteristics of Avi-GCPII.

Avi-GCPII is ineffectively processed by TEV protease

The AviTEV tag was designed with the specific cleavage site for the tobacco etch virus (TEV) protease to enable the removal of the tag from Avi-GCPII (see Fig. 1, panel A). TEV protease is known as one of the most specific proteolytic enzymes and is widely used for the processing of recombinant proteins [40]. The purified, tagged TEV protease [His-TEV(S219V)-Arg] was incubated with purified Avi-GCPII in two different ratios (equimolar and with a 100-fold molar excess of TEV protease to Avi-GCPII). Cleavage was performed in three different buffers (see "Materials and methods" section). The results were identical for all buffers used, and for simplicity, only the experiment using TBS is shown in Fig. 4. It is visible from the Western blot analysis that a 100-fold molar excess of TEV protease is needed to efficiently remove the AviTEV tag, suggesting that the cleavage by TEV protease proceeds inefficiently, and its use in large-scale experiments would not be feasible.

Avi-GCPII is processed by host protease

Interestingly, a cleavage within the N-terminal part of purified Avi-GCPII itself was observed. N-terminal sequencing analysis identified two cleavage sites within the Avi-GCPII molecule (see Fig. 1, panel A). A series of experiments was performed in order to determine whether the processing is due to auto-proteolysis or hydrolysis by some host contaminating protease. The data shown in Fig. 5 suggested that Avi-GCPII is probably cleaved by a contaminant serine protease, since addition of a specific serine protease inhibitor, Pefabloc, slowed down the processing. The intensive degradation of Avi-GCPII observed in the experiment with EDTA was probably caused by chelation of zinc and calcium ions within Avi-GCPII and the protein's subsequent structural destabilization by which more cleavage sites became accessible for the contaminant host protease. This contaminant protease is probably not co-purified during the standard purification of rhGCPII since no N-terminal cleavage was observed for rhGCPII (data not shown).

Additional experiments showed that the cleavage is also effectively slowed at 4 °C and no hydrolysis of purified Avi-GCPII was detected after 2 days incubation at this temperature. To ensure the integrity of our protein preparation, the potential degradation of Avi-GCPII was examined under the conditions of enzymatic assays and protein crystal growth. In both these conditions no Avi-GCPII processing whatsoever was observed (data not shown).

Discussion

Simple, efficient, and robust recombinant protein expression and purification is indispensable for many areas of molecular biology, from structural genomics to protein–protein interaction studies. Even though expression and purification in prokaryotic expression systems is reasonably characterized, the eukaryotic systems still remain a challenge. We aimed to develop a well-functioning one-step purification procedure utilizing a biotin acceptor peptide (BAP) as a purification tag, for its well-characterized properties of binding to streptavidin and its analogs, and *Drosophila* S2 cells as an expression system, for their relatively easy handling, possibility of large-scale growth in suspension, and high expression yields. As a target protein, we chose glutamate carboxypeptidase II. Even though a purification protocol for this protein has already been developed [19], it is quite laborious and not much versatile. Even a single amino acid mutation influences the purification yield and requires some optimization [41] and for the GCPII homologs, however close, the method needs to be re-developed. [27]. We decided to locate the AviTEV tag on the N-terminus of rhGCPII since its 3D structure indicates that it is more flexible than C-terminus of the molecule.

This purification set-up requires preparation of stable cell line expressing both *E. coli* biotin-protein ligase (*BirA*) and the target recombinant protein. Previously published results describing the influence of *BirA* cellular localization (cytoplasmic, within the ER, or in the secretory pathway) on the biotinylation efficiency of secreted recombinant proteins fused with BAP were not complete. For instance, only two subcellular localizations were compared in parallel, and the results varied significantly between mammalian [10,11] and insect systems [15]. Therefore, we decided to prepare three stable insect cell lines with *BirA* localized in cytoplasm (*BirA*), within the ER (BiP-*BirA*-KDEL), or in secretory pathway (BiP-*BirA*), and compared them in terms of the biotinylation efficiencies of secreted Avi-GCPII.

The cytosolic localization of *BirA* was shown to be the least effective (see Fig. 2). This finding contradicts the results of Yang et al, who determined that cytosolic *BirA* had a higher biotinylation
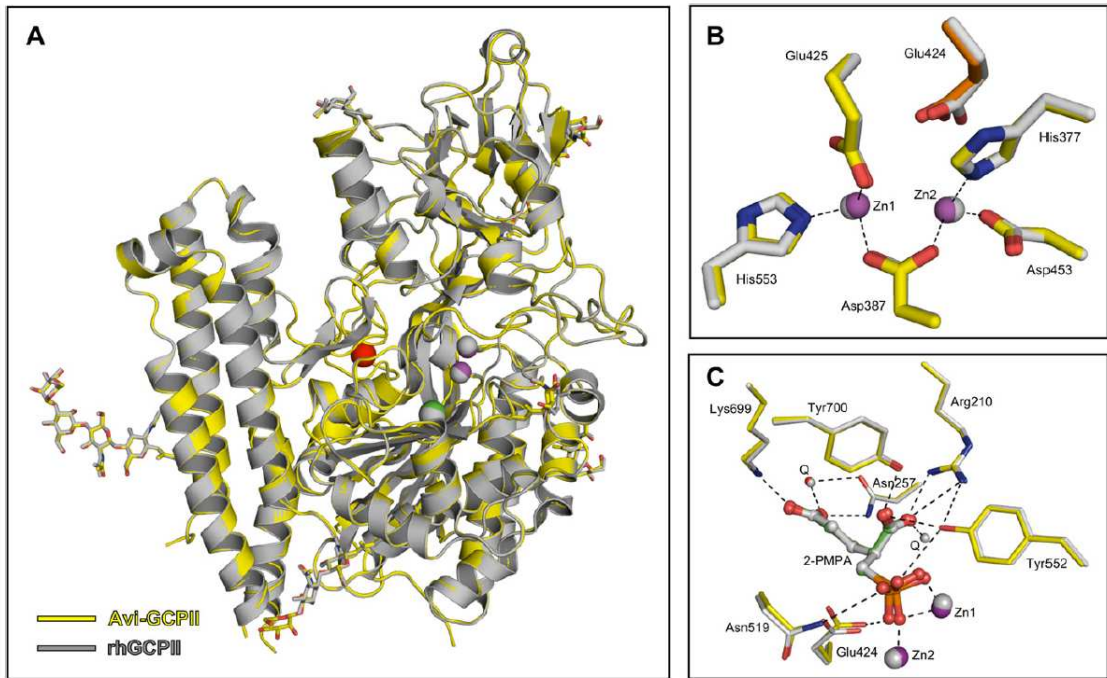
Fig. 3. Superposition of Avi-GCPII (3RBU) and rhGCPII (2PVW) structure. *Panel A:* The overall fold of Avi-GCPII and rhGCPII is identical. The protein backbone is shown in cartoon representation, sugar units in stick representation, and ions as spheres (Zn^{2+} – magenta, Cl$^-$ – green, Ca^{2+} – red for Avi-GCPII). Avi-GCPII is shown in yellow, rhGCPII in gray (including ions and sugars). Sugar oxygens and nitrogens are shown in red and blue, respectively. *Panel B:* Superposition of the active site residues/atoms. Residues coordinating Zn^{2+} ions are shown in yellow and catalytic glutamate in orange for Avi-GCPII (Zn^{2+} ions as magenta spheres) while all rhGCPII residues are shown in gray (including ions). Oxygen atoms are depicted in red and nitrogen atoms in blue. Coordination of the active site zinc ions in the Avi-GCPII structure is shown as dashed lines. *Panel C:* 2-PMPA interactions in the Avi-GCPII/rhGCPII active sites. Avi-GCPII is shown in yellow (Zn^{2+} ions as magenta spheres, 2-PMPA in green ball-and-stick representation, waters Q as red spheres); rhGCPII in gray (including ions, 2-PMPA, and waters). Oxygen atoms are depicted in red, nitrogen atoms in blue, and the phosphorus atom in orange. Direct H-bonding and coordination to Zn^{2+} ions in the Avi-GCPII structure are shown as dashed lines. The figures were created using the PyMOL Molecular Graphics System [43].

Table 2
Direct comparison of Avi-GCPII and rhGCPII enzymatic activity.

	Avi-GCPII			rhGCPII		
Substrate	K_m [µmol/L]	k_{cat} [per second]	k_{cat}/K_m [10^5/s·(mol/L)]	K_m [µmol/L]	k_{cat} [per second]	k_{cat}/K_m [10^5/s·(mol/L)]
Ac-Asp-Glu	0.53 ± 0.08[a]	0.46 ± 0.01[a]	8.66 ± 1.4	1.06 ± 0.18[a]	0.41 ± 0.02[a]	3.88 ± 1.06
Ac-Asp-Met	20.8 ± 3.3[b]	0.29 ± 0.01[b]	0.14 ± 0.02	25.2 ± 4.0[b]	0.34 ± 0.02[b]	0.13 ± 0.02
Inhibitor	K_i [pmol/L]			K_i [pmol/L]		
2-PMPA	370 ± 80[b]			540 ± 120[b]		

[a] Measurements were performed by radioactive assay.
[b] Measurements were performed by HPLC assay.
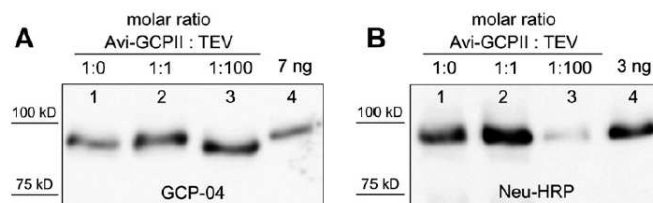
Fig. 4. Avi-GCPII cleavage by TEV protease. Purified Avi-GCPII was mixed with TEV protease in different ratios. The reactions were incubated overnight at 4 °C and then analyzed using Western blots. Blots were visualized with the monoclonal antibody GCP-04, which recognizes total Avi-GCPII (panel A), and Neu-HRP, which recognizes only biotinylated Avi-GCPII (panel B). (1) Purified Avi-GCPII without TEV protease; (2) equimolar mixture of Avi-GCPII and TEV protease; (3) Avi-GCPII with a 100-fold molar excess of TEV protease; 4. 7 ng (panel A) or 3 ng (panel B) of Avi-GCPII standard. Lanes 1–3 in both panels contained identical volumes of the analyzed samples.

Fig. 5. Inhibition of Avi-GCPII cleavage by protease class-specific inhibitors. Purified Avi-GCPII was incubated at room temperature, and samples were taken after 2 days (lanes 1,3,5,7,9,11) and 4 days (lanes 2,4,6,8,10,12) and analyzed on silver-stained reducing SDS–PAGE. Inhibitors tested: 2-PMPA (specific GCPII inhibitor; final concentration 200 µM; lanes 3,4), Pefabloc SC (serine protease inhibitor; final concentr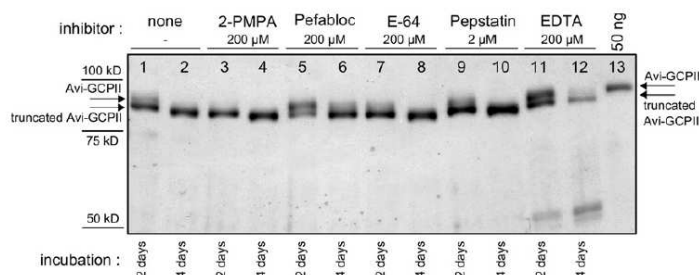ation 200 µM; lanes 5,6), E-64 (cysteine protease inhibitor; final concentration 200 µM; lanes 7,8), Pepstatin A (aspartate protease inhibitor; final concentration 2 µM; lanes 9,10), EDTA (metalloprotease inhibitor; final concentration 200 µM; lanes 11,12). The experiment without inhibitor was also performed (lanes 1, 2). Three microliters of the sample was loaded to each lane. 50 ng of purified Avi-GCPII was loaded to line 13 as a standard.

yield than the secreted form of *BirA* in insect cells [15]. This discrepancy might be due to the use of different peptide leading sequences for the secretion of *BirA* and target protein (BiP versus HLA-DR β leader sequence), by different localization of AviTag in the target molecule (N-terminal versus C-terminal), or by less obvious properties of a target protein or expression system. On the other hand, localizations of *BirA* within the ER and in the secretory pathway led to efficient Avi-GCPII biotinylation, indicating that the biotinylation in both cases probably proceeds within the ER. Only a slightly better relative biotinylation efficiency was determined for *BirA* localized within the ER compared to *BirA* localized in the secretory pathway. These data were consistent with the observations of Barat et al. in mammalian cells (even though we determined a much smaller difference between cells with secreted *BirA* and *BirA* retained within the ER) [11]. Additionally, it should be noted that using presented protocol for creation of stable S2 cell transfectants we obtained a polyclonal cell lines. When the transfection was done in duplicates, it showed higher variability in overall expression yields of biotinylated Avi-GCPII (Fig. 2, lanes 2 and 3) than was observed between cell lines with differently localized *BirA* (Fig. 2, lanes 2 and 4). These findings suggest that the careful optimization of the expression system is at least as important as proper localization of biotin ligase within the cell.

The purification procedure itself was optimized to provide the highest possible yield while preserving high homogeneity of the purified protein. Surprisingly, the use of non-dialyzed conditioned medium as a starting material for purification was shown to be the best option. Dialysis of the medium followed by optimization of ionic strength and/or addition of exogenous D-biotin resulted in lower yields and/or purity (data not shown). This effect might have been caused by some unknown additive present in the SF900II medium. We have also observed that by concentrating the conditioned medium prior to affinity purification, we improved greatly the purification yield. The explanation of this observation is not straightforward: it might be caused by increasing the effective concentration of both Avi-GCPII and mutein resin beads within the incubation mixture. Similar behavior was also observed during purifications of several Avi-GCPII mutants and homologs (data not shown).

Tags covalently attached to purified protein are useful tools for subsequent visualization or immobilization and are often retained with the target protein. In the case of AviTEV tag, the covalently attached biotin enables easy visualization, immobilization, or specific uptake of the target protein. Since the AviTEV tag is not effectively cleaved from its fusion partner by TEV protease, we focused on a detailed analysis of its influence on the biochemical features of rhGCPII.

We were able to crystallize Avi-GCPII under conditions identical to those used for the non-tagged enzyme, suggesting that the Avi-TEV tag does not influence the ability of Avi-GCPII to crystallize. In fact, we showed that the structure of Avi-GCPII is virtually identical to that of rhGCPII. A lack of interpretable electron density for the AviTEV tag indicates that this motif is likely disordered. Furthermore, we solved a structure of the AviTEV-tagged extracellular part of Naaladase L (amino acids 28–740), a GCPII homolog, in which the AviTEV tag was also not visible (manuscript in preparation). Those findings, together with a previously reported study of the structure of maltodextrin-binding protein fused with biotin acceptor peptide [42], supports the conclusion that the presence of AviTEV tag does not significantly affect the 3D structure of its fusion partner.

To determine the effect of AviTEV tag on Avi-GCPII enzymatic activity, kinetic constants for cleavage of GCPII substrates Ac-Asp-Glu and Ac-Asp-Met and the inhibition constant for the potent GCPII inhibitor 2-PMPA were determined for both Avi-GCPII and rhGCPII (see Table 2). The slightly improved catalytic efficiency of Avi-GCPII compared to rhGCPII might be explained by the milder conditions of the purification procedure used for Avi-GCPII. This notion was also supported by active site titration measurements. Purification via AviTEV tag led to Avi-GCPII molecules that were nearly 100% enzymatically active, while the standard four-step purification method yielded only 72% enzymatically active rhGCPII. The lower relative representation of enzymatically active enzyme in rhGCPII preparation compared to Avi-GCPII may be caused by complexity of purification (4 steps versus 1 step) and overall duration of purification procedure (approximately 5 days versus 2 days) in the former case. The inactive fraction of rhGCPII might partially bind the substrate/inhibitor and thus lower the observed catalytic efficiency of rhGCPII. The k_{cat} values for rhGCPII presented in Table 2 are not quite in agreement with previously published data [19,27]. This discrepancy might be caused by different methods of protein concentration determination (active site titration versus Bradford assay). Taken together, we can conclude that in this purification set-up AviTEV tag does not compromise the enzymatic activity of its fusion partner.

Even though the N-terminus part of Avi-GCPII molecule is disordered and accessible for host contaminant protease, the TEV protease showed to be very inefficient in cleaving off the tag. The poor processing may be caused by the arginine residue located at the P2′ position of the TEV cleavage site in Avi-GCPII molecule (see Fig. 1, panel A). In support of this hypothesis, we checked the enzymatic activity of the same preparation of TEV protease and determined it successfully cleaved different fusion protein containing TEV cleavage site (data not shown).

A potential versatility of this purification set-up was confirmed by successful purification of Avi-GCPII site-directed mutants and also several of its human paralogs and animal orthologs (data not shown). Furthermore, a secreted version of a different enzyme, carbonic anhydrase IX, with the AviTEV tag on its C-terminus was also successfully expressed and purified (Mader et al., manuscript in preparation). It might be relevant to mention that carbonic anhydrase XI is a type I transmembrane protein, and, consequently, the topology of the AviTEV tag location was the same as for Avi-GCPII)

In conclusion, we prepared a cell line of stably transfected *Drosophila* S2 cells with *BirA* localized within the ER and compared it with stable cell lines with the cytosolic and secreted forms of *BirA*. We showed that *BirA* localizations within both the ER and the secretory pathway lead to efficient biotinylation of target protein while the localization within ER showed slightly better biotinylation yield. Using this stable cell line we expressed, purified and characterized recombinant human GCPII. We achieved milligrams yields of pure protein per liter of culture and showed that AviTEV tag does not compromise the features of its fusion partner. Since the interaction is independent of target protein properties, we believe this purification set-up may represent a versatile and facile method for efficient expression and purification of secreted recombinant proteins in *Drosophila* S2 cells.

Acknowledgments

References

[1] N.M. Green, Avidin. 1. The use of (14-C)biotin for kinetic studies and for assay, Biochem. J. 89 (1963) 585–591.
[2] M.H. Qureshi, S.L. Wong, Design, production, and characterization of a monomeric streptavidin and its application for affinity purification of biotinylated proteins, Protein Expr. Purif. 25 (2002) 409–415.
[3] S.C. Wu, S.L. Wong, Engineering soluble monomeric streptavidin with reversible biotin binding capability, J. Biol. Chem. 280 (2005) 23225–23231.
[4] M.D. Lane, K.L. Rominger, D.L. Young, F. Lynen, The enzymatic synthesis of holotranscarboxylase from apotranscarboxylase and (+)-biotin. Ii. Investigation of the reaction mechanism, J. Biol. Chem. 239 (1964) 2865–2871.
[5] M.D. Lane, D.L. Young, F. Lynen, The enzymatic synthesis of holotranscarboxylase from apotranscarboxylase and (+)-biotin. Purification of the apoenzyme and synthetase; characteristics of the reaction, J. Biol. Chem. 239 (1964) 2858–2864.
[6] D. Beckett, E. Kovaleva, P.J. Schatz, A minimal peptide substrate in biotin holoenzyme synthetase-catalyzed biotinylation, Protein Sci. 8 (1999) 921–929.
[7] P.J. Schatz, Use of peptide libraries to map the substrate specificity of a peptide-modifying enzyme: a 13 residue consensus peptide specifies biotinylation in *Escherichia coli*, Biotechnology (NY) 11 (1993) 1138–1143.
[8] E. de Boer, P. Rodriguez, E. Bonte, J. Krijgsveld, E. Katsantoni, A. Heck, F. Grosveld, J. Strouboulis, Efficient biotinylation and single-step purification of tagged transcription factors in mammalian cells and transgenic mice, Proc. Natl. Acad. Sci. USA 100 (2003) 7480–7485.
[9] S. Duffy, K.L. Tsao, D.S. Waugh, Site-specific, enzymatic biotinylation of recombinant proteins in Spodoptera frugiperda cells using biotin acceptor peptides, Anal. Biochem. 262 (1998) 122–128.
[10] A. Predonzani, F. Arnoldi, A. Lopez-Requena, O.R. Burrone, In vivo site-specific biotinylation of proteins within the secretory pathway using a single vector system, BMC Biotechnol. 8 (2008) 41.
[11] B. Barat, A.M. Wu, Metabolic biotinylation of recombinant antibody by biotin ligase retained in the endoplasmic reticulum, Biomol. Eng. 24 (2007) 283–291.
[12] S. Driegen, R. Ferreira, A. van Zon, J. Strouboulis, M. Jaegle, F. Grosveld, S. Philipsen, D. Meijer, A generic tool for biotinylation of tagged proteins in transgenic mice, Transgenic Res. 14 (2005) 477–482.
[13] K. Sung, M.T. Maloney, J. Yang, C. Wu, A novel method for producing mono-biotinylated, biologically active neurotrophic factors: an essential reagent for single molecule study of axonal transport, J. Neurosci. Methods 200 (2011) 121–128.
[14] D. Juzumiene, C.Y. Chang, D. Fan, T. Hartney, J.D. Norris, D.P. McDonnell, Single-step purification of full-length human androgen receptor, Nucl. Recept. Signal. 3 (2005) e001.
[15] J. Yang, A. Jaramillo, R. Shi, W.W. Kwok, T. Mohanakumar, In vivo biotinylation of the major histocompatibility complex (MHC) class II/peptide complex by coexpression of BirA enzyme for the generation of MHC class II/tetramers, Hum. Immunol. 65 (2004) 692–699.
[16] T.G. Schmidt, A. Skerra, The Strep-tag system for one-step purification and high-affinity detection or capturing of proteins, Nat. Protoc. 2 (2007) 1528–1535.
[17] A. Skerra, T.G. Schmidt, Applications of a peptide ligand for streptavidin: the Strep-tag, Biomol. Eng. 16 (1999) 79–86.
[18] J.J. Lichty, J.L. Malecki, H.D. Agnew, D.J. Michelson-Horowitz, S. Tan, Comparison of affinity tags for protein purification, Protein Expr. Purif. 41 (2005) 98–105.
[19] C. Barinka, M. Rinnova, P. Sacha, C. Rojas, P. Majer, B.S. Slusher, J. Konvalinka, Substrate specificity, inhibition and enzymological analysis of recombinant human glutamate carboxypeptidase II, J. Neurochem. 80 (2002) 477–487.
[20] C. Barinka, P. Sacha, J. Sklenar, P. Man, K. Bezouska, B.S. Slusher, J. Konvalinka, Identification of the N-glycosylation sites on glutamate carboxypeptidase II necessary for proteolytic activity, Protein Sci. 13 (2004) 1627–1635.
[21] P. Buhler, P. Wolf, U. Elsasser-Beile, Targeting the prostate-specific membrane antigen for prostate cancer therapy, Immunotherapy 1 (2009) 471–481.
[22] A.A. Elgamal, E.H. Holmes, S.L. Su, W.T. Tino, S.J. Simmons, M. Peterson, T.G. Greene, A.L. Boynton, G.P. Murphy, Prostate-specific membrane antigen (PSMA): current benefits and future value, Semin. Surg. Oncol. 18 (2000) 10–16.
[23] A. Ghosh, W.D. Heston, Tumor target prostate specific membrane antigen (PSMA) and its regulation in prostate cancer, J. Cell. Biochem. 91 (2004) 528–539.
[24] J.H. Neale, R.T. Olszewski, L.M. Gehl, B. Wroblewska, T. Bzdega, The neurotransmitter N-acetylaspartylglutamate in models of pain, ALS, diabetic neuropathy, CNS injury and schizophrenia, Trends Pharmacol. Sci. 26 (2005) 477–484.
[25] R.E. Conway, N. Petrovic, Z. Li, W. Heston, D. Wu, L.H. Shapiro, Prostate-specific membrane antigen regulates angiogenesis by modulating integrin signal transduction, Mol. Cell. Biol. 26 (2006) 5310–5324.
[26] T. Liu, M. Jabbes, J.R. Nedrow-Byers, L.Y. Wu, J.N. Bryan, C.E. Berkman, Detection of prostate-specific membrane antigen on HUVECs in response to breast tumor-conditioned medium, Int. J. Oncol. 38 (2011) 1349–1355.
[27] K. Hlouchova, C. Barinka, V. Klusak, P. Sacha, P. Mlcochova, P. Majer, L Rulisek, J. Konvalinka, Biochemical characterization of human glutamate carboxypeptidase III, J. Neurochem. 101 (2007) 682–696.
[28] M.B. Robinson, R.D. Blakely, R. Couto, J.T. Coyle, Hydrolysis of the brain dipeptide N-acetyl-L-aspartyl-L-glutamate. Identification and characterization of a novel N-acetylated alpha-linked acidic dipeptidase activity from rat brain, J. Biol. Chem. 262 (1987) 14498–14506.
[29] W.S. Rasband, ImageJ. US National Institutes of Health, Bethesda, Maryland, USA. http://www.rsb.info.nih.gov/ij/, 1997–2008.
[30] Z. Otwinowski, W. Minor, Processing of X-ray diffraction data collected in oscillation mode, Methods Enzymol. 276 (1997) 307–326.
[31] C. Barinka, M. Rovenska, P. Mlcochova, K. Hlouchova, A. Plechanovova, P. Majer, T. Tsukamoto, B.S. Slusher, J. Konvalinka, J. Lubkowski, Structural insight into the pharmacophore pocket of human glutamate carboxypeptidase II, J. Med. Chem. 50 (2007) 3267–3273.
[32] G.N. Murshudov, A.A. Vagin, E.J. Dodson, Refinement of macromolecular structures by the maximum-likelihood method, Acta Crystallogr. D Biol. Crystallogr. 53 (1997) 240–255.
[33] P. Emsley, K. Cowtan, Coot: model-building tools for molecular graphics, Acta Crystallogr. D Biol. Crystallogr. 60 (2004) 2126–2132.
[34] V.B. Chen, W.B. Arendall 3rd, J.J. Headd, D.A. Keedy, R.M. Immormino, G.J. Kapral, L.W. Murray, J.S. Richardson, D.C. Richardson, MolProbity: all-atom structure validation for macromolecular crystallography, Acta Crystallogr. D Biol. Crystallogr. 66 (2010) 12–21.
[35] R.J. Leatherbarrow, GraFit Version 5, Erithacus Software Limited, Horley, UK, 2001.
[36] C. Woodward, J.K. Henderson, T. Wielgos, High-speed amino acid analysis (AAA) on 1.8 μm reversed-phase (RP) columns. Agilent Technologies App. Note (2007) 5989-6297EN.

[37] P. Sacha, J. Zamecnik, C. Barinka, K. Hlouchova, A. Vicha, P. Mlcochova, I. Hilgert, T. Eckschlager, J. Konvalinka, Expression of glutamate carboxypeptidase II in human brain, Neuroscience 144 (2007) 1361–1372.

[38] C. Barinka, J. Starkova, J. Konvalinka, J. Lubkowski, A high-resolution structure of ligand-free human glutamate carboxypeptidase II, Acta Crystallogr., Sect. F: Struct. Biol. Cryst. Commun. 63 (2007) 150–153.

[39] P.F. Jackson, D.C. Cole, B.S. Slusher, S.L. Stetz, L.E. Ross, B.A. Donzanti, D.A. Trainor, Design, synthesis, and biological activity of a potent inhibitor of the neuropeptidase N-acetylated alpha-linked acidic dipeptidase, J. Med. Chem. 39 (1996) 619–622.

[40] J. Phan, A. Zdanov, A.G. Evdokimov, J.E. Tropea, H.K. Peters 3rd, R.B. Kapust, M. Li, A. Wlodawer, D.S. Waugh, Structural basis for the substrate specificity of tobacco etch virus protease, J. Biol. Chem. 277 (2002) 50564–50572.

[41] P. Mlcochova, A. Plechanovova, C. Barinka, D. Mahadevan, J.W. Saldanha, L. Rulisek, J. Konvalinka, Mapping of the active site of glutamate carboxypeptidase II by site-directed mutagenesis, FEBS J. 274 (2007) 4731–4741.

[42] M.H. Bucher, A.G. Evdokimov, D.S. Waugh, Differential effects of short affinity tags on the crystallization of *Pyrococcus furiosus* maltodextrin-binding protein, Acta Crystallogr. D Biol. Crystallogr. 58 (2002) 392–397.

[43] Schrodinger, LLC, The PyMOL Molecular Graphics System, Version 1.3r1, 2010.

2.2.2 Paper II: Comparative analysis of monoclonal antibodies against GCPII

Motivation of the study

GCPII is involved in several human pathological conditions related to neurodegenerative and cancerous diseases, as has been extensively reviewed in the Introductory section (see section 1.7). Therefore, it is not surprising that monoclonal antibodies (mAbs) against this protein represent an intensively studied and used tool for GCPII specific targeting.

Unfortunately, even though there are many commercially available mAbs, only small portion of them is appropriately characterized in terms of their affinity and specificity. This issue may contribute to the inconsistent results concerning GCPII protein expression profile (see section 1.6). Additionally, the cross-reactivity of mAbs with close GCPII homologs, mainly human GCPIII and mouse GCPII/III (see section 1.9), has not been investigated for almost any available mAbs. The lack of knowledge of these basic characteristics may lead to erroneous interpretation of results obtained during every-day laboratory work as well as during advanced clinical testing of these mAbs.

Therefore, we decided to collect a panel of the most commonly used mAbs against GCPII and analyze them in both qualitative and quantitative manner.

Summary

In the presented study, we collected the 13 most frequently used mAbs against GCPII. We quantitatively characterized their binding to GCPII by enzyme-linked immunosorbent assay (ELISA) and surface plasmon resonance (SPR) while simultaneously determining their ability to recognize either native or denatured form of GCPII. Additionally, we investigated potential cross-reactivity of the studied mAbs against human GCPIII and mouse GCPII/III, and using a peptide library we mapped the epitopes of mAbs recognizing denature form of GCPII.

ELISA and SPR analyses revealed that mAbs J591, J415, D2B, 107-1A4, GCP-05, and 2G7 bind preferentially to GCPII in its native form, while mAbs YPSMA-1, YPSMA-2, GCP-02, GCP-04, and 3E6 bind solely to denatured form of GCPII. mAbs 24.4E6 and 7E11-C5.3 recognize both forms of GCPII in similar efficiency. Additionally, we determined that GCP-02 and 3E6 cross-react with denatured mouse GCPII, while GCP-04 recognizes denatured GCPII and GCPIII proteins from both human and mouse.

Finally, we assessed the applicability of these mAbs to routine experimental setups, including western blot (WB), immunohistochemistry (IHC), and flow cytometry (FC). The obtained results are summarized in Table 3.

Table 3: Summary of basic characteristics of anti-GCPII mAbs.
Each mAb is evaluated for its effectiveness on each of the analyzed methods. "-" stand for 'not applicable' while "+++" stands for 'highly efficient'.

Antibody	GCPII in native form		GCPII in denatured form		
	ELISA	FC	ELISA	WB	IHC
J591	+++	+++	+	+	-
J415	+++	+++	-	-	-
D2B	+++	+++	+	+	-
107-1A4	+++	+++	-	-	-
2G7	++	++	-	-	-
GCP-05	+	+++	-	-	-
7E11-C5.3	++	-	++	++	-
GCP-02	-	-	+++	+++	+++
GCP-04	-	-	+++	+++	+++
YPSMA-1	-	-	++	+++	+++
YPSMA-2	-	-	++	++	+++
3E6	-	-	++	++	++
24.4E6	+	-	+	+	++

This is a first comprehensive study of these highly important research tools for GCPII analysis and targeting. We hope that the presented data will enable more precise and efficient usage of these mAbs by the researchers in the future.

My contribution

I purified mAbs GCP-02 and 24.4E6 and conducted all ELISA, SPR and WB experiments. I also participated in FC and IHC experiments and wrote the draft of the manuscript.

Comparative Analysis of Monoclonal Antibodies Against Prostate-Specific Membrane Antigen (PSMA)

J. Tykvart,[1,2] V. Navrátil,[1,2] F. Sedlák,[1,3] E. Corey,[4] M. Colombatti,[5] G. Fracasso,[5] F. Koukolík,[6] C. Bařinka,[7] P. Šácha,[1,2] and J. Konvalinka[1,2]*

[1]Gilead Sciences and IOCB Research Centre, Institute of Organic Chemistry and Biochemistry, Academy of Sciences of the Czech Republic, Czech Republic
[2]Department of Biochemistry, Faculty of Natural Science, Charles University, Czech Republic
[3]First Faculty of Medicine, Charles University in Prague, Czech Republic
[4]Genitourinary Cancer Research Laboratory, Department of Urology, University of Washington, Seattle
[5]Department of Pathology and Diagnostics, Section of Immunology, University of Verona, Verona, Italy
[6]Department of Pathology and Molecular Medicine, Thomayer Teaching Hospital, Czech Republic
[7]Institute of Biotechnology, Academy of Sciences of the Czech Republic, Czech Republic

BACKGROUND. Prostate-specific membrane antigen (PSMA), also known as glutamate carboxypeptidase II (GCPII), is generally recognized as a diagnostic and therapeutic cancer antigen and a molecular address for targeted imaging and drug delivery studies. Due to its significance in cancer research, numerous monoclonal antibodies (mAbs) against GCPII have been described and marketed in the past decades. Unfortunately, some of these mAbs are poorly characterized, which might lead to their inappropriate use and misinterpretation of the acquired results.

METHODS. We collected the 13 most frequently used mAbs against GCPII and quantitatively characterized their binding to GCPII by enzyme-linked immunosorbent assay (ELISA) and surface plasmon resonance (SPR). Using a peptide library, we mapped epitopes recognized by a given mAb. Finally, we assessed the applicability of these mAbs to routine experimental setups, including Western blotting, immunohistochemistry, and flow cytometry.

RESULTS. ELISA and SPR analyses revealed that mAbs J591, J415, D2B, 107-1A4, GCP-05, and 2G7 bind preferentially to GCPII in native form, while mAbs YPSMA-1, YPSMA-2, GCP-02, GCP-04, and 3E6 bind solely to denatured GCPII. mAbs 24.4E6 and 7E11-C5.3 recognize both forms of GCPII. Additionally, we determined that GCP-02 and 3E6 cross-react with mouse GCPII, while GCP-04 recognizes GCPII and GCPIII proteins from both human and mouse.

CONCLUSION. This comparative analysis provides the first detailed quantitative characterization of the most commonly used mAbs against GCPII and can serve as a guideline for the scientific community to use them in a proper and efficient way. *Prostate 74: 1674–1690, 2014.*
© 2014 Wiley Periodicals, Inc.

INTRODUCTION

Over the past 20 years, prostate specific membrane antigen (PSMA), also known as glutamate carboxypeptidase II (GCPII), has been investigated for use in cancer diagnostics and targeted drug delivery due to its elevated and highly restricted expression in prostate adenocarcinoma [1]. In 1997, GCPII was also found to be expressed in the neovasculature of newly formed solid tumors [2–3]. This finding turned GCPII into an even more attractive target for diagnostic and therapeutic applications [4]. Furthermore, GCPII has become widely used as a model molecular address for various targeted drug delivery strategies due to its favorable features, including its topology (it is a transmembrane protein with the majority of the molecule facing outside of the cell [5]), ability to internalize ligands upon binding [6] and restricted tissue expression [7–11].

Several laboratories are currently studying GCPII from various perspectives, and the majority of them routinely use monoclonal antibodies (mAbs) in a variety of experimental methods [12–15]. There is a large pool of available anti-GCPII mAbs produced by both academia and industry. Unfortunately, some of them are not sufficiently well characterized to allow appropriate use and interpretation of results. This may occasionally lead to inconsistent or even contradictory results. For example, numerous research groups intensively studied the expression profile of GCPII in the human body. The researchers utilized several detection methods (immunohistochemistry (IHC) [2–3,16–22], Western blot (WB) [23–24], enzyme-linked immunosorbent assay (ELISA) [25]) and various mAbs (7E11-C5.3 [3,18–20,24–25], J591 [2,18], PEQ226.5 [18,25], 24.4E6 [20], YPSMA-1 [21], 3D16 [16], PM2J004.5 [17–18], GCP-04 [23], and 3E6 [22]). Taken together, the studies provided some clear and consistent results (e.g., GCPII was detected in prostate tissue in all studies) but also yielded some major inconsistencies and contradictions (e.g., expression of GCPII in tumor-associated neovasculature was detected by some scientists [16–17,22] but not others [20–21]; the expression of GCPII in brain was confirmed in some studies [20–21,24] but not others [3,18–19]).

Therefore, our objective was to gather the most frequently used mAbs against GCPII and perform their thorough analysis and comparison. These mAbs are listed in Table I.

Two mAbs from our collected panel are either in clinical use or advanced stage of clinical trials. 7E11-

C5.3 was the first mouse mAb developed against GCPII. It was generated in 1987 by immunizing mice with crude LNCaP cell lysate, and it recognizes the intracellular portion of GCPII [29]. The ^{111}In radioconjugate of 7E11-C5.3 (ProstaScint^{TM}) is currently the only anti-GCPII agent employed in clinical practice. It is used for detection of prostate cancer recurrence and metastases [26–28].

J591 is a second-generation mAb that recognizes the extracellular portion of GCPII. It was prepared and characterized in 1997 by Liu et al. J591 recognizes viable LNCaP cells expressing GCPII and enables visualization of GCPII in frozen tissue sections [2]. J591 has been intensively investigated for potential use in the clinic. Various conjugates of this mAb have been prepared and characterized as potential diagnostic and therapeutic agents, and some are now being tested in phase II clinical trials [31–39].

We could not possibly cover all available mAbs against GCPII, but we believe that we included most of those that are commonly used. The notable exceptions involve a panel of mAbs prepared in the laboratory of Dr. Ursula Elsässer-Beile (Universitätsklinikum Freiburg, Experimentelle Urologie, Germany) [61] and a panel of mAbs developed by Progenics [62–63]. These mAbs were unfortunately not provided to us for the purpose of this study.

We believe the results of this study will help clarify the inconsistent results published in the GCPII literature. We also hope that our observations will help scientists choose the most appropriate mAbs for their experiments and plan them in the most effective manner (e.g., information about the binding affinity of a particular mAb would enable facile estimation of its working concentration). Finally, we point out some misconceptions and the erroneous performances of some of the methods involving these mAbs, specifically Western blot and immunohistochemistry.

MATERIALS AND METHODS

Purification of Recombinant Avi-tagged Proteins

The extracellular portion of human GCPII with an N-terminal Avi-tag (Avi-GCPII) was prepared as previously described [64]. Human GCPII homologs (human GCPIII, mouse GCPII and mouse GCPIII) were prepared and denoted in a similar fashion. See Supplementary Material for more details.

TABLE I. List of mAbs Against GCPII Analyzed in this Study and Their Basic Characteristics (As Found in Appropriate Publications or Manufacturer's Datasheets)

Antibody	Isotype	Producer	Applications	Epitope	References
7E11-C5.3	IgG1	NA	WB, IHC-Fr/P, ICC, IP	intracellular (aa 1–7)	[3,18–20,24–30]
J591	IgG1	NA	IHC-Fr, IP, ICC, WB, ELISA	extracellular	[2,6,18,31–39]
J415	IgG1	NA	IHC-Fr, IP, ICC, ELISA	extracellular	[2,5,17]
D2B	IgG1	NA	IP, ICC, IHC-Fr, WB	extracellular	[40–45]
107-1A4	IgG1	Abcam (ab140348), Sigma (SAB4200257)	ELISA, IHC-P, IHC-Fr, ICC	extracellular	[46–47]
YPSMA-1	IgG2b	Abcam (ab19071), Anogen (MO-T40086A), LSBio (LS-B3040), Abnova (MAB4315), GeneTex (GTX19071), Santa Cruz (sc-59674)	IHC-Fr/P, WB, ELISA, ICC	extracellular (aa 716–723)	[9–10,21,48]
YPSMA-2	IgG2b	Anogen (MO-T40086B), Santa Cruz (sc-69665)	IHC-Fr/P, WB, ELISA	extracellular	[48]
3E6	IgG1	Dako (M3620)	IHC-P	extracellular (aa 57–134)	[22,49–52]
2G7	IgG1	NA	IP	extracellular	[53]
24.4E6	IgG1	NA	WB, IHC-P	extracellular (aa 638–657)	[20,54]
GCP-02	IgG1	NA	WB, IHC-P	extracellular	[55]
GCP-04	IgG1	Exbio (11–532), Abcam (ab66911)	WB, IHC-P	extracellular (aa 100–104)	[23,39,55–58]
GCP-05	IgG1	Exbio (11–539), Abcam (ab66912), Sigma (SAB4700282)	IP, ICC, FC	extracellular	[59–60]

WB, Western blot; ICC, immunocytochemistry; IP, immunoprecipitation; ELISA, enzyme-linked immunosorbent assay; FC, flow cytometry; IHC-Fr, immunohistochemistry performed on frozen tissue sections; IHC-P, immunohistochemistry performed on paraffin-embedded tissue sections; aa, amino acid; NA, not available. Positions of mAbs epitopes refer to GCPII sequence of accession number Q04609-1.

Preparation and Purchase of mAbs

The following mAbs were purchased from commercial sources: YPSMA-1 (Abcam), YPSMA-1 (Anogen), YPSMA-2 (Anogen), 3E6 (Dako) and GCP-05 (Exbio). Antibodies provided as lyophilized powders were reconstituted according to the manufacturer's protocol.

Antibodies D2B (referred to as anti-PSMA in [41]), 107-1A4 [46], GCP-02 [57], GCP-04 [57], 7E11-C5.3 [57] and 2G7 [53] were prepared as previously described.

Antibody 24.4E6 was purified from hybridoma supernatant that was kindly provided by Dr. Ching Y. Wang, using the same protocol as for 2G7 [53]. The purity of the final 24.4E6 preparation was approximately 50%, as assessed by silver-stained SDS-PAGE. Purified mAbs J415 and J591 were a kind gift from Dr. Neil H. Bander.

Concentration of all mAbs was determined by absorption at 280 nm except for 3E6, which was purchased as a dialyzed hybridoma supernatant. We used the 3E6 concentration stated by the manufacturer.

Characterization of mAb Binding by ELISA

All ELISA experiments were performed in a 96-well plate format at 25°C. First, the NeutrAvidin solution (Thermo Scientific) was non-specifically immobilized on the surface. Casein blocker was used to block the surface of each well. Mono-biotinylated human Avi-GCPII was then bound to the neutravidin in native binding buffer (for native GCPII ELISA assay) or in denaturing binding buffer (for denatured GCPII ELISA assay). To determine possible mAb cross-reactivity, human Avi-GCPIII, mouse Avi-GCPII and

mouse Avi-GCPIII were used in a similar fashion as human GCPII. For mAb 7E11-C5.3, intraGCPII peptide in native binding buffer was used instead of human Avi-GCPII. Then, solutions of various mAbs prepared by 2× serial dilution (11 concentrations in total) were added into the wells, followed by addition of HRP-conjugated goat anti-mouse polyclonal antibody. The chemiluminiscent substrate was added into each well, and the chemiluminiscence was measured. See Supplementary Material for more details.

Epitope Determination Assay

The protocol described for the native GCPII ELISA assay was also used for this experiment. A library of 83 biotinylated 18-mer peptides was synthesized. These peptides, which cover the entire sequence of human GCPII, were immobilized on a 96-well plate via neutravidin and then treated with the appropriate mAb. Experiments without any primary antibody and with indifferent mouse IgG were also performed as negative controls. See Supplementary Material for more details.

Characterization of mAb Binding by SPR

All SPR measurements were performed on a four-channel SPR sensor platform (PLASMON IV) developed at the Institute of Photonics and Electronics (IPE) of the Academy of Sciences of the Czech Republic, Prague [65–66]. First, a gold chip was functionalized with alkanethiols containing carboxylic terminal groups (Prochimia) in pure ethanol and then mounted to the prism on the SPR sensor. All experiments were performed at 25°C. Activation of carboxylic terminal groups on the sensor surface was performed in situ by injecting a solution of N-hydroxysuccinimide and N-ethyl-N-(dimethylaminopropyl) carbodiimide in pure water. Then, neutravidin was covalently immobilized on the chip surface, followed by a high ionic strength solution and ethanolamine to wash out non-covalently bound neutravidin and deactivate residual carboxylic groups, respectively. Recombinant human Avi-GCPII in PBS was immobilized to the prepared layer, followed by injection of an appropriate mAb (D2B, J591, J415, 107-1A4 or 2G7). Four different mAb concentrations in PBS were used for each experiment (association phase). Then, PBS was loaded to the chip to wash out the bound mAb (dissociation phase).

TraceDrawer 1.5 (Ridgeview Instruments AB) was used to calculate k_{on} and k_{off} parameters of mAb binding. Measurements were performed twice for each mAb. See Supplementary Material for more details.

Western Blotting

Western blots were performed using standard procedures and overnight incubation with appropriate mAbs, namely GCP-02, GCP-04, YPSMA-1, YPSMA-2, 3E6, 24.4E6, J591 (1 µg/ml) and D2B (10 µg/ml). See Supplementary Material for more details.

Immunohistochemistry

A prostate adenocarcinoma sample (Gleason score 3 + 4) was obtained by radical prostatectomy at Thomayer's Hospital in Prague. Patient consent and local ethical commission approval were obtained. Formalin-fixed paraffin-embedded tissues (3-µm-thick slides) were used for IHC that was performed according to a standard procedure with overnight incubation of the anti-GCPII mAbs at 4°C. The mAb concentration differed depending on the particular experiment, ranging from 0.01 µg/ml to 10 µg/ml. For visualization of antibody–antigen complexes, the slides were incubated with Histofine® Simple Stain™ MAX PO (MULTI) (Nichirei Biosciences Inc.). See Supplementary Material for more details.

Flow Cytometry

LNCaP and PC3 cells were grown under standard tissue culture conditions. After reaching 80% confluence, the cells were trypsinized, harvested, counted and diluted in 10% FBS/PBS to a final concentration 4×10^6 cells/ml.

The experiments were performed in a 96-well plate format with 2×10^5 cells in each well. All subsequent procedures were performed strictly at 4°C to prevent internalization of a bound primary antibody. An appropriate mAb was added into each well to reach a final concentration of 10 µg/ml. After 1 hour, cells were washed several times and incubated for another hour with secondary F(ab′) fragment donkey anti-mouse IgG (H + L) antibody conjugated with phycoerythrin (Jackson ImmunoResearch). Finally, the cells were diluted in 10% FBS/PBS, and single cell suspensions were measured on a BD LSRFortessa™ cell analyzer (Becton, Dickinson and Company). All experiments (all mAbs and both cell lines) were measured in triplicate. See Supplementary Material for more details.

RESULTS

We sorted the mAbs based on the nature of the antigen they recognize (i.e., GCPII in native or denatured form) since this feature predetermines mAb effectiveness in all the methods tested. Throughout

this manuscript, we use the term "GCPII in native form" to refer to the biophysical properties of GCPII, that is, properly folded and enzymatically active protein. We use the term "GCPII in denatured form" to refer to protein that has been heat-denatured in the presence of the detergents.

In this study, we used GCPII of two different origins. For ELISA, SPR, and WB experiments, we used the extracellular portion of recombinant human GCPII (Avi-GCPII) or its three homologs (human Avi-GCPIII, mouse Avi-GCPII, and mouse Avi-GCPIII) produced in insect cells with N-terminal biotin (covalently attached to the Avi-tag^{TM}) [64] while for FC, IHC, and WB experiments, we used GCPII endogenously expressed in LNCaP cells or prostate adenocarcinoma tissue.

Quantitative Analysis

The affinities of mAbs for Avi-GCPII were determined by ELISA and SPR. First, we used ELISA to qualitatively test the ability of the mAbs to bind Avi-GCPII in its native or denatured form. Based on these results, we measured a titration curve for each mAb and its appropriate antigen. From these measurements, we obtained the 50% saturation binding value, which describes the affinity of the mAb, and the maximal saturation signal value, which corresponds to the overall output signal of the mAb.

Using ELISA, we also tested mAb binding to three GCPII homologs (human Avi-GCPIII, mouse Avi-GCPII,

and mouse Avi-GCPIII). Additionally, to gain an even better understanding of the binding event, we used SPR to determine the kinetic profile of binding for the tight-binding mAbs against Avi-GCPII in native form.

ELISA Using Avi-GCPII in Native Form

mAbs that bind to Avi-GCPII in native form are listed in Table II. Our results show that mAbs 2G7, J415, J591, D2B and 107-1A4 bind Avi-GCPII very tightly (with nanomolar to high picomolar 50% saturation values), while GCP-05 and 24.4E6 bind Avi-GCPII much weakly (with submicromolar 50% saturation values). Moreover, a comparison of the maximal saturation values of the tight-binding mAbs showed an almost sevenfold difference in maximal signal output (2G7 vs. J591).

ELISA Using Denatured Avi-GCPII and mAb Epitope Mapping

mAbs that bind Avi-GCPII in denatured form are listed in Table III. The results show a wide range of 50%

TABLE III. Characteristics of mAb Binding to Denatured Human Avi-GCPII

Antibody	50% saturation	Maximal signal	Epitope	#
GCP-04	0.628 ± 0.066 nM	54	91–108	2
J591	3.06 ± 0.89 nM	1	ND	3
GCP-02	5.2 ± 1.2 nM	40	271–288	4
3E6	9.8 ± 1.7 nM	9	118–135	2
7E11-C5.3	9.9 ± 3.0 nM	NC	1–21	2
YPSMA-1	61 ± 17 nM	7	469–486	2
YPSMA-2	216 ± 55 nM	42	469–486	3
24.4E6	267 ± 49 nM	5	640–657	2

ELISA experiments under denaturing conditions were performed with various mAbs to measure their binding to Avi-GCPII (for 7E11-C5.3, a synthetic biotinylated peptide was used). "50% saturation" indicates the mAb concentration at which 50% of the maximal saturation signal was obtained. "#" stands for the number of measurements performed. "Maximal signal" shows the ratio of maximal saturation signals among all mAbs (the lowest maximal saturation signal was taken as standard). "Epitope" indicates the sequence of the biotinylated peptide used in the epitope determination assay. Positions of mAb epitopes refer to the GCPII sequence of accession number Q04609-1. The assay did not provide any positive results for J591. In the case of 7E11-C5.3, the sequence of intraGCPII peptide, which was used for measurement of saturation binding curve, is stated. The maximal signal value for 7E11-C5.3 was not calculated (NC) because a different amount of immobilized antigen was used in the experiment. 50% saturation values are shown as arithmetic means with weighted standard errors calculated from the individual measurements. The saturation curves for each mAb are shown in Fig. S1 in the Supplementary Material.

TABLE II. Characteristics of mAb Binding to Human Avi-GCPII in Native Form

Antibody	50% saturation	Maximal signal	#
D2B	0.072 ± 0.013 nM	4.8	2
J415	0.163 ± 0.022 nM	3.9	3
J591	1.40 ± 0.27 nM	6.9	3
2G7	2.89 ± 0.25 nM	1.0	2
107-1A4	3.81 ± 0.43 nM	2.6	2
24.4E6	365 ± 77 nM	NC	4
GCP-05	550 ± 130 nM	NC	2

ELISA experiments under native conditions were performed with various mAbs to measure their saturation binding curves to Avi-GCPII. "50% saturation" indicates the mAb concentration at which 50% of the maximal saturation signal was obtained. "#" stands for the number of measurements performed. "Maximal signal" shows the ratio of maximal saturation signals among all mAbs (the lowest maximal saturation signal was taken as the standard). The maximal signal values for GCP-05 and 24.4E6 were not calculated (NC) because a different amount of immobilized Avi-GCPII was used in those experiments. 50% saturation values are shown as arithmetic means with weighted standard errors calculated from the individual measurements. The saturation curves for each mAb are shown in Fig. S1 in the Supplementary Material.

saturation values (from subnanomolar for GCP-04 to submicromolar for 24.4E6 and YPSMA-2). The variation in the maximal saturation signals is even higher, with a 54-fold difference between mAbs GCP-04 and J591. In addition to the mAbs listed in Table III, we also observed detectable binding of D2B to denatured Avi-GCPII. However, due to the very low signal, we were unable to obtain an appropriate saturation-binding curve to characterize this interaction (data not shown). For measurements with 7E11-C5.3, we used a synthetic peptide (intraGCPII peptide) as antigen because the 7E11-C5.3 epitope lies within the intracellular portion of GCPII, which is not included in Avi-GCPII.

To further characterize the epitopes of the mAbs tested, we used a library of biotinylated peptides that cover the entire GCPII sequence. Using this library, we identified the epitopes of all tested mAbs except J591 and D2B. For 7E11-C5.3, GCP-04 and 24.4E6, we confirmed already known epitopes, and for 3E6, we substantially narrowed the previously suggested epitope. Furthermore, we identified the epitopes of YPSMA-1 (aa 469–486), YPSMA-2 (aa 469–486), and GCP-02 (aa 271–288).

ELISA Using Avi-GCPII Homologs

None of the tested mAbs recognize human GCPII homologs (human Avi-GCPIII, mouse Avi-GCPII, and mouse Avi-GCPIII) in native form. On the other hand, three of the 13 mAbs tested cross-react with the denatured form of the human GCPII homologs (see Table IV). GCP-02 and 3E6 recognize mouse Avi-GCPII with similar affinity as human Avi-GCPII, but GCP-02 has a much lower maximal saturation signal value toward the mouse enzyme. GCP-04 recognizes all tested homologs, binding to mouse Avi-GCPII with similar affinity as to human Avi-GCPII and recognizing both Avi-GCPIII proteins with approximately 10-fold lower affinity and threefold lower maximal saturation signal compared to their Avi-GCPII counterparts.

SPR Using Avi-GCPII in Native Form

To further characterize binding of the tested mAbs to Avi-GCPII, we determined their binding kinetics using SPR. Due to persistent problems with preparation of a stable denatured Avi-GCPII layer, we were only able to analyze mAb binding to Avi-GCPII in its native form. We performed this kinetic analysis for mAbs J415, J591, 107-1A4, D2B, and 2G7. GCP-05 and 24.4E6 did not provide sufficient signal for proper measurement.

The results (summarized in Table V) show similar kinetic profiles for mAbs J591 and 2G7, with dissociation

TABLE IV. Characteristics of mAb Binding to Denatured Avi-GCPII Homologs

Antibody	50% saturation	Maximal signal	Antigen	#
GCP-02	5.2 ± 1.2 nM	16.3	human GCPII	2
	2.52 ± 0.44 nM	1.0	mouse GCPII	3
3E6	9.8 ± 1.7 nM	1.0	human GCPII	2
	28.6 ± 3.0 nM	1.3	mouse GCPII	2
GCP-04	0.628 ± 0.066 nM	3.4	human GCPII	2
	2.62 ± 0.13 nM	2.9	mouse GCPII	2
	50.4 ± 9.3 nM	1.0	human GCPIII	2
	29.3 ± 3.3 nM	1.3	mouse GCPIII	3

ELISA experiments were performed under denaturing conditions with various mAbs to determine their binding affinity toward human Avi-GCPIII, mouse Avi-GCPII and mouse Avi-GCPIII. "50% saturation" indicates the antibody concentration at which 50% of maximal saturation signal was obtained. "#" stands for the number of measurements performed. "Maximal signal" shows the ratio of maximal saturation signals for one mAb and several GCPII homologs (the lowest maximal saturation signal was taken as the standard). 50% saturation values are shown as arithmetic means with weighted standard errors calculated from the individual measurements. The saturation curves for each mAb are shown in Fig. S1 in the Supplementary Material.

constants (K_D values) in the subnanomolar range. 107-1A4 had a very high association rate (k_{on} value) but also the highest dissociation rate (k_{off} value) leading to a similar K_D as those calculated for J591 and 2G7. J415 and D2B showed high k_{on} and very low k_{off} values. The k_{off} values were under the detection limit of our SPR instrument. However, our results indicate that the K_D

TABLE V. Kinetic Parameters of mAb Binding to Avi-GCPII in Native Form

Antibody	k_{on} $[10^4$ $(M^*s)^{-1}]$	k_{off} $[10^{-5}$ $s^{-1}]$	K_D $[10^{-9}$ M]
J415	110.5 ± 3.5	< 2	< 0.018
D2B	49.2 ± 3.1	< 2	< 0.041
107-1A4	46.1 ± 1.3	10.2 ± 3.8	0.221 ± 0.083
2G7	11.45 ± 0.78	4.1 ± 1.5	0.36 ± 0.13
J591	11.15 ± 0.64	8.4 ± 1.5	0.75 ± 0.14

Recombinant human Avi-GCPII was immobilized via biotin to the SPR chip. Four different concentrations of each mAb were applied to the layer, and their association and dissociation curves were measured. Each measurement was performed twice. The k_{on} and k_{off} values represent the average of both measurements with the deviation from the mean. The k_{off} values of J415 and 107-1A4 were below the detection limit of our SPR sensor and thus could not be reliably determined. The fitted binding curves for each mAb are shown in Figure S2 in the Supplementary Material.

The Prostate

values for these two mAbs are in the picomolar range. The SPR results are in agreement with the results from ELISA experiments, in which mAbs J415 and D2B displayed the lowest 50% saturation values.

Qualitative Analysis

To obtain additional information about the characteristics of the tested mAbs, we compared them using three basic techniques: Western blot (WB), immunohistochemistry (IHC) and flow cytometry (FC). In the WB analysis, the protein samples are denatured; therefore, we analyzed only those mAbs capable of binding to denatured GCPII. In the other two methods, we exploited a larger pool of mAbs because the methods can be performed under both native and denaturing conditions.

Comparison of mAbs in Western Blot

We used mAbs GCP-02, GCP-04, 3E6, YPSMA-1, YPSMA-2, 24.4E6, J591, D2B, and 7E11-C5.3 to detect GCPII by Western blot (see Fig. 1). Our sample set contained a dilution series of purified human Avi-GCPII and its three homologs, lysate from LNCaP cells (a cell line endogenously expressing GCPII) and lysate from prostate adenocarcinoma tissue (only the latter two samples were used with 7E11-C5.3 because this mAb has an intracellular epitope and thus does not recognize the recombinant protein constructs).

Our results show that all the mAbs are able to detect GCPII under WB conditions. Based on signal strength, the mAbs can be divided into three groups: (a) GCP-02, GCP-04 and YPSMA-1, yielding a strong signal even for low amounts of Avi-GCPII and lysates; (b) 3E6, YPSMA-2 and 7E11-C5.3, providing an average signal for detection of GCPII in lysates and the highest concentration of Avi-GCPII; and (c) 24.4E6, J591 and D2B, showing weak signals (for D2B, we had to increase the mAb concentration to obtain a detectable signal). Additionally, only mAbs GCP-02, GCP-04, and 3E6 were able to detect some of the human Avi-GCPII homologs, which is in agreement with
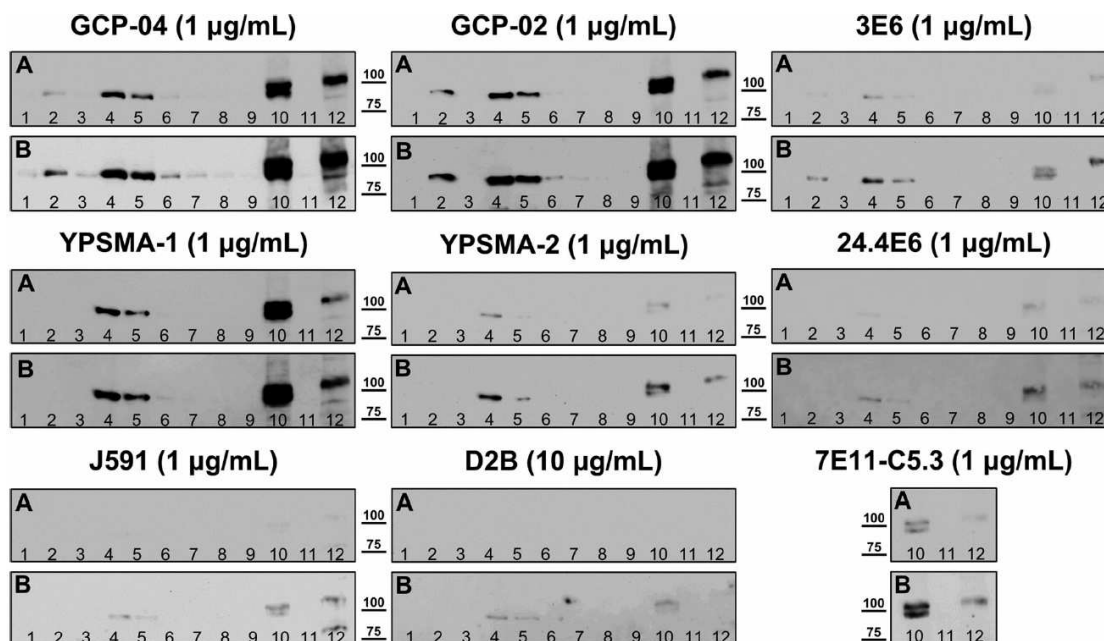

Fig. 1. Western blot detection of human GCPII and its homologs by anti-GCPII mAbs. Samples of purified human Avi-GCPII and its homologs (human Avi-GCPIII, mouse Avi-GCPII and Avi-GCPIII), lysate from LNCaP cells and lysate from prostate adenocarcinoma tissue were resolved by SDS-PAGE, blotted onto nitrocellulose membranes and incubated with various mAbs. Sample legend: 1. mouse Avi-GCPIII – 10 ng, 2. mouse Avi-GCPII – 10 ng, 3. human Avi-GCPIII – 10 ng, 4. human Avi-GCPII – 10 ng, 5. human Avi-GCPII – 5 ng, 6. human Avi-GCPII – 1 ng, 7. human Avi-GCPII – 500 pg, 8. human Avi-GCPII – 200 pg, 9. empty line, 10. LNCaP lysate – 20 μg total protein 11. empty line, 12. prostate adenocarcinoma lysate – 50 μg total protein. The chemiluminiscence detection was performed identically for all mAbs. **A:** Figures were not processed with a graphical editor. **B:** Contains the same figures as in panels A, but processed with a graphical editor (changes in color contrast and levels) to highlight the chemiluminiscence signal.

results from ELISA. In Figure 1, panels "A" serve for proper comparison of the signal outputs of the tested mAbs (images were not processed with a graphical editor), while panels "B" show images that were individually processed with a graphical editor to highlight the chemiluminiscence signal.

Comparison of mAbs in Immunohistochemistry

We prepared formalin-fixed paraffin-embedded tissue sections (this preparation method leads to complete denaturation of the sample proteins) from high-grade prostate adenocarcinoma and tested the ability of our mAb panel to visualize GCPII. We tested the mAbs at a concentration of $10 \, \mu g/ml$. As shown in Figure 2, only mAbs GCP-02, GCP-04, YPSMA-1, YPSMA-2, 3E6, and 24.4E6 provide visible staining of GCPII in tissue sections. Even though the strength of staining is different among these six mAbs, they all provided clear visualization of GCPII.

Additionally, we performed an experiment with these mAbs to map the dependence of the output signal on the mAb working concentration. As shown in Figure 3, all tested mAbs were able to visualize GCPII in tissue sections at a concentration $0.1 \, \mu g/ml$, and GCP-04 was effective even at concentration $0.01 \, \mu g/ml$.

Comparison of mAbs in Flow Cytometry

To assess the ability of the tested mAbs to bind GCPII in native form, we used flow cytometry and evaluated their binding to two prostate cancer cell lines: one endogenously expressing GCPII (LNCaP) and one lacking this expression (PC3). We incubated live cells with mAbs ($10 \, \mu g/ml$ final concentration) and investigated the potential binding.

Results from these experiments are summarized in Figure 4. Based on the overall fluorescent signal of the cells, the mAbs can be divided into two groups: a) mAbs that bind to LNCaP but not to PC3: J591, D2B, 107-1A4, J415, GCP-05, and 2G7 and b) mAbs that do not bind either LNCaP or PC3 cells: 24.4E6, GCP-02, GCP-04, 7E11-C5.3, YPMSA-1, YPSMA-2, and 3E6 (see Fig. 4A).

Additionally, the mAbs binding to LNCaP cells can be further divided based on their ability to distinguish the LNCaP and PC3 cell populations. J591, D2B, 107-1A4, GCP-05, and J415 are able to separate these populations quantitatively, while 2G7 provides approximately 60% separation of these populations (see Fig. 4B).

The results from all our presented experiments are summarized in a simplified form in Table VI. All tested mAbs are marked with "$+/-$" signs to indicate their

TABLE VI. Summary of Basic Characteristics of Anti-GCPII mAbs

Antibody	GCPII in native form		GCPII in denatured form		
	ELISA	FC	ELISA	WB	IHC-P
J591	+++	+++	+	+	−
J415	+++	+++	−	−	−
D2B	+++	+++	+	+	−
107-1A4	+++	+++	−	−	−
2G7	++	++	−	−	−
GCP-05	+	+++	−	−	−
7E11-C5.3*	++	−	++	++	−
GCP-02	−	−	+++	+++	+++
GCP-04	−	−	+++	+++	+++
YPSMA-1	−	−	++	+++	+++
YPSMA-2	−	−	++	++	+++
3E6	−	−	++	++	++
24.4E6	+	−	+	+	++

*for this mAb the intraGCPII peptide was used as antigen instead of GCPII protein. ELISA, enzyme-linked immunosorbent assay; WB, Western blot; FC, flow cytometry performed under native conditions; IHC-P, immunohistochemistry performed on paraffin-embedded tissue sections.

efficacy in the appropriate method ("$+++$" meaning the highest efficacy and "$-$" meaning not working at all).

Discussion

The form of the antigen (native or denatured) that a mAb recognizes and its appropriate binding constants are the two features that should suffice for the proper utilization of a given mAb. Therefore, in our study we did not aim to compare the efficacies of all mAbs in all applicable methods, but rather quantitatively analyze the binding of collected mAbs to their antigens. Our results, together with the understanding of a particular method's principles and some basic biochemical knowledge, should allow researchers to select the best mAb and conditions for their particular experiments.

Evaluation of Quantitative Analysis Data

The data obtained from quantitative analysis of mAbs from ELISA experiments can be used to estimate the efficacies of the mAbs in other methods, such as WB, IHC, and FC. We can evaluate this assumption based on the results presented in this study, including the 50% saturation value (which reflects binding affinity) and the maximal saturation signal obtained from ELISA analysis. Comparing
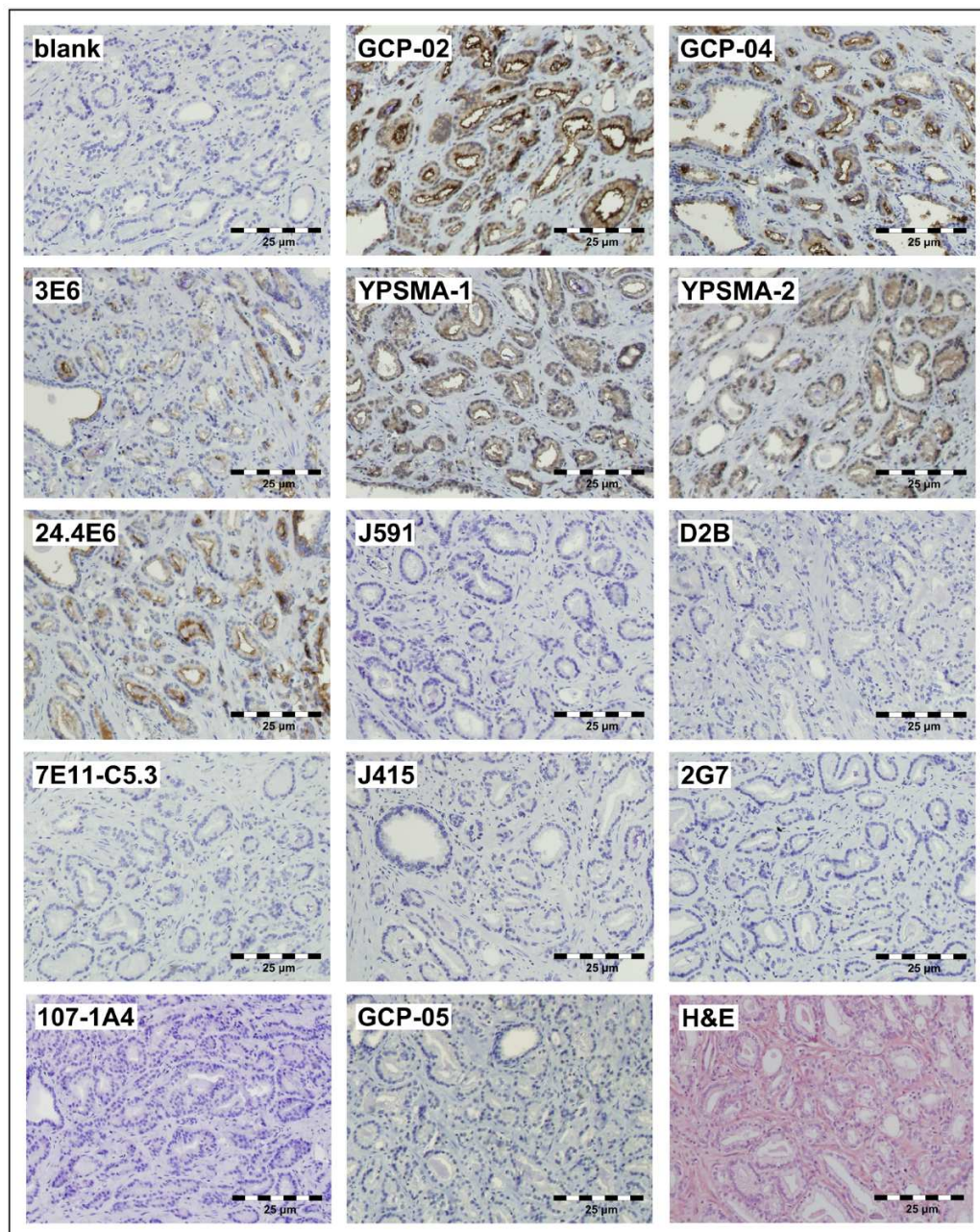
Fig. 2. Immunohistological staining of prostate adenocarcinoma tissue sections with anti-GCPII mAbs. Formalin-fixed paraffin-embedded sections were subjected to the panel of mAbs (all at 10 μg/ml concentration) to compare their abilities to visualize GCPII. The immunoperoxidase method was used for visualization of antibody-antigen complexes, followed by counterstaining with Harris' hematoxylin. Routine hematoxylin and eosin staining (H&E) was also performed to determine the morphological features of the cancer tissue. The specificity of staining was confirmed by processing one slide with omission of the primary antibody (blank).
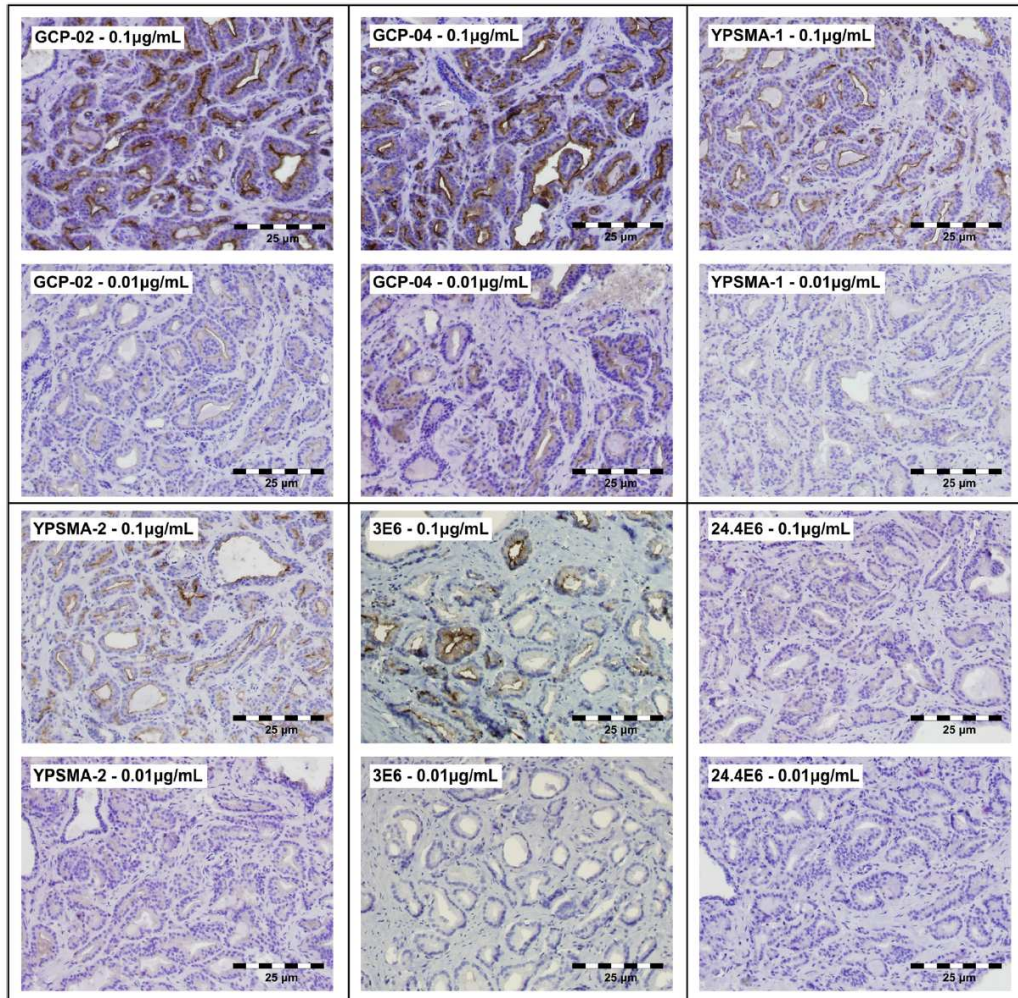
Fig. 3. Immunohistological staining of prostate adenocarcinoma tissue sections by different concentration of various anti-GCPII mAbs. Formalin-fixed paraffin-embedded tissue sections were subjected to two different concentrations (0.1 μg/ml and 0.01 μg/ml) of GCP-02, GCP-04, YPSMA-1, YPSMA-2, 3E6 and 24.4E6. The immunoperoxidase method was used for visualization of bound mAbs, followed by counterstaining with Harris' hematoxylin.

the 50% saturation value to the working mAb concentration used in a certain method (e.g., WB) indicates whether the mAb is saturated with the particular antigen. The maximal saturation signal provides an estimate of the maximal signal output given by the mAb in a particular method. However, it is important to keep in mind that these are only rough estimates because the conditions used for the method studied (e.g., WB) differ slightly from the conditions used for quantitative analysis (e.g., ELISA).

GCP-02 and GCP-04 should provide the best WB results based on the ELISA experiments, and they are indeed the most sensitive mAbs from the panel. YPSMA-2 has a high maximal saturation signal as well, but also a high 50% saturation value (the working concentration of mAbs in WB was approximately 7 nM). Therefore, it did not provide a very strong signal. In this case, increasing the mAb concentration should significantly improve the signal output. On the other hand, increasing the mAb concentration is unlikely to greatly improve the results for J591 and
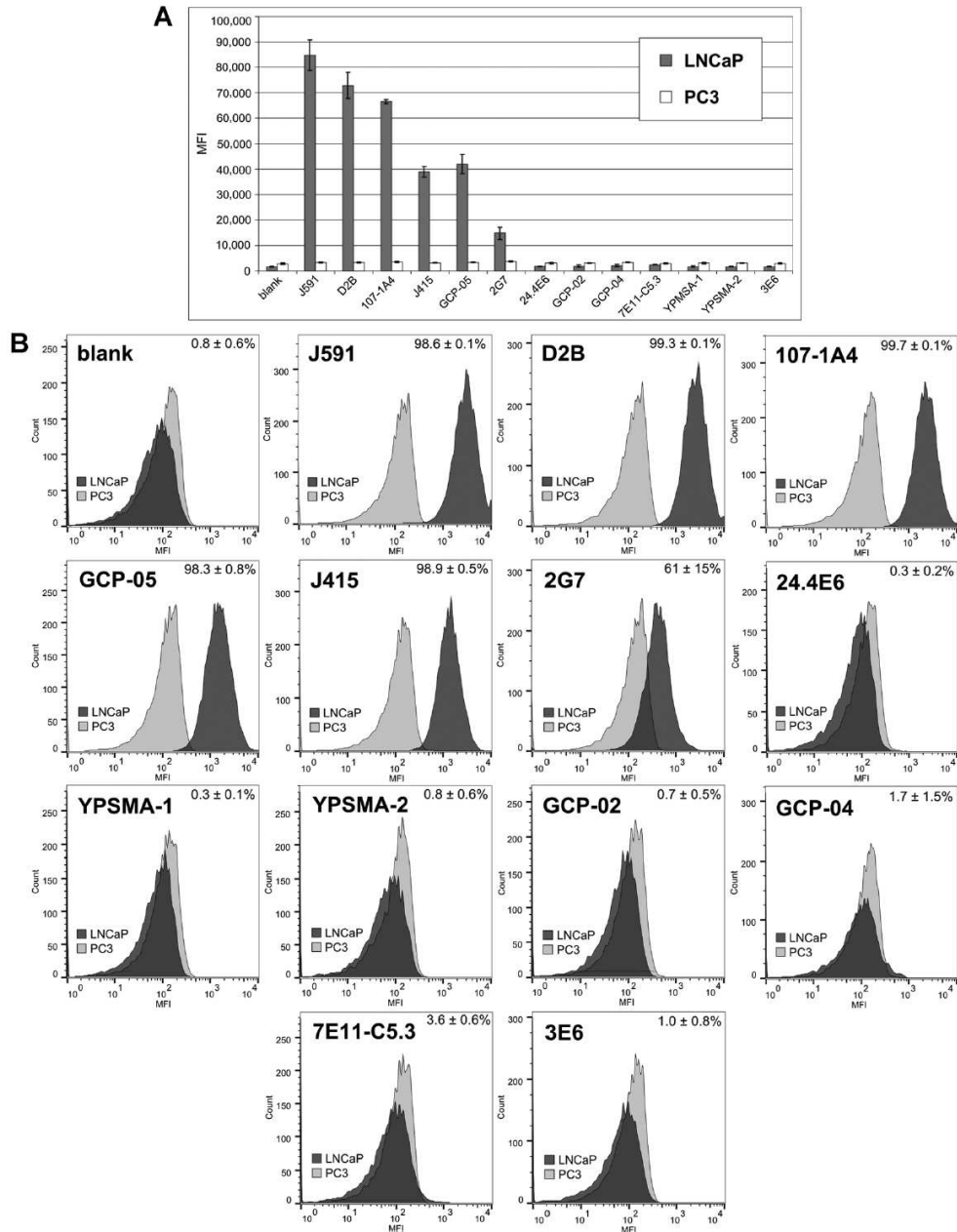
Fig. 4. Flow cytometry analysis of mAb binding efficacy to viable prostate cancer cell lines. Single cell suspensions of cell lines that possess (LNCaP) or lack (PC3) endogenous GCPII expression were mixed with the tested mAbs. The antibody-antigen complex was subsequently visualized by phycoerythrin-conjugated secondary antibody followed by flow cytometry analysis. For each measurement, 10,000 events (gated to analyze only living cells) were processed. **A:** Graph showing the mean fluorescent intensity (MFI) of each mAb for either LNCaP or PC3 cells. Each experiment was run in triplicate, and error bars represent the standard deviation. **B:** A series of histograms for each mAb showing the population distribution based on the fluorescent intensity. Each histogram was created from a single representative experiment. The LNCaP population is shown in dark grey and the PC3 population in light grey. The number in the top right corner of each histogram indicates the percentage of the LNCaP population that has a higher MFI signal than the highest 5% of the PC3 population. This number was calculated for each measurement (performed in triplicate), and the mean $\pm$ SEM is presented.

The Prostate

3E6 because they already have very low 50% saturation values, and their weak signals are likely caused by their low maximal saturation values.

A quantitative comparison of IHC staining is very difficult to perform. Nevertheless, it appears that GCP-02 and GCP-04 provided the strongest signals (see Fig. 2). The working concentration of mAbs in IHC was approximately 70 nM. Such a concentration should, based on the results from ELISA, provide the maximal saturation signal for all mAbs except YPSMA-1, YPSMA-2, and 24.4E6. For those mAbs, an additional increase in concentration should improve the signal output obtained upon staining. Even though we showed that many of the tested mAbs also work at lower concentrations (as low as 0.07 nM for GCP-04), it should be noted that we analyzed a sample of high-grade prostate adenocarcinoma with very high expression of GCPII; the expression will likely be much lower in other tissues. Therefore, we recommend following the 50% saturation values determined by ELISA (concentrations 10-fold higher than the 50% saturation value should provide the highest signal output) to estimate an appropriate mAb concentration for IHC experiments.

Interestingly, the mAb 7E11-C5.3 did not provide any visible staining in our IHC experiments, even though there is clear and repeated evidence of its expected "positive" performance throughout the literature (see references in Table I). To elucidate this result, we performed an additional experiment with two different antigen retrieval buffers (acidic and basic). This experiment showed that even though basic retrieval buffer slightly improved the staining, 7E11-C5.3 still provides very weak to no signal (see Fig. S3). This might indicate that the intracellular epitope of GCPII was not accessible under our experimental conditions (perhaps due to the cross-linking with the surrounding intracellular proteins during the fixation step by formaldehyde), suggesting that the IHC protocol would require additional optimization to work efficiently for this particular mAb. This result favors mAbs with epitopes located in the extracellular portion of GCPII (e.g., GCP-04 or YPSMA-1) over 7E11-C5.3, because these mAbs likely do not require such stringent and optimized experimental conditions to work efficiently.

Data from FC experiments are in general agreement with the estimations made from the ELISA results. J591, J415, D2B, and 107-1A4 provided the highest signals and full separation of the GCPII-positive and GCPII-negative cell populations. 2G7 showed average separation, which is probably caused by its low maximal signal value. mAb 7E11-C5.3 did not bind to viable LNCaP cells because the mAb was likely unable to access its intracellular epitope in our experimental

setup. Both 24.4E6 and 7E11-C5.3 were also tested in FC at a higher concentration (100 µg/ml), yielding the same negative results (data not shown).

Discrepancies in Proposed mAb Efficacies

Taken together, the results of our quantitative analysis can be used to estimate mAb efficacy in other methods. Nevertheless, we observed several examples of poor data correlation; namely, 7E11-C5.3 efficacy in IHC and FC, GCP-05 and 24.4E6 efficacy in FC and YPSMA-1 efficacy in WB. As discussed earlier, 7E11-C5.3 behaved differently than other tested mAbs mainly due to its different epitope localization (intracellular vs. extracellular).

GCP-05, which bound to Avi-GCPII weakly in ELISA, provided very good results in FC experiments. On the other hand mAb 24.4E6, which showed similar affinity to Avi-GCPII as GCP-05 in the ELISA assay, did not work in FC at all. There are at least two potential explanations for these discrepancies. First, there is a difference in experimental conditions (e.g., working with immobilized antigen in ELISA vs. working in solution in FC and use of different secondary antibodies or different binding buffers). This problem cannot be overcome and must always be taken into account. Second, the antigens used for ELISA and FC originate from different sources. We performed the ELISA experiments with recombinant Avi-GCPII protein expressed in insect cells, while FC was performed with human cell lines. Even though it has been repeatedly shown that the extracellular portion of GCPII produced in insect cells is properly folded, enzymatically active protein [64,67], there is a difference in the protein's post-translational modification, namely N-glycosylation, compared to that of its mammalian counterpart.

There is little information about the epitopes of mAbs binding to GCPII in native form and therefore we can only speculate about the influence of N-glycosylation on the binding of GCP-05. On the other hand, we have determined the approximate epitopes of mAbs that bind to denatured Avi-GCPII. As shown in Fig. S4, the epitope of 24.4E6 does not contain an N-glycosylation site, and therefore the discrepant results obtained from ELISA and FC experiments cannot be explained by this phenomenon. Contrary to 24.4E6 the determined epitope sequences of YPSMA-1, YPSMA-2, and 3E6 contain Asn residue which is N-glycosylated suggesting that these three mAbs could bound differently to GCPII expressed in insect and mammalian cells. However, the results from WB experiment where both recombinant Avi-GCPII from insect cells and endogenous GCPII were detected (see Fig. 1) shows that these mAbs recognize both forms of GCPII with similar affinity and

thus N-glycosylation does not play role in the recognition of GCPII by these mAbs.

Specificity of mAbs Against Different Forms of GCPII

Our results suggest that most mAbs recognize GCPII either in its native or denatured form. The exceptions are 24.4E6 and 7E11-C5.3 because their epitopes probably adopt the same conformation regardless of the GCPII state. Additionally, we observed binding of J591 and D2B to denatured GCPII, but in comparison to their affinity toward the native protein, this binding was negligible. We hypothesize that the process of denaturation in some methods was incomplete, and a small portion of the protein (or at least the appropriate antibody epitope) remained in the native state. This hypothesis is supported by the fact that epitope determination assays using the panel of synthetic peptides were inconclusive for J591 and D2B. This would suggest that these mAbs require some additional structural motive (secondary structure) for efficient binding and they do not bind to a single unstructured polypeptide chain.

On the other hand, 24.4E6 showed very similar binding to Avi-GCPII in both native and denaturing ELISA setups. Since for this particular mAb the amount of immobilized Avi-GCPII was identical (10 ng per well) in both experiments, the incomplete denaturation of Avi-GCPII in the denaturing ELISA setup or partial denaturation of Avi-GCPII in the native ELISA setup would not explain the observed binding. In addition, the epitope determination assay provided a positive result for 24.4E6, unlike J591 and D2B. Both facts support the finding that 24.4E6 can bind to both the native and denatured forms of Avi-GCPII.

Results from the epitope determination assay were also helpful in predicting and validating the cross-reactivities of the mAbs with close GCPII homologs in denatured form. In this case, cross-reactivity is exclusively dependent on the protein sequence similarity. Therefore, it was not surprising to observe cross-reactivity of 3E6 with mouse Avi-GCPII because the 3E6 epitope sequences of mouse and human GCPII are identical (see Fig. S4). We can also turn this approach around and narrow the determined 18 aa epitope for YPSMA-1 and YPSMA-2, which do not recognize mouse Avi-GCPII. Because the only difference between human and mouse GCPII in this region is Lys482, which is a Gln residue in mouse GCPII, the epitopes of these mAbs are likely located around this residue. Interestingly, the determined epitope for YPSMA-1 does not correspond to the suggested epitope (aa 716–723;

information taken from Abcam datasheet). To address this discrepancy, we tested two different batches of YPSMA-1, from Anogen and Abcam. Both these mAbs provided identical results in our epitope determination assay.

Advantages and Disadvantages of the Comparative Analysis Approach

Finally, we should note that we performed all qualitative experiments with the same mAb concentrations (with the exception of D2B in WB) because we focused primarily on comparative analysis of the tested mAbs. The consequence of this approach was that in some cases we performed an experiment with a mAb concentration that was too low compared to its corresponding 50% saturation value (e.g., YPSMA-2 in WB) and thus did not obtain optimal results.

Additionally, direct comparison of our results with those presented in the literature is difficult because use of different instrumentation and protocols can influence the results. Therefore, we decided to perform a large-scale comparative study of anti-GCPII mAbs rather than characterize only mAbs developed in our lab. For example, our results do not disprove the fact that J591 can recognize GCPII with sufficient sensitivity in WB if the experiment is performed with a different blotting device or by using a different blotting membrane or secondary antibody compared to our WB protocol [2] (in that study, 100 nM J591 was used). On the other hand, the result suggesting that J591 works with similar efficacy as GCP-04 in WB as presented by Wang et al. is quite surprising in light of our observations [58].

General Remarks on the Lack of Experimental Details in the Scientific Literature

Because comparative studies of mAbs in this field are lacking, it is very challenging to compare published results and determine their biological and/or clinical relevance. The situation is further complicated by the fact that the experimental sections of published papers often lack sufficient and precise descriptions of the experimental setups. For example, the amount of protein sample loaded onto a WB or the exact concentration of primary antibody used is often not mentioned in the figure legend or Methods section [20,39,48]. Sometimes, even the name of the mAb is not stated clearly and a generalized denotation, such as "antibody purchased from Abcam," is given instead (Abcam currently provides more than 30 different mAbs against GCPII) [68].

It is even more complicated for methods such as IHC or ICC, because these methods can generally be

performed under either native or denaturing conditions. Therefore, even if the mAb is suggested for use in IHC or ICC by its manufacturer, the researcher should always attempt to check the exact experimental conditions. For example, IHC from frozen tissue sections is generally thought to visualize antigen in its native form. But the experimental protocol often includes fixation with acetone or methanol, which leads to complete denaturation of the sample and therefore requires different mAbs for proper visualization. If these seemingly minor differences are not stated explicitly, it may lead to confusion. In the case of YPSMA-1, several manufacturers state that it works in ICC and IHC-Fr. These methods are generally thought to visualize native proteins. Therefore, it is not surprising that some studies used YPSMA-1 in experimental setups in which GCPII in native form was targeted, even though based on our results YPSMA-1 binds solely to denatured GCPII [10,69].

To avoid such pitfalls, precise description of experimental details is essential. Unfortunately, this is not the case for many studies, which use mAbs to visualize GCPII. For example, the dilution rather than the working concentration of 3E6, the most frequently used mAb for visualizing GCPII in IHC experiments, is almost exclusively stated in the literature [22,49–51]. Unfortunately, 3E6 is provided as dialyzed supernatant with its concentration determined by the producer, and this concentration varies batch-to-batch. For example, we used two batches of 3E6 (#10041132 and #10067501, which were provided at concentrations of $283\,\mu g/ml$ and $81\,\mu g/ml$, respectively) in our study. With such a difference in concentrations between the batches, it is not surprising that the dilution of 3E6 used varies from 1:20 to 1:200 in the literature [22,51]. Clearly, in this case there is no way to calculate the actual working concentration of 3E6. It is also worth noting that the customer purchases a volume of supernatant, so the actual amount of mAb purchased differs for each batch.

The lack of detailed information regarding experimental procedures may be partially caused by the ongoing efforts of scientific journals to reduce the length of published articles as much as possible; the Materials and Methods sections are most often the first choice for truncation. Even though this effort is understandable, it should not be done at the expense of scientific accuracy. The authors may try to overcome this issue by providing a simplified method description in the main text and full detailed experimental descriptions in the Supplementary Material (as is already suggested by some of scientific journals, e.g., *Science*).

CONCLUSION

We performed a thorough comparative analysis of 13 mAbs against GCPII. We divided them based on their abilities to bind GCPII in either native or denatured form and compared their efficacies in basic molecular biology methods (WB, IHC, and FC). We believe that our observations will help dissect some of the discrepancies in the published results and that they will be useful in helping researchers choose the most appropriate mAb for their experimental setup. We also dare to hope that the common inaccuracies in method descriptions that we pointed out will become less frequent in the future.

ACKNOWLEDGEMENT

REFERENCES

1. Ghosh A, Heston WD. Tumor target prostate specific membrane antigen (PSMA) and its regulation in prostate cancer. J Cell Biochem 2004;91(3):528–539.

2. Liu H, Moy P, Kim S, Xia Y, Rajasekaran A, Navarro V, Knudsen B, Bander NH. Monoclonal antibodies to the extracellular domain of prostate-specific membrane antigen also react with tumor vascular endothelium. Cancer Res 1997;57(17):3629–3634.

3. Silver DA, Pellicer I, Fair WR, Heston WD, Cordon-Cardo C. Prostate-specific membrane antigen expression in normal and malignant human tissues. Clin Cancer Res 1997;3(1):81–85.

4. Foss CA, Mease RC, Cho SY, Kim HJ, Pomper MG. GCPII imaging and cancer. Curr Med Chem 2012;19(9):1346–1359.

5. Mesters JR, Barinka C, Li W, Tsukamoto T, Majer P, Slusher BS, Konvalinka J, Hilgenfeld R. Structure of glutamate carboxypeptidase II, a drug target in neuronal damage and prostate cancer. EMBO J 2006;25(6):1375–1384.

6. Liu H, Rajasekaran AK, Moy P, Xia Y, Kim S, Navarro V, Rahmati R, Bander NH. Constitutive and antibody-induced

internalization of prostate-specific membrane antigen. Cancer Res 1998;58(18):4055–4060.

7. Javier DJ, Nitin N, Levy M, Ellington A, Richards-Kortum R. Aptamer-targeted gold nanoparticles as molecular-specific contrast agents for reflectance imaging. Bioconjug Chem 2008;19(6):1309–1312.

8. Kasten BB, Liu T, Nedrow-Byers JR, Benny PD, Berkman CE. Targeting prostate cancer cells with PSMA inhibitor-guided gold nanoparticles. Bioorg Med Chem Lett 2013;23(2):565–568.

9. Schol D, Fleron M, Greisch JF, Jaeger M, Frenz M, De Pauw E, De Pauw-Gillet MC. Anti-PSMA antibody-coupled gold nano-rods detection by optical and electron microscopies. Micron 2013;50:68–74.

10. Wang L, Li L, Guo Y, Tong H, Fan X, Ding J, Huang H. Construction and in vitro/in vivo targeting of PSMA-targeted nanoscale microbubbles in prostate cancer. Prostate 2013;73(11):1147–1158.

11. Xu W, Siddiqui IA, Nihal M, Pilla S, Rosenthal K, Mukhtar H, Gong S. Aptamer-conjugated and doxorubicin-loaded unimolec-ular micelles for targeted therapy of prostate cancer. Biomaterials 2013;34(21):5244–5253.

12. Osborne JR, Akhtar NH, Vallabhajosula S, Anand A, Deh K, Tagawa ST. Prostate-specific membrane antigen-based imaging. Urol Oncol 2013;31(2):144–154.

13. Vacchelli E, Aranda F, Eggermont A, Galon J, Sautes-Fridman C, Zitvogel L, Kroemer G, Galluzzi L. Trial watch: Tumor-targeting monoclonal antibodies in cancer therapy. Oncoimmunology 2014;3(1):e27048.

14. Vacchelli E, Vitale I, Tartour E, Eggermont A, Sautes-Fridman C, Galon J, Zitvogel L, Kroemer G, Galluzzi L. Trial watch: Anticancer radioimmunotherapy. Oncoimmunology 2013;2(9):e25595.

15. Vacchelli E, Eggermont A, Galon J, Sautes-Fridman C, Zitvogel L, Kroemer G, Galluzzi L. Trial watch: Monoclonal antibodies in cancer therapy. Oncoimmunology 2013;2(1):e22789.

16. Al-Ahmadie HA, Olgac S, Gregor PD, Tickoo SK, Fine SW, Kondagunta GV, Scher HI, Morris MJ, Russo P, Motzer RJ, Reuter VE. Expression of prostate-specific membrane antigen in renal cortical tumors. Mod Pathol 2008;21(6):727–732.

17. Baccala A, Sercia L, Li J, Heston W, Zhou M. Expression of prostate-specific membrane antigen in tumor-associated neo-vasculature of renal neoplasms. Urology 2007;70(2):385–390.

18. Chang SS, Reuter VE, Heston WD, Bander NH, Grauer LS, Gaudin PB. Five different anti-prostate-specific membrane anti-gen (PSMA) antibodies confirm PSMA expression in tumor-associated neovasculature. Cancer Res 1999;59(13):3192–3198.

19. Lopes AD, Davis WL, Rosenstraus MJ, Uveges AJ, Gilman SC. Immunohistochemical and pharmacokinetic characterization of the site-specific immunoconjugate CYT-356 derived from antiprostate monoclonal antibody 7E11-C5. Cancer Res 1990;50(19):6423–6429.

20. Kinoshita Y, Kuratsukuri K, Landas S, Imaida K, Rovito PM Jr, Wang CY, Haas GP. Expression of prostate-specific membrane antigen in normal and malignant human tissues. World J Surg 2006;30(4):628–636.

21. Mhawech-Fauceglia P, Zhang S, Terracciano L, Sauter G, Chadhuri A, Herrmann FR, Penetrante R. Prostate-specific membrane antigen (PSMA) protein expression in normal and neoplastic tissues and its sensitivity and specificity in prostate adenocarcinoma: An immunohistochemical study using mutiple tumour tissue microarray technique. Histopathology 2007;50(4):472–483.

22. Haffner MC, Kronberger IE, Ross JS, Sheehan CE, Zitt M, Muhlmann G, Ofner D, Zelger B, Ensinger C, Yang XJ, Geley S, Margreiter R, Bander NH. Prostate-specific membrane antigen expression in the neovasculature of gastric and colorectal cancers. Hum Pathol 2009;40(12):1754–1761.

23. Rovenska M, Hlouchova K, Sacha P, Mlcochova P, Horak V, Zamecnik J, Barinka C, Konvalinka J. Tissue expression and enzymologic characterization of human prostate specific mem-brane antigen and its rat and pig orthologs. Prostate 2008; 68(2):171–182.

24. Troyer JK, Beckett ML, Wright GL Jr. Detection and characteri-zation of the prostate-specific membrane antigen (PSMA) in tissue extracts and body fluids. Int J Cancer 1995;62(5):552–558.

25. Sokoloff RL, Norton KC, Gasior CL, Marker KM, Grauer LS. A dual-monoclonal sandwich assay for prostate-specific membrane antigen: Levels in tissues, seminal fluid and urine. Prostate 2000;43(2):150–157.

26. Ellis RJ, Kaminsky DA, Zhou EH, Fu P, Chen WD, Brelin A, Faulhaber PF, Bodner D. Ten-year outcomes: The clinical utility of single photon emission computed tomography/computed tomography capromab pendetide (Prostascint) in a cohort diagnosed with localized prostate cancer. Int J Radiat Oncol Biol Phys 2011;81(1):29–34.

27. Han M, Partin AW. Current clinical applications of the in-capromab pendetide scan (prostascint(r) scan, cyt-356). Rev Urol 2001;3(4):165–171.

28. Hinkle GH, Burgers JK, Neal CE, Texter JH, Kahn D, Williams RD, Maguire R, Rogers B, Olsen JO, Badalament RA. Multicenter radioimmunoscintigraphic evaluation of patients with prostate carcinoma using indium-111 capromab pendetide. Cancer 1998; 83(4):739–747.

29. Horoszewicz JS, Kawinski E, Murphy GP. Monoclonal antibodies to a new antigenic marker in epithelial prostatic cells and serum of prostatic cancer patients. Anticancer Res 1987;7(5B):927–935.

30. Troyer JK, Feng Q, Beckett ML, Wright GL Jr. Biochemical characterization and mapping of the 7E11-C5. 3 epitope of the prostate-specific membrane antigen. Urol Oncol 1995;1(1):29–37.

31. Tagawa ST, Milowsky MI, Morris M, Vallabhajosula S, Christos P, Akhtar NH, Osborne J, Goldsmith SJ, Larson S, Taskar NP, Scher HI, Bander NH, Nanus DM. Phase II study of Lutetium-177-labeled anti-prostate-specific membrane antigen monoclonal antibody J591 for metastatic castration-resistant prostate cancer. Clin Cancer Res 2013;19(18):5182–5191.

32. Tagawa ST, Akhtar NH, Nikolopoulou A, Kaur G, Robinson B, Kahn R, Vallabhajosula S, Goldsmith SJ, Nanus DM, Bander NH. Bone marrow recovery and subsequent chemotherapy following radiolabeled anti-prostate-specific membrane antigen monoclonal antibody j591 in men with metastatic castration-resistant prostate cancer. Front Oncol 2013;3:214.

33. Holland JP, Divilov V, Bander NH, Smith-Jones PM, Larson SM, Lewis JS. 89Zr-DFO-J591 for immunoPET of prostate-specific membrane antigen expression in vivo. J Nucl Med 2010;51(8):1293–1300.

34. Moffatt S, Papasakelariou C, Wiehle S, Cristiano R. Successful in vivo tumor targeting of prostate-specific membrane antigen with a highly efficient J591/PEI/DNA molecular conjugate. Gene Ther 2006;13(9):761–772.

35. Patri AK, Myc A, Beals J, Thomas TP, Bander NH, Baker JR Jr. Synthesis and in vitro testing of J591 antibody-dendrimer conjugates for targeted prostate cancer therapy. Bioconjug Chem 2004;15(6):1174–1181.

- 53 -

36. Kampmeier F, Williams JD, Maher J, Mullen GE, Blower PJ. Design and preclinical evaluation of a 99mTc-labelled diabody of mAb J591 for SPECT imaging of prostate-specific membrane antigen (PSMA). EJNMMI Res 2014;4(1):13.

37. Bandekar A, Zhu C, Jindal R, Bruchertseifer F, Morgenstern A, Sofou S. Anti-prostate-specific membrane antigen liposomes loaded with 225Ac for potential targeted antivascular alpha-particle therapy of cancer. J Nucl Med 2014;55(1):107–114.

38. Zhang F, Shan L, Liu Y, Neville D, Woo JH, Chen Y, Korotcov A, Lin S, Huang S, Sridhar R, Liang W, Wang PC. An anti-PSMA bivalent immunotoxin exhibits specificity and efficacy for prostate cancer imaging and therapy. Adv Healthc Mater 2013;2(5):736–744.

39. Baiz D, Hassan S, Choi YA, Flores A, Karpova Y, Yancey D, Pullikuth A, Sui G, Sadelain M, Debinski W, Kulik G. Combination of the PI3K inhibitor ZSTK474 with a PSMA-targeted immunotoxin accelerates apoptosis and regression of prostate cancer. Neoplasia 2013;15(10):1172–1183.

40. Lutje S, Rijpkema M, Franssen GM, Fracasso G, Helfrich W, Eek A, Oyen WJ, Colombatti M, Boerman OC. Dual-modality image-guided surgery of prostate cancer with a radiolabeled fluorescent anti-psma monoclonal antibody. J Nucl Med 2014.

41. Colombatti M, Grasso S, Porzia A, Fracasso G, Scupoli MT, Cingarlini S, Poffe O, Naim HY, Heine M, Tridente G, Mainiero F, Ramarli D. The prostate specific membrane antigen regulates the expression of IL-6 and CCL5 in prostate tumour cells by activating the MAPK pathways. PLoS One 2009;4(2): e4608.

42. Frigerio B, Fracasso G, Luison E, Cingarlini S, Mortarino M, Coliva A, Seregni E, Bombardieri E, Zuccolotto G, Rosato A, Colombatti M, Canevari S, Figini M. A single-chain fragment against prostate specific membrane antigen as a tool to build theranostic reagents for prostate cancer. Eur J Cancer 2013;49(9): 2223–2232.

43. Schmidt S, Fracasso G, Colombatti M, Naim HY. Cloning and characterization of canine prostate-specific membrane antigen. Prostate 2013;73(6):642–650.

44. Schmidt S, Gericke B, Fracasso G, Ramarli D, Colombatti M, Naim HY. Discriminatory role of detergent-resistant membranes in the dimerization and endocytosis of prostate-specific membrane antigen. PLoS One 2013;8(6):e66193.

45. Lutje S, van Rij CM, Franssen GM, Fracasso G, Helfrich W, Eek A, Oyen WJ, Colombatti M, Boerman OC. Targeting human prostate cancer with In-labeled D2B IgG, F(ab') and Fab fragments in nude mice with PSMA-expressing xenografts. Contrast Media Mol Imaging 2014.

46. Brown LG, Wegner SK, Wang H, Buhler KR, Arfman EW, Lange PH, Vessella RL. A novel monoclonal antibody 107-1A4 with high prostate specificity: Generation, characterization of antigen expression, and targeting of human prostate cancer xenografts. Prostate Cancer Prostatic Dis 1998;1(4):208–215.

47. Wang S, Diamond DL, Hass GM, Sokoloff R, Vessella RL. Identification of prostate specific membrane antigen (PSMA) as the target of monoclonal antibody 107-1A4 by proteinchip; array, surface-enhanced laser desorption/ionization (SELDI) technology. Int J Cancer 2001;92(6):871–876.

48. Mincheff M, Zoubak S, Altankova I, Tchakarov S, Makogonenko Y, Botev C, Ignatova I, Dimitrov R, Madarzhieva K, Hammett M, Pomakov Y, Meryman H, Lissitchkov T. Human dendritic cells genetically engineered to express cytosolically retained fragment of prostate-specific membrane antigen prime cytotoxic

49. Chaux A, Eifler J, Karram S, Al-Hussain T, Faraj S, Pomper M, Rodriguez R, Netto GJ. Focal positive prostate-specific membrane antigen (PSMA) expression in ganglionic tissues associated with prostate neurovascular bundle: Implications for novel intraoperative PSMA-based fluorescent imaging techniques. Urol Oncol 2013;31(5):572–575.

50. Minner S, Wittmer C, Graefen M, Salomon G, Steuber T, Haese A, Huland H, Bokemeyer C, Yekebas E, Dierlamm J, Balabanov S, Kilic E, Wilczak W, Simon R, Sauter G, Schlomm T. High level PSMA expression is associated with early PSA recurrence in surgically treated prostate cancer. Prostate 2011; 71(3):281–288.

51. Perner S, Hofer MD, Kim R, Shah RB, Li H, Moller P, Hautmann RE, Gschwend JE, Kuefer R, Rubin MA. Prostate-specific membrane antigen expression as a predictor of prostate cancer progression. Hum Pathol 2007;38(5):696–701.

52. Murphy GPS, WA), Boynton, Alton L. (Redmond, WA), Holmes, Eric H. (Bothell, WA), Tino, William Thomas (Redmond, WA); Northwest Biotherapeutics, Inc. (Seattle, WA), assignee. Monoclonal antibodies specific for the extracellular domain of prostate-specific membrane antigen. United States. 2000.

53. Knedlik T, Navratil V, Vik V, Pacik D, Sacha P, Konvalinka J. Detection and quantitation of glutamate carboxypeptidase II in human blood. Prostate 2014.

54. Kinoshita Y, Kuratsukuri K, Newman N, Rovito PM, Kaumaya PT, Wang CY, Haas GP. Targeting epitopes in prostate-specific membrane antigen for antibody therapy of prostate cancer. Prostate Cancer Prostatic Dis 2005;8(4):359–363.

55. Barinka C, Mlcochova P, Sacha P, Hilgert I, Majer P, Slusher BS, Horejsi V, Konvalinka J. Amino acids at the N- and C-termini of human glutamate carboxypeptidase II are required for enzymatic activity and proper folding. Eur J Biochem 2004;271(13):2782–2790.

56. Barinka C, Sacha P, Sklenar J, Man P, Bezouska K, Slusher BS, Konvalinka J. Identification of the N-glycosylation sites on glutamate carboxypeptidase II necessary for proteolytic activity. Protein Sci 2004;13(6):1627–1635.

57. Sacha P, Zamecnik J, Barinka C, Hlouchova K, Vicha A, Mlcochova P, Hilgert I, Eckschlager T, Konvalinka J. Expression of glutamate carboxypeptidase II in human brain. Neuroscience 2007;144(4):1361–1372.

58. Wang X, Ma D, Olson WC, Heston WD. In vitro and in vivo responses of advanced prostate tumors to PSMA ADC, an auristatin-conjugated antibody to prostate-specific membrane antigen. Mol Cancer Ther 2011;10(9):1728–1739.

59. Chen Z, Penet MF, Nimmagadda S, Li C, Banerjee SR, Winnard PT Jr, Artemov D, Glunde K, Pomper MG, Bhujwalla ZM. PSMA-targeted theranostic nanoplex for prostate cancer therapy. ACS Nano 2012;6(9):7752–7762.

60. Mlcochova P, Barinka C, Tykvart J, Sacha P, Konvalinka J. Prostate-specific membrane antigen and its truncated form PSM'. Prostate 2009;69(5):471–479.

61. Elsasser-Beile U, Wolf P, Gierschner D, Buhler P, Schultze-Seemann W, Wetterauer U. A new generation of monoclonal and recombinant antibodies against cell-adherent prostate specific membrane antigen for diagnostic and therapeutic targeting of prostate cancer. Prostate 2006;66(13):1359–1370.

62. Schulke N, Varlamova OA, Donovan GP, Ma D, Gardner JP, Morrissey DM, Arrigale RR, Zhan C, Chodera AJ, Surowitz KG, Maddon PJ, Heston WD, Olson WC. The homodimer of prostate-

T-cell responses to multiple epitopes. Cancer Gene Ther 2003; 10(12):907–917.

specific membrane antigen is a functional target for cancer therapy. Proc Natl Acad Sci U S A 2003;100(22):12590–12595.

63. Ma D, Hopf CE, Malewicz AD, Donovan GP, Senter PD, Goeckeler WF, Maddon PJ, Olson WC. Potent antitumor activity of an auristatin-conjugated, fully human monoclonal antibody to prostate-specific membrane antigen. Clin Cancer Res 2006; 12(8):2591–2596.

64. Tykvart J, Sacha P, Barinka C, Knedlik T, Starkova J, Lubkowski J, Konvalinka J. Efficient and versatile one-step affinity purification of in vivo biotinylated proteins: Expression, characterization and structure analysis of recombinant human glutamate carboxypeptidase II. Protein Expr Purif 2012;82(1):106–115.

65. Hegnerova K, Bockova M, Vaisocherova H, Kristofikova Z, Ricny J, Ripova D, Homola J. Surface plasmon resonance biosensors for detection of Alzheimer disease biomarker. Sensor Actuat B-Chem 2009;139(1):69–73.

66. Pimkova K, Bockova M, Hegnerova K, Suttnar J, Cermak J, Homola J, Dyr JE. Surface plasmon resonance biosensor for the detection of VEGFR-1–a protein marker of myelodysplastic syndromes. Anal Bioanal Chem 2012;402(1):381–387.

67. Barinka C, Rinnova M, Sacha P, Rojas C, Majer P, Slusher BS, Konvalinka J. Substrate specificity, inhibition and enzymological analysis of recombinant human glutamate carboxypeptidase II. J Neurochem 2002;80(3):477–487.

68. Liu N, Liang W, Ma X, Li X, Ning B, Cheng C, Ou G, Wang B, Zhang J, Gao Z. Simultaneous and combined detection of multiple tumor biomarkers for prostate cancer in human serum by suspension array technology. Biosens Bioelectron 2013;47:92–98.

69. Conway RE, Petrovic N, Li Z, Heston W, Wu D, Shapiro LH. Prostate-specific membrane antigen regulates angiogenesis by modulating integrin signal transduction. Mol Cell Biol 2006; 26(14):5310–5324.

SUPPORTING INFORMATION

Additional Supporting Information may be found in the online version of this article at the publisher's web-site

Supplementary Material

for article

Comparative analysis of monoclonal antibodies against prostate-specific membrane antigen (PSMA)

J. Tykvart[1,2], V. Navrátil[1,2], F. Sedlák [1,3], E. Corey[3], M. Colombatti[5], G. Fracasso[5], F. Koukolík[6], C. Bařinka[7], P. Šácha[1,2], J. Konvalinka[1,2*]

Table of contents:

Methods

Purification of recombinant Avi-tagged proteins

The extracellular portion of human GCPII with an N-terminal Avi-tag (Avi-GCPII) was prepared as previously described [62]. GCPII homologs (human GCPIII, mouse GCPII and mouse GCPIII) were prepared in a similar fashion.

Briefly, the DNA sequences coding for extracellular portions of human GCPIII, mouse GCPII or mouse GCPIII proteins were inserted into plasmid pMT/BiP/AviTEV/rhGCPII in place of the rhGCPII sequence (coding for extracellular portion of human GCPII), yielding plasmids encoding human GCPIII (pMT/BiP/AviTEV/rhGCPIII), mouse GCPII (pMT/BiP/AviTEV/rmGCPII) and mouse GCPIII (pMT/BiP/AviTEV/rmGCPIII). Subsequently, *Drosophila* S2 cells, stably transfected with *E. coli* biotin-protein ligase localized within the ER, were additionally transfected with the above-mentioned plasmids using calcium-phosphate transfection protocol (Life Technologies). Large-scale expressions of Avi-tagged proteins were performed, and one-step purification was carried out on Streptavidin Mutein Matrix™ (Roche), yielding >90% pure protein of interest.

The prepared proteins contain an Avi-tag™ and TEV cleavage site N-terminally fused with the extracellular portion of the respective protein (human GCPIII, aa 36-740; mouse GCPII, aa 45-752; mouse GCPIII, aa 36-740). The recombinant proteins are denoted human Avi-GCPIII, mouse Avi-GCPII and mouse Avi-GCPIII. The concentration of purified proteins was determined using a Biochrom30 amino acid analyzer (Biochrom) following the manufacturer's protocol.

Characterization of mAb binding by ELISA

ELISA experiments were performed in a 96-well plate format using polystyrene F96 Nunc MaxiSorp™ MicroWell™ plates (Thermo Scientific). All procedures were carried out at 25 °C. All incubations and washes were performed on a shaker at 200 RPM and 450 RPM, respectively.

First, 100 μL of 83.3 nM NeutrAvidin solution (Thermo Scientific) was immobilized in 100 mM sodium borate, pH 9.5, in each well for 1 h. The wells were washed twice with 250 μL of TBS (20 mM Tris-HCl, 150 mM NaCl, pH 7.4), incubated with 200 μL of Casein Buffer 20x-4x Concentrate 1 (SDT) diluted 20x in TBS for 1 h and washed twice with 250 μL of 0.05% Tween-20 in TBS. Then, an appropriate antigen was immobilized on neutravidin-coated wells.

1

For the native GCPII ELISA assay, 100 µL of 0.4 nM recombinant human Avi-GCPII in native binding buffer (0.1% Tween-20 in TBS) was used. In the case of antibodies GCP-05 and 24.4E6, 100 µL of 1 nM of Avi-GCPII was used to ensure sufficient signal read-out. For 7E11-C5.3, 100 µL of 10 nM intraGCPII peptide in native binding buffer was used. This peptide consists of the first 21 amino acids of the GCPII sequence with an N-terminal biotin linked through the ε-amino group of lysine and a TTDS (1-amino-4,7,10-trioxa-13-tridecanamine succinimic acid) linker. For the denatured GCPII ELISA assay, recombinant human Avi-GCPII, human Avi-GCPIII, mouse Avi-GCPII or mouse Avi-GCPIII stock solutions were denatured in 1% SDS solution for 15 min at 70 °C. Subsequently, these stock solutions were diluted at least 100-fold with denature binding buffer (50 mM Tris-HCl, 150 mM NaCl, 0.2% Tween-20, 0.08% SDS). A 100 µL aliquot of such prepared 1 nM protein solution was immobilized on neutravidin.

The protein/peptide solution was incubated for 1 h with pre-bound neutravidin and washed three times with 250 µL of 0.05% Tween-20 in TBS. Then, 100 µL of various mAbs solutions prepared by 2x serial dilution (11 concentrations in total) in 0.1% Tween-20 in TBS was incubated with immobilized antigen. Based on the signal strength, the highest concentration of the dilution series was either 67 nM or 670 nM. The antibody was incubated with antigen for 1 h, and wells were then washed three times with 250 µL of 0.05% Tween-20 in TBS. Afterwards, 100 µL of 2.7 nM HRP-conjugated goat anti-mouse antibody (Thermo Scientific) in 0.1% Tween-20 in TBS was added to each well and incubated for 1 h, followed by three washes with 250 µL of 0.05% Tween-20 in TBS.

The chemiluminiscence substrate was prepared (2.5 mM luminol (Sigma-Aldrich), 2 mM 4-iodophenol (Fisher Scientific), 0.018% hydrogen peroxide (Sigma-Aldrich), 100 mM Tris-HCl, pH 8.8). A 175 µL aliquot of substrate solution was added to each well, and the chemiluminiscence was immediately measured for 500 ms on an Infinite® M1000 PRO (TECAN).

Epitope determination assay

The protocol described for the native GCPII ELISA assay was also used for this experiment, with minor modifications. A library of 83 18-mer peptides (custom-made by PepScan, Lelystad) biotinylated at their N-termini and linked to the peptide through 6-aminohexanoic acid was synthesized. These peptides cover the entire sequence of human GCPII with nine amino acid overlap between the peptides. All cysteine residues in the library were substituted with serine to prevent the formation of disulfide bridges. Each peptide was

2

immobilized in one well of a 96-well plate (100 µL of 2.5 µM peptide solution) and treated with the appropriate primary mAb; YPSMA-1 (6.7 nM), YPSMA-2 (6.7 nM), GCP-02 (6.7 nM), GCP-04 (6.7 nM), 24.4E6 (6.7 nM), 3E6 (0.67 nM), J591 (6.7 nM) or D2B (6.7 nM). Experiments without any primary mAb and with indifferent mouse IgG (Thermo Scientific) were used as negative controls.

Characterization of mAb binding by SPR

All surface plasmon resonance measurements were performed on a four-channel SPR sensor platform (PLASMON IV) developed at the Institute of Photonics and Electronics (IPE), AS CR, Prague [63-64]. First, the SPR chip (provided by IPE) was loaded into a pure ethanol mixture of $HS-(CH_2)_{11}-PEG_4-OH$ and $HS-(CH_2)_{11}-PEG_6-O-CH_2-COOH$ alkanethiols (Prochimia; mixed in a 7:3 ratio) with a final concentration of 0.2 mM and incubated for 1 h at 37 °C. The chip was rinsed with ethanol and deionized water, dried with nitrogen flow and mounted to the prism on the SPR sensor. Experiments were performed at 25 °C.

Activation of carboxylic terminal groups on the sensor surface was performed *in situ* by injecting a solution of 0.1 M *N*-hydroxysuccinimide (NHS) and 0.5 M 1-ethyl-3-(3-dimethylaminopropyl)-carbodiimide hydrochloride (EDC) in deionized water (Biacore) for 5 min at a flow rate of 20 µL/min. The remainder of the experiment was performed at a flow rate of 30 µL/min. Afterwards, a 0.02 mg/mL neutravidin solution in 10 mM sodium acetate buffer, pH 5.0, was loaded for 8 min, followed by a high ionic strength solution (PBS with 0.5 M NaCl) and 1 M ethanolamine (Biacore) to wash out non-covalently bound neutravidin and deactivate residual carboxylic groups, respectively.

A 2.5 µg/mL solution of recombinant human Avi-GCPII in PBS was immobilized to achieve approximately 20% saturation of binding sites (e.g., around 3 nm change in the relative response signal). Antibody solutions of various concentrations were then loaded into each flow-channel for 10 min, followed by 20 min flow of PBS to observe antibody dissociation. The following antibody concentrations were used: D2B (4 µg/mL, 2 µg/mL, 1 µg/mL and 0.5 µg/mL), J415 (2 µg/mL, 1 µg/mL, 0.5 µg/mL and 0.25 µg/mL), J591 (20 µg/mL, 10 µg/mL, 5 µg/mL and 2.5 µg/mL), 2G7 (20 µg/mL, 10 µg/mL, 5 µg/mL and 2.5 µg/mL) and 107-1A4 (8 µg/mL, 4 µg/mL, 2 µg/mL and 1 µg/mL).

TraceDrawer 1.5 (Ridgeview Instruments AB) was used to calculate k_{on} and k_{off} parameters of antibody binding. The One-To-One interaction model for fitting was used for all antibodies except J415. We used the One-To-One model with mass diffusion correction for J415 due to the very high association rate of this antibody. Change in signal due to the bulk

3

effect was added manually for antibody 107-1A4. For all other mAbs, this effect was not observed and was manually set to zero. Measurements were performed twice for each mAb.

SDS-PAGE and Western blotting

Samples were resolved by reducing 0.1% sodium dodecyl sulfate polyacrylamide gel electrophoresis (SDS-PAGE). Following SDS-PAGE, the proteins were electroblotted onto a nitrocellulose membrane using a Trans-Blot® SD Semi-Dry Transfer Cell (Bio-Rad). The membrane was blocked with Casein Buffer 20x-4x Concentrate 1 (SDT) diluted 20-fold in TBS for 1 h and subsequently incubated overnight with GCP-02, GCP-04, YPSMA 1, YPSMA 2, 3E6, 24.4E6, J591 or D2B. All mAbs were diluted in blocking solution to a concentration of 1 μg/mL with the exception of antibody D2B, which was diluted to a concentration of 10 μg/mL. The membranes were washed several times with 0.05% Tween 20 in PBS and incubated for 1 h with HRP-conjugated goat anti-mouse antibody (1 mg/mL; Thermo Scientific) diluted in Casein Buffer in a 1:25,000 ratio. The membranes were washed several times with 0.05% Tween 20 in PBS, and the blots were developed using SuperSignal West Dura Chemiluminiscence Substrate (Thermo Scientific) according to the manufacturer's protocol. Reactive bands were visualized by 20 min exposition using 1x1 binning on a ChemiDoc-It™600 Imaging System (UVP).

Preparation of tissue slides for immunohistochemistry

A prostate adenocarcinoma sample (Gleason score grade 3+4) was obtained by radical prostatectomy at Thomayer's Hospital in Prague from a consented patient with the agreement of the local ethical commission. Subsequently, less-than-3-μm-thick slides of the formalin-fixed paraffin-embedded sample were prepared from the obtained tissue according to standard histological procedures. Samples for immunohistological staining were mounted on SuperFrost®PLUS microscope slides.

Comparison of IHC staining of prostate cancer tissues with various mAbs

The prepared slides were deparaffinized in xylene (incubated twice for 5 min) and rehydrated through decreasing concentrations of aqueous ethanol (incubated 3 min each in 99%, 96%, 70%, 50% and 30% ethanol and finally 5 min in pure water). Heat-induced antigen retrieval was performed in the appropriate buffer by warming to 95 °C in a water bath for 45 min. If not stated otherwise, acidic antigen retrieval buffer (10 mM sodium citrate, 0.1% Tween 20, pH 6.0) was used. For comparison study of antigen retrieval buffers, basic

4

buffer (10 mM Tris base, 1.2 mM EDTA, 0.1% Tween 20, pH not adjusted) was also used. Endogenous peroxidase activity was blocked with 1.5% hydrogen peroxide solution in PBS for 20 min. Afterwards, the slides were incubated for 1 h in 10% FBS/PBS followed by overnight incubation with various anti-GCPII mAbs at 4 °C. Concentration of the mAbs differed depending on the experiment. In experiments comparing the ability of various mAbs to visualize GCPII (Figure 2), the concentration was 10 µg/mL. In experiments with dilution series of mAbs (Figure 3), the concentrations were 0.01 µg/mL and 0.1 µg/mL. In experiments with different antigen retrieval buffers (Figure S3), the concentration of 7E11-C5.3 used was 10 µg/mL and the GCP-04 concentration was 1 µg/mL.

For visualization of antibody-antigen complexes, the slides were incubated with Histofine® Simple Stain™ MAX PO (MULTI) (Nichirei Biosciences Inc.) diluted 1:1 with 10% FBS/PBS for 1 h at 4 °C. Then, the bound antibody was visualized by either 30 sec (for 10 µg/mL concentration of primary antibody) or 90 sec (for lower concentrations of primary antibody) staining with diaminobenzidine solution using the stable DAB/Plus kit (Diagnostic BioSystems). Finally, all sections were counterstained with Harris' hematoxylin (Fluka Chemie) and mounted in mowiol solution (9.6% (w/V) Mowiol 4.88 (Merck), 24% (w/V) glycerol, 100 mM Tris-HCl, pH 8.5) for preservation.

Comparison of LNCaP and PC3 cell line staining by various mAbs using flow cytometry

LNCaP and PC3 cells were grown in 100 mm Petri dishes. LNCaP cells were grown in RPMI-1640 medium (Sigma-Aldrich) with addition of FBS (final concentration of 10%), while PC3 cells were grown in DMEM-High Glucose medium (GE Healthcare) containing L-glutamine (final concentration of 4 mM) and FBS (final concentration of 10%). After reaching 80% confluence, the cells were harvested using trypsin solution (0.25% (w/V) trypsin and 0.01% (w/V) EDTA in PBS). Cells were counted and their viability was determined with a Countess® Automated Cell Counter (Invitrogen) using a 0.4% solution of trypan blue (Sigma-Aldrich) in PBS.

If the viability of cells was higher than 90%, they were washed with PBS and suspended in 10% FBS/PBS. A 50 µL aliquot of 4 x 10^6 cells/mL cell suspension was placed into wells of a polypropylene 96-well plate (round bottom) and incubated 1 h at 4 °C. All following procedures were performed strictly at 4 °C to prevent internalization of a bound primary antibody. A 1 µL aliquot of antibody solution was added into each well to reach a final antibody concentration of 10 µg/mL. After 1 h, cells were pelleted (500 g, 2 min) and washed twice with 200 µL of 10% FBS/PBS. Then, the cell pellet was suspended in 50 µL of

5

a 2.5 μg/mL solution of secondary F(ab') fragment donkey anti-mouse IgG (H+L) antibody conjugated with phycoerythrin (Jackson ImmunoResearch) in 10% FBS/PBS and incubated for 1 h.

Finally, the cells were suspended in 200 μL of 10% FBS/PBS, and single cell suspensions were measured on a BD LSRFortessa™ cell analyzer (Becton, Dickinson and Company). An appropriate amount of cell suspension was injected to ensure 10,000 measured events for each well. The gates on side scatter and forward scatter were set to ensure measurement of viable cells. All experiments (all mAbs and both cell lines) were performed in triplicate.
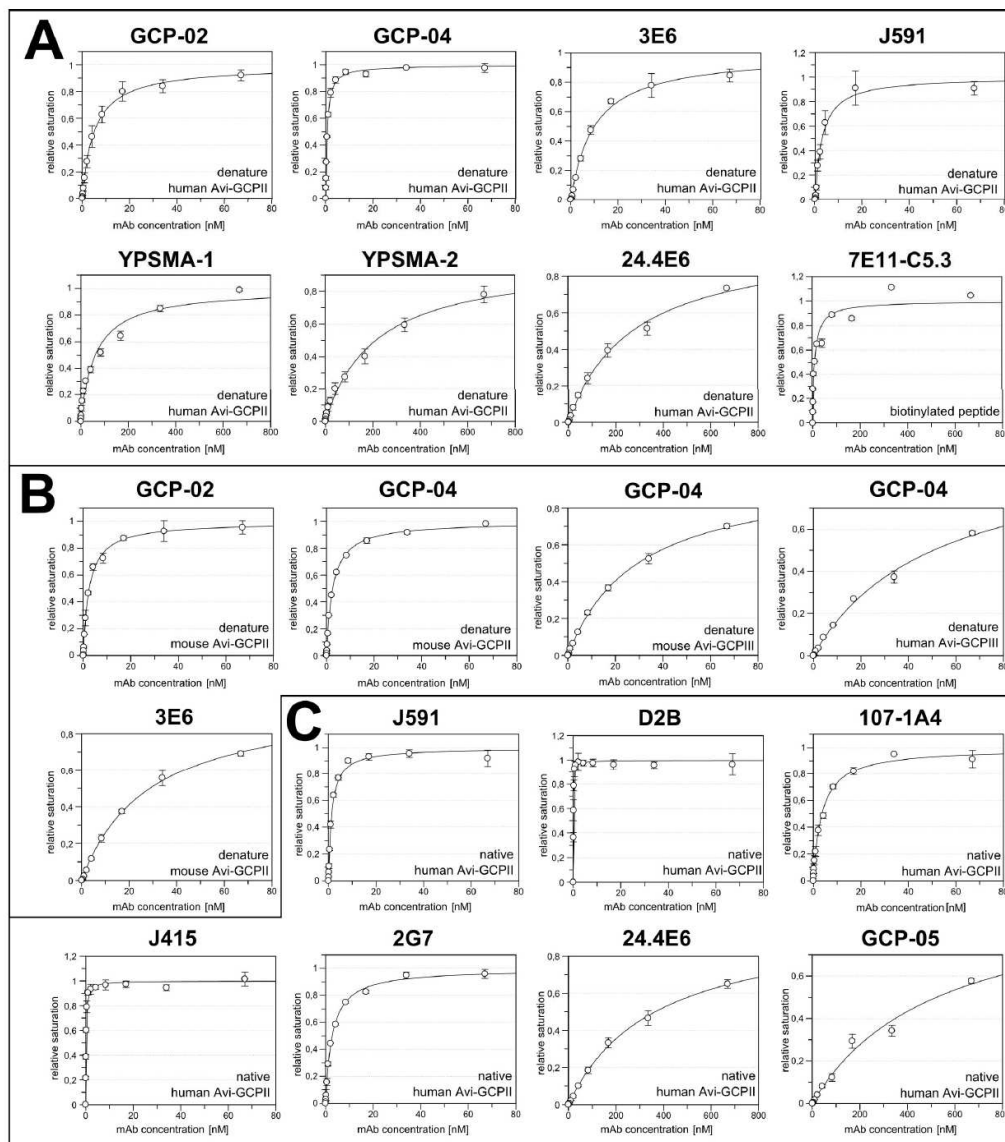
6

Figures

Figure S1: Binding curves of various anti-GCPII mAbs determined by ELISA.
Each mAb was measured at least twice (the precise number is shown in Tables 2-4). The error bars indicate standard deviations of the measurements. In the bottom-right corner of each binding curve, the experimental ELISA setup and the type of antigen are specified. For more experimental details, see the corresponding section in Supplementary Material. **Panel A:** Saturation binding curves for antibodies binding denatured extracellular portion of human GCPII. In the case of mAb 7E11-C5.3, the biotinylated peptide was used instead of the extracellular portion of GCPII. **Panel B:** Saturation binding curves for antibodies binding denatured extracellular portions of human GCPII homologs (human GCPIII, mouse GCPII and mouse GCPIII). **Panel C:** Saturation binding curves for antibodies binding native extracellular portion of human GCPII.
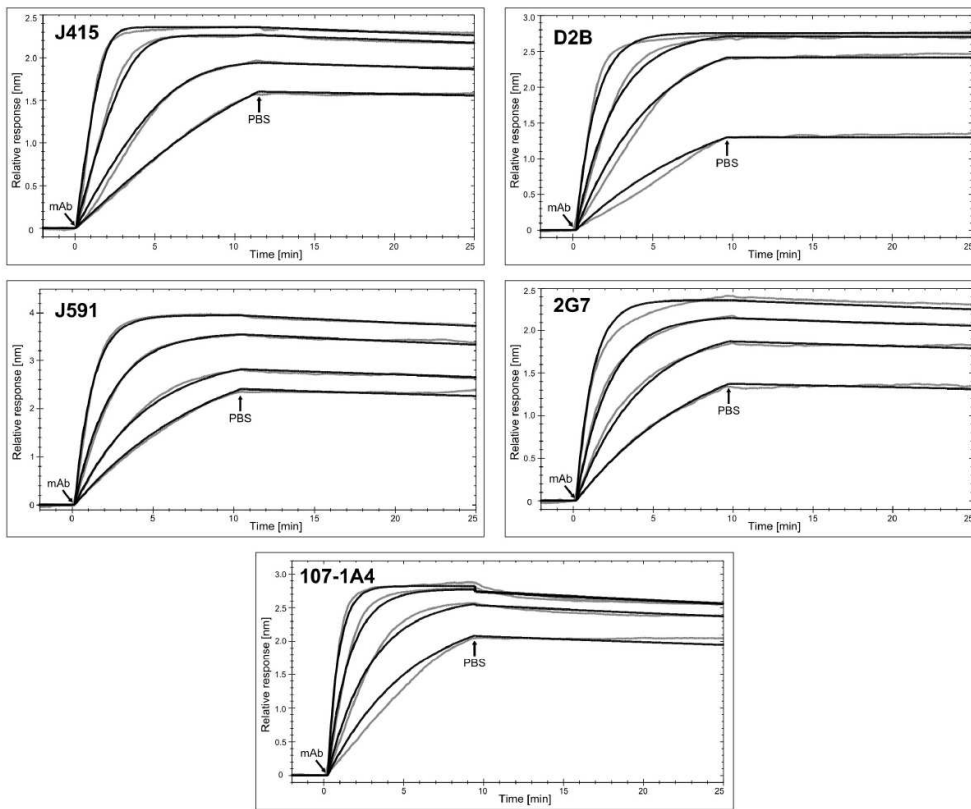
7

Figure S2: Kinetic analysis of various mAbs binding to GCPII in native form measured by SPR. Recombinant Avi-GCPII was immobilized through biotin-neutravidin interaction. Afterwards, four different concentrations of each mAb were applied to the immobilized Avi-GCPII. The concentration of mAbs were as follows: D2B (4 µg/mL, 2 µg/mL, 1 µg/mL and 0.5 µg/mL), J415 (2 µg/mL, 1 µg/mL, 0.5 µg/mL and 0.25 µg/mL), J591 (20 µg/mL, 10 µg/mL, 5 µg/mL and 2.5 µg/mL), 2G7 (20 µg/mL, 10 µg/mL, 5 µg/mL and 2.5 µg/mL) and 107-1A4 (8 µg/mL, 4 µg/mL, 2 µg/mL and 1 µg/mL). Kinetic curves were fitted in TraceDrawer 1.5 (Ridgeview Instruments AB). In the case of J415, the One-To-One model with mass diffusion correction was used. For 107-1A4, the bulk effect of running buffer was included. For more details, see the corresponding section in Supplementary Material.
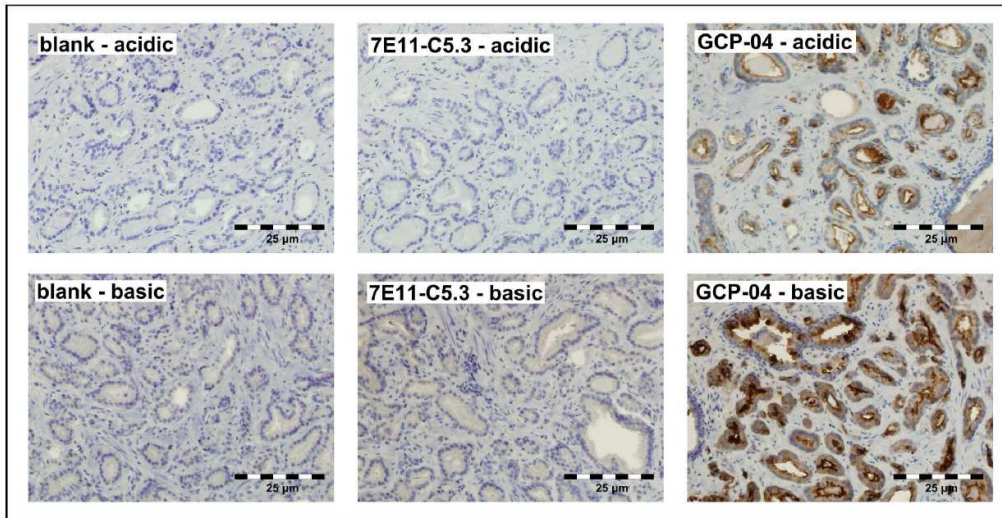
Figure S3: Immunohistological staining of GCPII in prostate adenocarcinoma tissue sections using two different antigen retrieval buffers.
Formalin-fixed paraffin-embedded tissues sections were subjected to two different antigen retrieval protocols (using either acidic citrate-based buffer or basic Tris/EDTA-based buffer) and two mAbs (7E11-C5.3 at 10 µg/mL concentration and GCP-04 at 1 µg/mL concentration) to compare their ability to visualize GCPII. The immunoperoxidase method was used for visualization of bound antibodies, followed by counterstaining with Harris' hematoxylin. For more details, see the corresponding section in Supplementary Material.

9
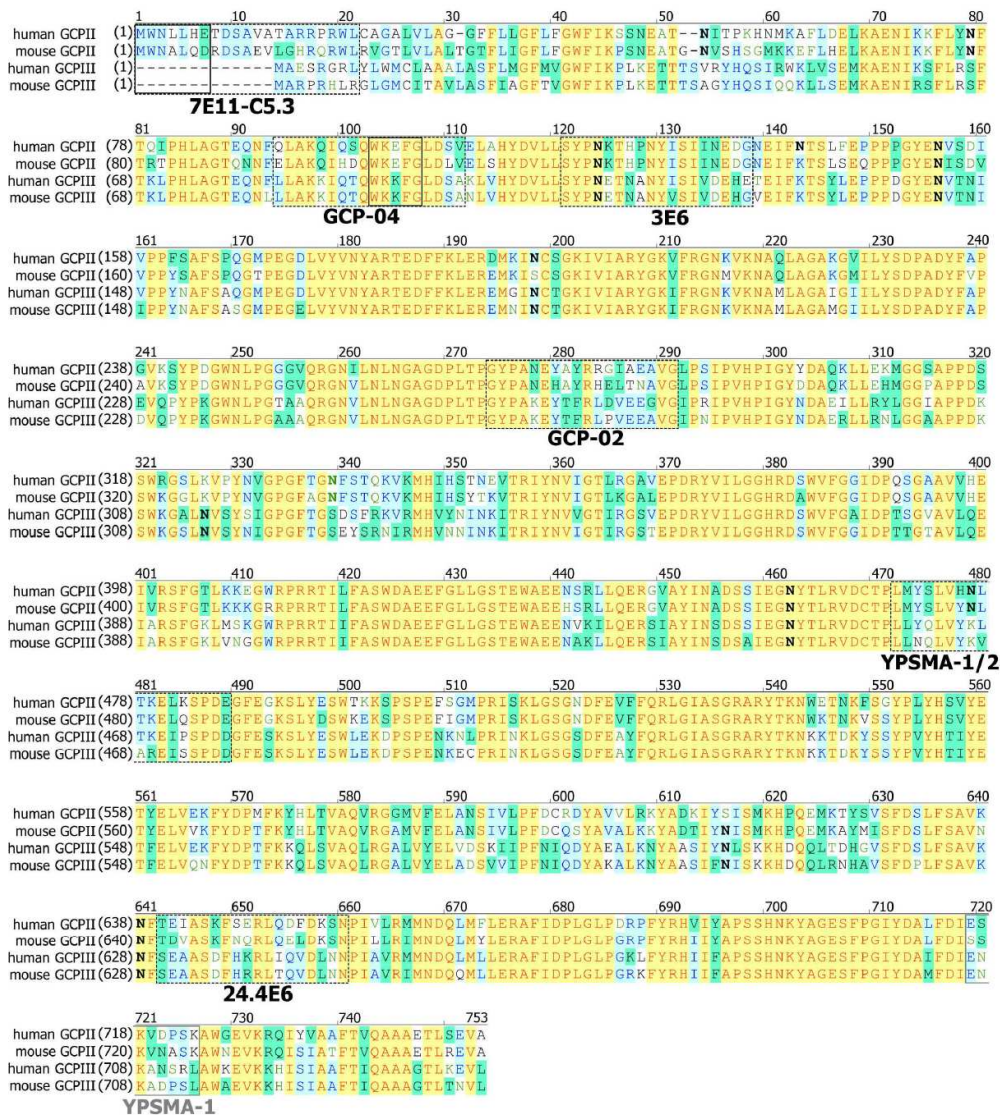
Figure S4: Alignment of protein sequences of human GCPII and GCPIII and their mouse counterparts, with epitopes of several mAbs highlighted.

Epitopes determined by epitope determination assay using a synthesized peptide library are marked with dashed black rectangles. Black rectangles mark previously known mAb epitopes that are more specific than those determined by epitope determination assay. A gray rectangle marks the previously reported epitope of YPSMA-1 mAb. Potential N-glycosylation sites are shown in bold. Yellow background and red letters indicate the same aa in all sequences. Dark green background shows aa with highly similar biophysical properties. Light green letters show aa with slightly similar biophysical properties. Light blue background with dark blue letters indicates the same aa for several of the aligned sequences.

10

2.2.3 Paper III: Structural and biochemical characterization of NAALADase L

Motivation of the study

Human *N*-acetylated alpha-linked acidic dipeptidase-like protein (NAALADase L) represents one of the closest GCPII homologs with approximately 37% sequence identity and conservation of zinc coordinating residues as well as catalytic glutamate. Even though the protein was identified in 1997 by Shneider *et al.* [197] only one additional study describing NAALADase L has been published to date [27]. Both these studies characterized expression and enzymatic activity of NAALADase L. However, they did not use purified recombinant protein and their results were somewhat inconsistent.

Therefore, we decided to prepare recombinant NAALADase L and thoroughly describe its structure, expression profile and enzymatic activity. Additionally, being a close GCPII homolog, we hoped that elucidation of a physiological role of NAALADase L could shed some light on the potential non-enzymatic function of GCPII; a question which is actively pursued in a GCPII research field.

Summary

Using previously established Avi-tag based expression and purification system, we prepared and purified extracellular portion of NAALADase L (Avi-NaalL) and its putative catalytically ineffective mutant Avi-NaalL(E416A). We prepared diffraction quality crystals of Avi-NaalL and refined the final model to 1.75 Å resolution (see Figure 11A, p. 68). The structure analysis revealed that Avi-NaalL structure is highly similar to that of GCPII, including complete conservation of amino acids indispensable for hydrolase activity.

Additionally, we analyzed the expression profile of NAALADase L on both mRNA and protein level. We detected high levels of mRNA coding for NAALADase L in several tissues such as testis, small intestine, colon, spleen, and ovary. On the other hand, we observed highly restricted expression of NAALADase L on a protein level detecting the expression predominantly in a small intestine. These data suggested that the mRNA coding for NAALADase L probably undergoes extensive alternative splicing.

Finally, we investigated the enzymatic activity of NAALADase L. We disproved its previously reported DPP IV-like activity and demonstrated that the recombinant protein derived from the *NAALADL1* gene possesses aminopeptidase activity. NAALADase L degrades peptide substrates from their N-termini until it reaches an acidic residue at P2' or

proline residue at P3'. If there is none of these amino acids present within the peptide sequence, NAALADase L processes the peptide to single amino acids. Furthermore, we identified Glu416 as a critical residue for proper enzymatic activity of NAALADase L probably functioning as a proton shuttle (see Figure 11B).
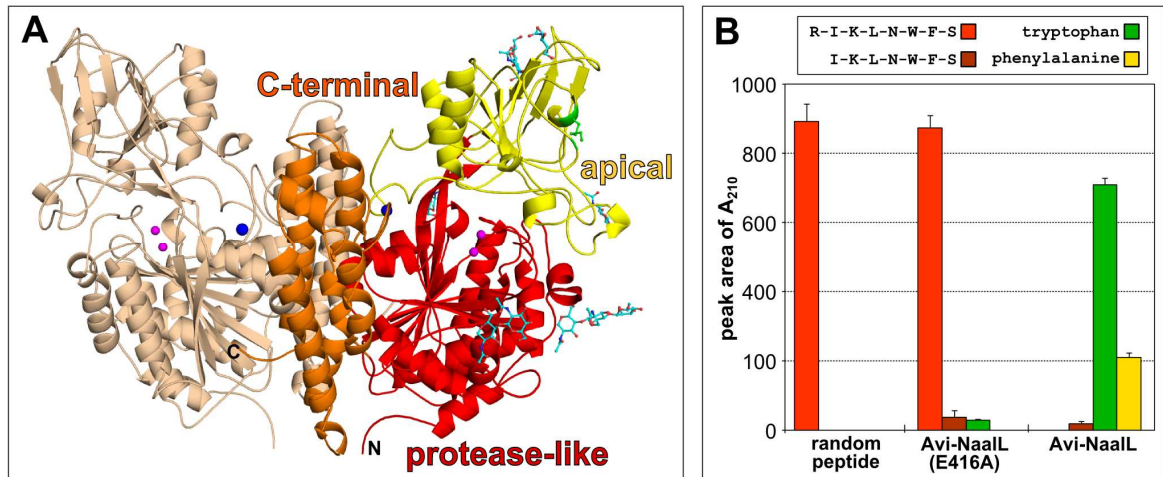

Figure 11: Structure and enzymatic activity analysis of NAALADase L.
Panel A: Overall structure of NAALADase L dimer shown in ribbon representation. One monomer is shown in wheat, and the other is colored based on its domain organization. The zinc ions are shown as magenta spheres and calcium ions as blue spheres. The carbohydrate moieties are depicted as cyan sticks with oxygen atoms in red and nitrogen in blue. The disulfide bond between Cys296 and Cys313 is shown as a green stick. **Panel B**: Cleavage analysis of a random peptide by NAALADase L showing that the putative inactive mutant is incapable of effective cleavage and that the NAALADase L is able to completely process the peptide to individual amino acids.

Based on NAALADase L newly identified enzymatic activity and highly restricted protein expression, we suggested a new name for this enzyme: human ileal aminopeptidase (HILAP) and hypothesized that this protein physiological role in human is likely connected to a peptide/protein degradation.
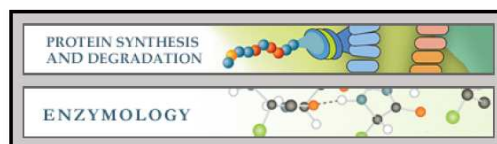
My contribution:

I prepared the expression plasmids and performed purification of Avi-tagged proteins, refined Avi-NaalL X-ray structure, conducted all enzymatic experiments except for the PICS analysis, performed protein expression profile analysis, and wrote the draft of the manuscript.

Structural and biochemical characterization of a novel aminopeptidase from human intestine*

Jan Tykvart[1,2], Cyril Bařinka[3], Michal Svoboda[1,5], Václav Navrátil[1,2], Radko Souček[1], Martin Hubálek[1], Martin Hradilek[1], Pavel Šácha[1,2], Jacek Lubkowski[4], Jan Konvalinka[1,2]

[1]Gilead Sciences and IOCB Research Centre, Institute of Organic Chemistry and Biochemistry, Academy of Sciences of the Czech Republic, Flemingovo n. 2, Prague 6, Czech Republic
[2]Department of Biochemistry, Faculty of Natural Science, Charles University, Albertov 6, Prague 2, Czech Republic
[3]Institute of Biotechnology, Academy of Sciences of the Czech Republic, Vídeňská 1083, Prague 4, Czech Republic
[4]National Cancer Institute, Center for Cancer Research, Macromolecular Crystallography Laboratory, building 539, Frederick, MD 21702-1201, USA
[5] Department of Physical and Macromolecular Chemistry, Faculty of Natural Science, Charles University, Albertov 6, Prague 2, Czech Republic

*Running title: *Characterization of a novel human aminopeptidase*

Corresponding author: Jan Konvalinka, Institute of Organic Chemistry and Biochemistry, ASCR, v.v.i.; Flemingovo n. 2, Prague 6, 166 10, Czech Republic; Tel: 00420 220 183 218, Fax: 00420 220 183 578; Email: jan.konvalinka@uochb.cas.cz

Background: A protein product of *NAALADL1* gene is a homolog of glutamate carboxypeptidase II, a metallopeptidase studied as a promising theranostic cancer agent.
Results: We solved x-ray structure and analyzed substrate specificity of *NAALADL1* gene product.
Conclusion: We demonstrated that the protein represents a novel human ileal aminopeptidase.
Significance: This study describes novel enzyme involved in protein/peptide digestion in small intestine and clarifies controversial previous reports.

ABSTRACT

N-acetylated alpha-linked acidic dipeptidase-like protein (NAALADase L), encoded by the *NAALADL1* gene, is a close homolog of glutamate carboxypeptidase II (GCPII), a metallopeptidase that has been intensively studied as a target for imaging and therapy of solid malignancies and neuropathologies. However, neither the physiological functions nor structural features of NAALADase L are known at present. Here, we report a thorough characterization of the protein product of the human *NAALADL1* gene, including heterologous overexpression and purification, structural and biochemical characterization, and analysis of its expression profile.

By solving the NAALADase L X-ray structure, we provide the first experimental evidence that it is a zinc-dependent metallopeptidase with a catalytic mechanism similar to that of GCPII, yet distinct substrate specificity. A proteome-based assay revealed that the *NAALADL1* gene product possesses previously unrecognized aminopeptidase activity, but no carboxy- or endopeptidase activity. These findings were corroborated by site-directed mutagenesis and identification of bestatin as a potent inhibitor of the enzyme. Analysis of *NAALADL1* gene expression at both the mRNA and protein levels revealed the small intestine as the major site of protein expression and points towards extensive alternative splicing of the *NAALADL1* gene transcript.

Taken together, our data imply that the *NAALADL1* gene product's primary physiological function is associated with the final stages of protein/peptide digestion and absorption in the human digestive system. Based on these results, we suggest a new name for this enzyme: human ileal aminopeptidase (HILAP).

1

INTRODUCTION

Human *N*-acetylated alpha-linked acidic dipeptidase-like protein (NAALADase L) is encoded by the *NAALADL1* gene localized at chromosome 11q12. The gene spans more than 14 kbp and contains 18 exons (1). Translation of the mRNA transcript yields a 740-amino-acid type II transmembrane protein. According to the MEROPS database, NAALADase L belongs to the M28B metallopeptidase subfamily (MEROPS ID: M28.011). Glutamate carboxypeptidase II (GCPII), which shares 37% sequence identity and 50% similarity with NAALADase L, is another member of this subfamily.

In 1997, Shneider *et al.* identified a NAALADase L protein (designated as I100) in rat ileum. They analyzed mRNA expression in rat and human tissues, raised polyclonal antibody against I100, and detected DPP IV activity in an immunoprecipitate from rat ileum (2). The only other report to date describing the *NAALADL1* gene product was published by Pangalos *et al.* in 1999 (1). These researchers performed a comparative analysis of the human *NAALADL1* gene product and its two close paralogs NAALADase I and NAALADase II, which are now known as GCPII and GCPIII, respectively. They gave the protein its current name, NAALADase L, based on the close homology of these enzymes. They cloned NAALADase L cDNA, identified its position in the human genome, analyzed its alternative splicing, and detected DPP IV activity in NAALADase L-transfected cell lysate. Additionally, they detected DPP IV activity in GCPII- and GCPIII-transfected cell lysates. However, this activity was subsequently not confirmed for GCPII and GCPIII in experiments with purified recombinant protein (3-4).

In the present study, we performed a thorough structural and biochemical characterization of the human *NAALADL1* gene product using a purified recombinant protein preparation to elucidate the physiological role of the protein.

EXPERIMENTAL PROCEDURES
Cloning NAALADase L cDNA and preparation of expression plasmids

Two plasmids, A (ID LIFESEQ95147340) and B (ID LIFESEQ4181072), containing cDNA coding for NAALADase L were purchased from Open Biosystems (now GE Healthcare). The extracellular portion of NAALADase L (AAs 28-740) was amplified from plasmid A, and *Bcl*I and *Xho*I restriction sites were introduced by PCR using primers FNAL28*Bcl*I (*aaa***tgatca**atccccaaaaaagccaactcactggc*) and RNAL740*Xho*I (*ttt***ctcgag***tcatcagaggtcagccacaggcc*). The PCR product was then ligated *via Bgl*II and *Xho*I restriction sites into pMT/BiP/V5-HisA (Life Technologies), resulting in pMT/BiP/rhNaalL28-740. Sequencing identified two mutations in pMT/BiP/rhNaalL28-740 (resulting in AA mutations L364P and L393P). Therefore, the mutated part of DNA was replaced with the corresponding DNA from plasmid B utilizing *Nco*I and *Kpn*I cleavage sites to insert leucine residues at the proper positions in the plasmid DNA. Additional sequencing confirmed that the mutations were repaired.

For preparation of N-terminal His-tagged NAALADase L, the extracellular portion of the protein (AA 28-740) was amplified from pMT/BiP/rhNaalL28-740 using primers FNAL28*Nde*I (*aaa***catatg**atccccaaaaaagccaactcactggc*) and RNAL740*Xho*I. The PCR product was then ligated into pET28b *via Nde*I and *Xho*I restriction sites, yielding pET28b-HisNaalL.

For preparation of N-terminal Avi-tagged NAALADase L, the extracellular portion of the protein (AA 28-740) was amplified from pMT/BiP/rhNaalL28-740 using primers FNAL28*Bcl*I and RNAL740*Xho*I. The PCR product was then ligated into pMT/BiP/AviTEV/rhGCPII (5) *via Bgl*II and *Xho*I restriction sites, yielding pMT/BiP/AviTEV/rhNaalL. The final protein construct contains an N-terminal AviTag™ (Avidity) sequence and TEV cleavage site.

The E416A mutation was introduced into pMT/BiP/AviTEV/rhNaalL using the QuikChange Site-Directed Mutagenesis Kit (Stratagene). Primers RNAL-E416A (*gccaatgagcccaaactc***cgc**agcccccccagctcgc*) and FNAL-E416A (*gcgagctgggggggct***gcg**gagtttgggctcattggc*) were used for the PCR reaction, which was performed according to the manufacturer's protocol, yielding pMT/BiP/AviTEV/rhNaalL(E416A).

2

The plasmid pET24a_HIVprD25N, which encodes HIV-1(D25N) protease, was created from pET24a_HIVprWT (6), which encodes wild-type HIV-1 protease, using the QuikChange Site-Directed Mutagenesis Kit (Stratagene) with primers RHIV-D25N (*gaagctctatta**aat**acaggagcagatgata*) and FHIV-D25N (*tatcatctgctcctgt**attt**aatagagcttc*) according to the manufacturer's protocol.

The sequences of all constructed plasmids were verified by DNA sequencing.

Preparation of His-NaalL protein for immunization

The plasmid pET28b-HisNaalL was used for large-scale expression of the extracellular portion (AAs 28-740) of NAALADase L with an N-terminal His-tag (His-NaalL) in *E. coli* BL21-CodonPlus-RIL cells using 1 mM IPTG for induction. His-NaalL was purified from inclusion bodies under denaturing conditions. First, the cell pellet was dissolved in running buffer (8 M urea, 0.5 M NaCl, 50 mM Na_2HPO_4, pH 8.0) and loaded onto a HisTrap HP (GE Healthcare) column using an ÄKTAexplorer LC system (GE Healthcare). The column was washed with running buffer containing 10 mM imidazole, and protein was eluted with 1 M imidazole. The elution fractions were pooled and used for mouse immunization.

Preparation of monoclonal antibody against NAALADase L

Monoclonal antibodies were prepared according to an established protocol (7). Briefly, Balb/c mice were intraperitoneally immunized with purified His-NaalL in 8 M urea (40 µg in 100 µL) mixed with an equal volume of incomplete Freund's adjuvant in 3-week intervals. Hybridoma cells, prepared by fusion of immune spleen cells and Sp/0 myeloma cells, were cloned by limited dilution and assayed for production of NAALADase L-specific antibodies by enzyme-linked immunosorbent assay. Positive selection was performed against His-NaalL and negative selections against rhGCPII and rhGCPIII prepared in our laboratory (3-4). Four positive hybridoma clones (1C11, 3C11, 3D10, and 4E9) were expanded, and conditioned medium from the most sensitive hybridoma clone (1C11) was used for immunoblots. Additionally, we tested the ability of all four hybridoma supernatants to immunoprecipitate native Avi-NaalL. The results indicated that these monoclonal antibodies bind specifically to the denatured form of NAALADase L (data not shown).

Expression and purification of Avi-NaalL and Avi-NaalL(E416A)

Preparation and purification of Avi-NaalL was performed as previously described (5). Briefly, *Drosophila* S2 cells expressing *E. coli* biotin-ligase (*BirA*) in the endoplasmic reticulum were transfected with pMT/BiP/AviTEV/rhNaalL (encoding the extracellular portion [AAs 28-740] of NAALADase L with an N-terminal Avi-tag and TEV protease cleavage site. Large-scale expression of Avi-NaalL was performed, and the conditioned medium was concentrated 10-fold. The recombinant protein was purified on Streptavidin Mutein Matrix™ (Roche), followed by size exclusion chromatography on Superdex™ 200 10/300 GL (GE Healthcare) in 10 mM bis-Tris propane, 150 mM NaCl, pH 7.4. The concentration of the final protein preparation was determined by amino acid analysis using a Biochrom30 amino acid analyzer (Biochrom).

The preparation of Avi-NaalL(E416A) mutant was performed analogously.

Expression and purification of HIV-1 protease and HIV-1(D25N) protease

HIV-1 protease was prepared as previously described (6).

HIV-1(D25N) protein was overexpressed in *E. coli* BL21(DE3)RIL (Novagen) transformed with pET24a_HIVprD25N expression plasmid. Insoluble recombinant protein, accumulated in the form of inclusion bodies, was isolated and solubilized in 50% (v/v) acetic acid. Solubilized protein was purified by gel chromatography in 50% (v/v) acetic acid, using a Superdex G75 16/60 gel filtration column (Amersham Bioscience). Fractions containing mutant HIV-1 protease were pooled, and the protein was subsequently refolded by drop-wise dilution into a 19-fold excess of water and additional dialysis against water for 3 h at 4 °C, followed by subsequent overnight dialysis against 50 mM MES, 10% (v/v) glycerol, 1 mM EDTA, 0.05% (v/v) 2-mercaptoethanol, pH 5.8. The purified protein was stored at −70°C.

Crystallization and data collection

3

Avi-NaalL stock solution (5 mg/mL) was mixed in a 1:1 ratio with reservoir solution (0.16 M magnesium formate and 16% [w/v] PEG 3350). Crystals were grown using the hanging drop vapor diffusion method at 293 K. Diffraction quality crystals (0.3x0.2x0.2 mm³) were obtained by seeding. For diffraction experiments, crystals were cryo-cooled in liquid nitrogen after transferring to cryo-protectant containing 0.16 M magnesium formate, 16% (w/v) PEG 3350, and 14% (v/v) glycerol. The diffraction data were collected at 100 K using synchrotron radiation at the Southeast Regional Collaborative Access Team sector 22 beamlines BM of the Advanced Photon Source (Argonne, IL, USA) with the X-ray wavelength tuned to 1.0000 Å. The complete dataset was collected from a single crystal and recorded on a MarMosaic 225 mm CCD detector. Data processing was performed with the HKL2000 software package (8).

Structure determination and refinement

The Avi-NaalL structure was solved by molecular replacement using the program Phaser (9) and coordinates of GCPII (PDB entry 2PVW) as a search model. Subsequent structural refinement was carried with the program Refmac 5.1 (10). During the refinement process, 1% of randomly selected reflections were kept aside for cross-validation (R_{free}). Refinement was interspersed with manual corrections aided by the program Coot (11). The stereochemical quality of the final model was evaluated using the Web server MolProbity (12). The final model and experimental amplitudes were deposited in the RCSB Protein Data Bank (entry code 4TWE).

Quantitative PCR (qPCR)

Amounts of *NAALADL1* gene transcript were quantified using two distinct sets of primers. The first set, NaalL_A, contained forward and reverse primers (sequences *cactgggctgccactacag* and *ttgtagacgctcacattcacct*) and fluorescent hydrolysis Universal ProbeLibrary Probe #3 (Roche). This set was designed to amplify NTs 945 to 1032 in *NAALADL1* transcript NM_005468, which covers the region containing exons 6 and 7 and corresponds to AAs 310 to 339 in the longest ORF. The expected size of the amplified product was 88 bases; the size of the possibly amplified genomic DNA was 758 bases. The second set,

NaalL_B, consisted of forward and reverse primers (sequences *atctcctccatggacattgc* and *gctgtgtggtaggtggggta*) and fluorescent hydrolysis Universal ProbeLibrary Probe #41 (Roche). This set was designed to amplify NTs 1580 to 1656 in *NAALADL1* transcript NM_005468, which covers the region containing exons 13 and 14 and corresponds to AAs 522 to 547 in the longest ORF. The expected size of the amplified product was 77 bases, while the size of the possibly amplified genomic DNA was 1024 bases.

All qPCR reactions (10 μl) were carried out in triplicate in sealed 96-well plates (FrameStar® 480, 4titude) using a LightCycler 480 II instrument (Roche). Each reaction consisted of LightCycler 480 Probe Master (Roche) diluted according to the manufacturer's protocol, forward and reverse primers (final concentration 1 μM each), fluorescent probe (final concentration of #3 was 100 nM; final concentration of #41 was 50 nM) and template DNA. Reaction mixtures without template DNA were prepared as controls. Moreover, interplate calibrators were included in each plate. Initial denaturation for 3 min at 95 °C was followed by 45 cycles of 10 sec at 95 °C, 30 sec at 66 °C, and 30 sec at 72 °C. The threshold cycle numbers (C_q) were then determined from fluorescence intensities acquired during the qPCR runs by the 2nd derivative maximum method using LightCycler 480 software (Roche). The presence and size of PCR products for all qPCR reactions was analysed by agarose gel electrophoresis.

A set of serial dilutions, ranging from 10^2 to 10^7 copies per reaction, of the pMT/BiP/AviTEV/rhNaalL plasmid was used for absolute quantification. The initial concentration of plasmid DNA prior to dilution was determined spectrophotometrically based on absorption at 260 nm (Nanodrop ND-1000, Thermo Scientific). The amount of *NAALADL1* transcript was then measured in 0.1 μl aliquots of tissue cDNA libraries obtained from Clontech (Human MTC Panel I and II).

To assess the selectivity of qPCR amplification, pcDNA4 plasmids with subcloned protein coding sequences of homologous human transcripts (ORF from NM_004476 coding AAs 1 to 750 of GCPII, ORF from NM_005467 coding AAs 1 to 740 of GCPIII) at concentrations of 10^6 copies per reaction were amplified in the same qPCR setup with both primer sets. Possible

4

products were inspected by agarose gel electrophoresis. Amplification of isolated human genomic DNA was tested in the same manner.

Human tissue lysate preparation

Human tissue lysates were prepared as described earlier (13). Briefly, human samples were obtained during autopsy performed 4–8 h postmortem. The samples were homogenized in 50 mM Tris-HCl, 150 mM NaCl, pH 7.5, supplemented with EDTA-free protease inhibitors (Roche). The samples were then sonicated using Soniprep 150 (Sanyo) three times for 10 sec on ice, and 1% (v/v) Triton X-100 was added. After 30 min incubation on ice, the suspension was centrifuged at 16000 g for 10 min, and the supernatants were stored at -80° C for further experiments.

SDS-PAGE and Western blotting

Protein samples were resolved by reducing sodium dodecyl sulfate polyacrylamide gel electrophoresis (SDS-PAGE). Gels were silver-stained for analysis of protein purification or stained with colloidal Coomassie G-250 for mass spectrometry analysis or electroblotted (100 V for 1 h) onto a nitrocellulose membrane using a Mini Trans-Blot® Cell wet blot system (Bio-Rad).

After blotting, membranes were blocked with casein (SDT), incubated overnight with hybridoma supernatant 1C11, washed three times with 0.05% (w/w) Tween 20 in PBS (PBST), incubated for 1 h with HRP-conjugated goat anti-mouse antibody (1 mg/mL; Thermo Scientific) diluted in casein in a 1:25000 ratio, and washed three times with PBST. Blots were developed using SuperSignal West Dura Chemiluminiscence Substrate (Thermo Scientific) according to the manufacturer's protocol. Reactive bands were visualized on a ChemiDoc-It™600 Imaging System (UVP; 20 min exposition, 1x1 binning).

MS analysis

Chosen gel sections were excised, destained, reduced with DTT, alkylated with iodoacetamide, and digested with trypsin for 10 h. Peptides were extracted and dissolved in 0.1% formic acid (FA). Samples were analyzed with an UltiMate 3000 RSLCnano system (Thermo Scientific) coupled to a TripleTOF 5600 mass spectrometer with a NanoSpray III source (AB Sciex). Peptides were separated on an Acclaim PepMap100 analytical column (3 μm, 250 mm × 75 μm ID, Thermo Scientific). The concentration of buffer B (0.1% FA in acetonitrile) was gradually increased from 5% to 30% in buffer A (0.1% aqueous FA) over 40 min. The MS mass range was set to 350–1250 m/z; in MS/MS mode, the instrument acquired fragmentation spectra within 100–1600 m/z. The program Protein Pilot 4.5 (AB Sciex) was used for protein identification against the UniProt *Homo sapiens* database (reviewed 12/20/2013).

Samples for PICS were analyzed in the same manner but without gel extraction and by applying a 95-min instead of a 40-min gradient. PICS results were searched against the UniProt *Homo sapiens* database containing typical MS contaminants (reviewed 06/23/2014).

LNCaP lysate preparation

LNCaP cells were grown in RPMI-1640 medium (Sigma-Aldrich) with addition of 10% (v/v) FBS. After reaching confluence, the cells were harvested and sonicated 4 times for 15 sec in lysis buffer (50 mM Tris-HCl, 150 mM NaCl, 1% [w/v] C12E8 [Affymetrix], 50 mM NaF, 1 mM Na_3VO_4, 1 mM β-glycerol phosphate, 2.5 mM $Na_4O_7P_2$, pH 7.4). Cell debris was removed by centrifugation (45000 g for 60 min at 4 °C), and protein concentration was determined by Bradford assay (14).

DPP IV activity assay

Protein samples, either purified recombinant Avi-tagged protein or LNCaP cell lysate, were incubated in 25 mM bis-Tris propane, 150 mM NaCl, pH 8.5, with 100 μM Gly-Pro-AMC (Sigma) for 15 h at 37 °C. The reactions were performed in triplicate in white 96-well polypropylene plates with V-bottoms. The fluorescence was measured on an Infinite® M1000 PRO (TECAN) with excitation and emission wavelengths/bandwidths of 335/5 nm and 450/10 nm, respectively.

Synthesis of dipeptides and dipeptide libraries

Substrate mixtures of the general formula Ac-Aaa-X-OH (where Aaa is one of 19 proteinogenic AAs [all except cysteine] and X is an equimolar mixture of all 19 AAs [all except cysteine]) were prepared by solid phase peptide

5

synthesis on 2-chlorotritylchloride resin (for C-terminal amino acids Asp, His, Pro, Trp) or on Wang resin (for all other C-terminal amino acids) using the Fmoc/tBu protection and DIC/HOBt coupling strategy described by Barlos *et al.* (15).

N-terminal acetylation was accomplished with acetic anhydride in the presence of DIEA. The completeness of all couplings was controlled by a ninhydrin test (16). A mixture of 94% trifluoracetic acid, 2% triisopropylsilane, 2% ethanedithiol, and 2% water was used for final cleavage from the resin. The peptides were freeze-dried from 10% acetic acid in water.

To confirm the presence and quantify the amount of all N-acetylated dipeptides in the mixtures, samples were analyzed by amino acid analysis using a Biochrom30 amino acid analyzer (Biochrom) following the manufacturer's protocol.

Carboxypeptidase activity assay

Reactions were performed in round-bottom 96-well PP plate. The enzyme (final concentration 0.25 μM) and 5 μL of N-acetylated dipeptide library (the final concentration of each individual dipeptide in the library was approximately 25 μM) were diluted with reaction buffer (25 mM bis-Tris propane, 150 mM NaCl, 0.001% [w/v] C12E8, pH 7.4) to a final volume of 50 μL. The reaction were then incubated at 37 °C for 15 h and subsequently analyzed on HPLC.

The cleaved free amino acids in the reaction mixtures were analyzed on an Agilent 1260 HPLC system (Agilent Technologies) equipped with an AccQ-Tag Ultra RP 130 Å column (1.7 μm, 100 mm × 2.1 mm ID, Waters) following a previously published protocol for amino acid analysis (17).

Enzymatic assay with peptides from PICS

Reactions were performed in 1.5 mL capped plastic vials in final volume of 40 μL. The final enzyme concentration was 1 μM for 15 h incubations and 0.1 μM for time-dependent cleavage analysis. The final concentration of substrate (peptide 52 or peptide 71) was 100 μM. Reactions were buffered with 25 mM bis-Tris propane, 150 mM NaCl, 0.001% (w/v) C12E8, pH 7.4. After stopping reactions by addition of 40 μL 1 M glycine-HCl, pH 2.4, mixtures were analyzed on an Agilent 6230 TOF LC/MS (Agilent Technologies) equipped with a Dual AJS ESI

source operated in the positive ion mode (acquisition 4 GHz, HiRes).

Separation of the peptides and AAs was conducted on the Acquity UPLC BEH-C18 130 Å column (1.7 μm, 100 mm × 2.1 mm ID, Waters) using a 10 min gradient from 2% to 100% mobile phase B (A: 0.1% aqueous FA, B: 0.1% FA in acetonitrile). The column temperature was 25 °C and the flow rate 0.3 ml/min.

HPLC analysis of aminopeptidase activity

Reactions were performed in round-bottom 96-well PP plates. For determination of kinetic parameters of IIDPNG peptide cleavage by Avi-NaalL the reactions with various concentration of the peptide ranging from 6 to 1600 μM were performed. The Avi-NaalL was first diluted in reaction buffer (25 mM bis-Tris propane, 150 mM NaCl, 0.001% [w/v] C12E8, pH 7.4) in final volume of 40 μL to ensure 10-20% conversion. The enzyme was then pre-incubated for 5 min at 37 °C and then 10 μL of various concentrations of peptide substrate (IIDPNG) was added to start the reaction. After 15 min the reactions were stopped by addition of 50 μL of stopping buffer (200 mM glycine-HCl, pH 2.4).

For determination of inhibition constant of bestatin 90 ng of Avi-NaalL, ensuring approximately 10% conversion, and various concentration ranging from 0.1 to 500 μM of bestatin hydrochloride (AppliChem) were mixed in reaction buffer in final volume of 40 μL. The reactions were pre-incubated for 5 min at 37 °C and then 10 μL of peptide substrate (IIDPNG; final concentration 50 μM) was added to start the reaction. After 15 min the reactions were stopped by addition of 50 μL of stopping buffer. Each reaction was performed in duplicate.

The reactions were subsequently analyzed on an Agilent 1260 HPLC system (Agilent Technologies) equipped with the Acquity UPLC BEH-C18 130 Å column (1.7 μm, 100 mm × 2.1 mm ID, Waters) using a 6 min gradient from 2% to 100% mobile phase B (A: 0.1% aqueous FA, B: 0.1% FA in acetonitrile). The column temperature was 25 °C, and the flow rate was 0.3 ml/min. The obtained data were then processed using GraFit v.5.0.11 (Erithacus Software Ltd.).

The catalytic efficiency of Avi-NaalL(E416A) mutant was determined in reaction buffer by incubation Avi-NaalL(E416A), final

6

concentration 10 µM, and peptide IIDPNG, final concentration 4 mM, at 37 °C. 2 µL of reaction mixture were withdrawn from the reaction after 60 min, 120 min, and 240 min, added to 100 µL of stopping buffer and subsequently analyzed on HPLC.

PICS assay

PICS was performed along previously published protocol with several modifications (18). Non-transfected HEK293T cells were grown in DMEM to 90% confluence and harvested by washing into PBS buffer. Cells were transferred into hypotonic lysis buffer containing protease inhibitors and lysed by sonication, followed by cysteine reduction and alkylation. Proteins were precipitated using TCA and resolubilized into 200 mM HEPES, pH 7.5. Following resolubilization, the proteome-derived peptide library was prepared by cleaving isolated denatured proteins into peptides with trypsin (Sigma Aldrich). After abolishing trypsin activity using 1 mM PMSF, a second round of sulfhydryl reduction and alkylation was performed. Primary amines on peptide N-termini and lysine side chains were blocked by formaldehyde-cyanoborohydride reductive dimethylation. Excess modification reagents were removed by gel filtration, and the peptide library was purified and transferred to HPLC-grade water using a C-18 solid phase extraction cartridge Sep-Pak (Waters) according to the manufacturer's protocol. The peptide concentration was adjusted to 2 mg/mL. The integrity of the peptide library was confirmed by LC-MS/MS analysis, and aliquots were stored at -80 °C until further use.

For the endopeptidase assay, the peptide library (final concentration 1 mg/mL) was incubated in 200 µL of 25 mM bis-Tris propane, 150 mM NaCl, pH 7.4, and 0.2 µM Avi-NaalL. The reaction was incubated for 12 h at 37 °C. Following incubation, the reaction was heat-inactivated for 30 min at 70 °C and titrated with 2 M HEPES, pH 8.5, to final pH 8.0.

Subsequently, newly formed free peptide N-termini (products of proteolytic cleavage) were *in vitro* biotinylated by addition of 350 µM sulfo-NHS-SS-biotin (Thermo-Scientific) for 4 h at room temperature. Biotinylated products were then immobilized on streptavidin agarose (Solulink) by 2 h incubation with mild agitation at room temperature, followed by washing. Additional washing steps (2 M urea followed by 20% isopropanol, 5% DMSO, and 5% acetonitrile, all in washing buffer [50 mM HEPES, 150 mM NaCl, pH 7.5]) were added to the original protocol, followed by ten washes with washing buffer. Immobilized peptides were eluted with 20 mM DTT, desalted using Pepclean C-18 reverse phase cartridges (Thermo Scientific) according to the manufacturer's protocol, and analyzed by mass spectrometry.

As negative controls, Avi-NaalL(E416A) and buffer alone (blank) were used. As positive controls, the HIV-1 protease cleavage profile in 100 mM sodium acetate, 300 mM NaCl, pH 7.4, was tested with wild-type and HIV-1(D25N) protease. The protease library ratio was 1:200, and the final enzyme concentration was 0.2 µM.

PICS data analysis

Data were analyzed using a series of predesigned queries in Microsoft Access database software. First, lists of identified peptides from each MS run were loaded into the database and filtered for peptides containing products of N-terminal modification by biotinylation. Second, peptides with confidence over 80% were picked for enzymatic reactions (Avi-NaalL or HIV-1 protease), while peptides with confidence over 10% were picked for control reactions (reactions with catalytically ineffective forms of the enzymes and blanks). To properly subtract the background signal, the list of peptides found in each enzymatic reaction was screened for peptides present in the blank reaction and the reaction with catalytically ineffective enzyme. Such peptides were then removed from processing. Finally, the enzymatic reactions were screened for peptides identified in the original unprocessed peptide library. Such peptides were also removed from the analysis.

The final cleared list of identified peptides was then mapped against the FASTA database used for proteomics database search. By identified peptide alignment with the database, the N-terminal portions of cleaved peptides (preceding the cleavage site) were determined. If there was more than one computationally identified AA for a given P position, the position was omitted from the processing, while the identified peptide sequence remained listed for downstream analysis. The final list of substrate peptides containing sequences of P'

7

amino acids identified in the MS experiment and four P amino acids identified computationally is shown in Table 2. The frequency of each AA in each position was then calculated and plotted, yielding substrate specificity matrix heat-maps.

RESULTS

We used an expression and purification system established in our laboratory to produce the extracellular portion (AAs 28–740) of human NAALADase L, designated Avi-NaalL, and its putative catalytically ineffective mutant Avi-NaalL(E416A) (5). These recombinant proteins, with a final purity greater than 95%, shown in Fig. 1, were used in all subsequent experiments.

X-ray structure of Avi-NaalL

We prepared diffraction quality crystals of human Avi-NaalL in hanging drops using a microseeding approach. We solved the structure by molecular replacement using the program Phaser, and refined the final model to 1.75 Å resolution (PDB code 4TWE; data collection and refinement statistics are shown in Table 1). As shown in Fig. 2A, the overall fold of Avi-NaalL is very similar to that of GCPII (PDB code 3BXM) with a root-mean-square deviation of 1.41 Å for the 646 equivalent Cα atoms (19). Guided by the well-described structural features of GCPII (20-21), we annotated the Avi-NaalL structure accordingly.

The Avi-NaalL monomer folds into three distinct domains: protease-like domain (residues 35–108 and 340–587), apical domain (residues 109–339), and C-terminal domain (residues 588–740). Two Avi-NaalL molecules in the asymmetric unit form a dimer with a buried surface area of more than 2300 Å^2. The dimerization interface mainly involves interactions between the C-terminal domain of the first monomer and the protease-like/apical domains of the second monomer (Fig. 2B). Size-exclusion chromatography data also indicated that the protein is dimeric with approximate relative molecular weight 250 kDa (Fig. 1), suggesting that this is likely its physiological quaternary structure. This quaternary arrangement is reminiscent of the dimerization pattern of both human transferrin receptor and GCPII (22).

Unlike GCPII, Avi-NaalL contains one intramolecular disulfide bridge, linking Cys296 with Cys313. The Avi-NaalL sequence also contains seven potential N-glycosylation motifs. We found clear electron density for at least one N-acetylglucoseamide moiety for all putative glycosylation sites except Asn274. A sequential alignment of NAALADase L and GCPII is shown in Fig. 2C and highlights several key structural features of these proteins.

A strong positive density peak representing a metal ion was observed in the *Fo-Fc* map of the Avi-NaalL structure. The metal is hepta-coordinated by the γ-carboxylates of Glu425 and Glu428, the main chain carbonyls of Leu261 and Thr258, and the side chain hydroxyl group of Thr258 (all at distances between 2.4 Å and 2.5 Å). The coordination sphere is completed by a water molecule (2.5 Å, Fig. 3A). In the final model the Ca^{2+} ion was modeled into this position. Our assumption of modeling calcium ion was guided by several lines of indirect evidence, including the favored pentagonal bipyramidal geometry of the coordination sphere, agreement with the electron density, "optimal" interatomic distances, and matching atomic displacement parameters (B-factors) of the metal and coordinating residues (23). Additionally, the identity of Ca^{2+} ion, occupying equivalent site in closely-related human GCPII, was confirmed experimentally before (20), thus strengthening our argument for calcium as a metal of choice. The exact structural and/or functional role of this cation, however, is not known at present and warrants further studies.

Avi-NaalL binds two Zn^{2+} ions, which are coordinated by the side chains of His368, Asp378, Glu417, Asp445, and His545 (Fig. 3B) at distances between 1.9–2.0 Å. These zinc-coordinating residues adopt the same conformation as in GCPII, forming the core of the Avi-NaalL active site. Glu416, analogous to Glu424 in GCPII (24), likely serves as a catalytic acid/base residue for peptide cleavage. Additionally, the presence of zinc ions was experimentally confirmed by fluorescent scanning of the Avi-NaalL protein crystal (data not shown). Similar to GCPII, Avi-NaalL also contains a *cis* peptide bond between Asp378 and Pro379, which is a hallmark of bimetallic peptidases.

Although Avi-NaalL was crystallized in the absence of a ligand, we detected an extensive positive electron density peak in the vicinity of the zinc ions (Fig. 3C). Unfortunately, we were unable to reliably model any molecule into this electron density. Moreover, this electron density peak spans

8

over the expected position of the catalytic hydroxyl ion, which therefore could not be modeled in the Avi-NaalL structure. In GCPII, this hydroxyl ion completes the tetrahedral coordination of zinc ions and acts as a nucleophilic agent during peptidic substrate cleavage (24).

The comparison of AAs that mediate ligand binding in GCPII with their Avi-NaalL counterparts is illustrated in Fig. 3D; the structure of inactive GCPII in complex with its endogenous substrate NAAG was used for comparison. We found two conserved residues that likely mediate substrate binding to Avi-NaalL, Arg198 and Tyr544. Their GCPII counterparts, Arg210 and Tyr552, interact with the C-terminal alpha carboxylic group and the carbonyl oxygen of the cleaved peptide bond of the GCPII substrate. The residues Arg534 and Arg536, which forms the so-called 'arginine patch' in GCPII, thus providing the GCPII substrate binding cleft with a positive charge and contributing to its preference for negatively charged peptide substrates, are not conserved in Avi-NaalL (Fig. 3E). Consequently, the chloride ion, which stabilizes the energetically unfavorable 'all-gauche' conformation of Arg534 in GCPII, is not present in the Avi-NaalL structure.

Expression pattern of the human *NAALADL1* gene product

We determined the amount of *NAALADL1* gene transcript in commercially available cDNA libraries normalized to set of control genes from several human tissues by quantitative PCR (qPCR). We used two primer sets, each consisting of a primer pair for amplification and a fluorescent probe for detection. The first set of amplification primers targeted the region spanning exons 6 and 7 (NaalL_A), while the second targeted the exons 13 to 14 (NaalL_B). The absolute amounts of *NAALADL1* transcripts detected are shown in Fig. 4A. We identified *NAALADL1* gene transcripts in several tissues, including the testis, colon, small intestine, ovary, spleen, and thymus.

On the other hand, using our newly developed mAb 1C11, we found that NAALADase L expression is primarily restricted to the small intestine (Fig. 4B). We interrogated the specificity of Western blots by mass spectrometry by analyzing several areas corresponding to positive Western blot signals (boxed in Fig. 4B). The small intestine tissue

sample (solid box) was the only one in which we identified the *NAALADL1* gene product (UniProt Accession number Q9UQQ1). We found 33 distinct peptides covering 41% of the sequence entry in the database. On the other hand, gel sections from ovary tissue (dashed box) did not contain NAALADase L, suggesting that 1C11 has non-specific cross-reactivity.

Enzymatic activities of NAALADase L
Putative DPP IV activity

Because both human and rat NAALADase L were previously reported to possess DPP IV activity (1-2), we attempted to confirm these findings using our purified protein preparations. As illustrated in Fig. 5, we were unable to detect any DPP IV activity for Avi-NaalL and Avi-GCPII, while the use of LNCaP lysate as a positive control resulted in a clear increase in fluorescence intensity.

Putative carboxypeptidase activity

Guided by our structural analysis of Avi-NaalL, we set out to investigate its putative carboxypeptidase activity. We synthesized and screened a dipeptide library encompassing 19 proteinogenic amino acids (all but cysteine). Our library consisted of 19 individual N-acetylated dipeptide mixtures, each mixture comprising 19 different dipeptides with defined N-terminal and variable C-terminal AAs (e.g., Ac-Ala-X-OH, Ac-Met-X-OH). After incubating each mixture with Avi-NaalL, released C-terminal AAs were detected using HPLC analysis. We used a catalytically ineffective mutant, Avi-NaalL(E416A), as a control. Additionally, we tested an active recombinant GCPII-preparation (Avi-GCPII) and its catalytically ineffective E424A mutant as a corresponding control pair (5,25).

The results of this carboxypeptidase activity assay presented as differential heat-maps of active and inactive protein preparation are illustrated in Fig. 6. The control experiment with Avi-GCPII indicates that the assay is reliable, as it confirms a clear preference for acidic residues (Glu/Asp) at both the C- and N-termini of the dipeptides (3). On the other hand, Avi-NaalL shows negligible activity and no preference for any AA at either the C- or N-terminus. These results demonstrate that Avi-NaalL does not possess

9

detectable carboxypeptidase activity against an N-acetylated peptide as a substrate.

Putative endopeptidase activity

We performed a proteomic identification of cleavage site (PICS) experiment to assess Avi-NaalL endopeptidase activity. This technique enables simultaneous characterization of both the S and S′ cleavage sites of an enzyme (18). We used a peptide library derived from the HEK293T cell proteome as substrate and included HIV-1 protease as positive control to assess the functionality of the assay. Additionally, Avi-NaalL(E416A) and HIV-1(D25N), the corresponding catalytically ineffective mutants, were included to ensure reliable background subtraction.

The specificity matrices, presented in the form of heat-maps, obtained from PICS are shown in Fig. 7. They summarize the sequences of peptide substrates for Avi-NaalL (72 individual sequences identified; a list of the peptides is shown in Table 2) and HIV-1 protease (over 160 individual sequences identified). For better clarity, we depicted matrices characterizing the percentage of individual AAs at a given position in the identified cleaved peptides in Fig. 7A. Fig. 7B illustrates the ratios of individual AA occurrence at a given position compared to the overall occurrence of that AA in the human genome. Our data for HIV-1 protease showed high similarity to those found in the MEROPS database, demonstrating that our PICS experimental set-up provides a reliable account of protease substrate specificity. The specificity matrix for Avi-NaalL revealed substantial enrichment of acidic residues (Glu/Asp) in the P2′ position and Pro residue in the P3′ position.

Novel aminopeptidase activity

To elaborate on the PICS results, we synthesized two of the identified peptides, peptide 52 (AVF/VDLEPT) and peptide 71 (GLFI/IDPNG), and assayed their processing by Avi-NaalL and Avi-NaalL(E416A).

During overnight incubation, both peptides were completely processed by wild-type Avi-NaalL, while its E416A mutant showed minimal activity (Fig. 8). Interestingly, we could identify only N-terminally truncated parts of the assayed peptides. Moreover, we detected free phenylalanine in both reactions, which most likely

originated from the N-terminal portion of the peptides. These data suggest that Avi-NaalL possesses aminopeptidase rather than endopeptidase activity. To confirm this assumption we performed a time-dependent analysis of hydrolysis of peptide 52 and found that Avi-NaalL indeed processes its peptide substrate sequentially from N-terminus (Fig. 9A).

To obtain more quantitative data on Avi-NaalL enzymatic activity we designed model peptide substrate derived from peptide 71 (I/IDPNG) from which only one Ile should be cleaved off by Avi-NaalL. Using this model substrate, we determined kinetic parameters of Avi-NaalL cleavage, $K_M = 210$ μM and $k_{cat} = 2.16$ s^{-1} (Fig. 9B), and also determined the inhibition constant of a common aminopeptidase inhibitor bestatin towards Avi-NaalL, $K_i = 10.7$ μM (Fig. 9C). Additionally, using high substrate concentration, thus modeling saturation state of the enzyme, we were able to determine the catalytic efficiency of the Avi-NaalL(E416A) mutant, $k_{cat} = 0.0011$ s^{-1}. This result confirmed our prediction that the Glu416 indeed serves as a proton shuttle residue which is crucial for proper catalytic efficiency of the enzyme.

Finally, to further corroborate the Avi-NaalL substrate specificity we designed a random peptide (RIKLNWFS) and assayed its degradation by Avi-NaalL. As shown in Fig. 10, we identified that the peptide was efficiently processed to single AAs by Avi-NaalL during overnight incubation; a finding that is in line with the expected cleavage pattern because the peptide contained neither an acidic residue nor Pro that could block the peptide processing. Moreover, this experiment also revealed the fact that Avi-NaalL is able to efficiently process longer oligopeptides as well as smaller tri- or dipeptides.

All these results demonstrate that Avi-NaalL is an aminopeptidase with wide substrate specificity. Additionally, the results strongly suggest that the apparent Avi-NaalL endopeptidase-like substrate specificity determined by PICS—acidic residues in P2′ and Pro in P3′ position—is actually a motif preventing further N-terminal processing of peptides by Avi-NaalL.

DISCUSSION
Structural features of the *NAALADL1* gene product

10

This is the first study to experimentally describe the structure of the *NAALADL1* gene product which is highly homologous to that of GCPII. The AAs coordinating two active site zinc ions and the catalytic acid/base residue (Glu416, Fig. 3B) in Avi-NaalL are identical to those in GCPII. On the other hand, the GCPII AAs participating in substrate recognition and formation of the arginine patch, which provides positive charge to the GCPII active site, are not conserved in Avi-NaalL. This structural comparison suggested that Avi-NaalL might bind the C-terminus of its potential peptide substrate and position it towards the catalytic acid/base residue to enable proteolysis. However, it also indicated that Avi-NaalL substrate specificity is likely different from that of GCPII.

Both GCPII and NAALADase L belong to the MH clan (family M28) of metallopeptidases. The primary feature of these peptidases is di-zinc active site centre with conserved zinc-coordinating AAs His, Asp, Glu, Asp/Glu, His with the first Asp coordinating both metal ions. Additionally, for all peptidase from this clan, an additional residue (Asp or Glu) has been identified which is important for catalysis and is placed adjacent to coordinating AAs in the motifs His-X-Asp or Glu-Glu. Based on the sequence and structural alignment of Avi-NaalL with other members of M28 family such as aminopeptidase S from *Streptomyces griseus* (SGAP) or GCPII, Glu416 most probably plays a role of acid/base catalytic residue in Avi-NaalL. This assumption is additionally supported by the enzymological data with the E416A mutant presented in this study.

Similarly to other families from MH clan (e.g., M20 family), the M28 family of peptidases contains both carboxypeptidases (GCPII) and aminopeptidases (SGAP). In the M20 family the peptidase enzymatic activity is determined by the sequence; more specifically by the presence of either Glu or Asp residue at the ambiguous position in the zinc coordination center. If Glu residue is present, the peptidase embodies carboxypeptidase activity (e.g., carboxypeptidase G2 from *Pseudomonas sp.*) while in the presence of Asp residue the peptidase acts as an aminopeptidase (e.g., aminopeptidase PepV from *Lactobacillus delbrueckii*) (26). Interestingly, this relationship is not observed in M28 family where

Asp coordinating residue is present in both GCPII and SGAP.

Considering tertiary and quaternary structure organization, Avi-NaalL adopts identical structure as GCPII, containing three domains and folding into the dimer, while aminopeptidases from M28 family, such as SGAP, are single-domain monomeric proteins. On the other hand, our enzymological data indicate that Avi-NaalL, like SGAP, possesses aminopeptidase activity. Therefore, we hypothesize that Avi-NaalL represents an evolutionary intermediate between GCPII and SGAP, sharing the same structural features with the former and the same enzymatic activity with the latter. The elucidation of Avi-NaalL reaction mechanism and substrate binding may hopefully lead to the identification of the comparable structure-activity dependence as was described for M20 family.

However, additional crystallographic studies, targeting complexes of the wild-type enzyme with a potent inhibitor (e.g., bestatin) or complexes of an catalytically ineffective mutant (e.g., Avi-NaalL[E416A]) with a substrate, will be needed to address these questions in detail.

Distribution of the *NAALADL1* gene product in human tissues

Although prior studies have described *NAALADL1* gene product expression in human tissues at the mRNA level, this is the first study which analyzes its expression profile at a protein level. Interestingly, the restricted expression of NAALADase L, which we detected only in the small intestine, did not correspond well with the results from our qPCR analysis, which showed wide tissue distribution (Fig. 4). False positive results from the qPCR assay or alternative splicing of the *NAALADL1* transcript are two possible explanations for these differences.

Amplification of plasmid *NAALADL1* transcript in our qPCR assay conditions was approximately 90% effective and showed linear dependence between the C_q values and the logarithm of the plasmid concentration over a complete range of standard concentrations for both primer sets. Moreover, we confirmed that both primer sets do not amplify transcripts of close NAALADase L homologs human GCPII/III or genomic DNA to a degree that would interfere with our qPCR assay (data not shown). These

11

additional experiments and the use of commercial cDNA libraries, which are normalized to several different housekeeping genes and pooled from numerous individuals, help ensure the reliability of our qPCR data.

Previously reported data on *NAALADL1* transcript expression by Pangalos *et al.*, amplifying the region between exons 14 and 16, showed wide tissue distribution (1). On the other hand, a study by Shneider *et al.*, using a large probe spanning exons 10–15, detected *NAALADL1* transcript only in the small intestine (2). The discrepancies between these two studies could be explained by alternative splicing of the *NAALADL1* transcript; short amplicons are more prone to recognize several splice variants, while long probes are more specific.

Data from the AceView database also support a high degree of alternative splicing of the *NAALADL1* transcript, describing more than 15 different splice variants (27). Among these variants, deletions of exon 11 (68 bp) or exon 13 (91 bp) are most common. The NaalL_A primer set, targeting exons 6 and 7, can detect both of these potential splice variants, while the NaalL_B primer set, targeting exons 13 and 14, cannot detect a variant lacking exon 13. This observation may be responsible for the different results in lung, ovary, and prostate tissues, in which NaalL_A but not NaalL_B primer sets amplified the *NAALADL1* transcript (Fig. 4A).

Taken together, both the presented and previously published data support the hypothesis that the *NAALADL1* transcript undergoes extensive alternative splicing. This processing may function as a regulatory mechanism of NAALADase L expression.

Putative activities of NAALADase L

We were unable to detect the previously reported DPP IV activity in our enzyme preparation. The previous reports used either polyclonal antibody immunoprecipitate (2) or crude cell lysate (1-2). Due to the ubiquitous presence of DPP IV activity in mammalian cells (28), we suggest that their results may have been false-positive. Furthermore, one of these studies also reported DPP IV activity for GCPII and GCPIII, which was subsequently disproved by experiments with purified recombinant protein (3-4).

The results from our carboxypeptidase assay, which suggest slow but specific Avi-NaalL cleavage of N-acetylated dipeptides with identical C- and N-termini, can be explained by sequential N-terminal degradation of the tested dipeptides. The free N-terminal AA, present in the reaction mixture 19 times more frequently than other AAs, would be detected preferentially, leading to a false-positive signal. The release of free N-terminal AA could be explained either by the ability of Avi-NaalL to cleave the N-acetyl moiety from the dipeptide or by incomplete N-acetylation during library synthesis.

Aminopeptidase activity of NAALADase L

After ruling out the potential carboxypeptidase activity of Avi-NaalL, we used PICS, a more general method, to probe potential Avi-NaalL proteolytic activity. PICS enables not only analysis of endopeptidase activity but, in theory, also determination of aminopeptidase activity. Since the method is based on MS analysis of P' regions of the cleaved peptides (i.e., the C-terminal fragments of putative peptide substrates) which are assigned by the peptide spectrum matching against proteomic database, the cleavage of even one AA from the N-terminus of putative peptide substrate can be detected. However, because the downstream sequences of different peptides are often identical, the determination of the "P sequence" can be ambiguous. We identified approximately 15% of peptides in our assay with more than one possible P sequence. We omitted these P sequences from the analysis (see Table 2 and Experimental procedures for more details about a data analysis).

The PICS data suggested that Avi-NaalL prefers an acidic residue at P2' and a Pro residue at P3'. Interestingly, individual analysis of 72 peptide sequences revealed that Asp/Glu in the P2' position (31 peptides identified) and Pro in the P3' position (25 peptides identified) are almost mutually exclusive. Of those 56 peptides, Glu/Asp and Pro were present simultaneously only in two cases. This observation led us to assume that these AAs do not form a conserved substrate recognition motif for Avi-NaalL. Indeed, subsequent enzymatic analyses revealed that the identified cleavage pattern acts as a stopping point for N-terminal peptide degradation rather than as a substrate recognition motif. Nevertheless, these

12

results confirmed the potential of PICS for characterization of aminopeptidase substrate specificity.

It should be noted that the peptides used for our PICS experiments were dimethylated at their N-termini. This suggests that Avi-NaalL is capable of cleaving off N-terminal AAs with blocked primary amine groups. However, this assumption conflicts somewhat with the results from the carboxypeptidase assay, in which N-acetylated dipeptides were inefficiently processed by Avi-NaalL. A likely explanation for this phenomenon is incomplete dimethylation of the peptide library, which would leave some peptides accessible to Avi-NaalL degradation.

Subsequent analysis of two individual peptides identified by PICS confirmed the aminopeptidase activity of Avi-NaalL. We were able to detect only the P' portion of peptide substrates. Additionally, we identified individual AAs that were present in the N-terminal portions of the analyzed peptides (Phe in peptide 52 and 71 or Phe and Trp in random peptide). Moreover, reactions with prolonged incubation times revealed that either Asp/Glu at P2' or Pro at P3' is sufficient to significantly decrease the cleavage efficacy, but only the combination of both AAs completely prevents peptide degradation (Fig. 8, peptide 52). The inhibition experiment with bestatin together with detection of complete degradation of random peptide showed that Avi-NaalL likely belongs to the group of aminopeptidases that are able to cleave a variety of AAs from the peptide N-terminus, such as bovine lens aminopeptidase and SGAP (29). Even though we perform quantitative analysis of Avi-NaalL cleavage of a model substrate, an additional analysis of Avi-NaalL substrate specificity and cleavage efficacy will be necessary for proper classification of this novel aminopeptidase.

Nevertheless, our data clearly demonstrate that the *NAALADL1* gene product possesses different enzymological activity than GCPII. Because the protein product ("NAALADase L") currently bears the same EC number as GCPII (EC 3.4.17.21), a new EC number for this enzyme should be appointed. Additionally, considering that the name NAALADase L (*N*-acetylated alpha-linked acidic dipeptidase-like) does not in fact describe the enzyme's features and is rather misleading, we suggest renaming the enzyme human ileal aminopeptidase (HILAP), to reflect its actual enzymatic activity and expression profile.

To conclude, we solved the X-ray structure of the extracellular portion of the human *NAALADL1* gene product and showed that it is very similar to the GCPII structure, including complete conservation of all AAs necessary for peptidase activity. Analysis of *NAALADL1* gene product expression showed high levels of corresponding mRNA in several tissues. However, the protein was identified predominantly in small intestine, implying that the corresponding mRNA undergoes extensive alternative splicing. We disproved the previously reported DPP IV-like activity of the enzyme and demonstrated that a recombinant protein derived from the *NAALADL1* gene possesses aminopeptidase activity. The enzyme degrades peptide substrates from their N-termini until it reaches an acidic residue at P2' or proline residue at P3'. This activity is inhibited by the specific aminopeptidase inhibitor bestatin.

Given its restricted expression profile and wide substrate specificity, we suggest that the physiological functions of the *NAALADL1* gene product are likely associated with the final stages of protein digestion in the human body and suggest a new name for this enzyme: human ileal aminopeptidase (HILAP).

13

References

1. Pangalos, M. N., Neefs, J. M., Somers, M., Verhasselt, P., Bekkers, M., van der Helm, L., Fraiponts, E., Ashton, D., and Gordon, R. D. (1999) Isolation and expression of novel human glutamate carboxypeptidases with N-acetylated alpha-linked acidic dipeptidase and dipeptidyl peptidase IV activity. *The Journal of biological chemistry* **274**, 8470-8483

2. Shneider, B. L., Thevananther, S., Moyer, M. S., Walters, H. C., Rinaldo, P., Devarajan, P., Sun, A. Q., Dawson, P. A., and Ananthanarayanan, M. (1997) Cloning and characterization of a novel peptidase from rat and human ileum. *The Journal of biological chemistry* **272**, 31006-31015

3. Barinka, C., Rinnova, M., Sacha, P., Rojas, C., Majer, P., Slusher, B. S., and Konvalinka, J. (2002) Substrate specificity, inhibition and enzymological analysis of recombinant human glutamate carboxypeptidase II. *Journal of neurochemistry* **80**, 477-487

4. Hlouchova, K., Barinka, C., Klusak, V., Sacha, P., Mlcochova, P., Majer, P., Rulisek, L., and Konvalinka, J. (2007) Biochemical characterization of human glutamate carboxypeptidase III. *Journal of neurochemistry* **101**, 682-696

5. Tykvart, J., Sacha, P., Barinka, C., Knedlik, T., Starkova, J., Lubkowski, J., and Konvalinka, J. (2012) Efficient and versatile one-step affinity purification of in vivo biotinylated proteins: expression, characterization and structure analysis of recombinant human glutamate carboxypeptidase II. *Protein Expr Purif* **82**, 106-115

6. Kozisek, M., Saskova, K. G., Rezacova, P., Brynda, J., van Maarseveen, N. M., De Jong, D., Boucher, C. A., Kagan, R. M., Nijhuis, M., and Konvalinka, J. (2008) Ninety-nine is not enough: molecular characterization of inhibitor-resistant human immunodeficiency virus type 1 protease mutants with insertions in the flap region. *J Virol* **82**, 5869-5878

7. Langone, J. J., and Van Vunakis, H. (1986) Immunological techniques. Part I: Hybridoma technology and monoclonal antibodies. *Methods Enzymol.* **121**, 1-947

8. Otwinowski, Z., and Minor, W. (1997) Macromolecular Crystallography. Part A: Processing of X-ray Diffraction Data Collected in Oscillation Mode. *Methods Enzymol.* **276**, 307-326

9. McCoy, A. J., Grosse-Kunstleve, R. W., Adams, P. D., Winn, M. D., Storoni, L. C., and Read, R. J. (2007) Phaser crystallographic software. *J Appl Crystallogr* **40**, 658-674

14

10. Murshudov, G. N., Vagin, A. A., and Dodson, E. J. (1997) Refinement of macromolecular structures by the maximum-likelihood method. *Acta Crystallogr D Biol Crystallogr* **53**, 240-255

11. Emsley, P., and Cowtan, K. (2004) Coot: model-building tools for molecular graphics. *Acta Crystallogr D Biol Crystallogr* **60**, 2126-2132

12. Chen, V. B., Arendall, W. B., 3rd, Headd, J. J., Keedy, D. A., Immormino, R. M., Kapral, G. J., Murray, L. W., Richardson, J. S., and Richardson, D. C. (2010) MolProbity: all-atom structure validation for macromolecular crystallography. *Acta crystallographica. Section D, Biological crystallography* **66**, 12-21

13. Rovenska, M., Hlouchova, K., Sacha, P., Mlcochova, P., Horak, V., Zamecnik, J., Barinka, C., and Konvalinka, J. (2008) Tissue expression and enzymologic characterization of human prostate specific membrane antigen and its rat and pig orthologs. *The Prostate* **68**, 171-182

14. Bradford, M. M. (1976) A rapid and sensitive method for the quantitation of microgram quantities of protein utilizing the principle of protein-dye binding. *Anal Biochem* **72**, 248-254

15. Barlos, K., Chatzi, O., Gatos, D., and Stavropoulos, G. (1991) 2-Chlorotrityl chloride resin. Studies on anchoring of Fmoc-amino acids and peptide cleavage. *Int J Pept Protein Res* **37**, 513-520

16. Kaiser, E., Colescott, R. L., Bossinger, C. D., and Cook, P. I. (1970) Color test for detection of free terminal amino groups in the solid-phase synthesis of peptides. *Anal Biochem* **34**, 595-598

17. Woodward, C., Henderson, J. K., and Wielgos, T. (2007) High-speed amino acid analysis(AAA) on 1.8 lm reversed-phase (RP) columns. . *Agilent Technologies App. Note* 5989-6297EN

18. Schilling, O., Huesgen, P. F., Barre, O., Auf dem Keller, U., and Overall, C. M. (2011) Characterization of the prime and non-prime active site specificities of proteases by proteome-derived peptide libraries and tandem mass spectrometry. *Nat Protoc* **6**, 111-120

19. Krissinel, E. (2012) Enhanced fold recognition using efficient short fragment clustering. *Journal of Molecular Biochemistry* **1**

15

20. Mesters, J. R., Barinka, C., Li, W., Tsukamoto, T., Majer, P., Slusher, B. S., Konvalinka, J., and Hilgenfeld, R. (2006) Structure of glutamate carboxypeptidase II, a drug target in neuronal damage and prostate cancer. *EMBO J* **25**, 1375-1384

21. Pavlicek, J., Ptacek, J., and Barinka, C. (2012) Glutamate Carboxypeptidase II: An Overview of Structural Studies and Their Importance for Structure-Based Drug Design and Deciphering the Reaction Mechanism of the Enzyme. *Current Medicinal Chemistry* **19**, 1300-1309

22. Lawrence, C. M., Ray, S., Babyonyshev, M., Galluser, R., Borhani, D. W., and Harrison, S. C. (1999) Crystal structure of the ectodomain of human transferrin receptor. *Science* **286**, 779-782

23. Zheng, H., Chruszcz, M., Lasota, P., Lebioda, L., and Minor, W. (2008) Data mining of metal ion environments present in protein structures. *J Inorg Biochem* **102**, 1765-1776

24. Klusak, V., Barinka, C., Plechanovova, A., Mlcochova, P., Konvalinka, J., Rulisek, L., and Lubkowski, J. (2009) Reaction mechanism of glutamate carboxypeptidase II revealed by mutagenesis, X-ray crystallography, and computational methods. *Biochemistry* **48**, 4126-4138

25. Navratil, M., Ptacek, J., Sacha, P., Starkova, J., Lubkowski, J., Barinka, C., and Konvalinka, J. (2014) Structural and biochemical characterization of the folyl-poly-gamma-l-glutamate hydrolyzing activity of human glutamate carboxypeptidase II. *FEBS J* **281**, 3228-3242

26. Lindner, H. A., Lunin, V. V., Alary, A., Hecker, R., Cygler, M., and Menard, R. (2003) Essential roles of zinc ligation and enzyme dimerization for catalysis in the aminoacylase-1/M20 family. *J Biol Chem* **278**, 44496-44504

27. Thierry-Mieg, D., and Thierry-Mieg, J. (2006) AceView: a comprehensive cDNA-supported gene and transcripts annotation. *Genome Biol* **7 Suppl 1**, S12 11-14

28. Sedo, A., and Malik, R. (2001) Dipeptidyl peptidase IV-like molecules: homologous proteins or homologous activities? *Biochim Biophys Acta* **1550**, 107-116

29. Taylor, A. (1996) *Chapter I:Aminopeptidases, occurence, regulation and nomenclature. In: Taylor A. editor. The Aminopeptidases*, Landes Bioscience Publishers, Austin, TX

30. Weiss, M. S. (2001) Global indicators of X-ray data quality. *Journal of Applied Crystallography* **34**, 130-135

16

31.   Cheng, Y., and Prusoff, W. H. (1973) Relationship between the inhibition constant (K1) and the concentration of inhibitor which causes 50 per cent inhibition (I50) of an enzymatic reaction. *Biochem Pharmacol* **22**, 3099-3108

17

ACKNOWLEDGEMENTS

FOOTNOTES

Abbreviation used: AA, amino acid; Avi-GCPII, extracellular portion of GCPII with N-terminal AviTEV tag; AMC, aminomethylcoumarine; Avi-NaalL, extracellular portion of NAALADase L with N-terminal AviTEV tag; cDNA, complementary deoxyribonucleic acid; DIC, N,N'-diisopropylcarbodiimide; DIEA, N,N-diisopropylethylamine; DPP IV, dipeptidyl peptidase IV; FA, formic acid; Fmoc, fluorenylmethyloxycarbonyl ; GCPII/III, glutamate carboxypeptidase II/III; HILAP, human ileal aminopeptidase; His-NaalL, extracellular portion of NAALADase L with N-terminal His tag; His-tag, hexahistidine tag; HOBt, 1-hydroxybenzotriazole; I100, 100-kDa brush border membrane protein; NAAG, N-acetyl-L-aspartyl-L-glutamate; NAALADase I/II/L, *N*-acetylated alpha-linked acidic dipeptidase I/II/-like; NTs, nucleotides; PDB, protein data bank; PICS, proteomic identification of cleavage site; PSMA, prostate-specific membrane antigen; qPCR, quantitative polymerase chain reaction; rhGCPII/III, extracellular portion of recombinant human GCPII/III; SGAP, aminopeptidase from *Streptomyces griseus;* tBu, *tert*-butyl; TEV, tobacco etch virus

FIGURES AND TABLE LEGENDS

Table 1: Data Collection and Refinement Statistics for Avi-NaalL
[a] $R_{pim} = \Sigma_{hkl} (1/(n-1))^{0.5} \Sigma^{n}_{j=1} |I_{hkl,j} - \langle I_{hkl} \rangle| / \Sigma_{hkl} \Sigma_j I_{hkl,j}$ (30) [b] estimated by SFcheck [c] R value = $||F_o| - |F_c||/|F_o|$, where F_o and F_c are the observed and calculated structure factors, respectively. [d] R_{free} is equivalent to the R value but is calculated for 1% of the reflections selected at random and omitted from the refinement process. [e] as determined by MolProbity (12). *the data in parentheses refer to the highest-resolution shell. Amino acids of the AviTEV-tag and first seven N-terminal amino acids of Avi-NaalL are disordered and not modeled in the structure.

Table 2: List of Avi-NaalL peptidic substrates sequences determined by PICS.
Sequences are written in one-letter AA coding from N- to C-terminus. A dash marks the putative cleavage site.

Figure 1: SDS-PAGE and SEC analysis of Avi-NaalL(E416A) affinity purification.
Concentrated conditioned medium from S2 cells mixed with equilibration buffer (fraction L) was mixed with Streptavidin Mutein Matrix overnight. The medium was separated from the resin (fraction FT), and the resin was washed with washing buffer (fraction W1). The resin was then transferred to elution buffer (fraction W2). After 1 h incubation, Avi-NaalL(E416A) was eluted with an excess of D-biotin (fractions E1-E4). Samples were loaded on the gel and silver-stained; L, FT – 1 µl; W1, W2 – 15 µl; E1 – 1 µl; E2 – 10 µl; E3, E4 – 15 µl. The quaternary fold of Avi-NaalL(E416A) was subsequently analyzed using FPLC system and Superdex™ 200 10/300 column. Prior the analysis, the column was calibrated by LMW and HMW Gel Filtration Calibration Kits (GE Healthcare) following manufacturer's protocol.

18

Figure 2: X-ray structure of Avi-NaalL and its structural and sequential comparison to GCPII.
Panel A: Alignment of Avi-NaalL (PDB code 4TWE) and GCPII (PDB code 3BXM) structures. Both are shown in ribbon representation. GCPII is shown in gray. Avi-NaalL is color-coded based on its domain organization: protease-like domain – red, apical domain – yellow, C-terminal domain – orange. The zinc ions are shown as magenta spheres and calcium ion as blue sphere. **Panel B:** Overall structure of Avi-NaalL dimer shown in ribbon representation. One monomer is shown in wheat, and the other is colored based on its domain organization. The zinc ions are shown as magenta spheres and calcium ions as blue spheres. The carbohydrate moieties are depicted as cyan sticks with oxygen atoms in red and nitrogen in blue. The disulfide bond between Cys296 and Cys313 is shown as a green stick. The top-view of the dimer illustrates the extensive dimerization interface. **Panel C:** Sequential alignment of GCPII and NAALADase L. Conserved AAs are highlighted in yellow and similar AAs in cyan. The domain organization of NAALADase L is indicated by arrows above the sequence colored as follows: intracellular domain – black, transmembrane domain – gray, protease-like domain – red, apical domain – yellow, C-terminal domain – orange. The catalytic acid/base Glu is marked with blue star. Residues coordinating the zinc ions are black-boxed. N-glycosylation sites are shown as blue circles, shaded if electron density for corresponding N-acetylglucoseamide was detected. AAs coordinating the calcium ion are shown as red circles and Cys residues forming the disulfide bond as green circles. AAs participating in NAAG binding in GCPII are marked with magenta circles.

Figure 3: Detailed features of the Avi-NaalL structure compared with the GCPII structure.
Avi-NaalL residues are shown in green and GCPII residues in gray. Oxygens are colored red and nitrogens blue. **Panel A:** Calcium ion hepta-coordination shell in Avi-NaalL with electron density map. The calcium ion is coordinated by the Glu425 and Glu428 side chain carboxyl groups, the Thr258 hydroxyl group, the carbonyl oxygens of Leu261 and Thr258, and a water molecule. Interactions are depicted as dashed lines with distances shown. The calcium ion is shown as a blue sphere and water as red sphere. The *2Fo-Fc* map (contoured to 1 σ) is shown in blue, while the *Fo-Fc* map (contoured to 3 σ) is colored green for positive and red for negative electron density peaks. **Panel B:** Superposition of the zinc ion coordination shells in Avi-NaalL and GCPII (PDB code 2PVW). The coordination shell of the active-site zincs is identical for both proteins, utilizing the side chains of His368, Asp378, Glu417, Asp445, and His545 in Avi-NaalL. Additionally, the position of the Glu416 side chain is identical to the position of the catalytic glutamate (Glu424) in GCPII. Interactions are depicted as dashed lines with distances shown. **Panel C:** Electron density map around the Avi-NaalL active site. The *2Fo-Fc* map (contoured to 1 σ) is shown in blue, while the *Fo-Fc* map (contoured to 3 σ) is colored green for positive and red for negative electron density peaks. Zinc ions are shown as magenta spheres and waters as red spheres. **Panel D:** Superposition of AAs contributing to substrate binding in GCPII with the Avi-NaalL structure. The structure of GCPII E424A mutant (PDB code 3BXM) with bound N-acetyl-L-aspartyl-L-glutamate (NAAG), an endogenous GCPII substrate, is shown. Zinc ions in the GCPII structure are shown as gray spheres and in Avi-NaalL as magenta spheres. Interactions of NAAG with GCPII are depicted as dashed lines. **Panel E:** Superposition of the arginine patch in the GCPII (PDB code 3BXM) structure with Avi-NaalL. GCPII water molecule and chloride ion are depicted as gray spheres and Avi-NaalL waters as green spheres. Interactions of both GCPII and Avi-NaalL are depicted as dashed lines with distances shown.

Figure 4: *NAALADL1* gene product expression in human tissues.
Panel A: Quantitative PCR (qPCR) determination of *NAALADL1* mRNA. Two sets of primers (NaalL_A and NaalL_B) were used to independently assess the level of *NAALADL1* transcripts in different human tissues. "No. of transcripts" indicates the number of transcripts determined in 0.1 μL of normalized cDNA library, with values showing the mean of triplicate measurements. Error bars represent standard deviations (for more experimental details, see Experimental procedures). **Panel B:** Western blot analysis of human tissue samples. Tissue lysates (50 μg total protein) were loaded onto the gel with recombinant Avi-NaalL (5 ng) as a control. Samples were incubated with 1C11 hybridoma supernatant overnight, and the

19

antibody-antigen complex was visualized using HRP-conjugated anti-mouse secondary antibody. The dashed squares indicate false-positive signals, while the solid box marks NAALADase L (as determined by MS; data not shown).

Figure 5: Determination of Avi-NaalL DPP IV activity.
DPP IV activity was assayed using the fluorogenic substrate Gly-Pro-AMC (exc./em. 335 nm/450 nm). Potential DPP IV activity of recombinant Avi-NaalL (1 µg) was assessed. Avi-GCPII (1 µg) and substrate alone (blank) were used as negative controls, while LNCaP lysate (10 µg total protein) was used as a positive control. The reactions were incubated for 15 h at 37 °C. Each reaction was performed in triplicate and is shown as a mean with standard deviation.

Figure 6: Heat-maps reflecting qualitative determination of carboxypeptidase activity.
Recombinant Avi-NaalL and Avi-GCPII were incubated with 19 different N-acetylated dipeptide libraries of the general formula Ac-Aaa-X-OH (Aaa – constant amino acid, X – mixture of 19 proteinogenic AAs). After 15 h incubation at 37 °C, the free amine groups of cleaved C-terminal AAs were modified, and the AAs were detected by HPLC. Avi-NaalL(E416A) and Avi-GCPII(E424A), catalytically ineffective mutants of both enzymes, were used for background subtraction. The color-coding corresponds to the percentage of conversion of the particular AA in the reaction mixture; the overall amount of each AA in dipeptide libraries was detected by amino acid analysis prior to the experiment.

Figure 7: Heat-maps of proteomic identification of cleavage site (PICS) results.
PICS experiments were performed as described in Experimental procedures with Avi-NaalL and its catalytically ineffective mutant Avi-NaalL(E416A) and with HIV-1 protease and its catalytically ineffective mutant HIV-1(D25N) protease (positive control). Briefly, the proteins were incubated overnight with a peptide library derived from the HEK293T proteome. Cleaved peptides were subsequently isolated from the reaction mixture *via* biotin modification of newly formed primary amino groups. The peptides were identified by LC-MS/MS analysis, and their corresponding prime parts were determined by sequence alignment with a human proteome database. The MEROPS substrate profile of HIV-1 protease is presented for comparison (http://merops.sanger.ac.uk/cgi-bin/pepsum?id=A02.001). **Panel A:** Heat-maps illustrate in grayscale the percentage of individual AAs at a particular position relative to the scissile peptide bond. Four positions (P4′–P4) are shown. **Panel B:** Heat-maps illustrate ratios of individual AA occurrence at a given position compared to the overall occurrence of that AA in the human genome. Ratios above 1 (i.e., preferred by the protease analyzed) are shown in shades of green, while ratios below 1 (i.e., rejected by the protease analyzed) are shown in shades of red.

Figure 8: Avi-NaalL-catalyzed hydrolysis of two peptide substrates identified by PICS.
Recombinant Avi-NaalL was mixed with peptide (peptide 52 or peptide 71) in final concentrations of 1 µM and 100 µM, respectively. The specificity of cleavage was investigated using the catalytically ineffective mutant Avi-NaalL(E416A). Reaction mixtures were incubated for 15 h at 37 °C and analyzed using LC/MS. Peptide sequences or individual AA were identified based on their molecular mass and are shown in the legend. The amounts of peptide or AA were determined using absorption at 210 nm. Each reaction was done in duplicate and the result is shown as a mean with standard error.

Figure 9: Quantitative analysis of Avi-NaalL aminopeptidase activity.
Panel A: Time-dependent analysis of the peptide 52 cleavage by Avi-NaalL. Recombinant Avi-NaalL was mixed with peptide 52 in final concentrations of 0.1 µM and 100 µM, respectively. Reactions were performed at 37 °C and were stopped at times ranging from 5 min to 90 min and analyzed by LC/MS. The relative amount of individual peptides or AA is plotted against reaction time in panels A1-A5. **Panel B:** Determination of kinetic parameters of model peptide substrate (I/IDPNG) cleavage by Avi-NaalL. The enzyme was incubated with various concentrations of substrate, ranging from 6.3 to 1600 µM, for 15 min at 37 °C. The reactions mixtures were subsequently analyzed using HPLC. Each reaction was done in

20

duplicate and the result is shown as a mean with standard error. The kinetic parameters were obtained by non-linear fit of the data using GraFit v.5.0.11 (Erithacus Software Ltd.). The reciprocal linear plot is also illustrated for comparison. **Panel C:** Determination of inhibition constant of aminopeptidase specific inhibitor bestatin towards Avi-NaalL. Various concentration of bestatin, ranging from 0.1 to 500 μM, was incubated with Avi-NaalL and a model substrate (I/IDPNG) for 15 min at 37 °C. The reactions mixtures were subsequently analyzed using HPLC. Each reaction was done in duplicate and the result is shown as a mean with standard error. The IC_{50} value was obtained by non-linear fit of the data using GraFit v.5.0.11 (Erithacus Software Ltd.) and the K_i value was then calculated using Cheng-Prussof equation for competitive mode of inhibition (31).

Figure 10: Processing of a random peptide by Avi-NaalL
Recombinant Avi-NaalL was mixed with the peptide RIKLNWFS in final concentrations of 1 μM and 100 μM, respectively. The specificity of cleavage was investigated using the catalytically ineffective mutant Avi-NaalL(E416A). Reaction mixtures were incubated for 15 h at 37 °C and analyzed using LC/MS. The peptide sequences or individual AAs were identified based on their molecular mass and are shown in the legend. The amounts of peptide or AAs were determined by absorption at 210 nm. Each reaction was done in duplicate and the result is shown as a mean with standard error.

21

Table 1

PDB code	4TWE
Data collection statistics:	
Space group	*I*222
Temperature (K)	100
Cell parameters: a; b; c (Å)	98.5; 174.8; 208.0
No. of molecules in AU	2
Wavelength (Å)	1.000
Resolution limits (Å)	30.0 – 1.75
Highest resolution shell (Å)	1.78 – 1.75
No. of unique refl.	177979 (8822)*
Multiplicity	7.6 (7.5)
Completeness (%)	99.7 (99.4)
R_{pim} (%)[a]	2.9 (20.0)
Average $I/\sigma(I)$	22.1 (4.2)
Wilson B (Å^2)[b]	31.7
Refinement statistics:	
Resolution range (Å)	29.14 – 1.75
Highest resolution shell (Å)	1.80 – 1.75
No. of refl. in working set	172688 (12359)
No. of refl. in test set	1757 (112)
R value (%)[c]	0.167 (0.202)
R_{free} value (%)[d]	0.187 (0.231)
RMSD bond length (Å)	0.020
RMSD angle (º)	1.74
No. of atoms in AU	13236
No. of protein atoms in AU	11535
No. of ion atoms in AU	6
No. of solvent molecules in AU	1695
Mean B value (Å^2)	26.64
Mean B value of protein atoms (Å^2)	25.0
Mean B of solvent molecules (Å^2)	38.1
Ramachandran plot statistics[e]:	
Res. in favored regions (%)	97.2
Res. in allowed regions (%)	99.8
Outliers	Val373A/B, Ala450A

22

Table 2

#	Peptide sequence	#	Peptide sequence
1	–RFIPR	37	KISKG–ANPVEIR
2	–EDTNLCAIHAK	38	QEARK–AITEQKQK
3	KA–FYPEEISSMVLTK	39	SMKKA–AEVLNK
4	–EAPLNPK	40	NEEDA–AELVALAQAVNAR
5	–MDLEK	41	KEMVR–ADLINKK
6	GVVD–SEDLPLNISR	42	TRARF–EELCSDLFR
7	–RFLPR	43	RGVVD–SEDIPLNLSR
8	QN–IIPASTGAAK	44	MNTFS–VVPSPK
9	GV–VDSEDLPLNISR	45	VCDGK–VSVHVIEGDHR
10	L–VDLEPGTMDSVR	46	AHSSM–VGVNLPQK
11	–ALERLLR	47	QAFYM–VGPIEEAVAK
12	A–VFPSIVGR	48	RGNPT–VEVDLFTSK
13	–MDIER	49	ATRAA–VEEGIVLGGGCALLR
14	D–PPDVLDR	50	FIRGV–VDSEDIPLNLSR
15	EKSY–ELPDGQVITIGNER	51	NPTVE–VDLFTSK
16	–IEPIDEYCVQQLK	52	PRAVF–VDLEPTVIDEVR
17	EKS–YELPDGQVITIGNER	53	QYRAL–TVPELTQQMFDAK
18	FRA–AVPSGASTGIYEALELR	54	ITSDP–TEATAVGAVEASFK
19	DDEEF–ELPEFVEPFLK	55	PPEDP–SVPVALNIGK
20	GDEGG–FAPNILENK	56	DPSRY–ISPDQLADLYK
21	DIYNF–FSPLNPVR	57	VLKRG–LKPSCTIIPL
22	YDAMA–GDFVNMVEK	58	HLYRG–IFPVLCK
23	RKQSL–GELIGTLNAAK	59	KSGVK–IHVSDQELQSANASVDDSR
24	LLDPM–GGIVMTNDGNAILR	60	GCELK–ADKDYHFK
25	RDNIQ–GITKPAIR	61	KACQS–IYPLHDVFVR
26	PGAGR–GYNSIGR	62	INKKC–YEMASHLR
27	PSATL–HLSNIPPSVSEEDLK	63	LYDER–SVHKVEPITK
28	GETKS–FYPEEVSSMVLTK	64	VASRG–LDVEDVK
29	TRARF–EELNADLFR	65	MDMDM–SPLRPQNYLFGCELK
30	QRTVK–HPTLLQDPDLR	66	DVYKG–LLPEELTPLILATQK
31	TRAAV–EEGIVLGGGCALLR	67	KNQVA–LNPQNTVFDAK
32	GVVDS–EDLPLNISR	68	LLPEE–LTPLILATQK
33	GVVDS–EDIPLNLSR	69	TSWPR–PIFGSLHHVPDLSCR
34	QHPPK–DSSGQHVDVSPTSQR	70	SMGRG–RDWNVDLIPK
35	DPFDQ–DDWGAWQK	71	RGLFI–IDPNGVIK
36	QRIKA–AVPSIK	72	PHAKK–KSKISASRK

23
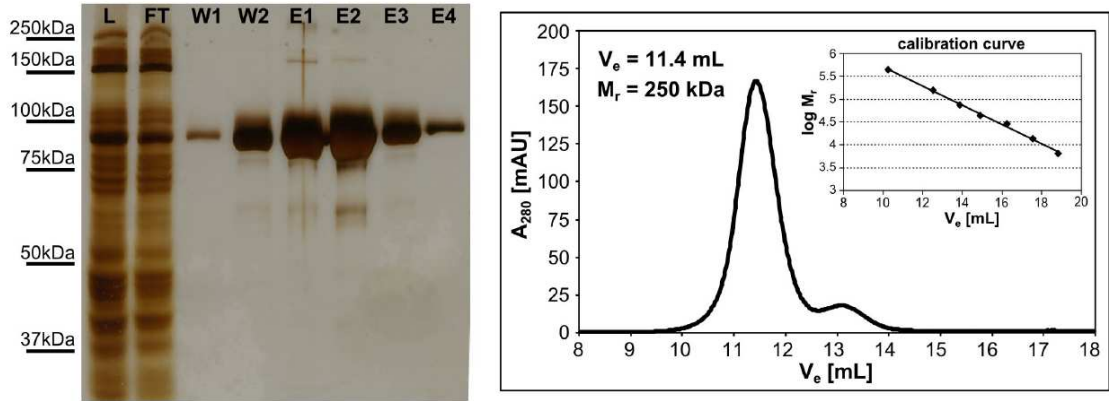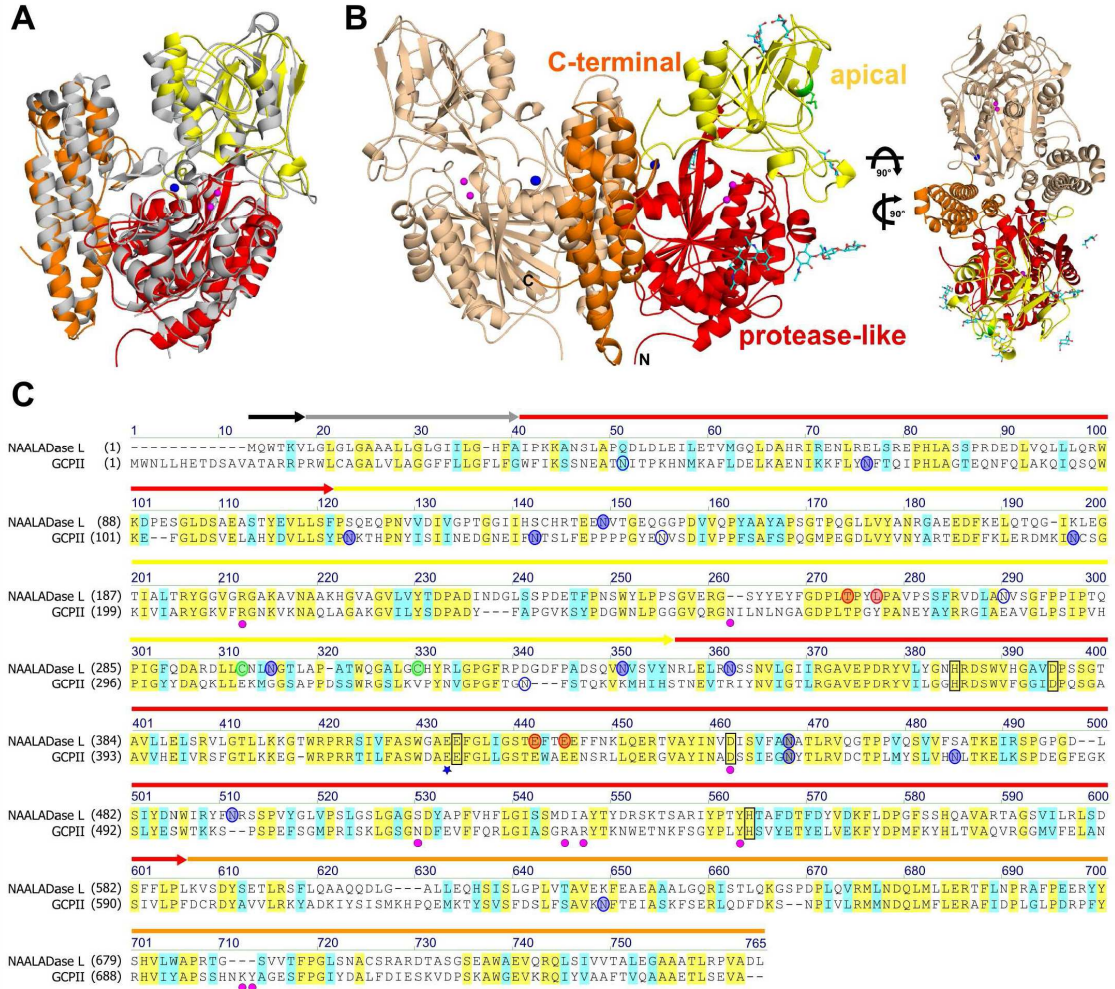
Figure 1

Figure 2

Figure 3
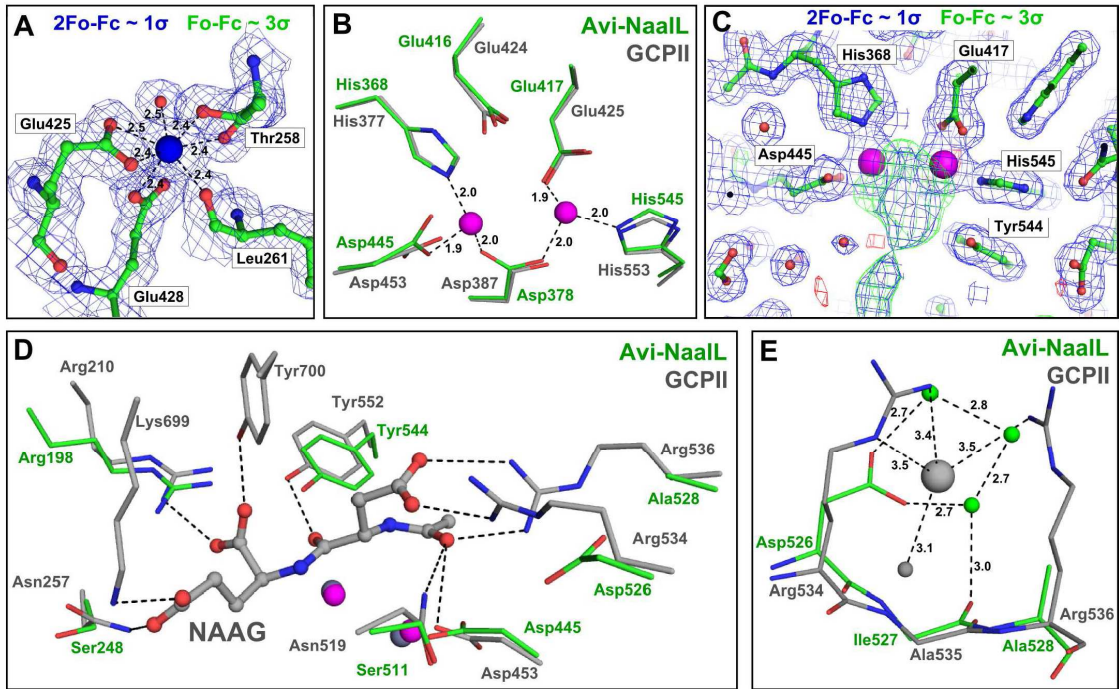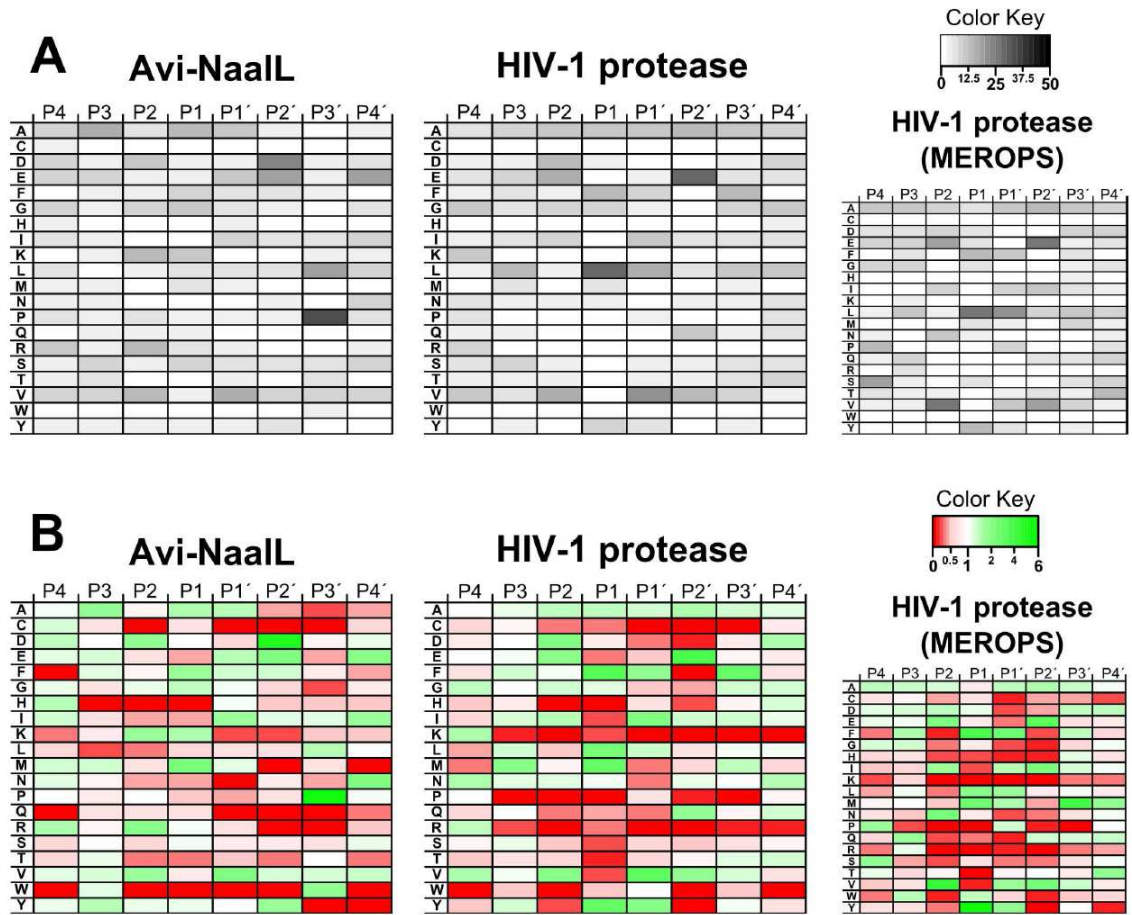
Figure 4
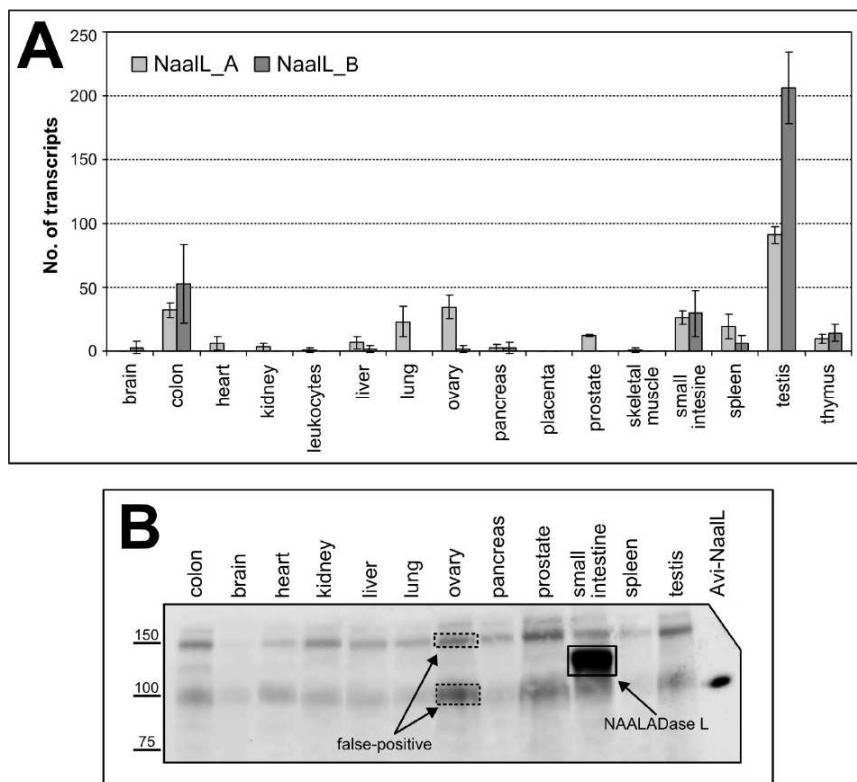
Figure 5
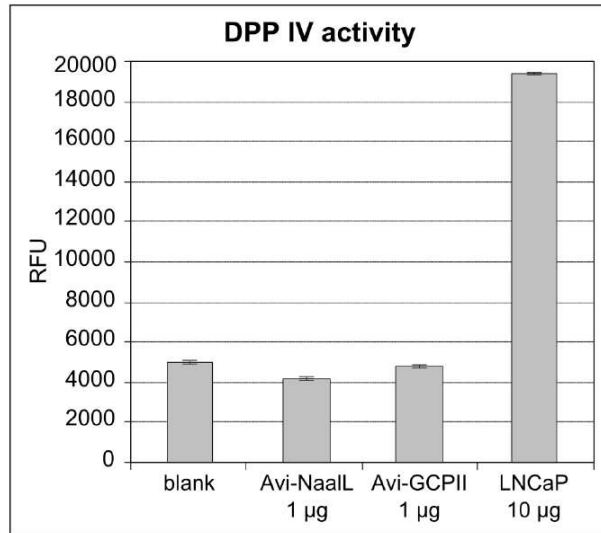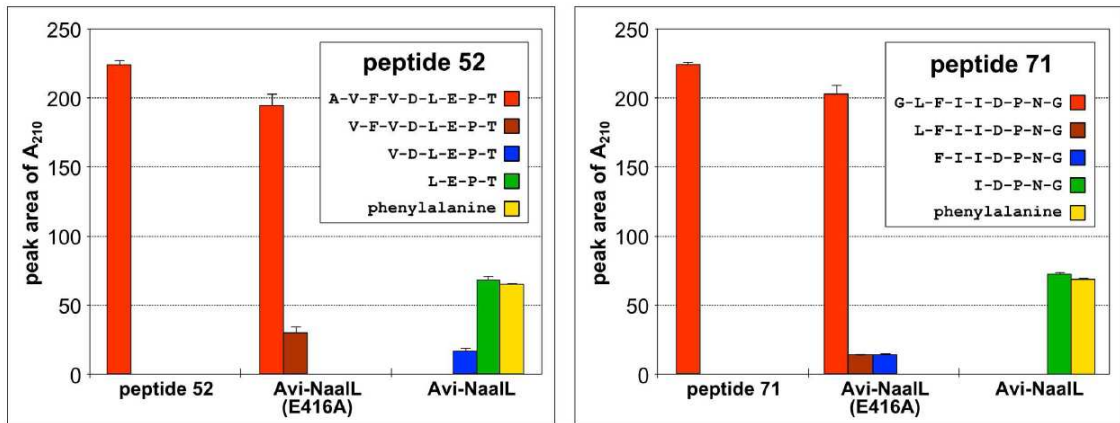
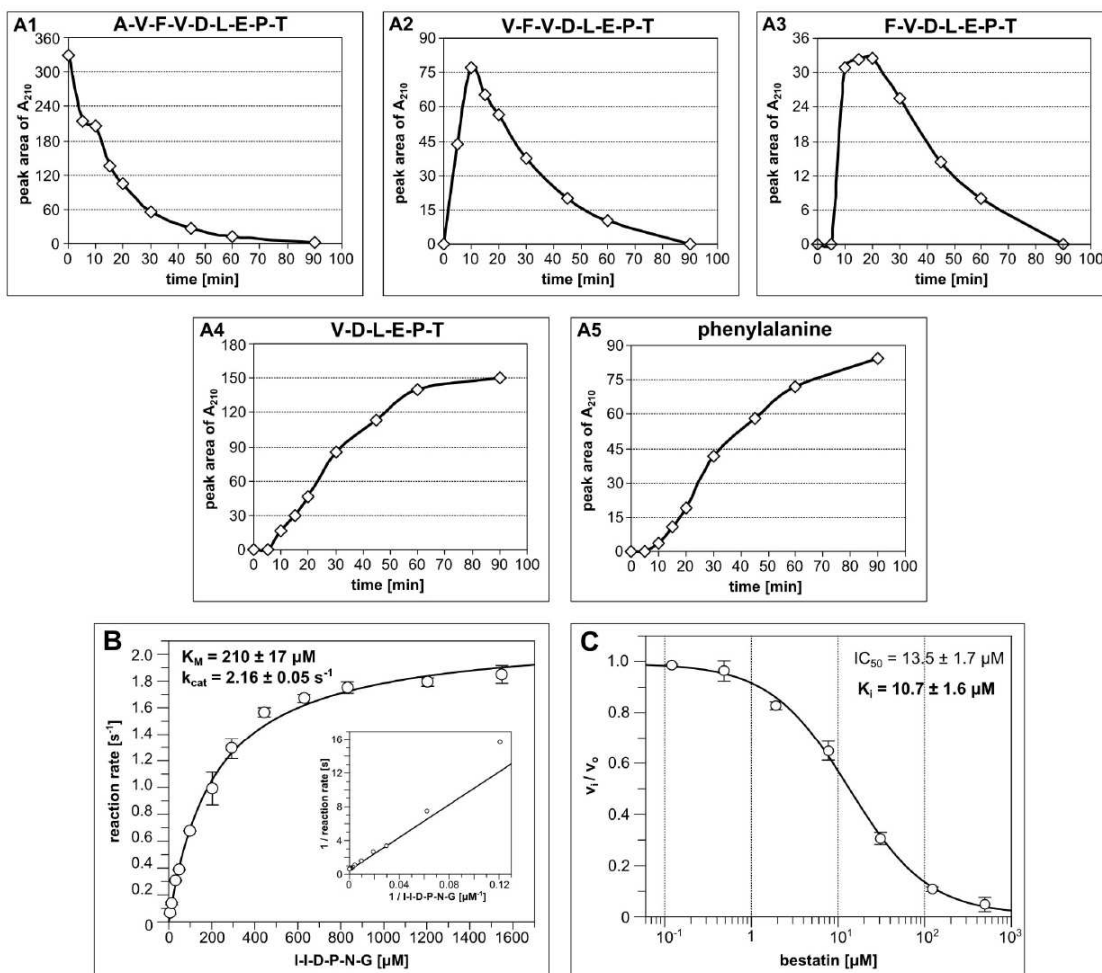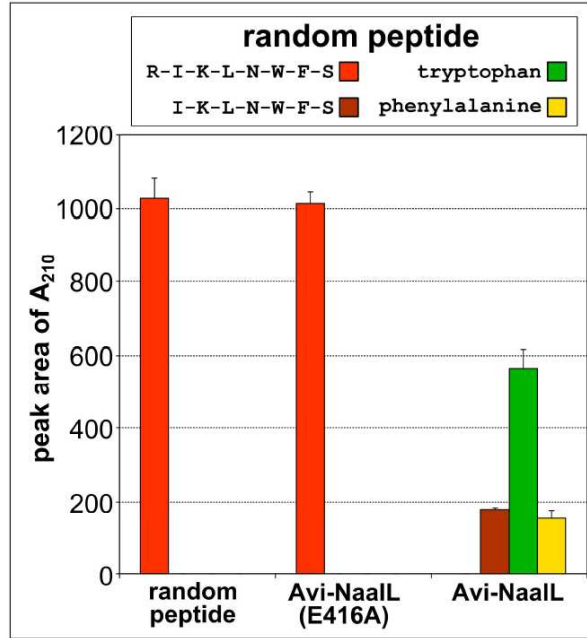**Figure 6**
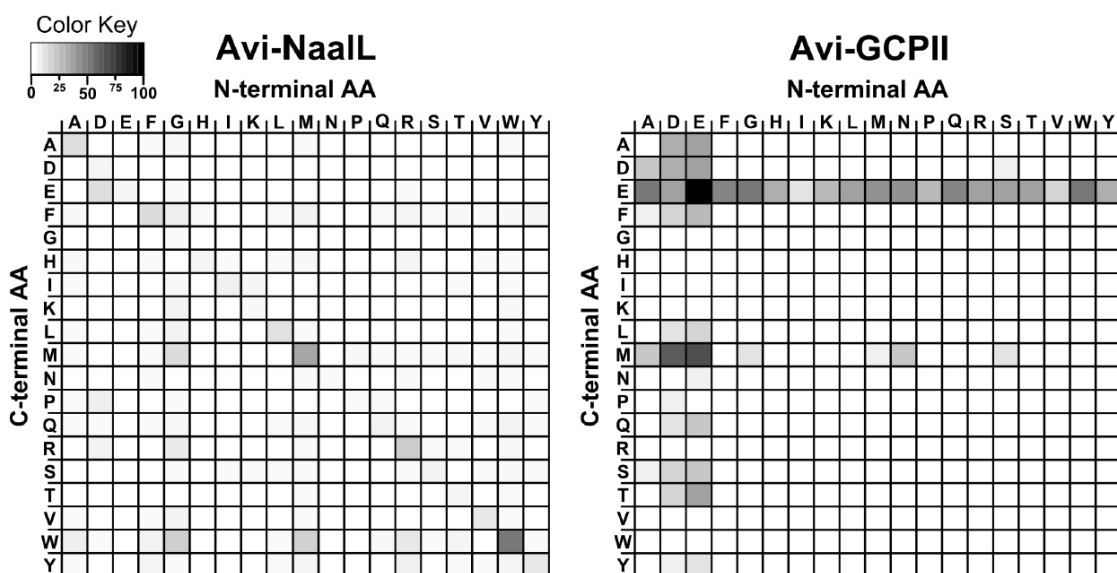
Figure 7

Figure 8

Figure 9

Figure 10

Chapter 3: Discussion and conclusion

As reviewed in the Introductory section, GCPII represents a promising target for diagnostic and therapy of prostate cancer as well as other solid tumors. Additionally, the inhibition of GCPII enzymatic activity seems to be neuroprotective suggesting the key role of the enzyme in the neuropathological conditions; most probably through its role in glutamate-mediated neurotoxicity. Lastly, due to the convenient protein topology, inducible internalization upon ligand binding and favorable expression profile, GCPII is frequently used as a model molecule for various specific-targeting delivery studies.

To enable effective use of GCPII in all these research areas, a reliable and efficient technique for its preparation is essential. We present here a new Avi-tag™-based purification protocol for preparation of recombinant GCPII in eukaryotic expression system. The system provides high-yields of homogenous protein in one-step purification set-up and does not demand extensive instrumentation, which makes it highly cost-effective. Moreover, we demonstrate the high versatility of our system by its application to several other proteins topologically identical to GCPII, such as GCPIII or NAALADase L. Additional advantage of this purification system is that the purified protein is specifically modified by biotin at the side chain amino group of lysine residue within the Avi-tag. Such specific protein modification enables facile protein visualization, immobilization or isolation by various commercially available streptavidin or neutravidin conjugates. We have extensively utilized this feature in both following studies presented in the thesis.

Monoclonal antibodies against GCPII represent not only indispensable tool for common laboratory work in GCPII-related research, but also one of the key clinical molecular agents to specifically target GCPII. Therefore, it is not surprising that there are various mAbs commercially available in the market and several mAb-conjugates are currently in the late stages of clinical trials. Unfortunately, even though mAbs against GCPII clearly play an important role in GCPII-related research, they are mostly very poorly characterized which may lead to their improper use or misinterpretation of obtained data. The presented study aims to address this issue by collecting and characterizing the most commonly used mAbs against GCPII.

This study targets two main knowledge-gaps which we have identified in this field. Firstly, mAbs have been mostly described based on the methods for which they should be used instead of the nature of antigen (native or denatured) they recognize. The current

description often lead to the confusion since there are several basic mAb-based techniques, such as IHC or fluorescent microscopy, which can be performed in both native and denature set-ups. Therefore, we decided to primarily sort out the mAbs based on their ability to bind either denature or native form of GCPII. This distinction based on the nature of the recognized antigen should provide the researchers with sufficient information for effective use of the corresponding mAbs in any given method.

Secondly, even though several close GCPII paralogs, such as GCPIII or NAALADase L, have been identified in the past decade, the potential cross-reactivity of available GCPII-specific mAbs against these proteins has not been investigated at all. Similarly, the issue of mAbs cross-reactivity with GCPII orthologs, such as mouse or rat GCPII, has also been largely ignored. Since potential unknown cross-reactivity may significantly influence the obtained results, for example in targeting GCPII-specific tissues in humans or in analyzing mouse xenograft models, we decided to probe all collected mAbs against closest and most relevant GCPII homologs; mouse GCPII, mouse GCPIII and human GCPIII.

The described lack of proper mAbs description may be the reason for several major inconsistencies identified in GCPII research which involve methods utilizing mAbs, such as GCPII protein expression determined by western blotting, ELISA or IHC (see section 1.6). We hope that our study will help the researchers to use available anti-GCPII mAbs more appropriately and efficiently in the future, which might ultimately lead to diminishing of such inconsistencies in published results.

Since we performed quantitative characterization of collected mAbs, the obtained dissociation constants for respective antigen-antibody complexes can be easily applied to optimize the appropriate protocol for highest possible signal output while keeping the mAb consumption to a minimum. Moreover, if the mAb with described cross-reactivity is used, the working mAb concentration can be adjusted in order to minimize the cross-reactivity or visualize both potential antigens; depending on individual researcher's need.

Finally, we would like to stress out that the motivation for performing this study was not to advertise one mAb over the other, but primarily provide a comprehensive characterization of given mAbs and point out the misleading information which can be found in some of the analyzed mAbs datasheets. For example, the mAb YPSMA-1 has been used in some studies for recognition of native GCPII, while it clearly recognizes only the denature form of the protein [118, 203]. This incorrect use of YPSMA-1 may be explained by the fact that its datasheet states the application of this mAb on the methods

such as IHC on frozen tissue slides, immunocytochemistry or flow-cytometry; the methods which are generally recognized as the techniques working with a native antigen. We hope that our presented data will help to prevent the repetition of such unfortunate use of anti-GCPII mAbs in the future.

Even though GCPII has been investigated for more than two decades as specific marker of prostate cancer, the physiological connection of increased expression level of GCPII with development of this pathological condition has not been conclusively identified yet. Based on the close structural homology to transferrin receptor, the putative role of GCPII in prostate cancer as a receptor rather than an enzyme has been proposed by several research groups (see section 1.7.2). However, the putative partner of GCPII has not yet been identified. To reveal potential non-enzymatic function of GCPII, a characterization and determination of physiological functions of its close homologs may be useful. Therefore, we decided to characterize NAALADase L and determine its physiological function.

By determination of its X-ray structure, we demonstrated that NAALADase L has very similar secondary and tertiary structure as GCPII. This fact together with the conservation of essential amino acids (zinc coordinating amino acids and catalytic acid/base glutamate) suggested that it might embody similar enzymatic activity to that of GCPII. Surprisingly, we identified that NAALADase L acts as an aminopeptidase rather than carboxypeptidase. This fact together with restricted protein expression of NAALADase L in the small intestine indicated that its physiological role will probably be associated with the protein/peptide degradation and led us to propose a new name for this enzyme: human ileal aminopeptidase (HILAP).

The presented data suggest that even though HILAP is highly homologous to GCPII on the structural level, its specialized physiological function does not make this protein a good candidate from which GCPII non-enzymatic role in pathological conditions could be derived.

On the other hand, HILAP may represent an interesting molecule for study of molecular evolution of M28 family of metallopeptidases. This family of metallopeptidases comprises both amino- and carboxypeptidases. These aminopeptidases, such as aminopeptidase S from *Streptomyces griseus*, are single-domain enzymes, while carboxypeptidases, such as GCPII, are structurally more complex molecules, consisting of three domains and forming dimeric quaternary structure. This may make the HILAP

a potential evolutionary "intermediate" of these two enzyme sub-families having similar enzymatic activity as the first and the structure as the second. Even though this pilot study described HILAP from both structural and enzymological point of view, additional studies will be necessary to address these issues in more detail.

To conclude, we presented here optimization and validation of an efficient purification set-up which is generally applicable for secreted proteins, such as the extracellular portion of GCPII. Moreover, we performed thorough characterization, in both quantitative and qualitative manner, of the most commonly used mAbs against GCPII. The results of these studies will hopefully contribute to more concise and efficient GCPII-related research thus facilitating the preparation of clinically applicable agents for targeting pathological conditions such as prostate carcinoma. Finally, we describe here a biochemical characterization of a close GCPII homolog, HILAP, which suggested that this protein probably represents an important element in the molecular evolution of M28 family of metallopeptidases and its physiological role is likely connected to the peptide/protein degradation.

References

1. Robinson MB, Blakely RD, Couto R, Coyle JT: **Hydrolysis of the brain dipeptide N-acetyl-L-aspartyl-L-glutamate. Identification and characterization of a novel N-acetylated alpha-linked acidic dipeptidase activity from rat brain**. *J Biol Chem* 1987, **262**(30):14498-14506.

2. Horoszewicz JS, Kawinski E, Murphy GP: **Monoclonal antibodies to a new antigenic marker in epithelial prostatic cells and serum of prostatic cancer patients**. *Anticancer Res* 1987, **7**(5B):927-935.

3. Halsted CH: **Jejunal brush-border folate hydrolase. A novel enzyme**. *West J Med* 1991, **155**(6):605-609.

4. Pinto JT, Suffoletto BP, Berzin TM, Qiao CH, Lin S, Tong WP, May F, Mukherjee B, Heston WD: **Prostate-specific membrane antigen: a novel folate hydrolase in human prostatic carcinoma cells**. *Clin Cancer Res* 1996, **2**(9):1445-1451.

5. Carter RE, Feldman AR, Coyle JT: **Prostate-specific membrane antigen is a hydrolase with substrate and pharmacologic characteristics of a neuropeptidase**. *Proc Natl Acad Sci U S A* 1996, **93**(2):749-753.

6. Luthi-Carter R, Barczak AK, Speno H, Coyle JT: **Molecular characterization of human brain N-acetylated alpha-linked acidic dipeptidase (NAALADase)**. *J Pharmacol Exp Ther* 1998, **286**(2):1020-1025.

7. Halsted CH, Ling EH, Luthi-Carter R, Villanueva JA, Gardner JM, Coyle JT: **Folylpoly-gamma-glutamate carboxypeptidase from pig jejunum. Molecular characterization and relation to glutamate carboxypeptidase II**. *J Biol Chem* 1998, **273**(32):20417-20424.

8. Luthi-Carter R, Barczak AK, Speno H, Coyle JT: **Hydrolysis of the neuropeptide N-acetylaspartylglutamate (NAAG) by cloned human glutamate carboxypeptidase II**. *Brain Res* 1998, **795**(1-2):341-348.

9. Luthi-Carter R, Berger UV, Barczak AK, Enna M, Coyle JT: **Isolation and expression of a rat brain cDNA encoding glutamate carboxypeptidase II**. *Proc Natl Acad Sci U S A* 1998, **95**(6):3215-3220.

10. O'Keefe DS, Su SL, Bacich DJ, Horiguchi Y, Luo Y, Powell CT, Zandvliet D, Russell PJ, Molloy PL, Nowak NJ *et al*: **Mapping, genomic organization and promoter analysis of the human prostate-specific membrane antigen gene**. *Biochim Biophys Acta* 1998, **1443**(1-2):113-127.

11. Good D, Schwarzenberger P, Eastham JA, Rhoads RE, Hunt JD, Collins M, Batzer M, Theodossiou C, Kolls JK, Grimes SR: **Cloning and characterization of the prostate-specific membrane antigen promoter**. *J Cell Biochem* 1999, **74**(3):395-405.

12. Noss KR, Wolfe SA, Grimes SR: **Upregulation of prostate specific membrane antigen/folate hydrolase transcription by an enhancer**. *Gene* 2002, **285**(1-2):247-256.

13. Watt F, Martorana A, Brookes DE, Ho T, Kingsley E, O'Keefe DS, Russell PJ, Heston WD, Molloy PL: **A tissue-specific enhancer of the prostate-specific membrane antigen gene, FOLH1**. *Genomics* 2001, **73**(3):243-254.

14. Bzdega T, Turi T, Wroblewska B, She D, Chung HS, Kim H, Neale JH: **Molecular cloning of a peptidase against N-acetylaspartylglutamate from a rat hippocampal cDNA library**. *J Neurochem* 1997, **69**(6):2270-2277.

15. Cao KY, Mao XP, Wang DH, Xu L, Yuan GQ, Dai SQ, Zheng BJ, Qiu SP: **High expression of PSM-E correlated with tumor grade in prostate cancer: a new alternatively spliced variant of prostate-specific membrane antigen**. *Prostate* 2007, **67**(16):1791-1800.

16. O'Keefe D, Bacich D, Heston WW: **Prostate Specific Membrane Antigen**. In: *Prostate Cancer*. Edited by Chung LK, Isaacs W, Simons J: Humana Press; 2001: 307-326.

17. Su SL, Huang IP, Fair WR, Powell CT, Heston WD: **Alternatively spliced variants of prostate-specific membrane antigen RNA: ratio of expression as a potential measurement of progression**. *Cancer Res* 1995, **55**(7):1441-1443.

18. Williams T, Kole R: **Analysis of prostate-specific membrane antigen splice variants in LNCap cells**. *Oligonucleotides* 2006, **16**(2):186-195.

19. Grauer LS, Lawler KD, Marignac JL, Kumar A, Goel AS, Wolfert RL: **Identification, purification, and subcellular localization of prostate-specific membrane antigen PSM' protein in the LNCaP prostatic carcinoma cell line**. *Cancer Res* 1998, **58**(21):4787-4789.

20. Lapidus RG, Tiffany CW, Isaacs JT, Slusher BS: **Prostate-specific membrane antigen (PSMA) enzyme activity is elevated in prostate cancer cells**. *Prostate* 2000, **45**(4):350-354.

21. Barinka C, Sacha P, Sklenar J, Man P, Bezouska K, Slusher BS, Konvalinka J: **Identification of the N-glycosylation sites on glutamate carboxypeptidase II necessary for proteolytic activity**. *Protein Sci* 2004, **13**(6):1627-1635.

22. Ghosh A, Heston WD: **Effect of carbohydrate moieties on the folate hydrolysis activity of the prostate specific membrane antigen**. *Prostate* 2003, **57**(2):140-151.

23. Mlcochova P, Barinka C, Tykvart J, Sacha P, Konvalinka J: **Prostate-specific membrane antigen and its truncated form PSM'**. *Prostate* 2009, **69**(5):471-479.

24. Cunha AC, Weigle B, Kiessling A, Bachmann M, Rieber EP: **Tissue-specificity of prostate specific antigens: comparative analysis of transcript levels in prostate and non-prostatic tissues**. *Cancer Lett* 2006, **236**(2):229-238.

25. Chang SS, O'Keefe DS, Bacich DJ, Reuter VE, Heston WD, Gaudin PB: **Prostate-specific membrane antigen is produced in tumor-associated neovasculature**. *Clin Cancer Res* 1999, **5**(10):2674-2681.

26. Israeli RS, Powell CT, Corr JG, Fair WR, Heston WD: **Expression of the prostate-specific membrane antigen**. *Cancer Res* 1994, **54**(7):1807-1811.

27. Pangalos MN, Neefs JM, Somers M, Verhasselt P, Bekkers M, van der Helm L, Fraiponts E, Ashton D, Gordon RD: **Isolation and expression of novel human glutamate carboxypeptidases with N-acetylated alpha-linked acidic dipeptidase and dipeptidyl peptidase IV activity**. *J Biol Chem* 1999, **274**(13):8470-8483.

28. Renneberg H, Friedetzky A, Konrad L, Kurek R, Weingartner K, Wennemuth G, Tunn UW, Aumuller G: **Prostate specific membrane antigen (PSM) is expressed in various human tissues: implication for the use of PSM reverse transcription polymerase chain reaction to detect hematogenous prostate cancer spread**. *Urol Res* 1999, **27**(1):23-27.

29. Rawlings ND, Waller M, Barrett AJ, Bateman A: **MEROPS: the database of proteolytic enzymes, their substrates and inhibitors**. *Nucleic Acids Res* 2014, **42**(Database issue):D503-509.

30. Rawlings ND, Barrett AJ: **Structure of membrane glutamate carboxypeptidase**. *Biochim Biophys Acta* 1997, **1339**(2):247-252.

31. Mesters JR, Barinka C, Li W, Tsukamoto T, Majer P, Slusher BS, Konvalinka J, Hilgenfeld R: **Structure of glutamate carboxypeptidase II, a drug target in neuronal damage and prostate cancer**. *EMBO J* 2006, **25**(6):1375-1384.

32. Rajasekaran SA, Anilkumar G, Oshima E, Bowie JU, Liu H, Heston W, Bander NH, Rajasekaran AK: **A novel cytoplasmic tail MXXXL motif mediates the internalization of prostate-specific membrane antigen**. *Mol Biol Cell* 2003, **14**(12):4835-4845.

33. Davis MI, Bennett MJ, Thomas LM, Bjorkman PJ: **Crystal structure of prostate-specific membrane antigen, a tumor marker and peptidase**. *Proc Natl Acad Sci U S A* 2005, **102**(17):5981-5986.

34. Barinka C, Starkova J, Konvalinka J, Lubkowski J: **A high-resolution structure of ligand-free human glutamate carboxypeptidase II**. *Acta Crystallogr Sect F Struct Biol Cryst Commun* 2007, **63**(Pt 3):150-153.

35. Barinka C, Rovenska M, Mlcochova P, Hlouchova K, Plechanovova A, Majer P, Tsukamoto T, Slusher BS, Konvalinka J, Lubkowski J: **Structural insight into the pharmacophore pocket of human glutamate carboxypeptidase II**. *J Med Chem* 2007, **50**(14):3267-3273.

36. Navratil M, Ptacek J, Sacha P, Starkova J, Lubkowski J, Barinka C, Konvalinka J: **Structural and biochemical characterization of the folyl-poly-gamma-l-glutamate hydrolyzing activity of human glutamate carboxypeptidase II**. *FEBS J* 2014, **281**(14):3228-3242.

37. Pavlicek J, Ptacek J, Cerny J, Byun Y, Skultetyova L, Pomper MG, Lubkowski J, Barinka C: **Structural characterization of P1'-diversified urea-based inhibitors of glutamate carboxypeptidase II**. *Bioorg Med Chem Lett* 2014, **24**(10):2340-2345.

38. Tykvart J, Schimer J, Barinkova J, Pachl P, Postova-Slavetinska L, Majer P, Konvalinka J, Sacha P: **Rational design of urea-based glutamate carboxypeptidase II (GCPII) inhibitors as versatile tools for specific drug targeting and delivery**. *Bioorg Med Chem* 2014, **22**(15):4099-4108.

39. Wang H, Byun Y, Barinka C, Pullambhatla M, Bhang HE, Fox JJ, Lubkowski J, Mease RC, Pomper MG: **Bioisosterism of urea-based GCPII inhibitors: Synthesis and structure-activity relationship studies**. *Bioorg Med Chem Lett* 2010, **20**(1):392-397.

40. Zhang AX, Murelli RP, Barinka C, Michel J, Cocleaza A, Jorgensen WL, Lubkowski J, Spiegel DA: **A remote arene-binding site on prostate specific membrane antigen revealed by antibody-recruiting small molecules**. *J Am Chem Soc* 2010, **132**(36):12711-12716.

41. Barinka C, Byun Y, Dusich CL, Banerjee SR, Chen Y, Castanares M, Kozikowski AP, Mease RC, Pomper MG, Lubkowski J: **Interactions between human glutamate carboxypeptidase II and urea-based inhibitors: structural characterization**. *J Med Chem* 2008, **51**(24):7737-7743.

42. Barinka C, Hlouchova K, Rovenska M, Majer P, Dauter M, Hin N, Ko YS, Tsukamoto T, Slusher BS, Konvalinka J *et al*: **Structural basis of interactions between human glutamate carboxypeptidase II and its substrate analogs**. *J Mol Biol* 2008, **376**(5):1438-1450.

43. Klusak V, Barinka C, Plechanovova A, Mlcochova P, Konvalinka J, Rulisek L, Lubkowski J: **Reaction mechanism of glutamate carboxypeptidase II revealed by mutagenesis, X-ray crystallography, and computational methods**. *Biochemistry* 2009, **48**(19):4126-4138.

44. Pavlicek J, Ptacek J, Barinka C: **Glutamate carboxypeptidase II: an overview of structural studies and their importance for structure-based drug design and deciphering the reaction mechanism of the enzyme**. *Curr Med Chem* 2012, **19**(9):1300-1309.

45. Neale JH, Bzdega T, Wroblewska B: **N-Acetylaspartylglutamate: the most abundant peptide neurotransmitter in the mammalian central nervous system**. *J Neurochem* 2000, **75**(2):443-452.

46. Barinka C, Rinnova M, Sacha P, Rojas C, Majer P, Slusher BS, Konvalinka J: **Substrate specificity, inhibition and enzymological analysis of recombinant human glutamate carboxypeptidase II**. *J Neurochem* 2002, **80**(3):477-487.

47. Serval V, Barbeito L, Pittaluga A, Cheramy A, Lavielle S, Glowinski J: **Competitive inhibition of N-acetylated-alpha-linked acidic dipeptidase activity by N-acetyl-L-aspartyl-beta-linked L-glutamate**. *J Neurochem* 1990, **55**(1):39-46.

48. Jackson PF, Cole DC, Slusher BS, Stetz SL, Ross LE, Donzanti BA, Trainor DA: **Design, synthesis, and biological activity of a potent inhibitor of the neuropeptidase N-acetylated alpha-linked acidic dipeptidase**. *J Med Chem* 1996, **39**(2):619-622.

49. Majer P, Jackson PF, Delahanty G, Grella BS, Ko YS, Li W, Liu Q, Maclin KM, Polakova J, Shaffer KA *et al*: **Synthesis and biological evaluation of thiol-based inhibitors of glutamate carboxypeptidase II: discovery of an orally active GCP II inhibitor**. *J Med Chem* 2003, **46**(10):1989-1996.

50. Yamamoto T, Hirasawa S, Wroblewska B, Grajkowska E, Zhou J, Kozikowski A, Wroblewski J, Neale JH: **Antinociceptive effects of N-acetylaspartylglutamate (NAAG) peptidase inhibitors ZJ-11, ZJ-17 and ZJ-43 in the rat formalin test and in the rat neuropathic pain model**. *Eur J Neurosci* 2004, **20**(2):483-494.

51. Chen Y, Foss CA, Byun Y, Nimmagadda S, Pullambhatla M, Fox JJ, Castanares M, Lupold SE, Babich JW, Mease RC *et al*: **Radiohalogenated prostate-specific membrane antigen (PSMA)-based ureas as imaging agents for prostate cancer**. *J Med Chem* 2008, **51**(24):7933-7943.

52. Jackson PF, Tays KL, Maclin KM, Ko YS, Li W, Vitharana D, Tsukamoto T, Stoermer D, Lu XC, Wozniak K *et al*: **Design and pharmacological activity of phosphinic acid based NAALADase inhibitors**. *J Med Chem* 2001, **44**(24):4170-4175.

53. Majer P, Hin B, Stoermer D, Adams J, Xu W, Duvall BR, Delahanty G, Liu Q, Stathis MJ, Wozniak KM *et al*: **Structural optimization of thiol-based inhibitors of glutamate carboxypeptidase II by modification of the P1' side chain**. *J Med Chem* 2006, **49**(10):2876-2885.

54. Tsukamoto T, Majer P, Vitharana D, Ni C, Hin B, Lu XC, Thomas AG, Wozniak KM, Calvin DC, Wu Y *et al*: **Enantiospecificity of glutamate carboxypeptidase II inhibition**. *J Med Chem* 2005, **48**(7):2319-2324.

55. Kozikowski AP, Zhang J, Nan F, Petukhov PA, Grajkowska E, Wroblewski JT, Yamamoto T, Bzdega T, Wroblewska B, Neale JH: **Synthesis of urea-based inhibitors as active site probes of glutamate carboxypeptidase II: efficacy as analgesic agents**. *J Med Chem* 2004, **47**(7):1729-1738.

56. Kozikowski AP, Nan F, Conti P, Zhang J, Ramadan E, Bzdega T, Wroblewska B, Neale JH, Pshenichkin S, Wroblewski JT: **Design of remarkably simple, yet potent urea-based inhibitors of glutamate carboxypeptidase II (NAALADase)**. *J Med Chem* 2001, **44**(3):298-301.

57. Ferraris DV, Shukla K, Tsukamoto T: **Structure-activity relationships of glutamate carboxypeptidase II (GCPII) inhibitors**. *Curr Med Chem* 2012, **19**(9):1282-1294.

58. Schomburg I, Chang A, Placzek S, Sohngen C, Rother M, Lang M, Munaretto C, Ulas S, Stelzer M, Grote A *et al*: **BRENDA in 2013: integrated reactions, kinetic data, enzyme function data, improved disease classification: new options and contents in BRENDA**. *Nucleic Acids Res* 2013, **41**(Database issue):D764-772.

59. Troyer JK, Beckett ML, Wright GL, Jr.: **Detection and characterization of the prostate-specific membrane antigen (PSMA) in tissue extracts and body fluids**. *Int J Cancer* 1995, **62**(5):552-558.

60. Kinoshita Y, Kuratsukuri K, Landas S, Imaida K, Rovito PM, Jr., Wang CY, Haas GP: **Expression of prostate-specific membrane antigen in normal and malignant human tissues**. *World J Surg* 2006, **30**(4):628-636.

61. Dumas F, Gala JL, Berteau P, Brasseur F, Eschwege P, Paradis V, Lacour B, Philippe M, Loric S: **Molecular expression of PSMA mRNA and protein in primary renal tumors**. *Int J Cancer* 1999, **80**(6):799-803.

62. Gala JL, Loric S, Guiot Y, Denmeade SR, Gady A, Brasseur F, Heusterspreute M, Eschwege P, De Nayer P, Van Cangh P *et al*: **Expression of prostate-specific membrane antigen in transitional cell carcinoma of the bladder: prognostic value?** *Clin Cancer Res* 2000, **6**(10):4049-4054.

63. Chang SS, Reuter VE, Heston WD, Bander NH, Grauer LS, Gaudin PB: **Five different anti-prostate-specific membrane antigen (PSMA) antibodies confirm PSMA expression in tumor-associated neovasculature**. *Cancer Res* 1999, **59**(13):3192-3198.

64. Lopes AD, Davis WL, Rosenstraus MJ, Uveges AJ, Gilman SC: **Immunohistochemical and pharmacokinetic characterization of the site-specific immunoconjugate CYT-356 derived from antiprostate monoclonal antibody 7E11-C5**. *Cancer Res* 1990, **50**(19):6423-6429.

65. Silver DA, Pellicer I, Fair WR, Heston WD, Cordon-Cardo C: **Prostate-specific membrane antigen expression in normal and malignant human tissues**. *Clin Cancer Res* 1997, **3**(1):81-85.

66. Sokoloff RL, Norton KC, Gasior CL, Marker KM, Grauer LS: **A dual-monoclonal sandwich assay for prostate-specific membrane antigen: levels in tissues, seminal fluid and urine**. *Prostate* 2000, **43**(2):150-157.

67. Mhawech-Fauceglia P, Zhang S, Terracciano L, Sauter G, Chadhuri A, Herrmann FR, Penetrante R: **Prostate-specific membrane antigen (PSMA) protein expression in normal and neoplastic tissues and its sensitivity and specificity in prostate adenocarcinoma: an immunohistochemical study using mutiple tumour tissue microarray technique**. *Histopathology* 2007, **50**(4):472-483.

68. Haffner MC, Laimer J, Chaux A, Schafer G, Obrist P, Brunner A, Kronberger IE, Laimer K, Gurel B, Koller JB *et al*: **High expression of prostate-specific membrane antigen in the tumor-associated neo-vasculature is associated with worse prognosis in squamous cell carcinoma of the oral cavity**. *Mod Pathol* 2012, **25**(8):1079-1085.

69. Liu H, Rajasekaran AK, Moy P, Xia Y, Kim S, Navarro V, Rahmati R, Bander NH: **Constitutive and antibody-induced internalization of prostate-specific membrane antigen**. *Cancer Res* 1998, **58**(18):4055-4060.

70. Huang X, Bennett M, Thorpe PE: **Anti-tumor effects and lack of side effects in mice of an immunotoxin directed against human and mouse prostate-specific membrane antigen**. *Prostate* 2004, **61**(1):1-11.

71. Mlcochova P: **Dissertation thesis: Structure, activity and metabolism of human glutamate carboxypeptidase**. *Department of Biochemistry, Faculty of Science, Charles University in Prague* 2007:33-36.

72. Willard SS, Koochekpour S: **Glutamate, glutamate receptors, and downstream signaling pathways**. *Int J Biol Sci* 2013, **9**(9):948-959.

73. Watkins JC, Evans RH: **Excitatory amino acid transmitters**. *Annu Rev Pharmacol Toxicol* 1981, **21**:165-204.

74. Carozzi V, Marmiroli P, Cavaletti G: **Focus on the role of Glutamate in the pathology of the peripheral nervous system**. *CNS Neurol Disord Drug Targets* 2008, **7**(4):348-360.

75. Kew JN, Kemp JA: **Ionotropic and metabotropic glutamate receptor structure and pharmacology**. *Psychopharmacology (Berl)* 2005, **179**(1):4-29.

76. Ozawa S, Kamiya H, Tsuzuki K: **Glutamate receptors in the mammalian central nervous system**. *Prog Neurobiol* 1998, **54**(5):581-618.

77. Wisden W, Seeburg PH: **Mammalian ionotropic glutamate receptors**. *Curr Opin Neurobiol* 1993, **3**(3):291-298.

78. Bruno V, Battaglia G, Copani A, D'Onofrio M, Di Iorio P, De Blasi A, Melchiorri D, Flor PJ, Nicoletti F: **Metabotropic glutamate receptor subtypes as targets for neuroprotective drugs**. *J Cereb Blood Flow Metab* 2001, **21**(9):1013-1033.

79. Skerry TM, Genever PG: **Glutamate signalling in non-neuronal tissues**. *Trends Pharmacol Sci* 2001, **22**(4):174-181.

80. Arundine M, Tymianski M: **Molecular mechanisms of glutamate-dependent neurodegeneration in ischemia and traumatic brain injury**. *Cell Mol Life Sci* 2004, **61**(6):657-668.

81. Doble A: **The role of excitotoxicity in neurodegenerative disease: implications for therapy**. *Pharmacol Ther* 1999, **81**(3):163-221.

82. Choi DW: **Ionic dependence of glutamate neurotoxicity**. *J Neurosci* 1987, **7**(2):369-379.

83. Rahn KA, Slusher BS, Kaplin AI: **Glutamate in CNS neurodegeneration and cognition and its regulation by GCPII inhibition**. *Curr Med Chem* 2012, **19**(9):1335-1345.

84. Dodd PR: **Excited to death: different ways to lose your neurones**. *Biogerontology* 2002, **3**(1-2):51-56.

85. Zhong C, Luo Q, Jiang J: **Blockade of N-acetylaspartylglutamate peptidases: a novel protective strategy for brain injuries and neurological disorders**. *Int J Neurosci* 2014.

86. Neale JH: **N-acetylaspartylglutamate is an agonist at mGluR(3) in vivo and in vitro**. *J Neurochem* 2011, **119**(5):891-895.

87. Wroblewska B, Wroblewski JT, Pshenichkin S, Surin A, Sullivan SE, Neale JH: **N-acetylaspartylglutamate selectively activates mGluR3 receptors in transfected cells**. *J Neurochem* 1997, **69**(1):174-181.

88. Bruno V, Battaglia G, Casabona G, Copani A, Caciagli F, Nicoletti F: **Neuroprotection by glial metabotropic glutamate receptors is mediated by transforming growth factor-beta**. *J Neurosci* 1998, **18**(23):9594-9600.

89. Thomas AG, Liu W, Olkowski JL, Tang Z, Lin Q, Lu XC, Slusher BS: **Neuroprotection mediated by glutamate carboxypeptidase II (NAALADase) inhibition requires TGF-beta**. *Eur J Pharmacol* 2001, **430**(1):33-40.

90. Thomas AG, Olkowski JL, Slusher BS: **Neuroprotection afforded by NAAG and NAALADase inhibition requires glial cells and metabotropic glutamate receptor activation**. *Eur J Pharmacol* 2001, **426**(1-2):35-38.

91. Sanabria ER, Wozniak KM, Slusher BS, Keller A: **GCP II (NAALADase) inhibition suppresses mossy fiber-CA3 synaptic neurotransmission by a presynaptic mechanism**. *J Neurophysiol* 2004, **91**(1):182-193.

92. Zhao J, Ramadan E, Cappiello M, Wroblewska B, Bzdega T, Neale JH: **NAAG inhibits KCl-induced [(3)H]-GABA release via mGluR3, cAMP, PKA and L-type calcium conductance**. *Eur J Neurosci* 2001, **13**(2):340-346.

93. Valivullah HM, Lancaster J, Sweetnam PM, Neale JH: **Interactions between N-acetylaspartylglutamate and AMPA, kainate, and NMDA binding sites**. *J Neurochem* 1994, **63**(5):1714-1719.

94. Trombley PQ, Westbrook GL: **Excitatory synaptic transmission in cultures of rat olfactory bulb**. *J Neurophysiol* 1990, **64**(2):598-606.

95. Westbrook GL, Mayer ML, Namboodiri MA, Neale JH: **High concentrations of N-acetylaspartylglutamate (NAAG) selectively activate NMDA receptors on mouse spinal cord neurons in cell culture**. *J Neurosci* 1986, **6**(11):3385-3392.

96. Bergeron R, Coyle JT, Tsai G, Greene RW: **NAAG reduces NMDA receptor current in CA1 hippocampal pyramidal neurons of acute slices and dissociated neurons**. *Neuropsychopharmacology* 2005, **30**(1):7-16.

97. Greene R: **Circuit analysis of NMDAR hypofunction in the hippocampus, in vitro, and psychosis of schizophrenia**. *Hippocampus* 2001, **11**(5):569-577.

98. Puttfarcken PS, Handen JS, Montgomery DT, Coyle JT, Werling LL: **N-acetyl-aspartylglutamate modulation of N-methyl-D-aspartate-stimulated [3H]norepinephrine release from rat hippocampal slices**. *J Pharmacol Exp Ther* 1993, **266**(2):796-803.

99. Jones HE, Sillito AM: **The action of the putative neurotransmitters N-acetylaspartylglutamate and L-homocysteate in cat dorsal lateral geniculate nucleus**. *J Neurophysiol* 1992, **68**(3):663-672.

100. Losi G, Vicini S, Neale J: **NAAG fails to antagonize synaptic and extrasynaptic NMDA receptors in cerebellar granule neurons**. *Neuropharmacology* 2004, **46**(4):490-496.

101. Carozzi VA, Chiorazzi A, Canta A, Lapidus RG, Slusher BS, Wozniak KM, Cavaletti G: **Glutamate carboxypeptidase inhibition reduces the severity of chemotherapy-induced peripheral neurotoxicity in rat**. *Neurotox Res* 2010, **17**(4):380-391.

102. Thomas AG, Corse AM, Coccia CF, Bilak MM, Rothstein JD, Slusher BS: **NAALADase inhibition protects motor neurons against chronic glutamate toxicity**. *Eur J Pharmacol* 2003, **471**(3):177-184.

103. Xi ZX, Li X, Peng XQ, Li J, Chun L, Gardner EL, Thomas AG, Slusher BS, Ashby CR, Jr.: **Inhibition of NAALADase by 2-PMPA attenuates cocaine-induced relapse in rats: a NAAG-mGluR2/3-mediated mechanism**. *J Neurochem* 2010, **112**(2):564-576.

104. Neale JH, Olszewski RT, Gehl LM, Wroblewska B, Bzdega T: **The neurotransmitter N-acetylaspartylglutamate in models of pain, ALS, diabetic neuropathy, CNS injury and schizophrenia**. *Trends Pharmacol Sci* 2005, **26**(9):477-484.

105. Zhang W, Murakawa Y, Wozniak KM, Slusher B, Sima AA: **The preventive and therapeutic effects of GCPII (NAALADase) inhibition on painful and sensory diabetic neuropathy**. *J Neurol Sci* 2006, **247**(2):217-223.

106. Zhang W, Slusher B, Murakawa Y, Wozniak KM, Tsukamoto T, Jackson PF, Sima AA: **GCPII (NAALADase) inhibition prevents long-term diabetic neuropathy in type 1 diabetic BB/Wor rats**. *J Neurol Sci* 2002, **194**(1):21-28.

107. Ghadge GD, Slusher BS, Bodner A, Canto MD, Wozniak K, Thomas AG, Rojas C, Tsukamoto T, Majer P, Miller RJ *et al*: **Glutamate carboxypeptidase II inhibition protects motor neurons from death in familial amyotrophic lateral sclerosis models**. *Proc Natl Acad Sci U S A* 2003, **100**(16):9554-9559.

108. Harada C, Harada T, Slusher BS, Yoshida K, Matsuda H, Wada K: **N-acetylated-alpha-linked-acidic dipeptidase inhibitor has a neuroprotective effect on mouse retinal ganglion cells after pressure-induced ischemia**. *Neurosci Lett* 2000, **292**(2):134-136.

109. Yao V, Berkman CE, Choi JK, O'Keefe DS, Bacich DJ: **Expression of prostate-specific membrane antigen (PSMA), increases cell folate uptake and proliferation and suggests a novel role for PSMA in the uptake of the non-polyglutamated folate, folic acid**. *Prostate* 2010, **70**(3):305-316.

110. Yao V, Bacich DJ: **Prostate specific membrane antigen (PSMA) expression gives prostate cancer cells a growth advantage in a physiologically relevant folate environment in vitro**. *Prostate* 2006, **66**(8):867-875.

111. Lambert LA, Mitchell SL: **Molecular evolution of the transferrin receptor/glutamate carboxypeptidase II family**. *J Mol Evol* 2007, **64**(1):113-128.

112. Lawrence CM, Ray S, Babyonyshev M, Galluser R, Borhani DW, Harrison SC: **Crystal structure of the ectodomain of human transferrin receptor**. *Science* 1999, **286**(5440):779-782.

113. Ananias HJ, van den Heuvel MC, Helfrich W, de Jong IJ: **Expression of the gastrin-releasing peptide receptor, the prostate stem cell antigen and the prostate-specific membrane antigen in lymph node and bone metastases of prostate cancer**. *Prostate* 2009, **69**(10):1101-1108.

114. Barwe SP, Maul RS, Christiansen JJ, Anilkumar G, Cooper CR, Kohn DB, Rajasekaran AK: **Preferential association of prostate cancer cells expressing prostate specific membrane antigen to bone marrow matrix**. *Int J Oncol* 2007, **30**(4):899-904.

115. Gordon IO, Tretiakova MS, Noffsinger AE, Hart J, Reuter VE, Al-Ahmadie HA: **Prostate-specific membrane antigen expression in regeneration and repair**. *Mod Pathol* 2008, **21**(12):1421-1427.

116. Haffner MC, Kronberger IE, Ross JS, Sheehan CE, Zitt M, Muhlmann G, Ofner D, Zelger B, Ensinger C, Yang XJ *et al*: **Prostate-specific membrane antigen expression in the neovasculature of gastric and colorectal cancers**. *Hum Pathol* 2009, **40**(12):1754-1761.

117. Chang SS, Reuter VE, Heston WD, Gaudin PB: **Metastatic renal cell carcinoma neovasculature expresses prostate-specific membrane antigen**. *Urology* 2001, **57**(4):801-805.

118. Conway RE, Petrovic N, Li Z, Heston W, Wu D, Shapiro LH: **Prostate-specific membrane antigen regulates angiogenesis by modulating integrin signal transduction**. *Mol Cell Biol* 2006, **26**(14):5310-5324.

119. Bivalacqua TJ, Musicki B, Usta MF, Champion HC, Kadowitz PJ, Burnett AL, Hellstrom WJ: **Endothelial nitric oxide synthase gene therapy for erectile dysfunction**. *Curr Pharm Des* 2005, **11**(31):4059-4067.

120. Duda DG, Fukumura D, Jain RK: **Role of eNOS in neovascularization: NO for endothelial progenitor cells**. *Trends Mol Med* 2004, **10**(4):143-145.

121. Foss CA, Mease RC, Cho SY, Kim HJ, Pomper MG: **GCPII imaging and cancer**. *Curr Med Chem* 2012, **19**(9):1346-1359.

122. Siegel R, Ma J, Zou Z, Jemal A: **Cancer statistics, 2014**. *CA Cancer J Clin* 2014, **64**(1):9-29.

123. Weissleder R: **Molecular imaging in cancer**. *Science* 2006, **312**(5777):1168-1171.

124. Mease RC: **Radionuclide based imaging of prostate cancer**. *Curr Top Med Chem* 2010, **10**(16):1600-1616.

125. Mease RC, Foss CA, Pomper MG: **PET imaging in prostate cancer: focus on prostate-specific membrane antigen**. *Curr Top Med Chem* 2013, **13**(8):951-962.

126. Ellis RJ, Kaminsky DA, Zhou EH, Fu P, Chen WD, Brelin A, Faulhaber PF, Bodner D: **Ten-year outcomes: the clinical utility of single photon emission computed tomography/computed tomography capromab pendetide (Prostascint) in a cohort diagnosed with localized prostate cancer**. *Int J Radiat Oncol Biol Phys* 2011, **81**(1):29-34.

127. Zuckier LS, DeNardo GL: **Trials and tribulations: oncological antibody imaging comes to the fore**. *Semin Nucl Med* 1997, **27**(1):10-29.

128. Troyer JK, Feng Q, Beckett ML, Wright GL, Jr.: **Biochemical characterization and mapping of the 7E11-C5.3 epitope of the prostate-specific membrane antigen**. *Urol Oncol* 1995, **1**(1):29-37.

129. Bander NH: **Technology insight: monoclonal antibody imaging of prostate cancer**. *Nat Clin Pract Urol* 2006, **3**(4):216-225.

130. Nanus DM, Milowsky MI, Kostakoglu L, Smith-Jones PM, Vallabahajosula S, Goldsmith SJ, Bander NH: **Clinical use of monoclonal antibody HuJ591 therapy: targeting prostate specific membrane antigen**. *J Urol* 2003, **170**(6 Pt 2):S84-88; discussion S88-89.

131. Holland JP, Divilov V, Bander NH, Smith-Jones PM, Larson SM, Lewis JS: **89Zr-DFO-J591 for immunoPET of prostate-specific membrane antigen expression in vivo**. *J Nucl Med* 2010, **51**(8):1293-1300.

132. Evans MJ, Smith-Jones PM, Wongvipat J, Navarro V, Kim S, Bander NH, Larson SM, Sawyers CL: **Noninvasive measurement of androgen receptor signaling with a positron-emitting radiopharmaceutical that targets prostate-specific membrane antigen**. *Proc Natl Acad Sci U S A* 2011, **108**(23):9578-9582.

133. Vallabhajosula S, Kuji I, Hamacher KA, Konishi S, Kostakoglu L, Kothari PA, Milowski MI, Nanus DM, Bander NH, Goldsmith SJ: **Pharmacokinetics and biodistribution of 111In- and 177Lu-labeled J591 antibody specific for prostate-specific membrane antigen: prediction of 90Y-J591 radiation dosimetry based on 111In or 177Lu?** *J Nucl Med* 2005, **46**(4):634-641.

134. Bander NH, Trabulsi EJ, Kostakoglu L, Yao D, Vallabhajosula S, Smith-Jones P, Joyce MA, Milowsky M, Nanus DM, Goldsmith SJ: **Targeting metastatic prostate cancer with radiolabeled monoclonal antibody J591 to the extracellular domain of prostate specific membrane antigen**. *J Urol* 2003, **170**(5):1717-1721.

135. Kampmeier F, Williams JD, Maher J, Mullen GE, Blower PJ: **Design and preclinical evaluation of a 99mTc-labelled diabody of mAb J591 for SPECT imaging of prostate-specific membrane antigen (PSMA)**. *EJNMMI Res* 2014, **4**(1):13.

136. Nargund V, Al Hashmi D, Kumar P, Gordon S, Otitie U, Ellison D, Carroll M, Baithun S, Britton KE: **Imaging with radiolabelled monoclonal antibody (MUJ591) to prostate-specific membrane antigen in staging of clinically localized prostatic carcinoma: comparison with clinical, surgical and histological staging**. *BJU Int* 2005, **95**(9):1232-1236.

137. Pandit-Taskar N, O'Donoghue JA, Beylergil V, Lyashchenko S, Ruan S, Solomon SB, Durack JC, Carrasquillo JA, Lefkowitz RA, Gonen M *et al*: **Zr-huJ591 immuno-PET imaging in patients with advanced metastatic prostate cancer**. *Eur J Nucl Med Mol Imaging* 2014.

138. Tagawa ST, Akhtar NH, Nikolopoulou A, Kaur G, Robinson B, Kahn R, Vallabhajosula S, Goldsmith SJ, Nanus DM, Bander NH: **Bone marrow recovery and subsequent chemotherapy following radiolabeled anti-prostate-specific membrane antigen monoclonal antibody j591 in men with metastatic castration-resistant prostate cancer**. *Front Oncol* 2013, **3**:214.

139. Tagawa ST, Milowsky MI, Morris M, Vallabhajosula S, Christos P, Akhtar NH, Osborne J, Goldsmith SJ, Larson S, Taskar NP *et al*: **Phase II study of Lutetium-177-labeled anti-prostate-specific membrane antigen monoclonal antibody J591 for metastatic castration-resistant prostate cancer**. *Clin Cancer Res* 2013, **19**(18):5182-5191.

140. Milowsky MI, Nanus DM, Kostakoglu L, Vallabhajosula S, Goldsmith SJ, Bander NH: **Phase I trial of yttrium-90-labeled anti-prostate-specific membrane antigen monoclonal antibody J591 for androgen-independent prostate cancer**. *J Clin Oncol* 2004, **22**(13):2522-2531.

141. Elsasser-Beile U, Wolf P, Gierschner D, Buhler P, Schultze-Seemann W, Wetterauer U: **A new generation of monoclonal and recombinant antibodies against cell-adherent prostate specific membrane antigen for diagnostic and therapeutic targeting of prostate cancer**. *Prostate* 2006, **66**(13):1359-1370.

142. Alt K, Wiehr S, Ehrlichmann W, Reischl G, Wolf P, Pichler BJ, Elsasser-Beile U, Buhler P: **High-resolution animal PET imaging of prostate cancer xenografts with three different 64Cu-labeled antibodies against native cell-adherent PSMA**. *Prostate* 2010, **70**(13):1413-1421.

143. Elsasser-Beile U, Reischl G, Wiehr S, Buhler P, Wolf P, Alt K, Shively J, Judenhofer MS, Machulla HJ, Pichler BJ: **PET imaging of prostate cancer xenografts with a highly specific antibody against the prostate-specific membrane antigen**. *J Nucl Med* 2009, **50**(4):606-611.

144. Imai K, Takaoka A: **Comparing antibody and small-molecule therapies for cancer**. *Nat Rev Cancer* 2006, **6**(9):714-727.

145. Foss CA, Mease RC, Fan H, Wang Y, Ravert HT, Dannals RF, Olszewski RT, Heston WD, Kozikowski AP, Pomper MG: **Radiolabeled small-molecule ligands for prostate-specific membrane antigen: in vivo imaging in experimental models of prostate cancer**. *Clin Cancer Res* 2005, **11**(11):4022-4028.

146. Mease RC, Dusich CL, Foss CA, Ravert HT, Dannals RF, Seidel J, Prideaux A, Fox JJ, Sgouros G, Kozikowski AP *et al*: **N-[N-[(S)-1,3-Dicarboxypropyl]carbamoyl]-4-[18F]fluorobenzyl-L-cysteine, [18F]DCFBC: a new imaging probe for prostate cancer**. *Clin Cancer Res* 2008, **14**(10):3036-3043.

147. Barrett J, LaFrance N, Coleman RE, Goldsmith S, Stubbs J, Petry N, Vallabhajosula S, Maresca K, Femia F, Babich J: **Targeting metastatic prostate cancer [PCa] in patients with 123I-MIP1072 & 123I-MIP1095**. *J NUCL MED MEETING ABSTRACTS* 2009, **50**(2_MeetingAbstracts):522-.

148. Banerjee SR, Foss CA, Castanares M, Mease RC, Byun Y, Fox JJ, Hilton J, Lupold SE, Kozikowski AP, Pomper MG: **Synthesis and evaluation of technetium-99m- and rhenium-labeled inhibitors of the prostate-specific membrane antigen (PSMA)**. *J Med Chem* 2008, **51**(15):4504-4517.

149. Kularatne SA, Zhou Z, Yang J, Post CB, Low PS: **Design, synthesis, and preclinical evaluation of prostate-specific membrane antigen targeted (99m)Tc-radioimaging agents**. *Mol Pharm* 2009, **6**(3):790-800.

150. Sharkey RM, Goldenberg DM: **Targeted therapy of cancer: new prospects for antibodies and immunoconjugates**. *CA Cancer J Clin* 2006, **56**(4):226-243.

151. Goldenberg DM: **Targeted therapy of cancer with radiolabeled antibodies**. *J Nucl Med* 2002, **43**(5):693-713.

152. Buhler P, Wolf P, Elsasser-Beile U: **Targeting the prostate-specific membrane antigen for prostate cancer therapy**. *Immunotherapy* 2009, **1**(3):471-481.

153. Elsasser-Beile U, Buhler P, Wolf P: **Targeted therapies for prostate cancer against the prostate specific membrane antigen**. *Curr Drug Targets* 2009, **10**(2):118-125.

154. Ma D, Hopf CE, Malewicz AD, Donovan GP, Senter PD, Goeckeler WF, Maddon PJ, Olson WC: **Potent antitumor activity of an auristatin-conjugated, fully human monoclonal antibody to prostate-specific membrane antigen**. *Clin Cancer Res* 2006, **12**(8):2591-2596.

155. Wang X, Ma D, Olson WC, Heston WD: **In vitro and in vivo responses of advanced prostate tumors to PSMA ADC, an auristatin-conjugated antibody to prostate-specific membrane antigen**. *Mol Cancer Ther* 2011, **10**(9):1728-1739.

156. Kantoff P, Petrylak D, Pomerantz M, Israel R, Olson W, Ramakrishna T, Morris S: **First-in-human phase I trial of prostate-specific membrane antigen antibody drug conjugate (PSMA ADC) in taxane-refractory prostate cancer**. *ASCO Annu Meet* 2010:Abstract no. TPS245

157. Ballangrud AM, Yang WH, Charlton DE, McDevitt MR, Hamacher KA, Panageas KS, Ma D, Bander NH, Scheinberg DA, Sgouros G: **Response of LNCaP spheroids after treatment with an alpha-particle emitter (213Bi)-labeled anti-prostate-specific membrane antigen antibody (J591)**. *Cancer Res* 2001, **61**(5):2008-2014.

158. Li Y, Tian Z, Rizvi SM, Bander NH, Allen BJ: **In vitro and preclinical targeted alpha therapy of human prostate cancer with Bi-213 labeled J591 antibody against the prostate specific membrane antigen**. *Prostate Cancer Prostatic Dis* 2002, **5**(1):36-46.

159. McDevitt MR, Barendswaard E, Ma D, Lai L, Curcio MJ, Sgouros G, Ballangrud AM, Yang WH, Finn RD, Pellegrini V *et al*: **An alpha-particle emitting antibody ([213Bi]J591) for radioimmunotherapy of prostate cancer**. *Cancer Res* 2000, **60**(21):6095-6100.

160. McDevitt MR, Finn RD, Ma D, Larson SM, Scheinberg DA: **Preparation of alpha-emitting 213Bi-labeled antibody constructs for clinical use**. *J Nucl Med* 1999, **40**(10):1722-1727.

161. Morris MJ, Divgi CR, Pandit-Taskar N, Batraki M, Warren N, Nacca A, Smith-Jones P, Schwartz L, Kelly WK, Slovin S *et al*: **Pilot trial of unlabeled and indium-111-labeled anti-prostate-specific membrane antigen antibody J591 for castrate metastatic prostate cancer**. *Clin Cancer Res* 2005, **11**(20):7454-7461.

162. Smith-Jones PM, Vallabhajosula S, Navarro V, Bastidas D, Goldsmith SJ, Bander NH: **Radiolabeled monoclonal antibodies specific to the extracellular domain of prostate-specific membrane antigen: preclinical studies in nude mice bearing LNCaP human prostate tumor**. *J Nucl Med* 2003, **44**(4):610-617.

163. Vallabhajosula S, Goldsmith SJ, Kostakoglu L, Milowsky MI, Nanus DM, Bander NH: **Radioimmunotherapy of prostate cancer using 90Y- and 177Lu-labeled J591 monoclonal antibodies: effect of multiple treatments on myelotoxicity**. *Clin Cancer Res* 2005, **11**(19 Pt 2):7195s-7200s.

164. Henry MD, Wen S, Silva MD, Chandra S, Milton M, Worland PJ: **A prostate-specific membrane antigen-targeted monoclonal antibody-chemotherapeutic conjugate designed for the treatment of prostate cancer**. *Cancer Res* 2004, **64**(21):7995-8001.

165. Wolf P, Alt K, Buhler P, Katzenwadel A, Wetterauer U, Tacke M, Elsasser-Beile U: **Anti-PSMA immunotoxin as novel treatment for prostate cancer? High and specific antitumor activity on human prostate xenograft tumors in SCID mice**. *Prostate* 2008, **68**(2):129-138.

166. Wolf P, Gierschner D, Buhler P, Wetterauer U, Elsasser-Beile U: **A recombinant PSMA-specific single-chain immunotoxin has potent and selective toxicity against prostate cancer cells**. *Cancer Immunol Immunother* 2006, **55**(11):1367-1373.

167. Wolf P, Alt K, Wetterauer D, Buhler P, Gierschner D, Katzenwadel A, Wetterauer U, Elsasser-Beile U: **Preclinical evaluation of a recombinant anti-prostate specific membrane antigen single-chain immunotoxin against prostate cancer**. *J Immunother* 2010, **33**(3):262-271.

168. Buhler P, Molnar E, Dopfer EP, Wolf P, Gierschner D, Wetterauer U, Schamel WW, Elsasser-Beile U: **Target-dependent T-cell activation by coligation with a PSMA x CD3 diabody induces lysis of prostate cancer cells**. *J Immunother* 2009, **32**(6):565-573.

169. Buhler P, Wolf P, Gierschner D, Schaber I, Katzenwadel A, Schultze-Seemann W, Wetterauer U, Tacke M, Swamy M, Schamel WW *et al*: **A bispecific diabody directed against prostate-specific membrane antigen and CD3 induces T-cell mediated lysis of prostate cancer cells**. *Cancer Immunol Immunother* 2008, **57**(1):43-52.

170. Hillier S, Merkin R, Maresca K, Zimmerman C, Barrett J, Tesson M, Eckelman W, Mairs R, Joyal J, Babich J: **[131I] MIP-1375, a small molecule prostate-specific membrane antigen (PSMA) inhibitor for targeted therapy of prostate cancer (PCa)**. In: *Society of Nuclear Medicine Annual Meeting Abstracts: 2011*. Soc Nuclear Med: 361.

171. Cerchia L, Giangrande PH, McNamara JO, de Franciscis V: **Cell-specific aptamers for targeted therapies**. *Methods Mol Biol* 2009, **535**:59-78.

172. Hicke BJ, Stephens AW, Gould T, Chang YF, Lynott CK, Heil J, Borkowski S, Hilger CS, Cook G, Warren S *et al*: **Tumor targeting by an aptamer**. *J Nucl Med* 2006, **47**(4):668-678.

173. Lupold SE, Hicke BJ, Lin Y, Coffey DS: **Identification and characterization of nuclease-stabilized RNA molecules that bind human prostate cancer cells via the prostate-specific membrane antigen**. *Cancer Res* 2002, **62**(14):4029-4033.

174. Dassie JP, Liu XY, Thomas GS, Whitaker RM, Thiel KW, Stockdale KR, Meyerholz DK, McCaffrey AP, McNamara JO, 2nd, Giangrande PH: **Systemic administration of optimized aptamer-siRNA chimeras promotes regression of PSMA-expressing tumors**. *Nat Biotechnol* 2009, **27**(9):839-849.

175. Ni X, Zhang Y, Ribas J, Chowdhury WH, Castanares M, Zhang Z, Laiho M, DeWeese TL, Lupold SE: **Prostate-targeted radiosensitization via aptamer-shRNA chimeras in human tumor xenografts**. *J Clin Invest* 2011, **121**(6):2383-2390.

176. Zhang L, Radovic-Moreno AF, Alexis F, Gu FX, Basto PA, Bagalkot V, Jon S, Langer RS, Farokhzad OC: **Co-delivery of hydrophobic and hydrophilic drugs from nanoparticle-aptamer bioconjugates**. *ChemMedChem* 2007, **2**(9):1268-1271.

177. Farokhzad OC, Cheng J, Teply BA, Sherifi I, Jon S, Kantoff PW, Richie JP, Langer R: **Targeted nanoparticle-aptamer bioconjugates for cancer chemotherapy in vivo**. *Proc Natl Acad Sci U S A* 2006, **103**(16):6315-6320.

178. Farokhzad OC, Jon S, Khademhosseini A, Tran TN, Lavan DA, Langer R: **Nanoparticle-aptamer bioconjugates: a new approach for targeting prostate cancer cells**. *Cancer Res* 2004, **64**(21):7668-7672.

179. Dhar S, Kolishetti N, Lippard SJ, Farokhzad OC: **Targeted delivery of a cisplatin prodrug for safer and more effective prostate cancer therapy in vivo**. *Proc Natl Acad Sci U S A* 2011, **108**(5):1850-1855.

180. Dhar S, Gu FX, Langer R, Farokhzad OC, Lippard SJ: **Targeted delivery of cisplatin to prostate cancer cells by aptamer functionalized Pt(IV) prodrug-PLGA-PEG nanoparticles**. *Proc Natl Acad Sci U S A* 2008, **105**(45):17356-17361.

181. Rovenska M, Hlouchova K, Sacha P, Mlcochova P, Horak V, Zamecnik J, Barinka C, Konvalinka J: **Tissue expression and enzymologic characterization of human prostate specific membrane antigen and its rat and pig orthologs**. *Prostate* 2008, **68**(2):171-182.

182. Bacich DJ, Pinto JT, Tong WP, Heston WD: **Cloning, expression, genomic localization, and enzymatic activities of the mouse homolog of prostate-specific membrane antigen/NAALADase/folate hydrolase**. *Mamm Genome* 2001, **12**(2):117-123.

183. Wu LY, Johnson JM, Simmons JK, Mendes DE, Geruntho JJ, Liu T, Dirksen WP, Rosol TJ, Davis WC, Berkman CE: **Biochemical characterization of prostate-specific membrane antigen from canine prostate carcinoma cells**. *Prostate* 2014, **74**(5):451-457.

184. Aggarwal S, Ricklis RM, Williams SA, Denmeade SR: **Comparative study of PSMA expression in the prostate of mouse, dog, monkey, and human**. *Prostate* 2006, **66**(9):903-910.

185. Lai CL, van den Ham R, van Leenders G, van der Lugt J, Mol JA, Teske E: **Histopathological and immunohistochemical characterization of canine prostate cancer**. *Prostate* 2008, **68**(5):477-488.

186. Lai CL, van den Ham R, van Leenders G, van der Lugt J, Teske E: **Comparative characterization of the canine normal prostate in intact and castrated animals**. *Prostate* 2008, **68**(5):498-507.

187. Hlouchova K, Navratil V, Tykvart J, Sacha P, Konvalinka J: **GCPII variants, paralogs and orthologs**. *Curr Med Chem* 2012, **19**(9):1316-1322.

188. O'Keefe DS, Bacich DJ, Heston WD: **Comparative analysis of prostate-specific membrane antigen (PSMA) versus a prostate-specific membrane antigen-like gene**. *Prostate* 2004, **58**(2):200-210.

189. Barinka C, Mlcochova P, Sacha P, Hilgert I, Majer P, Slusher BS, Horejsi V, Konvalinka J: **Amino acids at the N- and C-termini of human glutamate carboxypeptidase II are required for enzymatic activity and proper folding**. *Eur J Biochem* 2004, **271**(13):2782-2790.

190. Bzdega T, Crowe SL, Ramadan ER, Sciarretta KH, Olszewski RT, Ojeifo OA, Rafalski VA, Wroblewska B, Neale JH: **The cloning and characterization of a second brain enzyme with NAAG peptidase activity**. *J Neurochem* 2004, **89**(3):627-635.

191. Hlouchova K, Barinka C, Klusak V, Sacha P, Mlcochova P, Majer P, Rulisek L, Konvalinka J: **Biochemical characterization of human glutamate carboxypeptidase III**. *J Neurochem* 2007, **101**(3):682-696.

192. Collard F, Vertommen D, Constantinescu S, Buts L, Van Schaftingen E: **Molecular identification of beta-citrylglutamate hydrolase as glutamate carboxypeptidase 3**. *J Biol Chem* 2011, **286**(44):38220-38230.

193. Miyake M, Kakimoto Y, Sorimachi M: **Isolation and identification of beta-citryl-L-glutamic acid from newborn rat brain**. *Biochim Biophys Acta* 1978, **544**(3):656-666.

194. Miyake M, Kakimoto Y, Sorimachi M: **A gas chromatographic method for the determination of N-acetyl-L-aspartic acid, N-acetyl-alpha-aspartylglutamic acid and beta-citryl-L-glutamic acid and their distributions in the brain and other organs of various species of animals**. *J Neurochem* 1981, **36**(3):804-810.

195. Miyake M, Kume S, Kakimoto Y: **Correlation of the level of beta-citryl-L-glutamic acid with spermatogenesis in rat testes**. *Biochim Biophys Acta* 1982, **719**(3):495-500.

196. Hlouchova K, Barinka C, Konvalinka J, Lubkowski J: **Structural insight into the evolutionary and pharmacologic homology of glutamate carboxypeptidases II and III**. *FEBS J* 2009, **276**(16):4448-4462.

197. Shneider BL, Thevananther S, Moyer MS, Walters HC, Rinaldo P, Devarajan P, Sun AQ, Dawson PA, Ananthanarayanan M: **Cloning and characterization of a novel peptidase from rat and human ileum**. *J Biol Chem* 1997, **272**(49):31006-31015.

198. Sedo A, Malik R: **Dipeptidyl peptidase IV-like molecules: homologous proteins or homologous activities?** *Biochim Biophys Acta* 2001, **1550**(2):107-116.

199. Liu T, Toriyabe Y, Berkman CE: **Purification of prostate-specific membrane antigen using conformational epitope-specific antibody-affinity chromatography**. *Protein Expr Purif* 2006, **49**(2):251-255.

200. Slusher BS, Robinson MB, Tsai G, Simmons ML, Richards SS, Coyle JT: **Rat brain N-acetylated alpha-linked acidic dipeptidase activity. Purification and immunologic characterization**. *J Biol Chem* 1990, **265**(34):21297-21301.

201. Xiao Z, Jiang X, Beckett ML, Wright GL, Jr.: **Generation of a baculovirus recombinant prostate-specific membrane antigen and its use in the development of a novel protein biochip quantitative immunoassay**. *Protein Expr Purif* 2000, **19**(1):12-21.

202. Beckett D, Kovaleva E, Schatz PJ: **A minimal peptide substrate in biotin holoenzyme synthetase-catalyzed biotinylation**. *Protein Sci* 1999, **8**(4):921-929.

203. Wang L, Li L, Guo Y, Tong H, Fan X, Ding J, Huang H: **Construction and in vitro/in vivo targeting of PSMA-targeted nanoscale microbubbles in prostate cancer**. *Prostate* 2013, **73**(11):1147-1158.

Abbreviations

AA	amino acid
ADC	antibody-drug conjugate
AMPA	α-amino-3-hydroxy-5-methyl-4-isoxasolepropionate
BCG	β-citryl-L-glutamate
BH4	tetrahydrobiopterin
bp	base pair
BRENDA	Braunschweig Enzyme Database
CNS	central nervous system
CT	computed tomography
cAMP	cyclic adenosine monophosphate
ELISA	enzyme-linked immunosorbent assay
eNOS	nitric oxide synthase
EST	expressed sequence tag
FC	flow-cytometry
FOLH	folate hydrolase
GCPII/III	glutamate carboxypeptidase II/III
IHC	immunohistochemistry
i/mGluR	ionotropic/metabotropic glutamate receptor
IUBMB	International Union of Biochemistry and Molecular Biology
LNCaP	lymph node carcinoma of the prostate
mAb	monoclonal antibody
mGluR$_3$	metabotropic glutamate receptors type 3
mRNA	messenger ribonucleic acid
NAAG	*N*-acetyl-L-aspartyl-L-glutamate
NAALADase I/II/L	*N*-acetylated alpha-linked acidic dipeptidase I/II/like
NCBI	National Center for Biotechnology Information
NMDA	*N*-methyl-D-aspartate
NMR	nuclear magnetic resonance
PAK	p21-associated kinase
PCa	prostate carcinoma
PDB	protein data bank
PE40	truncated form of *Pseudomonas* exotoxin
PET	positron emission tomography
2-PMPA	2-(phosphonomethyl)pentanedioic acid
PSMA	prostate-specific membrane antigen
PSMAL	prostate-specific membrane antigen-like
PSME	enhancer of *FOLH1* gene
RCSB	Research Collaboratory for Structural Bioinformatics
rhGCPII	recombinant human GCPII (AAs 44-750)
SAR	structure-activity relationship
scFv	single-chain fragment variable
shRNA	short hairpin ribonucleic acid
siRNA	small interfering ribonucleic acid
SPECT	single-photon emission computed tomography
SPR	surface plasmon resonance
TGF-β	tumor growth factor β
THFs	5-methyl-tetrahydrofolates
WB	western blot

List of Figures and Tables